THE UNIVERSITY
of EDINBURGH

Synaptic Vesicle Recycling in Preclinical Models of Intellectual Disability, Autism Spectrum Disorder, and Epilepsy

Katherine Bonnycastle

THE UNIVERSITY *of* EDINBURGH

Doctor of Philosophy
The University of Edinburgh
2018

Declaration

I, Katherine Bonnycastle, have composed this thesis. All of the experimental procedures and data analysis presented in this work are my own unless otherwise specified, see below. Furthermore, no part of the following work has ever been submitted for any other degree or professional qualification.

Dr Rona Wilson, Centre for Integrative Physiology, prepared some of the wildtype hippocampal cultures for the dynamin-1 work.

Dr Dinesh Soares, American Chemical Society, performed all of the *in silico* modelling for the dynamin-1 mutants studied.

13/12/2017

Table of contents

Table of figures

Table of tables

Acknowledgements

Firstly, I would like to thank Professor Mike Cousin, for accepting to take me on as an MSc student and then again as a PhD student. I would also like to thank Mike and Professor Peter Kind for proposing such an interesting project. I would like to thank them both for their encouragement and feedback throughout this process and for allowing me to go to NCBS in India to work on a collaborative project. I look forward to continuing working with them as a SidB postdoc. I would especially like to thank Mike for getting my thesis drafts turned around to me in record time!

A special thank you to Dr Jamie Marland for his help and supervision at the beginning of this project. A big thank you to all the current and former members of the Cousin Lab for all their help and thoughtful scientific insight. I would particularly like to thank Dr Rona Wilson for all her work in tissue culture, Dr Karen Smillie for guidance with the GTPase assay, Dr Callista Harper for all her help with imaging and analysis and changing the microscope bulb and Dr Jessica Nicholson-Fish for help with VAMP4-pH analysis. I would also like to thank the current and former members of the Kind lab, particularly Dr Lindsay Mizen and Dr Adam Jackson for all the help and information they provided me regarding the rat models. I would also like to thank Dr Wayne Lam and Dr Dinesh Soares for providing me with patient data and modelling data for the dynamin-1 results chapter. I would also like to thank the BRR staff for looking after my colonies. I would also like to thank Dr Christos Gkogkas and Prof Ian Gold for additional guidance. I would also like to thank all of the HRB support staff including Carol Wollaston, James Griffiths and Laura Butterworth.

I would also like to acknowledge the CIP studentship and the Global Research Award that have provided me with funding for me to undertake this PhD.

Of course, I would not have survived this PhD without my office mates in 176 and all the other PhD students and postdocs who I have met along the way, especially my work besties Catherine and Amy without whom I would have never had even a semblance of work-life balance. I would also like to thank everyone at Tribe Yoga who helped keep me calm during my final year.

I would also like to thank all my friends back home for all their emotional support and for dealing with the five-hour time difference, especially Cath, Emmanuelle and Sarah, for their moral support and for continuing to make me laugh even when experiments weren't going

quite right. Thank you also to Marc who has been incredibly understanding throughout this last year.

Last but not least, I would also like to thank my parents and sister for their financial and emotional support. Thank you for being so supportive and putting up with me only talking about neuroscience for the last 3 years (okay 4.5+ years). Thank you for all the weekend calls and putting up with no lie-ins. Thank you for all the visits and for filling my fridge and freezer on your holidays. And finally, thank you for helping make the distance between us seem a lot shorter than it actually is.

Abstract

The development of the central nervous system is dysregulated in neurodevelopmental disorders such as intellectual disability, autism spectrum disorder, and epilepsy. These three disorders have different clinical features, yet there is high comorbidity between them. They can be difficult to study due to their highly complex aetiologies, however there are various monogenic diseases that can cause all of them, including *SYNGAP1* haploinsufficiency where the synaptic guanosine triphosphatase (GTPase)-activating protein (SYNGAP) protein levels are highly reduced; Fragile X syndrome where the fragile X mental retardation protein (FMRP) is no longer translated; and *DNM1* epileptic encephalopathy where mutations in the *Dynamin1* gene alter the protein function. These monogenic conditions are synaptopathies as the proteins affected play important roles in synapse stability and neurotransmission.

Because of the high comorbidity between these disorders, it is hypothesised that there may be a common mechanism underlying them. We hypothesise that a deficit in presynaptic vesicle recycling may be part of a common mechanism underlying intellectual disability, autism spectrum disorder, and epilepsy especially in *SYNGAP1* haploinsufficiency, Fragile X syndrome, and *DNM1* epileptic encephalopathy. Using various fluorescent presynaptic activity reporters including synaptic pHluorins, tetramethylrhodamine dextran and calcium dyes to compare presynaptic activity in *in vitro* models of these monogenic conditions, we found differences in synaptic vesicle (SV) endocytosis in the genetically altered conditions compared to wildtype controls.

We observed various SV endocytosis defects in clathrin-mediated endocytosis (CME) or activity-dependent bulk endocytosis (ADBE) in our models. We observed enhanced CME in *SynGAP1* KO mouse hippocampal neurons. This enhanced SV endocytosis was accompanied by decreased SV cargo on the plasma membrane. Rat *SynGAP1* KO hippocampal neurons did not display enhanced SV endocytosis, nor

did neurons with the GTPase-activating (GAP) domain of SynGAP deleted. This was perhaps due to the altered time course of development between these rodent species. In mouse and rat models of Fragile X syndrome, CME was not altered compared to wildtype controls. However, in a rat model, we observed fewer nerve terminals undergoing ADBE which is the dominant SV endocytosis mode during elevated neuronal activity. *De novo* epileptic encephalopathy-associated mutations in *DNM1* had differential effects on SV recycling through both CME and ADBE. Mouse hippocampal neurons overexpressing $Dyn1_{R237W}$, $Dyn1_{I289F}$ and $Dyn1_{H396D}$ all showed less CME compared to overexpression of $Dyn1_{WT}$. Moreover, fewer nerve terminals overexpressing $Dyn1_{H396D}$ were found to undergo ADBE. We also found that a large-conductance potassium (BK) channel opener can accelerate clathrin-mediated endocytosis and thus may be able to rescue the impaired SV endocytosis caused by these mutants.

Although there is not yet a common underlying pathway at the presynaptic level between these conditions, SV recycling dysfunction is present across all of these models. Furthermore, we propose an axis of pathophysiology model where optimal SV endocytosis is required for optimised neural performance. We propose that either decreased or increased SV endocytosis can lead to the synaptic dysfunction observed in these models.

Lay abstract

Neurodevelopmental disorders are a group of disorders that disrupt brain development. Intellectual disability, autism spectrum disorder and epilepsy are complex neurodevelopmental disorders that can present themselves together. They can be difficult to study as they can have multiple genetic and environmental causes. *SYNGAP1* haploinsufficiency, Fragile X syndrome and *DNM1* epileptic encephalopathy are common genetic causes of these disorders. In *SYNGAP1* haploinsufficiency, SYNGAP protein levels are highly reduced. In Fragile X syndrome, the fragile X mental retardation protein (FMRP) is absent. In *DNM1* epileptic encephalopathy, mutations in the protein dynamin-1 alter its function. These single-gene disorders impair neuronal function as the affected proteins all play important roles in communication across nerve cells.

In this project we looked at synaptic vesicle recycling in the brain of mouse and rat models of these three conditions. Synaptic vesicles are little membrane packages that contain the transmitter that is used for communication between nerve cells. Synaptic vesicles undergo cycles: with the appropriate stimulation, they fuse with the cell membrane to release their content, then parts of the cell membrane are taken back up again to form new synaptic vesicles. Individual vesicles can be taken up from the cell membrane in a process called clathrin-mediated endocytosis (CME). During higher levels of neuronal activity, a large portion of the membrane can be taken up to form a large membrane compartment from which individual synaptic vesicles can then be formed. This process is activity-dependent bulk endocytosis (ADBE).

We found defects in synaptic vesicle recycling, particularly impaired membrane retrieval in each model. In a mouse model of *SYNGAP1* haploinsufficiency, we saw enhanced membrane retrieval and less protein stuck on the cell membrane. We did not observe this in our rat model. This may be due to differences in development across mice and rats. In both mouse and rat models of Fragile X syndrome, we

observed that there was no difference in membrane retrieval through CME. However, in a rat model, we observed that there were fewer nerve structures that could undergo ADBE at high neuronal activity. For our *DNM1* epileptic encephalopathy model, we expressed human mutations into mouse neurons and observed that some of these mutations impaired membrane retrieval through CME, while others impaired membrane retrieval through both CME and ADBE. Interestingly, we also found a drug which had been developed for stroke treatment that could enhance membrane retrieval through CME and thus may be able rescue the impaired CME that we observe in this model.

Although there is not yet a common deficit between these conditions, SV recycling dysfunction is present across all of these models. Furthermore, we propose a model where optimal membrane retrieval is required for optimised neural performance. We propose that either decreased or increased membrane retrieval may lead to the neuronal dysfunction observed in these models.

List of publications

Marland, J.R., Hasel, P., **Bonnycastle, K**., and Cousin, M.A. (2016). Mitochondrial Calcium Uptake Modulates Synaptic Vesicle Endocytosis in Central Nerve Terminals. J. Biol. Chem. 291, 2080-2086.

List of abbreviations

[Ca2+]i	Intracellular free calcium concentration
ADBE	Activity-dependent bulk endocytosis
ADHD	Attention deficit hyperactivity disorder
AMPA	α-amino-3-hydroxy-5-methyl-4-isoxazolepropionic
AMPAR	α-amino-3-hydroxy-5-methyl-4-isoxazolepropionic acid receptor
ANOVA	Analysis of variance
AP	Action potential
AP-1	Adaptor protein-1
AP-5	DL-2-Amino-5-phosphonopentanoic acid
ASD	Autism spectrum disorder
ASPA	Animals (Scientific Procedures) Act
ATP	Adenosine triphosphate
ATPase	Adenosine triphosphatase
AZ	Active zone
BDNF	Brain-derived neurotrophic factor
BK channel	Big potassium channel
BSA	Bovine serum albumin
BSE	Bundle signalling element
Ca^{2+}	Calcium
CaMKII	Ca^{2+}/calmodulin-dependent protein kinase II
Cdk5	Cyclin-dependent kinase 5
CHC	Clathrin heavy chain
CIP4	cell division control protein 42 (Cdc42)- interacting protein 4
cKO	Conditional knockout
CLC	Clathrin light chain
CME	Clathrin-mediated endocytosis
CNQX	6-cyano-7-nitroquinoxaline-2,3-dione
cTKO	Conditional triple knockout
CYFIP1	Cytoplasmic FMRP-interacting protein-1
DHPG	3,5-dihydroxyphenylglycine

DIV	Day *in vitro*
DKO	Double knockout
DMEM	Dulbecco's Modified Eagle Medium
DMSO	Dimethyl sulfoxide
DNM1	*Dynamin1*
dNTP	Deoxynucleotide
DRG	Dorsal root ganglion
Dyn	Dynamin
EEG	Electroencephalography
eIF4E	Eukaryotic translation initiation factor 4E
eps15	Epidermal growth factor receptor substrate 15
ERK	Extracellular signal-regulated kinase
ESCRT	Endosomal sorting complex required for transport
BAR	Bin-amphiphysin-Rvs161/167
FBS	Foetal bovine serum
FCHo	Fer/Cip4 homology domain-only protein
FMR1	*Fragile X mental retardation 1*
FMRP	Fragile X mental retardation protein
FXS	Fragile X syndrome
GABA	Gamma-aminobutyric acid
GAP	Guanosine triphosphatase (GTPase)-activating protein
GED	Guanosine triphosphatase (GTPase) effector domain
GFP	Green fluorescent protein
GSK3β	Glycogen synthase kinase 3β
GTP	Guanosine triphosphate
GTPase	Guanosine triphosphatase
H^+	Hydrogen
HA	Hemagglutinin
Het	Heterozygous
Hom	Homozygous
HRP	Horseradish peroxidase
HSC-70	Heat shock cognate 70

ID	Intellectual disability
IP	Immunoprecipitation
IQ	Intelligence quotient
IRES	Internal ribosomal entry site
K^+	Potassium
KD	Knock-down
KO	Knockout
LEH	Long Evans Hooded
LRRTM	Leucine-rich repeat transmembrane protein
LTD	Long-term depression
MAPK	Mitogen-activated protein kinase
mCer	mCerulean
MEM	Minimum essential medium
mEPSC	Mini excitatory postsynaptic current
mGluR	Metabotropic glutamate receptor
mTOR	Mammalian target of rapamycin
mTORC2	Mammalian target of rapamycin complex 2
Munc	Mammalian uncoordinated protein
NB	Neurobasal
NMDA	N-Methyl-D-aspartic acid
NMDAR	N-Methyl-D-aspartic acid receptors
NSF	N-ethylmaleimide-sensitive factor
NSID	Non-syndromic intellectual disability
PBS	Phosphate buffered saline
PCR	Polymerase chain reaction
PDK1	Phosphatidylinositol-dependent kinase 1
PDL	Poly-D-lysine
PFA	Paraformaldehyde
-pH	pHluorin
PH	Pleckstrin homology
Pi	Inorganic phosphates
PI3K	Phosphatidylinositol 3-kinase

PIP2	Phosphatidylinositol 4,5-bisphosphate
PLK2	Polo-like kinase 2
PND	Post-natal day
PRD	Proline-rich domain
PSD	Postsynaptic density
RIM	Rab3-interacting molecule
ROI	Region of interest
RRP	Readily releasable pool
SAP102	Synapse-associate protein 102
SD	Sprague Dawley
SEM	Standard error of the mean
SH3	Src homology 3
shRNA	short hairpin ribonucleic acid
siRNA	short interfering ribonucleic acid
SNAP-25	Synaptosomal-associated protein 25
SNARE	Soluble N-ethylmaleimide-sensitive factor-attachment protein receptor
STD	Short-term depression
STED	Stimulated emission depletion
SV	Synaptic vesicle
SV2A	Synaptic vesicle glycoprotein 2A
SYNGAP	Synaptic guanosine triphosphatase (GTPase)-activating protein
sypHy	Synaptophysin-pHluorin
TARP	Transmembrane AMPA receptor regulatory proteins
TKO	Triple knockout
TMR	Tetramethylrhodamine
TTX	Tetrodotoxin
UV	Ultraviolet
VAMP4	Vesicle-associated membrane protein-4
vGAT	Vesicular GABA transporter
vGLUT	Vesicular glutamate transporter
WT	Wildtype

1. Introduction

1.1. Neurodevelopmental disorders

Neurodevelopmental disorders are a heterogeneous group of disorders of nervous system development. There are various genetic factors and epigenetic modifications that are associated with neurodevelopmental conditions, some of which are yet to be elucidated or fully understood (Sontheimer, 2015; van Loo and Martens, 2007). There is a complex interplay between genes and prenatal or postnatal environmental factors that can give rise to these disorders, making them difficult to study (van Loo and Martens, 2007).

The incidence of neurodevelopmental disorders is approximately 1 in 30 live births (Sontheimer, 2015). In the United States, the economic cost of neurodevelopmental disorders is $81.5–167 billion per year (Schettler, 2001; Szpir, 2006). Although these disorders are very common and present an important economic burden, very little is still known about them and how to treat them.

The pathophysiology underlying neurodevelopmental disorders remains poorly understood. The cellular dysfunction appears to be vastly different within and across different neurodevelopmental disorders due to their complex aetiologies. This makes it difficult to develop new drugs and treatment strategies. The one thing these disorders do have in common is that they impair the correct development of the brain (Andreae and Burrone, 2017; Hulbert and Jiang, 2017; Krol and Feng, 2017; Moretto et al., 2017).

In this work we have chosen to study three highly comorbid neurodevelopmental disorders: intellectual disability (ID), autism spectrum disorder (ASD) and epilepsy to determine whether there is any convergence across their pathophysiology.

1.1.1. Intellectual disability (ID)

ID, previously mental retardation (American Psychiatric Association and American Psychiatric Association. Task Force on DSM-IV, 1994), is characterised by deficits in intellectual and adaptive functioning across conceptual, social and practical domains (American Psychiatric Association and American Psychiatric Association. DSM-5 Task Force, 2013). Individuals can experience varying degrees of these deficits. Intelligence quotient (IQ) tests allow for the diagnosis of ID in late childhood or early adulthood (IQ< 70). The IQ score also permits the severity classification of affected individuals (Mefford et al., 2012). However, these scores cannot assess the extent of adaptive functioning deficits in social skills and personal independence which are better indicators of treatment and care options (American Psychiatric Association and American Psychiatric Association. DSM-5 Task Force, 2013; Mefford et al., 2012).

Despite ID diagnosis only occurring in late childhood, ID can be identified in early childhood from developmental delays across motor, cognitive, and speech functions (Mefford et al., 2012). It is a highly prevalent disorder that affects 2-3 % of the global population (Leonard and Wen, 2002; Ropers and Hamel, 2005). This is due to the broad definition of symptoms of the disorder which allows it to encompass various phenotypes that can be due to both syndromic and non-syndromic causes.

As with other neurodevelopmental disorders, there are a multitude of genetic and non-genetic factors that can cause intellectual disability. Different single-gene mutations, both autosomal and X-linked, have been shown to give rise to the disorder

(Mefford et al., 2012). This heterogeneity of risk factors may underlie some of the diversity of the phenotypes associated with ID. Multiple psychiatric and neurodevelopmental disorders present themselves with lower intellectual functioning, suggesting that there may be some similar underlying mechanisms across these disorders.

1.1.2. Autism spectrum disorder (ASD)

ASD is characterised by difficulties in social communication and social interaction, and restricted, stereotyped, repetitive behaviours or fixed interests (American Psychiatric Association and American Psychiatric Association. DSM-5 Task Force, 2013). These behaviours can vary in severity across the autism spectrum. ASD is often comorbid with other neurodevelopmental disorders including attention deficit hyperactivity disorder (ADHD) (Leyfer et al., 2006; Simonoff et al., 2008; Joshi et al., 2010), anxiety (Simonoff et al., 2008), ID (McCarthy, 2007) and epilepsy (Mazarati et al., 2017). ID is present in 50-70 % of individuals with ASD (Mefford et al., 2012) and epilepsy is present in 4-38 % of individuals with ASD (S. Thomas et al., 2017).

The disorder was first observed in children displaying obsessive behaviours and impaired affective and social interactions (Kanner, 1943). Individuals are diagnosed with ASD around 3 years of age using a battery of psychological questionnaires (Johnson et al., 2007), behavioural observations, and interviews with caregivers (American Psychiatric Association and American Psychiatric Association. DSM-5 Task Force, 2013). This age is when autistic behaviours become apparent, however certain symptoms of the behaviour can be observed at an earlier age, including language delays and lack of affective behaviour (Johnson et al., 2007).

The prevalence of ASD has increased throughout the past 30 years. Currently, 1 in 68 children in the United States (Developmental Disabilities Monitoring Network Surveillance Year 2010 Principal Investigators and Centers for Disease Control and Prevention (CDC), 2014), and 3.8:1000 boys and 0.8:1000 girls in the United Kingdom (B. Taylor et al., 2013) are diagnosed with ASD. It is unclear whether this increase in prevalence is due to more accurate diagnostic tests, a change in diagnostic criteria, more awareness of these disorders or a higher incidence rate (Charman, 2002).

ASDs have a complex aetiology with several known and unknown genetic, epigenetic, and environmental causes (Banerjee et al., 2014). They have an important heritable component as shown by multiple twin studies (Folstein and Rutter, 1977; Ritvo et al., 1985; Rosenberg et al., 2009). These multiple causes give rise to different autistic phenotypes of differing severity. Unsurprisingly, there is no treatment for this disorder, however certain associated symptoms including epilepsy and anxiety can be partially relieved by appropriate medication.

The increased excitation and decreased inhibition model (Rubenstein and Merzenich, 2003) was developed to attempt to explain how so many different genetic causes produce the same autistic phenotypes. This model proposes that there is an excitatory/inhibitory imbalance that underlies most behavioural, social and cognitive impairments observed in ASD. This model also postulates that the severity of the excitatory/inhibitory imbalance determines the severity of ASD phenotypes. This imbalance can be due to increased excitation or decreased inhibition or a combination of both in different circuits (Rubenstein and Merzenich, 2003). Studies have lent support to this model by showing that increasing excitation/inhibition ratio can replicate ASD-related phenotypes in WT mice (Yizhar et al., 2011).

1.1.3. Epilepsy

Epilepsy is characterised by repeated seizures due to bursts of neuronal hyperactivity (Avanzini and Franceschetti, 2003; Bozzi et al., 2012). These events of spontaneous neuronal firing can be contained to a specific region of the brain or spread across both hemispheres, with the most epileptogenic regions being the cortex and the hippocampus (Avanzini and Franceschetti, 2003; Pitkanen and Sutula, 2002). Recurrent seizures can result in changes in synaptic plasticity due to neuronal loss, neurogenesis, axonal branching and glial proliferation (reviewed in Pitkanen and Sutula, 2002).

Epilepsy is a common neurological disorder (Sander and Shorvon, 1996) affecting 7.3:1000 individuals in the United Kingdom (J. Wright et al., 2000). The prevalence of epilepsy increases with age (J. Wright et al., 2000). In certain cases, however, it is considered a neurodevelopmental disorder because it is due to the disruption of prenatal neuronal proliferation and migration, and postnatal circuit remodelling during developmental critical periods (reviewed in Bozzi et al., 2012).

1.2. Monogenic causes of neurodevelopmental disorders

Neurodevelopmental disorders have highly complex aetiologies and most of their pathophysiology is still not well understood. ID, ASD, and epilepsy are highly comorbid, suggesting a common mechanism underlying these disorders. Since monogenic conditions allow for study of tractable model systems, this work focusses on three monogenic conditions causing ID, ASD and epilepsy: *SYNGAP1* haploinsufficiency, Fragile X syndrome and *DNM1* epileptic encephalopathy.

1.2.1. SYNGAP1 haploinsufficiency

SYNGAP1 haploinsufficiency is due to mutations in the *SYNGAP1* gene resulting in loss of function of the brain-specific synaptic guanosine triphosphatase (GTPase)-activating protein (SYNGAP). Most described patient mutations are deletions or missense mutations leading to dysfunctional proteins (reviewed in Parker et al., 2015). Since the first mutations in *SYNGAP1* were characterised (Hamdan et al., 2009), *SYNGAP1* haploinsufficiency has been identified as an important cause of non-syndromic ID (NSID) (C. F. Wright et al., 2015). The ID caused by *SYNGAP1* haploinsufficiency is highly comorbid with epilepsy and ASD (Parker et al., 2015). There is also some evidence suggesting that loss of SYNGAP may also lead to syndromic ID in a subset of patients who display distinct facial features, typical myoclonic, absence, and drop attack seizures, hyperexcitability, sleep disturbances and aggressive behaviour (Parker et al., 2015).

SynGAP is a highly abundant protein enriched at excitatory postsynaptic densities (PSDs) (H. J. Chen et al., 1998; Kim et al., 1998). SynGAP was identified in a cDNA screen as a novel protein that could interact with the PDZ domains of the PSD-95/ synapse-assiciated protein (SAP) 102 family of proteins (Kim et al., 1998). The N-terminal of the protein contains a pleckstrin homology (PH) domain, a C2 domain and a Ras-GTPase activating (RasGAP) domain (Kim et al., 1998). The GAP and C2 domains of SynGAP can also act as a RapGAP (Krapivinsky et al., 2004; Pena et al., 2008). Its C-terminal contains a phosphorylation site for Ca^{2+}/calmodulin-dependent protein kinase II (CaMKII) (H. J. Chen et al., 1998; Walkup et al., 2015). Phosphorylation of SynGAP1 by CaMKII, cyclin-dependent kinase 5 (Cdk5) or polo-like kinase 2 (PLK2) increases its RasGAP and RapGAP activity to different extents (Krapivinsky et al., 2004; Lee et al., 2011; Walkup et al., 2015).

SynGAP can be alternatively spliced to produce multiple isoforms with distinct N-termini and C-termini (Figure 1.1) (Kim et al., 2003; W. Li et al., 2001; A. C.

McMahon et al., 2012). SynGAP has five isoforms with distinct C-termini: α1, α2, β1/2, β3/4, γ, with the α1 and β isoforms being the most abundant in the brain (W. Li et al., 2001). These isoforms have different distribution patterns across the forebrain. The α1 isoform colocalises with PSD-95 at excitatory synapses in rat hippocampal neuron cultures and β isoforms preferentially colocalises with gephyrin in culture suggesting their presence at inhibitory synapses (Moon et al., 2008). The SynGAPα1 isoform is tightly associated with synaptic structures, whereas the β isoforms formed more extra-synaptic clusters in dendrites (Moon et al., 2008). Additionally, there is evidence of SynGAPβ isoforms in the nucleus of cultured hippocampal neurons (Moon et al., 2008). There are also three alternative spice variants of the N-terminus: A, B, C (Kim et al., 2003; W. Li et al., 2001) due to the use of different promoters (A. C. McMahon et al., 2012).

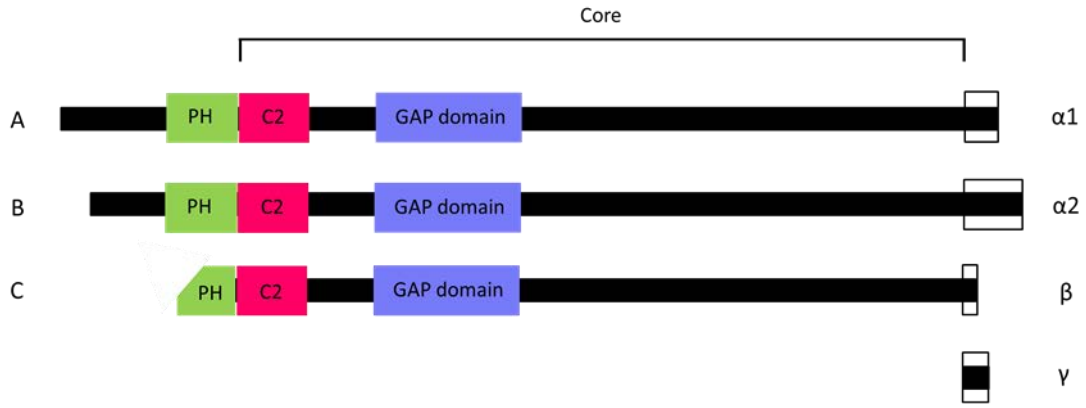

Figure 1.1 SynGAP isoforms and domain structure

Adapted from McMahon et al. (2010)
SynGAP is composed of a pleckstrin homology (PH) domain, a C2 domain and a GTPase activating (GAP) domain in its N-terminus. SynGAP can be alternatively spliced to produce multiple isoforms with distinct N-termini (A, B, C) and C-termini (α1, α2, β1/2, β3/4, γ).

The different SynGAP isoforms have distinct effects on synaptic function (A. C. McMahon et al., 2012). SynGAP Aα2 expressed in forebrain neurons decreased mini excitatory postsynaptic current (mEPSC) amplitude whereas SynGAP Bα2 and Cα2 increased mEPSC amplitude. Thus, SynGAPα2 can regulate mEPSC amplitude in an

N-terminus splice variant-dependent manner (A. C. McMahon et al., 2012). SynGAP Bα2 isoforms also showed increased mEPSC frequency which may suggest an increased release probability of presynaptic neurotransmitter. SynGAP Aα1 showed decreased mEPSC frequency (A. C. McMahon et al., 2012). Overexpression of GFP-SynGAP was also found to decrease mEPSC frequency (Rumbaugh et al., 2006). No other isoforms tested produced any effect on mEPSC frequency compared to control (A. C. McMahon et al., 2012). This suggests that SynGAP can both positively and negatively impact synaptic strength depending on isoform expression.

Activation of SynGAP can regulate extracellular signal-regulated kinase (ERK) signalling downstream of N-Methyl-D-aspartic acid receptors (NMDARs) (Komiyama et al., 2002) which in turn leads to inhibition of protein translation (Barnes et al., 2015; Rumbaugh et al., 2006; C. C. Wang et al., 2013). Short interfering RNA (siRNA)-mediated knock-down of SynGAP in cortical networks leads to increased protein synthesis (C. C. Wang et al., 2013). SynGAP regulates the α-amino-3-hydroxy-5-methyl-4-isoxazolepropionic acid receptor (AMPAR) content of the plasma membrane by suppressing AMPAR synthesis through inhibition of the mitogen-activated protein kinase (MAPK)/ERK pathway (C. C. Wang et al., 2013). Altering the number of AMPAR at the plasma membrane directly impacts synaptic strength (reviewed in Anggono and Huganir, 2012).

As previously stated, SynGAP, particularly the SynGAPα1 isoform, can bind any of the three PDZ domains of PSD-95 (Kim et al., 1998). This competitive binding of the PDZ of PSD-95 can regulate AMPAR docking and synapse structure by preventing neuroligins, leucine-rich repeat transmembrane proteins (LRRTMs) and transmembrane AMPA receptor regulatory proteins (TARPs) from binding (Walkup et al., 2016). Phosphorylation of SynGAP by CaMKII or PLK2 reduces its binding to PSD-95, thus allowing modification of the PSD structure. This modification of PSD structure includes more insertion of AMPAR in the plasma membrane through binding of TARPs with the PDZ domains of PSD-95 (Walkup et al., 2016). In a

mouse model of *SynGAP1* haploinsufficiency, there was altered protein composition of the PSD with increased LRRTM, TARP and neuroligin-2 associated with PSD-95 (Walkup et al., 2016). This altered composition of the synapse may, in part, mediate some of the deficits in synaptic plasticity observed in models of *SynGAP1* haploinsufficiency.

Mice with homozygous deletion of SynGAP die within 5 days of birth (Komiyama et al., 2002) due to increased apoptosis measured by caspase-3 activation (Knuesel et al., 2005). Caspase-3 is a key degradative enzyme in apoptosis and can be used to measure of amount of apoptosis occurring (Rami, 2003). Interestingly neuronal apoptosis appears to be inversely correlated with SynGAP expression levels suggesting a role for SynGAP in the apoptosis pathway (Knuesel et al., 2005). However how SynGAP regulates apoptosis is not well understood.

Mice with heterozygous deletion of *SynGAP1* (*SynGAP1* Het) show impaired synaptic plasticity during critical periods of synapse formation (Aceti et al., 2015; Clement et al., 2012). SynGAP's pattern of expression would suggest a role in development, with expression peaking by post-natal day (PND) 14. SynGAP levels then decrease in adulthood (Kim et al., 1998; Porter et al., 2005; Clement et al., 2012). There is already evidence for premature maturation of hippocampal synapses in *SynGAP1* Het mice by PND 7 (Aceti et al., 2015) with significantly increased hippocampal neurotransmission at PND 14 associated with an increase in the AMPA/NMDA currents (Clement et al., 2012). The maturation of excitatory synapses requires a change in glutamate receptors inserted into the plasma membrane. An increase in AMPA/NMDA currents is suggestive of a more mature synapse where AMPAR-mediated neurotransmission is dominant (Hall et al., 2007). mEPSC frequency and amplitude are increased in *SynGAP1* Het dentate gyrus granule neurons (Clement et al., 2012). Dendritic spine density is unchanged between Het and WT neurons, however spine morphology was different in Het

neurons with more mushroom-type spines and fewer stubby-type spines at PND 14. This phenotype persists into adulthood (Clement et al., 2012).

At PND 21, *SynGAP1* Het cortical pyramidal neurons were bigger and displayed more dendritic branching and longer dendrites. They appeared to be more similar to adult neurons and were already undergoing pruning which is characteristic of mature neurons (Aceti et al., 2015). However, during adulthood, there is no longer any difference between WT and *SynGAP1* Het neuron gross morphology in the cortex (Aceti et al., 2015).

Temporally inducing SynGAP haploinsufficiency during adulthood did not alter AMPA/NMDA current ratio (Clement et al., 2012). This suggests an important role for SynGAP in controlling dendritic spine maturation during development. Furthermore, using a Cre-Lox system to express SynGAP during adulthood was not able to rescue the impaired behavioural phenotypes including decreased anxiety, (more time spent in the open arm the elevated plus maze) and hyperactivity (more locomotion in an open field), suggesting a critical role of SynGAP during circuit formation (Clement et al., 2012).

SynGAP also plays an important role in circuit connectivity. Hippocampal slices from *SynGAP1* Het mice display enhanced protein synthesis-dependent metabotropic glutamate receptor- mediated long-term depression (mGluR-LTD) (Barnes et al., 2015). This exaggerated mGluR-LTD is due to dysregulated ERK1/2 signalling leading to enhanced protein synthesis.

Thus, SynGAP is necessary for correct synapse formation and circuit connectivity during development. This critical role in development makes *SYNGAP1*

haploinsufficiency an important model for elucidating underlying mechanisms for neurodevelopmental disorders.

1.2.2. Fragile X syndrome (FXS)

FXS, also known as Martin-Bell Syndrome (Martin and Bell, 1943), is one of the most common monogenic causes of ID and ASD, accounting for 5 % of all cases (Mefford et al., 2012). Epilepsy is also present in 10-20 % of cases of FXS (Berry-Kravis, 2002).

FXS syndrome is caused by the loss of the *Fragile X mental retardation 1* (*FMR1*) gene product fragile X mental retardation protein (FMRP) (Pieretti et al., 1991). Most cases of FXS, are caused by a CGG trinucleotide expansion in the 5' untranslated region of the *FMR1* gene on the X chromosome. This expansion leads to hypermethylation of the promoter, repressing the transcription of FMR1 (Bell et al., 1991; Sutcliffe et al., 1992; Verkerk et al., 1991). This trinucleotide repeat gives rise to a constricted and elongated "fragile" appearance of the X chromosome during metaphase (Hecht and Bixenman, 1990). The allele is classed as normal (up to 40 repeats), a pre-mutation (40 to 200 repeats) or a full mutation (over 200 repeats) depending on the number of CGG repeats (Fu et al., 1991). Loss of FMRP can also be due to large intragenic deletions in *FMR1* (Hirst et al., 1995; Lugenbeel et al., 1995; Meijer et al., 1994) or single point mutations (Collins et al., 2010; Gronskov et al., 2011). There has also been one report of FXS in a patient with present though non-functional FMRP present (De Boulle et al., 1993). Genotyping revealed a single missense point mutation I304N (De Boulle et al., 1993). This mutation was found to prevent FMRP from associating with polyribosomes (Feng et al., 1997).

FMR1 is segregated in an X-linked manner with reduced penetrance in females (Rousseau et al., 1995). It affects 1:5000 males (Coffee et al., 2009) and 1:6000-8000

females (Hagerman, 2008). Alongside the ASD, ID and epilepsy-associated cognitive disabilities, individuals with FXS also present a distinct physical appearance that aids in the diagnosis of the syndrome. These include large prominent ears, macroorchidism and hyperextensible metacarpophalangeal joints (Lachiewicz et al., 2000).

FMRP is expressed ubiquitously with high expression throughout the brain and in the testes (Gholizadeh et al., 2015; Tamanini et al., 1997). In the brain, expression peaks within the first postnatal week and plateaus in adulthood (Gholizadeh et al., 2015; Till et al., 2012; Till et al., 2015).

FMRP acts as an mRNA-binding protein that represses the translation of its target mRNAs downstream of mGluRs. FMRP can directly inhibit protein translation during the initiation or elongation phase. It forms an inhibitory complex with cytoplasmic FMRP-interacting protein-1 (CYFIP1) and eukaryotic translation initiation factor 4E (eIF4E) to inhibit translation initiation in an activity dependent manner (Napoli et al., 2008). FMRP can also supress the translation of its estimated 748 target mRNAs by directly binding polyribosomes (Feng et al., 1997) to stall their translocation (Darnell et al., 2011).

FMRP is also present in the presynapse in discrete granules, Fragile X granules (FXGs), in axons in certain regions of the mouse brain (Christie et al., 2009). The expression pattern of FXGs is correlated with periods of rich synaptic plasticity and circuit remodelling (Akins et al., 2012; Christie et al., 2009). These FXGs can associate with ribosomes and mediate the translation of specific mRNAs depending on the brain region and developmental period (Chyung et al., 2017).

FMRP is important regulator of protein synthesis-dependent synaptic plasticity. In fact, hippocampal mGluR-LTD is exaggerated in *Fmr1* KO mice (Huber et al., 2002). FMRP does not play a role in the other common LTD form, NMDAR-LTD (Huber et al., 2002). In WT, activation of Group 1 mGluRs leads to the rapid increase in FMRP synthesis and thus the suppression of target mRNA translation (Hou et al., 2006; Weiler et al., 1997). During mGluR-LTD, FMRP is rapidly degraded by the ubiquitin-proteasome pathway (Hou et al., 2006). After degradation, there is an increase in levels of proteins whose transcripts are targets of FMRP (Hou et al., 2006).

In *Fmr1* KO mouse hippocampal slices, both synaptic stimulation-induced and chemically-induced (using the Group 1 mGluR agonist 3,5-dihydroxyphenylglycine, DHPG) mGluR-LTD is enhanced (Hou et al., 2006; Huber et al., 2002; Zhang et al., 2009). Although mGluR-LTD is translation-dependent in WT, in KO, mGluR-LTD is resistant to both the inhibition of protein synthesis and the inhibition of the ERK signalling cascade (Hou et al., 2006; Nosyreva and Huber, 2006). This suggests that this form of plasticity is protein-synthesis independent in this syndrome. Thus, different mechanisms underlie mGluR-LTD in the presence or absence of FMRP.

The altered dendritic spine morphology observed in FXS may also underlie some of the impaired synaptic plasticity. Although there is a discrepancy in terms of dendritic spine phenotype reported in FXS, most *post mortem* studies of mouse brains show age and region-specific differences in dendritic spine morphology. Dendritic spines play an important role in network connectivity as they receive input from most excitatory synapses (Alvarez and Sabatini, 2007). Defects in spine morphology in FXS include an age-specific increase in length and density compared to wild type (WT) (Galvez and Greenough, 2005) and higher density of filopodia and thin spines in spiny stellate neurons with fewer mushroom spines in *Fmr1* KO mice (Till et al., 2012). A region-specific immature spine morphology can also be observed in the hippocampus of *Fmr1* KO mice (Levenga et al., 2011). More recently, stimulated

emission depletion (STED) microscopy was used to obtain better spatial resolution for the imaging of dendritic spines. This study revealed that there were only subtle differences in spine development or morphology in *Fmr1* KO mouse brains during development compared to WT (Wijetunge et al., 2014).

FMRP can promote maturation of synapses and cell-to-cell connections between the third and fifth postnatal weeks (Patel et al., 2014; Zang et al., 2013). Furthermore, FMRP can also regulate connectivity of cortical circuits during critical periods of connection possibly by promoting the pruning of unnecessary connections through the elimination of synapses in an activity-dependent manner (Patel et al., 2014; Pfeiffer et al., 2010; Zang et al., 2013).

The mGluR theory of FXS was proposed based on the phenotypes observed in models of FXS and described above. This theory suggests that the core deficits in FXS can be explained by overactive signalling by group 1 mGluRs (Bear et al., 2004). As previously described, mGluRs work in opposition to FMRP to regulate protein translation. In the absence FMRP, there is excessive translation of these proteins by group 1 mGluRs activation of the ERK signalling cascade (Osterweil et al., 2010). The increased levels of basal protein synthesis (Osterweil et al., 2010) and protein expression (Darnell and Klann, 2013; Klemmer et al., 2011; Tang et al., 2015; Zalfa et al., 2003) then mediates the different phenotypes reported in FXS from exaggerated hippocampal mGluR-LTD to altered circuit connectivity (Bear et al., 2004; Dolen and Bear, 2009). Several studies lend support to this theory and have shown that genetically (Dolen et al., 2007) or pharmacologically (de Vrij et al., 2008; A. M. Thomas et al., 2012; Yan et al., 2005) reducing mGluR5 activity corrects multiple phenotypes of *Fmr1* KO mice (reviewed in Robertson, 2013). Furthermore, treatments regulating the ERK signalling pathway, downstream of group 1 mGluRs, have also been shown to rescue the behavioural, protein synthesis and cellular deficits observed in FXS (Gantois et al., 2017; Osterweil et al., 2013).

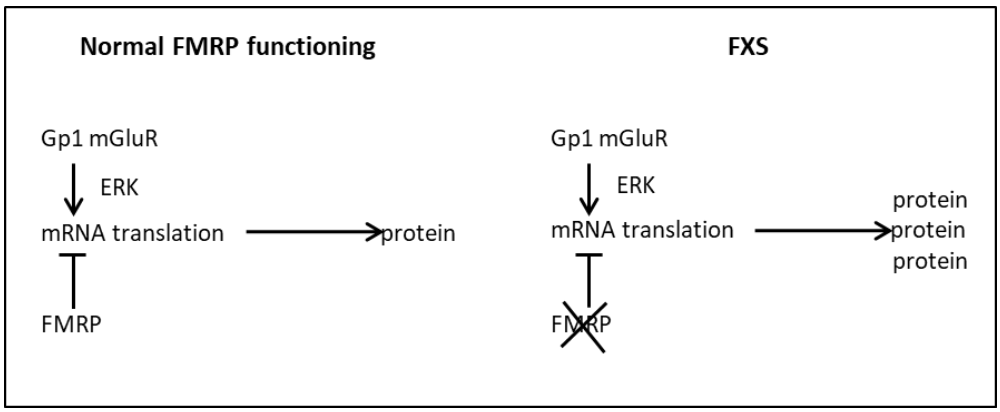

Figure 1.2 The mGluR theory of FXS

Figure adapted from Dolen and Bear, 2009.
FMRP works in opposition to mGluRs to negatively regulate mRNA translation. In the absence of FMRP, as is the case in FXS, there is no negative regulation of translation, thus the translation of mGluR-associated transcripts is upregulated.

It is important to note however that modulating group 1 mGluR activity cannot correct all of the deficits observed in mouse models of FXS, suggesting that FMRP may play another protein translation-independent role. In the presynapse, FMRP plays important roles in mediating ion channel gating in a protein synthesis-independent manner (reviewed in Ferron, 2016). It is hypothesised that the presynaptic phenotype in FXS models is independent of its role in protein translation (Deng and Klyachko, 2016), despite 30.4 % of the presynaptic proteome's mRNAs being targets of FMRP (Darnell et al., 2011). FMRP can regulate action potential (AP) duration by directly binding to large conductance voltage and Ca^{2+}-gated big potassium (BK) channel to modulate their gating (Deng et al., 2013; Myrick et al., 2015). FMRP also directly binds Slack sodium channels (Brown et al., 2010) and controls their gating. These channels are involved in maintaining neuronal firing during sustained neural activity (Bhattacharjee and Kaczmarek, 2005). FMRP can also control the density of N-type calcium channels on the plasma membrane to regulate $[Ca^{2+}]_i$ (Ferron et al., 2014).

There is increasing evidence that some of the impairments in neurotransmission and synaptic plasticity have presynaptic origins. At *Fmr1* KO CA3-CA1 hippocampal

synapses there is increased synaptic response to high frequency stimulation due to increased Ca^{2+} influx in these conditions (Deng et al., 2011). Baseline synaptic transmission is not affected at CA3-CA1 synapses, however (X. S. Wang et al., 2014). These synapses also display reduced short-term depression (STD) at high frequency stimulation due to faster synaptic vesicle (SV) recycling as determined by faster FM1-43 destaining and enlarged SV pools. In fact, both the size of the readily releasable pool (RRP) and reserve pool are increased in this model (Deng et al., 2011). Additionally, during repetitive activity, there is an increased release probability at the CA3-CA1 synapses, but quantal size remains the intact (X. S. Wang et al., 2014).

In WT conditions, FMRP regulates the short-term plasticity described above by directly interacting with BK channels (Deng et al., 2013; Deng and Klyachko, 2016; Myrick et al., 2015). FMRP can regulate AP duration and thus regulate neurotransmitter release. It does this through binding the β4 regulatory subunit of the BK channel and modulating its Ca^{2+} sensitivity (Deng et al., 2013). Loss of FMRP causes reduced channel activity and excessive AP broadening which in turns leads to increased presynaptic Ca^{2+} influx, increased synaptic transmission and the deficits in short-term plasticity (Deng et al., 2013). Furthermore, genetically (Deng and Klyachko, 2016) or pharmacologically (Hebert et al., 2014) enhancing BK channel activity in the absence of FMRP is sufficient to rescue multiple synaptic and behavioural phenotypes associated with FXS. Therefore, deficits in presynaptic activity observed in *Fmr1* KO mice can be mediated by BK channel activity.

In the peripheral nervous system, dorsal root ganglion (DRG) neurons display increased SV exocytosis at high frequency stimulation with unchanged rate and amount of endocytosis with short hairpin RNA (shRNA) mediated knock-down (KD) of FMRP (Ferron et al., 2014). This enhanced SV exocytosis may be due to increased presynaptic Ca^{2+} currents observed with FMRP KD. FMRP can directly interact with N-type voltage gated Ca^{2+} channels to regulate their density on the plasma membrane

(Ferron et al., 2014). FMRP can regulate N-type Ca^{2+} channel expression through directly binding them and targeting them for proteasomal degradation (Ferron et al., 2014). This suggests, that in the absence of FMRP, there is increased channel density which mediates the increased presynaptic Ca^{2+} influx and altered neurotransmission.

The loss of FMRP results in impaired synaptic and circuit function at both the postsynapse and the presynapse which is why FXS is characterised as a synaptopathy. The various presynaptic and postsynaptic phenotypes caused by the loss of FMRP make this a very robust model for studying synaptic dysfunction in neurodevelopmental disorders.

1.2.3. Dynamin1 (DNM1) epileptic encephalopathy

Epileptic encephalopathies comprise a group of childhood-onset severe seizure disorders where the epilepsy contributes to a disrupted cerebral functioning which can progress and worsen with time (Berg et al., 2010). *De novo* mutations in synaptic transmission genes including *CDKL5*, *KCNQ2*, *STXBP1*, *DNM1*, *SLC1A2* and *CACNA1A* can give rise to epileptic encephalopathies (Asinof et al., 2015; Asinof et al., 2016; Boumil et al., 2010; Dhindsa et al., 2015; Epi4K Consortium et al., 2013; Epi4K Consortium, 2016; Fahrner et al., 2016; Nakashima et al., 2016). Two common disorders included in epileptic encephalopathies are infantile spasms and Lennox-Gastaut syndrome (Epi4K Consortium et al., 2013). Lennox-Gastaut syndrome is characterised by drug-resistant seizures of multiple types including tonic, atonic, and atypical absences, abnormal brain wave activity reported by electroencephalography (EEG) study and ID (Asadi-Pooya, 2017). *De novo* mutations in *DNM1* account for approximately 2 % of cases of infantile spasms or Lennox-Gastaut syndrome (Epi4K Consortium et al., 2013).

Dynamin-1 (dyn1), the gene product of *DNM1*, was first described as a mechanochemical enzyme that could regulate microtubule bundling in a nucleotide-dependent manner (Obar et al., 1990; Paschal et al., 1987; Shpetner and Vallee, 1989). The first evidence of dyn1's involvement in endocytosis came from the *Drosophila melanogaster shibire* temperature sensitive mutant (*shibire*^{ts}). The *shibire* gene encodes multiple forms of dynamin (M. S. Chen et al., 1991; van der Bliek and Meyerowitz, 1991). These proteins play an essential role in SV endocytosis, as the *shibire*^{ts} mutant exhibited muscle paralysis at restrictive temperatures, due to depletion of SVs at the neuromuscular junction because of impaired SV endocytosis (Grigliatti et al., 1973; Poodry and Edgar, 1979).

There are three genes that encode different dynamin isoforms in mammals. Dyn1 is selectively expressed in the brain at high levels throughout postnatal development and adulthood (Cao et al., 1998; Cook et al., 1996; Faire et al., 1992; Nakata et al., 1991). Dyn2 is ubiquitous, but expressed at lower levels in the brain where it may play a housekeeping role (Raimondi et al., 2011). Dyn3 is also expressed in the brain, however in lower levels that dyn1 (Cao et al., 1998; Cook et al., 1996). There is thought to be some functional overlap between the proteins as revealed by the generation of *Dnm* KO animal models (discussed below) (Ferguson et al., 2007; Raimondi et al., 2011).

Dyn1 is composed of a GTPase domain (G domain) responsible for guanosine triphosphate (GTP) hydrolysis, a bundle signalling element (BSE) composed of a three-helix bundle and required for correct folding of the protein, the stalk through which dyn1 can dimerise, a PH domain where phosphoinositides can bind, a GTPase effector domain (GED) that regulates GTPase activity, and a proline-rich domain (PRD) which mediates its interactions with the Src homology 3 (SH3) domains of other synaptic proteins (Figure 1.3) (reviewed in Ferguson and De Camilli, 2012).

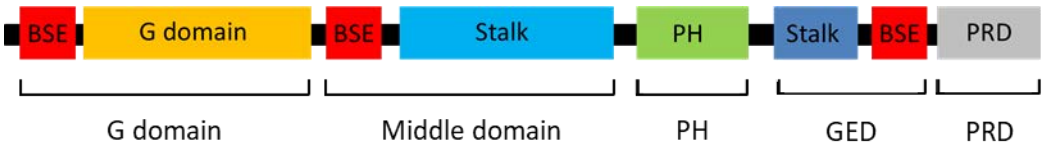

Figure 1.3 Domain structure of dyn1

Adapted from Faelber et al. (2011)
The G domain of dyn1 comprises a bundle signalling element (BSE) and G domain and it mediates GTP hydrolysis. The middle domain comprises a BSE and the stalk through which dyn1 can self-assemble. The pleckstrin homology (PH) domain is where phosphoinositides bind. The GTPase effector domain (GED) of dyn1 comprises a stalk domain as well as a BSE, this domain mediates GTPase activity. The PRD domain can mediate dyn1's binding with SH3 domains.

Dyn1 plays an important role in SV endocytosis. Dyn1 is recruited to invaginating membranes where it forms a helical "collar" structure around the neck of budding vesicles (Sweitzer and Hinshaw, 1998; Takei et al., 1995). This step is independent of GTP-binding (Shnyrova et al., 2013). Upon GTP hydrolysis, and conformational change, there is constriction and subsequent fission of the plasma membrane and formation of SVs (Damke et al., 2001; Marks et al., 2001; Sweitzer and Hinshaw, 1998). At least two-rungs of dynamin are required for fission to occur (Shnyrova et al., 2013).

Evidence obtained from *Dnm1* KO mice suggests that dyn1 may not be essential for plasma membrane SV endocytosis. *Dnm1* KO mice appeared normal at birth, however they died within 2 weeks. There were fewer and heterogeneously-shaped SVs present in cortical neurons as revealed by electron microscopy. SV recycling was impaired during stimulation, leading to an accumulation of interconnected clathrin-coated buds at cortical synapses (Ferguson et al., 2007; Hayashi et al., 2008). Additionally, endocytic capacity was saturated at a lower frequency stimulus load in *Dnm1* KO neurons compared to WT, suggesting dyn1 plays a critical role in SV endocytosis (Ferguson et al., 2007; Hayashi et al., 2008). There was still some SV occurring in this model due to the functional overlap of dyn1 and dyn3 (Raimondi et al., 2011). The *Dnm3* KO mouse did not appear to have any SV recycling deficits,

however *Dnm1/3* double KO (DKO) mice died within hours of birth, suggesting a more severe effect of the DKO compared to *Dnm1* KO or *Dnm3* KO (Ferguson et al., 2007; Raimondi et al., 2011). In both *Dnm1* KO and DKO neurons there is increased cargo stranded on the membrane due to impaired endocytosis (Ferguson et al., 2007; Raimondi et al., 2011). There is an activity-dependent increase in number of endocytic intermediates and clathrin-coated pits accumulated in DKO neurons due to the impaired SV endocytosis. There is also loss of functional SVs (Raimondi et al., 2011). This presynaptic phenotype could be reversed by silencing synaptic activity in culture with tetrodotoxin (TTX), perhaps suggesting a compensatory role of dyn2 in maintaining a low rate of SV recycling (Ferguson et al., 2007; Raimondi et al., 2011; Tanifuji et al., 2013). As expected, *Dnm1/3* DKO neurons display a reduction in evoked EPSCs due to the reduced number of SVs in nerve terminals (Lou et al., 2012; Raimondi et al., 2011). These neurons displayed decreased release probability rather than accelerated depression, suggesting that there are mechanisms in place to sustain neuronal activity in the presence of decreased SVs (Lou et al., 2012).

Dnm1/2/3 conditional triple KO (cTKO) mice die a few hours after birth (Fan et al., 2016), similar to the *Dnm1/3* DKO (Raimondi et al., 2011). *Dnm1/2/3* triple KO (TKO) mouse embryonic fibroblasts show impaired transferrin uptake suggesting impaired clathrin-mediated endocytosis (CME) (Park et al., 2013). These cells also displayed long, narrow, deeply invaginated pits (Park et al., 2013) similar to what is seen in *Dnm1* KO and *Dnm1/3* DKO nerve terminals (Ferguson et al., 2007; Raimondi et al., 2011).

Both GTP binding and hydrolysis are required for membrane fission by dyn1, as using a non-hydrolisable form of GTP (GTPγS) impaired endocytosis (Marks et al., 2001; Takei et al., 1995). However, GTP hydrolysis is not sufficient for endocytosis, conformational change induced by GTPase activity is also required (Damke et al., 2001; Marks et al., 2001; Sweitzer and Hinshaw, 1998). Dyn1 GTPase activity is required for both CME (Hinshaw and Schmid, 1995; van der Bliek et al., 1993) and

activity-dependent bulk endocytosis (ADBE) (Clayton et al., 2009; Clayton et al., 2010; Smillie and Cousin, 2012). GTP hydrolysis by the dyn1 "collar" induces constriction of the underlying membrane tube which then undergoes scission once it reaches a critically narrow radius (Dar et al., 2015).

The GTPase activity of dyn1 can be differentially modulated. Dyn1 is usually present as homotetramers (Muhlberg et al., 1997) and can self-assemble into rings which stimulates its GTPase activity 5-10 fold (Hinshaw and Schmid, 1995; Warnock et al., 1996). The self-assembly of dyn1 is mediated by the stalk domain (Ramachandran et al., 2007). Dyn1 also contains a GED located in the stalk (Sever et al., 2000). This GED functions as a GAP, since addition of an exogenous dyn1 GED increased unassembled dyn1's GTPase activity 6-fold (Sever et al., 2000). Artificial templates such as microtubules or phospholipids also increase GTPase activity 50 fold (Barylko et al., 1998; Barylko et al., 2001; Lin et al., 1997; Tuma et al., 1993; Zheng et al., 1996). Dyn1 can bind the SH3 domains of multiple proteins through its PRD (Faelber et al., 2011). SH3 domains can differentially stimulate dyn1 assembly and GTPase activity (Gout et al., 1993; Krishnan et al., 2015). Some SH3 domains impair GTPase activity such as the cell division control protein 42 (Cdc42)- interacting protein 4 (CIP4) SH3 domain. Others enhance it including the SH3 domains of intersectin-1a (Krishnan et al., 2015) and amphiphysin-1 (Krishnan et al., 2015; Yoshida and Takei, 2005).

Dyn1's GTPase activity and subsequent conformational change is sufficient for membrane fission, however *in vivo* different functions of dyn1 are also required to ensure efficient SV endocytosis. The PH domain must be inserted in the plasma membrane to produce the membrane curvature required for dyn1 assembly in helical formation around budding vesicle (Ramachandran et al., 2009; Shnyrova et al., 2013). Self-assembly of dyn1 into more complex helical structures are also required (Boumil et al., 2010; Ramachandran et al., 2007). Dyn1 is recruited to the clathrin lattice of early stage clathrin coated pits (M. J. Taylor et al., 2011; M. J. Taylor et al.,

2012). This leads to the recruitment of more dyn1 as well as actin and the N- Bin-amphiphysin-Rvs161/167 (BAR) proteins amphiphysin-1 and endophilin which are required for fission. Through a feedback loop, actin serves as a scaffold to maintain dynamin and N-BAR proteins at scission sites (M. J. Taylor et al., 2012).

Dyn1 contains two phosphorylation sites at the C-terminus, serine 774 (S774) and S778 that can both be phosphorylated by Cdk5 *in vitro* (Tan et al., 2003). Dyn1 is constitutively phosphorylated in resting neurons. It becomes dephosphorylated by calcineurin upon depolarisation of the nerve terminal in an activity-dependent manner (Clayton et al., 2009). *In vivo*, Cdk5 phosphorylates dyn1 at S778. This phosphorylation primes dynamin for rephosphorylation at S774 by glycogen synthase kinase 3β (GSK3β) (Clayton et al., 2010). Dyn1's dephosphorylation by calcineurin is required for its interaction with syndapin-1 which is required for ADBE but not CME (Clayton et al., 2009) (see section 1.3.2).

Dyn1 phosphorylation can also be modulated by neuronal activity. For example, during high frequency stimulation, protein kinase B/Akt becomes activated by phosphorylation on Threonine 308 (T308) and S473 (Alessi et al., 1997; Sarbassov et al., 2005). This is indirectly mediated by phosphatidylinositol 3-kinase (PI3K) activation through Ca^{2+} microdomains due to increased neuronal activity (Nicholson-Fish, Cousin et al., 2016; Smillie and Cousin, 2012). PI3K can then activate upstream activators of Akt including phosphatidylinositol-dependent kinase 1 (PDK1) that can phosphorylate T308 and mammalian target of rapamycin (mTOR) complex 2 (mTORC2) that can phosphorylate S473. Additionally, the brain-derived neurotrophic factor (BDNF) can activate Akt through activation of PI3K (Nicholson-Fish et al., 2016; Smillie et al., 2013). This suggests that an extracellular signalling molecule can affect SV endocytosis. GSK3β is inhibited by Akt phosphorylation on S9/21 and thus cannot phosphorylate dyn1. This allows dyn1 to be maximally dephosphorylated by calcineurin and allows ADBE to occur (Smillie and Cousin, 2012). Dyn1's activity-dependent dephosphorylation and subsequent

rephosphorylation (Figure 1.2) are required for correct functioning of ADBE at nerve terminals (Clayton et al., 2010; Smillie and Cousin, 2012).

Deficits observed in patients with epileptic encephalopathy due to heterozygous mutations in *DNM1* may result from dyn1 dysfunction impairing efficient neurotransmission and SV endocytosis. Thus, these models are appropriate for elucidating the role of defective SV recycling in neurodevelopmental disorders.

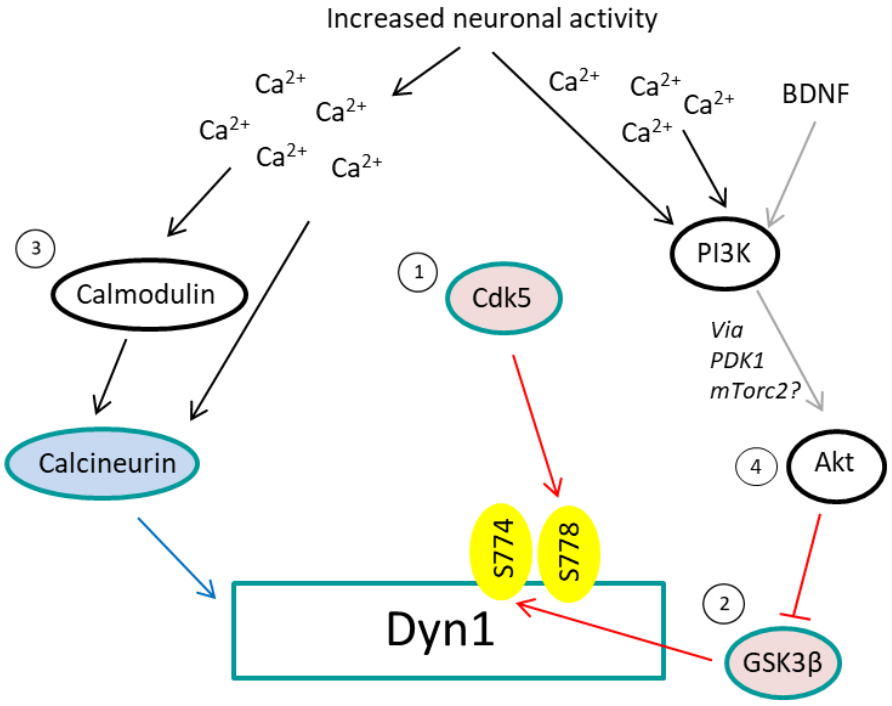

Figure 1.4 Dyn1 dephosphorylation-rephosphorylation cycle

Figure adapted from Smillie and Cousin (2011)
(1) Cdk5 is constitutively active and can phosphorylate dyn1 at rest on S778. (2) Once it has been primed by Cdk5, constitutively active GSK3β can phosphorylate dyn1 on S778. Upon increased neuronal activity: (3) Ca^{2+} and calmodulin activate the phosphatase calcineurin which dephosphorylates dyn1; (4) PI3K can activate Akt which through phosphorylation inhibits constitutively active GSK3β allowing dyn1 to be dephosphorylated.
GSK3β can then rephosphorylate dyn1 after it has been primed by Cdk5 phosphorylation. Blue arrow indicates dephosphorylation, red arrows indicate phosphorylation, grey arrows are proposed methods of activation.

1.3. Synaptic vesicle (SV) recycling

Neurotransmission allows for the transmission of information between neurons. The arrival of action potentials (APs) at nerve terminals lead to depolarisation of the nerve terminal and activation of voltage-gated Ca^{2+} channels. The high intracellular free calcium concentration ($[Ca^{2+}]_i$) triggers fusion of SVs and release of neurotransmitters. Chemical signals received across synapses are then transformed into electrical currents, through signalling downstream of neurotransmitter receptors, to allow signal transduction across neuronal networks to sustain neuronal activity (Sudhof, 2004).

1.3.1. SV Exocytosis

Neurons transmit signals by release of neurotransmitters in response to APs. The neurotransmitters are packaged in SVs. The vacuolar H^+-adenosine triphosphatase (ATPase) mediates the acidification of SVs which is necessary for refilling them with neurotransmitter. The vacuolar H^+-ATPase uses energy from ATP hydrolysis to create an electrochemical gradient across SV membranes to drive H^+ influx leading SVs to acidify. SVs are filled through neurotransmitter-specific transporters that can exchange lumenal H^+ for cytoplasmic neurotransmitter (reviewed in Edwards, 2007). Upon AP and calcium influx, these neurotransmitter-filled SVs fuse with the presynaptic membrane and release their content into the synaptic cleft where they can bind their target receptors (Sudhof, 2004).

SVs dock and fuse at the presynaptic active zone (AZ). The AZ is a large protein-dense structure located across the synaptic cleft from PSDs. The AZ can link SVs to voltage-gated Ca^{2+} channels through its dense protein scaffolding to facilitate SV fusion. The AZ can also organise presynaptic receptors and membrane composition through which it can mediate synaptic plasticity in the presynapse (Sudhof and Rizo, 2011).

SV exocytosis is mediated by the soluble N-ethylmaleimide-sensitive factor (NSF)-attachment protein receptor (SNARE) complex (reviewed in Rizo and Xu, 2015; Sudhof and Rizo, 2011). Synaptobrevin-2 on SVs can interact with synaptosomal-associated protein 25 (SNAP-25) and syntaxin-1 on the plasma membrane to form the SNARE complex. These proteins work together to bridge the SV to the plasma membrane for docking. Different AZ proteins including the scaffolds piccolo and bassoon, Rab3-interacting molecules (RIMs) and RIM-binding proteins may also be involved in the SV docking process (reviewed in Rizzoli, 2014). In particular, RIMs may interact with SVs to ensure their docking at the AZ (Haucke et al., 2011). RIMs can also mediate Ca^{2+} channel tethering at the AZ (Kaeser et al., 2011). Therefore, SVs are docked in proximity to Ca^{2+} channels ensuring optimal Ca^{2+}-sensing of the SV fusion machinery.

SVs can be primed once they are docked at the AZ. Priming is essential to ensure SVs can undergo fusion. RIMs, mammalian uncoordinated (Munc)-13 and Munc-18 are required for this step (reviewed in Rizo and Xu, 2015; Rizzoli, 2014). RIM can directly bind to Munc-13 to regulate its activity. Munc-13 and Munc-18 cooperate to promote correct assembly of the SNARE complex for efficient SV fusion (Lai et al., 2017). Together, they can promote the correct assembly the syntaxin-1-SNAP-25 sub-complex. Munc13 can additionally ensure the correct assembly of syntaxin-1-synaptobrevin-2 sub-complex (Lai et al., 2017). Complexin can also bind the SNARE complex to maintain its stability and increase SV fusion probability (Trimbuch and Rosenmund, 2016).

During evoked release, Ca^{2+} enters the nerve terminal and binds to the SV protein synaptotagmin-1 with low affinity. Ca^{2+}-bound synaptotagmin-1 interacts with both the SNARE complex and the plasma membrane to promote SV fusion. Synaptotagmin-1 is thought to promote membrane curvature (Martens et al., 2007) to

bring the SV closer to the plasma membrane and leads to the opening of the fusion pore. The primed SV can then completely merge with the plasma membrane at the fusion pore to release neurotransmitters. Munc-18 and protein chaperones are also required for efficient SV exocytosis. After SV fusion, the zippered SNARE complex must be disassembled by the ATPase NSF and SNAP proteins to allow subsequent rounds of SV fusion (Rizo and Xu, 2015; Sudhof and Rizo, 2011).

The SVs in the nerve terminal can be divided into two pools that can be mobilised by APs (reviewed in Alabi and Tsien, 2012; Rizzoli and Betz, 2005): the readily releasable pool (RRP), which, as the name states, is made up of primed SVs already situated near the AZ ready to be released, and the reserve pool which contains the SVs that are only mobilised during high intensity stimulation. There is also an additional pool, the resting pool, which accounts for 50 % of all the SVs in the nerve terminal. The SVs in this pool remain unreleased even after intense stimulation (Alabi and Tsien, 2012). There is evidence that this pool of SVs participates is spontaneous release, independent of APs (Fredj and Burrone, 2009) to modulate network maturation and homeostasis (Kavalali, 2015).

1.3.2. SV Endocytosis

There are a limited number of SVs in the nerve terminal (N. Harata et al., 2001). New SVs need to be formed to ensure that neurotransmission is continued, especially during sustained neuronal activity. New SVs can be formed through endocytosis of a portion of the plasma membrane. Once new SVs are formed, they are acidified, filled with neurotransmitter, as previously described, and prepared to undergo another round of exocytosis (H. T. McMahon and Boucrot, 2011).

There are several different SV endocytosis pathways (Figure 1.5). 1- CME (section 1.3.2.1) by which individual SVs are endocytosed by means of a clathrin coat

(Heuser and Reese, 1973). 2- ADBE (section 1.3.2.2) where a large invagination forms an endosome from the presynaptic membrane from which individual SVs can then be formed (Miller and Heuser, 1984). 3- Ultrafast endocytosis (section 1.3.2.3) occurs on the edge of the active zone where a portion of the plasma membrane is retrieved. This form of endocytosis occurs 200-fold faster than in CME (Watanabe, Liu et al., 2013; Watanabe, Rost et al., 2013). 4- Kiss-and-run is when the SV does not fully fuse with the synaptic membrane at the AZ and thus retrieved intact (Alabi and Tsien, 2013; Fesce et al., 1994; N. C. Harata et al., 2006). The mode of endocytosis that the SVs undergo depends on multiple factors including the nerve terminal, the intensity of stimulation, the duration of stimulation and the proteins present (reviewed in Cousin, 2017; Kononenko and Haucke, 2015; H. T. McMahon and Boucrot, 2011; Saheki and De Camilli, 2012; Watanabe and Boucrot, 2017).

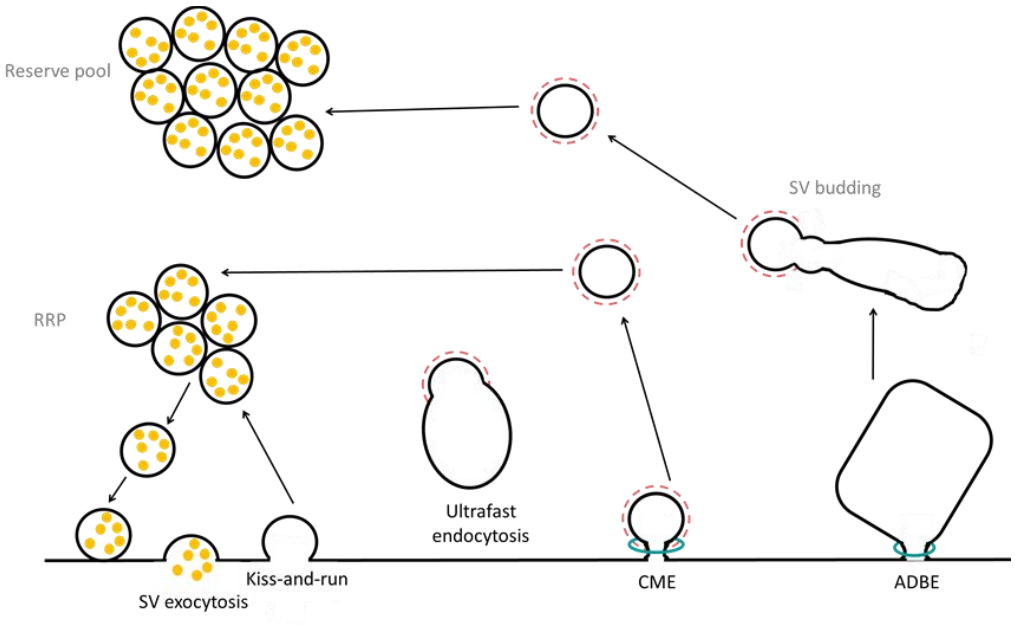

Figure 1.5 SV endocytosis

Adapted from Clayton et al. (2007)
Different modes of SV endocytosis occurring at the nerve terminal: kiss-and-run, ultrafast endocytosis, clathrin-mediated endocytosis (CME) and activity-dependent bulk endocytosis (ADBE). CME preferentially refills the RRP whereas ADBE refills the reserve pool that is only mobilised upon high neuronal activity. It is still unclear which pool is refilled through ultrafast endocytosis. CME and SV budding from ultrafast endosomes and bulk endosomes are clathrin-dependent (pink cages).

1.3.2.1.Clathrin-mediated endocytosis (CME)

CME is the major form of endocytosis that occurs after physiological stimuli (Granseth et al., 2006). CME can retrieve individual SVs on the order of tens of seconds (Granseth et al., 2006). CME is composed of different stages: nucleation, invagination, fission and uncoating (reviewed in H. T. McMahon and Boucrot, 2011; Saheki and De Camilli, 2012).

Nucleation occurs in the periactive zone of synaptic terminals. Phosphatidylinositol 4,5-bisphosphate (PIP2) initiates the nucleation process by recruiting the F-BAR Fer/Cip4 homology domain-only protein (FCHo) to bind it at the plasma membrane. FCHo can then recruit epidermal growth factor receptor substrate 15 (eps15) and intersectins to form the initial scaffolding around the nucleation site to recruit adaptor and accessory proteins (Henne et al., 2010). They can also induce curvature of the plasma membrane. Intersectin contains five SH3 domains through which it can interact with dynamin-1 and synaptojanin (Saheki and De Camilli, 2012).

Adaptor protein-2 (AP-2) and AP180, as well as epsins are among the proteins that are recruited to the nucleated pit. These proteins bind to the plasma membrane and can continue to induce curvature. AP-2 can directly bind to FCHo. This interaction activates AP-2 through a conformational change which promotes cargo recognition and binding (Hollopeter et al., 2014). The adaptor proteins AP-2 and AP180 can recognise and recruit cargo proteins through cargo-specific amino acid motifs and sequences (Saheki and De Camilli, 2012).

Once clathrin adaptors have been recruited, clathrin can be recruited to the plasma membrane invagination by AP180 and AP-2 (Ford et al., 2001). AP-2, AP180 and epsin then promote the clathrin cage formation (H. T. McMahon and Boucrot, 2011). Synaptotagmin-1 can also directly interact with AP-2 to promote clathrin cage

assembly (Haucke and De Camilli, 1999). Clathrin forms triskelia composed of three molecules of clathrin light chain (CLC) and three molecules of clathrin heavy chain (CHC). Once the clathrin has polymerised, it stabilises the curvature of the membrane and forms a clathrin-coated bud (H. T. McMahon and Boucrot, 2011).

During the nucleation stage, the different proteins recruited can also start the invagination process by promoting membrane curvature. As previously mentioned, the F-BAR protein FCHo can promote membrane curvature (Saheki and De Camilli, 2012). Epsin can also directly deform and curve the plasma membrane through inserting its amphipathic α-helix into the plasma membrane upon binding PIP2 (Ford et al., 2002). Other proteins with BAR domains have been proposed to mediate membrane invagination including endophilin (Verstreken et al., 2002) and amphiphysin-1 (Di Paolo et al., 2002). Disruption of the actin cytoskeleton impaired SV endocytosis and the transport of SVs into SV clusters suggesting a critical role of actin in CME (Shupliakov et al., 2002). Actin is proposed to serve as a scaffold surrounding the invaginating clathrin-coated pit. It may tether other required molecules in place during this process (Sankaranarayanan et al., 2003).

Dyn1 is recruited by amphiphysin-1 and endophilin to the clathrin cage at the formation of clathrin-coated pits through its PRD domain interacting with the SH3 domains of these BAR proteins (M. J. Taylor et al., 2011; M. J. Taylor et al., 2012). Dyn1 mediates the fission of the clathrin-coated vesicle from the plasma membrane. Dyn1 can self-assemble into helical rings “collars” around the necks of invaginating SVs (Sweitzer and Hinshaw, 1998; Takei et al., 1995). Dyn1 undergoes a conformational change mediated by GTP hydrolysis leading to constriction at the neck of the clathrin-coated pit and fission of the plasma membrane to form SVs (Damke et al., 2001; Marks et al., 2001; Sweitzer and Hinshaw, 1998). Genetic or pharmacological disruption of dyn1 impairs CME, suggesting that dyn1 plays a critical role in SV recycling through this pathway (Schmid and Frolov, 2011) (Also see section 1.2.3).

The clathrin coat is immediately disassembled by heat shock cognate 70 (HSC-70), auxilin, and synaptojanin following fission. Synaptojanin is recruited to clathrin-coated SVs through its interaction with endophilin (Gad et al., 2000; Verstreken et al., 2003). Synaptojanin dephorylates the nucleation protein PIP2 which results in the removal of the adaptor and accessory proteins from the SV membrane (H. T. McMahon and Boucrot, 2011). Auxilin can then recruit HSC-70 to the clathrin coat and promote its ATPase activity. Through ATP hydrolysis, HSC-70 can disrupt clathrin-clathrin interactions to dissociate the clathrin coat (Lemmon, 2001). After uncoating, SVs recycled through CME join the RRP to undergo further rounds of exocytosis (Cheung et al., 2010).

CME occurs during low levels of neuronal activation (Granseth et al., 2006). There is only enough clathrin present in nerve terminals to recycle ~7 % of SVs simultaneously through CME (Lopez-Murcia et al., 2014; Wilhelm et al., 2014). Therefore, upon elevated neuronal activity another mode of endocytosis must occur to ensure sustained neurotransmission.

1.3.2.2.Activity-dependent bulk endocytosis (ADBE)

ADBE occurs at synapses during high frequency stimulation (Clayton et al., 2008; Nguyen et al., 2012) when endocytosis of individual SVs by CME cannot maintain synaptic transmission. During high frequency stimulation, there is invagination of a large portion of the plasma membrane which goes on to form a bulk endosome. Individual SVs can then bud off from this large bulk endosome structure (reviewed in Clayton and Cousin, 2009a).

ADBE is thought to be dyn1-dependent (Clayton et al., 2007; Clayton et al., 2009; Clayton et al., 2010; Kononenko et al., 2014; Nguyen et al., 2012). Our group has

shown that in order for ADBE to occur, dyn1 must undergo an activity-dependent dephosphorylation-rephosphorylation cycle (Clayton et al., 2007; Clayton et al., 2009; Clayton et al., 2010). Upon high intensity stimulation, there is a large influx of Ca^{2+} in nerve terminals which activates calmodulin. Together, Ca^{2+} and calmodulin can activate the phosphatase calcineurin. Calcineurin then dephosphorylates dyn1 allowing ADBE to occur.

Dephosphorylated dyn1 can bind the SH3 domain of syndapin-1 (Anggono et al., 2006). This interaction with syndapin-1 is required for ADBE to occur (Clayton et al., 2009). Syndapin-1 is a neuronal protein in the BAR family (reviewed in Quan and Robinson, 2013). Syndapin-1 has an F-BAR domain at it's N-terminus (Quan and Robinson, 2013). F-BAR domains preferentially interact with membranes that have a shallow curvature (Henne et al., 2007; Shimada et al., 2007). Although the exact role of syndapin-1 in ADBE remains unknown, it is possible that it can bind to and facilitate the curvature of large bulk endosomes (Clayton et al., 2009) Furthermore, it may serve to recruit dephosphorylated dyn1 to large bulk endosomes.

ADBE can be abolished by genetically or pharmacologically inhibiting GSK3β and preventing its phosphorylation of dyn1 (Clayton et al., 2010). Additionally, overexpressing dominant-negative mutants of dyn1 which prevent GSK3β phosphorylation at S774 inhibit ADBE (Clayton et al., 2009). siRNA-mediated KD of Dyn1 and dyn3 or dyn2 also impaired endocytic retrieval at high frequency stimulation, purported to be ADBE (Kononenko et al., 2014).

Dyn1's GTPase activity is also required for bulk endosome fission from the plasma membrane. Pharmacologically blocking dyn1's activity with dynasore inhibited ADBE (Clayton et al., 2009). However, it is important to note that dynasore still arrests endocytosis in *Dnm* TKO cells, meaning that it may not be acting via dyn

GTPase activity (Park et al., 2013). Taken together, this provides evidence of the importance of dyn1 and the phosphorylation of S774 for the triggering of ADBE.

Interestingly, other groups have suggested that ADBE may be dyn1-independent, as ADBE can still occur in *Dnm1/3* DKO neurons (Wu et al., 2014). Large bulk endosomes could still be generated in DKO nerve terminals following depolarisation by high K^+ concentration or high frequency electrical stimulation (Wu et al., 2014). Additionally, new fully functional SVs could be generated from these endosomes, suggesting that dyn1 does not play a role in SV budding (Wu et al., 2014). This would suggest that ADBE is dyn-independent. However, it is important to note that there are a few caveats to this study. *Dnm1/3* DKO mice die shortly after birth however their neurons do not appear morphologically different to WT neurons in culture (Raimondi et al., 2011). This could suggest that there is a compensatory mechanism that can mediate neuronal activity in culture. This compensatory mechanism may act through dyn2 which is still expressed at low levels in these neurons (Raimondi et al., 2011). There is overlapping function between the three dynamin proteins (Hayashi et al., 2008; Raimondi et al., 2011). Dyn2 may be able to sustain neuronal activity in the absence of the other two isoforms (Ferguson et al., 2007; Hayashi et al., 2008; Raimondi et al., 2011). Indeed, *Dnm1* KO (Ferguson et al., 2007) and *Dnm1/3* DKO neurons (Raimondi et al., 2011) can still undergo some CME despite its dependence on dyn1.

Actin is another protein which has been proposed to modulate ADBE. Interestingly, the PI3K-Akt pathway that is required to mediate the dyn1 dephosphorylation-rephosphorylation cycle required for ADBE can also promote actin remodelling in chicken embryo fibroblasts (Qian et al., 2004). This perhaps hints to a convergence of actin and dyn1 activation to promote ADBE. In retinal bipolar cells, stimulus-dependent growth of the actin network through actin polymerisation was required for ADBE. The actin remodelling in this model was also dependent on Ca^{2+} and PI3K signalling (Holt et al., 2003). Actin polymerisation is proposed to be essential for the

budding of recyclosome vesicles from the bulk endosomes at amphibian neuromuscular junctions (Nguyen et al., 2012). Actin polymerisation is also required for ADBE in neurosecretory chromaffin cells (Gormal et al., 2015). In these cells, actin forms a contractile ring around the neck of large plasma membrane invaginations. Along with myosin-2, the actin rings can constrict the neck of the bulk endosome precursors. Dyn2 GTPase activity then mediates fission from the plasma membrane (Gormal et al., 2015). Finally, in hippocampal neurons, ADBE was impaired by preventing actin polymerisation by treatment with latrunculin-A (Kononenko et al., 2014). Therefore, actin remodelling and polymerisation may be required for efficient membrane retrieval by ADBE.

Endophilin has also been proposed to mediate ADBE (Kononenko et al., 2014). Endophilin is a N-BAR domain-containing protein that can directly bind the lipid bilayer to promote curvature (Farsad et al., 2001). Endophilin can form complexes with dyn1 on lipid tubules to regulate its fission activity (Farsad et al., 2001). Therefore, endophilin may act to reshape the membrane to promote ADBE.

After formation of the bulk endosome, budding off of individual SVs occur. These newly formed SVs replenish the reserve pool (Cheung et al., 2010; Cheung and Cousin, 2012). This process is proposed to be clathrin-dependent and cannot occur when endogenous clathrin is disrupted, even though bulk-endosome formation is clathrin-independent and can occur under these conditions (Heerssen et al., 2008; Kasprowicz et al., 2008; Kononenko et al., 2014). Budding of SVs from bulk endosomes also requires adaptor proteins (Cheung and Cousin, 2012; Kononenko et al., 2014) that can mediate SV formation and SV cargo retrieval (reviewed in Cousin, 2017). The adaptor proteins AP-1 and AP-3 can both mediate SV budding suggesting perhaps a separate and sequential role of these two adaptor proteins in this process (Cheung and Cousin, 2012). Additionally, AP-2, clathrin's major adaptor protein, is involved in budding as AP-2 cKO results in accumulation of bulk endosomes without the subsequent formation of SVs (Kononenko et al., 2014).

There is some evidence suggesting that the budding of SVs may be clathrin-independent (Wu et al., 2014). In *Dnm1/3* DKO neurons, lentiviral KD of CHC did not impair SV reformation from bulk endosomes after high frequency stimulation. In fact, reformation of SVs and depletion of bulk endosomes occurred to the same extent in both the CHC KD and control conditions (Wu et al., 2014). However as previously mentioned, the *Dnm1/3* DKO neuron model may be flawed due to excessive compensation in the absence of dynamin.

SV budding from bulk endosomes is also Ca^{2+}-dependent (Cheung and Cousin, 2013). There is fluid phase uptake of Ca^{2+} from the extracellular milieu into the bulk endosome during its formation. Acidification of the bulk endosomes through the vacuolar H^{+}-ATPase leads to Ca^{2+} efflux from the endosome into the cytoplasm. This Ca^{2+} can then activate calcineurin which is required for SV budding (Cheung and Cousin, 2013). In fact, buffering intracellular or intra-endosomal Ca^{2+} disrupted SV budding from bulk endosomes. Additionally, pharmacologically inhibiting the vacuolar H^{+}-ATPase or calcineurin also prevented SV budding (Cheung and Cousin, 2013). Taken together this suggests that Ca^{2+} activation of the phosphatase calcineurin is required for ADBE both to signal bulk endosome formation and SV budding.

Our group has also identified an ADBE-specific cargo: the vesicle-associated membrane protein-4 (VAMP4) (Nicholson-Fish et al., 2015). VAMP4 was found to be enriched on bulk endosomes and essential for efficient ADBE (Nicholson-Fish et al., 2015). VAMP4 had previously been reported to mediate Ca^{2+}-dependent asynchronous release through interacting with a subset of SNARE proteins (Raingo et al., 2012). This provides further evidence for a role of ADBE for preferentially replenishing a pool of SVs for asynchronous release (see Bacaj et al., 2013;

Evstratova et al., 2014; Y. C. Li et al., 2017; Nicholson-Fish et al., 2015; Raingo et al., 2012).

Some key molecules in ADBE have been identified, however there are still many unknowns regarding the trafficking of endocytic pathway including whether or not bulk endosomes fuse with other endosomal pathways before SV budding occurs (reviewed in Cousin, 2015).

1.3.2.3.Ultrafast endocytosis

Ultrafast endocytosis is a mode of endocytosis that was recently discovered at the neuromuscular junction of *Caenorhabditis elegans* and is thought to be evolutionarily conserved across species (Watanabe et al., 2013; Watanabe et al., 2013). This form of endocytosis can be triggered by a single AP under physiologically relevant conditions in both intact *Caenorhabditis elegans* and dissociated mouse hippocampal neurons (Watanabe et al., 2013; Watanabe et al., 2013). Interestingly, no CME is observed at physiological temperatures using these stimulation conditions (Watanabe et al., 2014). This suggests that ultrafast endocytosis may be the dominant endocytic mode during mild stimulation. Ultrafast endocytosis occurs on a much more rapid scale of any previously defined modes of endocytosis (Watanabe et al., 2013; Watanabe et al., 2013; Watanabe and Boucrot, 2017).

SV exocytosis triggered by a single pulse of blue light exciting an exogenously expressed channelrhodopsin triggers ultrafast endocytosis on the edge of active zones within 50 ms of stimulation (Watanabe et al., 2013; Watanabe et al., 2013). The majority of SVs are recycled through ultrafast endocytosis under these stimulation conditions (Watanabe et al., 2013). Addition of membrane to the nerve terminal through SV exocytosis is required for ultrafast endocytosis to occur. Immediately

following SV exocytosis (within 50-100 ms) shallow endocytic pits begin to form on the edge of the active zone. These shallow pits then form deeper invaginations which are thought to be precursors of "large vesicles". These "large vesicles" have the surface area of approximately 2-4 SVs and scale with the amount of SV exocytosis occurring at the AZ (Watanabe et al., 2013; Watanabe et al., 2013). Within 300 ms of stimulation, the "large vesicles" are resolved into smaller SVs (Watanabe et al., 2013; Watanabe et al., 2013).

Ultrafast endocytosis is actin-dependent as disruption of actin polymerisation by latrunculin-A inhibits the formation of endocytic structures after SV exocytosis (Watanabe et al., 2013). Ultrafast endocytosis is also mediated by dyn1 activity. Genetic (Watanabe et al., 2013) or pharmacological disruption (Watanabe et al., 2013) of dyn1 prevents the formation of "large vesicles". Instead, there are large deep invaginations that remain attached to the plasma membrane. This suggests that perhaps dyn1's GTPase activity is required for membrane fission in this form of endocytosis. Additionally, at physiological temperatures, clathrin is required for SV budding from endosomes, although it is not required for the formation of ultrafast endosomes (Watanabe et al., 2014). This is similar to; the role that clathrin is proposed to play in ADBE (Heerssen et al., 2008; Kasprowicz et al., 2008; Kononenko et al., 2014), perhaps suggesting a common underlying mechanism relating these two endocytic modes.

1.4. Monitoring SV recycling

Different live-cell imaging reporters can be used to measure the SV exocytosis and endocytosis occurring in neuronal cultures. These include styryl dyes, synaptic pHluorins (reviewed in Kavalali and Jorgensen, 2014; Ryan, 2001) and fluorescent dextrans (Clayton and Cousin, 2009b). Styryl dyes are amphipathic dyes that can label SV membranes. In brief, uptake of styryl dyes allow for the visualisation of SV trafficking through different endocytic pathways. FM dyes have different properties

and can thus report different modes of endocytosis with FM1-43 reporting both CME and ADBE, and FM2-10 only reporting CME (Clayton and Cousin, 2009b; Richards et al., 2000). In this work we used pHluorins (described in section 1.4.1) and fluorescent dextran (described in section 1.4.2) to monitor SV exocytosis and endocytosis through CME and ADBE in our models of neurodevelopmental disorders.

1.4.1. pHluorins

PHluorins are modified pH-sensitive green fluorescent proteins (GFPs), (Miesenbock et al., 1998). Their fluorescence is quenched by acid. Fusing pHluorins to the lumen of synaptic proteins allows the synaptic pHluorin to report SV recycling (Miesenbock et al., 1998; Sankaranarayanan et al., 2000). When the pHluorin is in the acidic lumen of the SV it remains quenched. It is possible to observe an exocytosis-dependent increase in fluorescence signal as SVs fuse with the plasma membrane, exposing the pHluorin to a neutral pH ~7.4 (Miesenbock et al., 1998; Sankaranarayanan et al., 2000; Sankaranarayanan and Ryan, 2000). After endocytosis, SVs are reacidified through the vacuolar H^+-ATPase. This proton pump creates an electrochemical gradient across the SV membrane which is required for neurotransmitter loading into the SV (reviewed in Edwards, 2007). Once the SV has been reacidified after endocytosis, the pHluorin is once again quenched, therefore pHluorins report the reacidification of SVs. This reacidification of endocytosed SVs occurs on the order of ~5 s (Atluri and Ryan, 2006; see also Egashira et al., 2015), whereas endocytosis occurs on a slower timescale $\tau \sim 15$ s, (Granseth et al., 2006), making endocytosis the rate limiting step. Thus, pHluorins provide a real-time method of visualising SV exocytosis and endocytosis due to the rapid kinetics of reacidification.

1.4.1.1.Synaptophysin-pHluorin (sypHy) and vesicular glutamate transporter-pHluorin (vGLUT-pH)

Both synaptophysin-pHluorin (sypHy) and vesicular glutamate transporter-pHluorin (vGLUT-pH) produce the characteristic fluorescence trace with increased fluorescence upon SV exocytosis which returns to baseline following SV endocytosis and subsequent reacidification (Figure 1.4). SypHy was created by fusing the pHluorin into the second intra-vesicular loop of synaptophysin-1 (Granseth et al., 2006). For vGLUT-pH, the pHluorin was fused to the first lumenal loop of vGLUT (Voglmaier et al., 2006). These reporters are targeted to SVs and have good signal-to noise ratios due to low surface expression on the plasma membrane (Granseth et al., 2006; Sankaranarayanan and Ryan, 2000; Voglmaier et al., 2006). SypHy and vGLUT-pH fluorescence traces were not altered in the presence of a GSK3 antagonist CT99021 (Nicholson-Fish et al., 2015) which has previously been shown to impair ADBE but not CME (Clayton et al., 2010). Therefore, these two pHluorins preferentially report CME and do not seem to report ADBE (Nicholson-Fish et al., 2015).

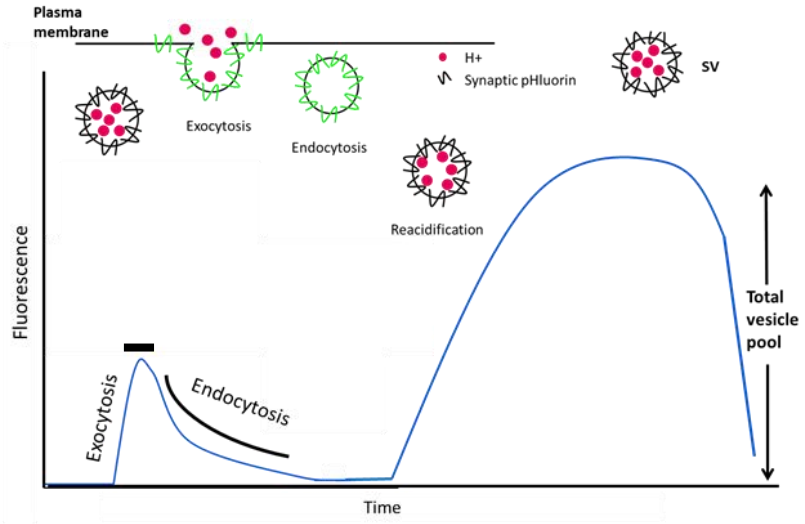

Figure 1.6 Synaptic pHluorin imaging

Figure adapted from Sankaranarayanan (2000)
Fluorescence trace as a response to SV exocytosis and endocytosis. When the lumen of the SV becomes exposed to a neutral pH during exocytosis, the pH-sensitive GFP in the lumen of the SV becomes unquenched and fluoresces. When the SV is endocytosed and reacidified, the pHluorin becomes quenched once again. Bar indicates stimulation.

1.4.1.2.Vesicle-associated membrane protein-4-pHluorin (VAMP4-pH)

A new pHluorin was recently identified as a reporter of ADBE. VAMP4-pH was the only reporter that showed impaired response with genetic or pharmacological block of ADBE compared to sypHy, vGLUT-pH, synaptobrevin-2-pHluorin and synaptotagmin-1-pHluorin (Nicholson-Fish et al., 2015). VAMP4-pH was created by fusing the pHluorin into C-terminal lumenal domain of VAMP4 (Nicholson-Fish et al., 2015). VAMP4 was also found to be enriched on bulk endosomes compared to clathrin-coated vesicles, providing further evidence that this protein is a cargo of ADBE (Nicholson-Fish et al., 2015).

VAMP4-pH expressed in nerve terminals displays a different fluorescence response compared to sypHy and vGLUT-pH (Nicholson-Fish et al., 2015; Raingo et al., 2012). The combination of fluorescence traces from all nerve terminals usually results in a fluorescence trace that does not significantly deviate from baseline during stimulation. However, when individual nerve terminals are assessed on stimulation, VAMP4-pH fluorescence can either increase or decrease. The decrease in fluorescence ("down" trace) represents the slow acidification of bulk endosomes. The increase in fluorescence ("up" trace) represents asynchronous release (Figure 1.5).

VAMP4-pH is more localised at the plasma membrane than sypHy or vGLUT-pH. More fluorescence is therefore unquenched resulting in high levels of baseline fluorescence. Upon high frequency stimulation, when ADBE is recruited, fluorescence decreases over time in line with the slow reacidification of bulk endosomes (Nicholson-Fish et al., 2015; Nicholson-Fish, Smillie et al., 2016). Although it has been demonstrated that all nerve terminals can undergo ADBE, they do not all undergo ADBE upon every high frequency stimulation (Nicholson-Fish et al., 2016). Nerve terminals that do not undergo ADBE show a slow increase in

fluorescence upon high frequency stimulation. This increase in fluorescence is proposed to be due to VAMP4-dependent asynchronous release (Raingo et al., 2012). The sorting of VAMP4-pH time traces into "up" or "down" traces allows for ADBE to be monitored at individual nerve terminals.

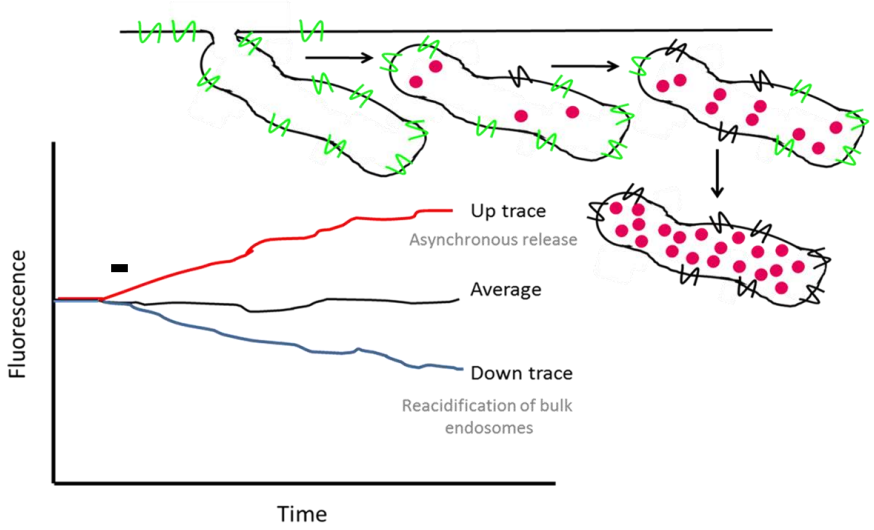

Figure 1.7 VAMP4-pH imaging

VAMP4-pH allows for ADBE recruitment to be monitored at individual nerve terminals. VAMP4-pH fluorescence traces can be sorted into "up" traces representing asynchronous release adding more VAMP4 to the plasma membrane and "down" traces representing ADBE and the slow reacidification of bulk endosomes. Bar indicates high frequency stimulation.

1.4.2. Tetramethylrhodamine (TMR) dextran uptake

Dextrans are large polysaccharides that can be used as inert fluid phase markers. Upon high frequency stimulation, 40 kDa fluorescent tetramethylrhodamine (TMR) dextran is preferentially internalised by ADBE due to its large size (Berthiaume et al., 1995; Clayton and Cousin, 2009b; Holt et al., 2003; Teng et al., 2007). Dextran is not found in SVs suggesting it is not being endocytosed via the CME pathway (Holt et al., 2003; Teng et al., 2007). TMR dextran fluorescence at nerve terminals does not correlate with the extent of ADBE occurring, perhaps due to the low number of bulk endosomes present at each nerve terminal and the limited number of dextran

particles that can fit into each bulk endosome. Background TMR puncta display similar fluorescence intensities to internalised TMR dextran fluorescence (Clayton and Cousin, 2009b). However, TMR dextran can provide information about the number of nerve terminals that undergo ADBE upon high frequency stimulation, similar to how VAMP4-pH reports ADBE (Clayton and Cousin, 2009b). Therefore, TMR dextran is a selective reporter for nerve terminals undergoing ADBE.

1.5. Hypothesis

ID, ASD and epilepsy are difficult to study due to the complex interplay of genetic, epigenetic and environmental factors underlying the disorders. A common mechanism is thought to underlie these three neurodevelopmental disorders, due to their high comorbidity. FXS, *SYNGAP1* haploinsufficiency and *DNM1* epileptic encephalopathy are monogenic diseases that can cause these disorders. Furthermore, they are all characterised by impaired synaptic function and there is evidence for presynaptic deficits in each condition. *Fmr1* KO hippocampal neurons show altered SV recycling and SV pool sizes (Deng et al., 2011; Deng et al., 2013; Ferron et al., 2014). During development, *SynGAP1* Het mice show altered mEPSC frequency in the forebrain which may be a sign of altered release probability (Clement et al., 2012). Correct functioning of dyn1 is required for SV endocytosis and thus necessary for maintained neurotransmission (Damke et al., 2001; Ferguson et al., 2007; Marks et al., 2001).

Based on these findings, we hypothesize that altered SV recycling in the presynapse is an important pathological feature of ID, ASD and epilepsy, particularly in models of FXS, *SYNGAP1* haploinsufficiency and *DNM1* epileptic encephalopathy.

1.6. Aims

The overarching aims of this work were to characterise SV exocytosis and endocytosis deficits in models of *SYNGAP1* haploinsufficiency, FXS, and *DNM1* epileptic encephalopathy using synaptic pHluorins, and large fluorescent TMR dextran. These live-cell imaging techniques provide ways to track SV recycling independently through either the CME or the ADBE modes to isolate which pathway may be defective in these models. Additionally, these experiments can provide insight into the roles that these proteins and their different domains play in different components of SV recycling. Repeating the same imaging assay on various preclinical models of neurodevelopmental disorders can elucidate whether these disorders may all use a converging SV recycling pathway to disrupt neuronal development and synaptic plasticity. Furthermore, we also aimed to see whether some of the impaired SV recycling defects observed could be rescued with pharmacological treatment.

2. Materials and methods

2.1. Materials

Unless specified otherwise, general reagents were acquired from Sigma Aldrich (Gillingham, UK). All other reagents used can be found in Table 2.1.

Reagent	Source	Reagent	Source
Genotyping reagents			
GoTaq DNA polymerase	Promega, Wisconsin USA; M7841	Hyperladder 1 kb DNA markers	Bioline, London UK; 33053
Green Reaction Buffer	Promega, Wisconsin USA; M7841	GoTaq Green Master Mix	Promega, Wisconsin USA M7122
Deoxynucleotides (dNTPs)	Invitrogen, Paisley UK, 18427013	Proteinase K	Promega, Wisconsin USA; V3021
RedSafe	Chembio, UK; 21141		
Cell culture reagents			
Papain	Worthington Biochemical Corporation, USA; LK003178	Cytosine arabinofuranoside	Sigma Aldrich, Gillingham, UK; C1768
DMEM F12	Gibco, Paisley, UK; 21331-020	Poly-D-lysine	Sigma Aldrich, Gillingham, UK; P7886
FBS	BioSera, France; S1810-500	Boric acid	Sigma Aldrich, Gillingham, UK; B6768
Penicillin/ streptomycin	Gibco, Paisley, UK; 15140-122	Lipofectamine 2000	ThermoFisher Scientific, UK; 11668027
Neurobasal	Gibco, Paisley, UK; 21103-049	Minimal Essential Medium	Gibco, Paisley, UK; 21090-022
B-27 supplement	Gibco, Paisley, UK; 17504-044	Dulbecco's Modified Eagle Medium	Gibco, Paisley, UK; 41966-029
L-glutamine	Gibco, Paisley, UK; 25030-024	Opti-MEM reduced-serum medium	Gibco, Paisley, UK; 31985-047
Laminin	Sigma Aldrich, Gillingham, UK, L2020	Trypsin	Irvine Scientific, USA; 9342
Site-directed mutagenesis reagents			
Pfu DNA polymerase 10 x buffer	Promega, Wisconsin USA; M7741	Pfu DNA polymerase	Promega, Wisconsin USA ; M7741

Live-cell imaging reagents			
Cyano-7-nitroquinoxaline-2,3-dione	Abcam, UK; ab120271	Bafilomycin A1	Cayman Chemical Company, Ann Arbor Michigan, USA; 11038
DL-2-Amino-5-phosphonopentanoic acid	(AP-5, Abcam, UK; ab120044)	Fluo-5F	ThermoFisher Scientific, UK; F14222
MaxiPost	Bio-Techne Ltd, UK; 4949/90)	Tetramethylrhodamine dextran, 40,000 MW	Life Technologies, Paisley, UK; D1842
Dimethyl sulfoxide	Sigma Aldrich, Gillingham, UK; D8418		
Immunofluorescence staining and fixed-cell imaging reagents			
Paraformaldehyde	Sigma Aldrich, Gillingham, UK; 47608	FluorSave Reagent	(Calbiochem, USA; 345789).
Bovine serum albumin	Roche Diagnostics GmbH, Germany; 10735078001		
GTPase assay reagents			
Protease inhibitors,	Sigma Aldrich, Gillingham, UK; P8849	Guanosine triphosphate	Sigma Aldrich, Gillingham, UK; G5884
Phenylmethane sulfonyl fluoride,	Sigma Aldrich, Gillingham, UK; P7626	Malachite green carbinol base	Sigma Aldrich, Gillingham, UK; 229105
GFP-fusion proteins	ChromoTek GmbH, Germany; gta-20	Ammonium molybdate tetrahydrate	Sigma Aldrich, Gillingham, UK; A7302
Bradford solution	Applichem, Germany; A6932		

Table 2.1 Table of reagents with sources and catalog numbers

2.2. Animals

All procedures involving animals were carried out in accordance with the Animals (Scientific Procedures) Act (ASPA) 1986 under a project license and delegated personal licence authority. Furthermore, severity recordings were taken for each animal in accordance with Home Office legislation. All animals were group housed as recommended by ASPA 1986. Colonies were maintained in facilities with a 12:12 hour light: dark cycle with food (standard chow) and drink *ad libitem*.

2.2.1. WT mice

WT mice on the C57BL/6J (Jackson Labs) from the in-house colony were set up for weekly timed matings. Embryos of either sex were used for tissue culture.

2.2.2. Fmr1 KO mouse

A breeding colony was established and maintained for the transgenic *Fmr1* $^{-/y}$ mice. In these KO mouse models, exon 5 of *Fmr1* was replaced with a neomycin resistance cassette, disrupting the gene and thus inactivating it (The Dutch-Belgian Fragile X Consortium, 1994). *Fmr1* heterozygous females on the C57BL/6J (Jackson Labs) background were set up for weekly timed matings with WT males on the same background to produce either *Fmr1*$^{-/y}$ or wildtype males. Male embryos from pregnant females were used for tissue culture.

2.2.3. Fmr1 KO Sprague Dawley rat

Commercially available *Fmr1* KO Sprague Dawley (*Fmr1* SD) rats were obtained from Sigma Advanced Genetic Engineering (SAGE) Labs (St. Louis, Missouri, USA), now part of Horizon Discovery. These rats were generated through a zinc finger-mediated 122 bp deletion in Exon 8 of *Fmr1* (Hamilton et al., 2014).

2.2.4. Fmr1 KO Long Evans Hooded rat

Fmr1 KO Long Evans Hooded (*Fmr1* LEH) rats were designed by the Centre for Integrative (University of Edinburgh) and engineered by Horizon Discovery. In this KO model, the coding region of exon 1 was replaced by an eGFPnlsSV40pA cassette.

For both Fmr1 rat models, heterozygous females were set up for weekly timed matings with WT males on the same background (Charles River labs) to produce either *Fmr1*$^{-/y}$ or wildtype males. Male embryos from were used for tissue culture.

2.2.5. SynGAP1 KO mouse

A breeding colony was established and maintained for the transgenic *SynGAP*$^{-/+}$ mice. The deletion of the C2 and GAP domains were caused by the insertion of a hemagglutinin (HA) tag with stop codons and internal ribosomal entry site (IRES)-lacZ-polyA · MC1neo-polyA cassette (Komiyama et al., 2002). SynGAP het males or females on the C57BL/6JOla (Harlan) background were bred with WT mice on the same background to maintain the colony.

2.2.6. *SynGAP1 GAP deletion Long Evans Hooded rat*

SynGAP1 GAP deletion LEH rats were designed by the Centre for Integrative Physiology, (University of Edinburgh) and engineered by Horizon Discovery. Briefly, deletion of the GAP domain was obtained by using zinc finger motifs to delete exons 8-12 coding for the GAP domain of the protein, resulting in a deletion encompassing amino acids 255 to 705.

2.2.7. SynGAP1 KO Long Evans Hooded rat

SynGAP1 KO LEH rats were designed by the centre for Integrative Physiology, (University of Edinburgh) and engineered by Horizon Discovery (Saint-Louis, Missouri). Briefly, CRISPR/Cas9 technology was used to create a 2-base insertion and a 1-base deletion introducing stop codons in exon 8.

For all *SynGAP* animals, Het x Het crossings were set up for embryonic cultures to obtain WT, Het and KO embryos in the case of the KO animals and WT, Het and Hom for the *SynGAP GAP* LEH. Both male and female embryos were used for tissue culture.

2.3. Genotyping

2.3.1. Fmr1 KO mouse

For the *Fmr1* mice, the HotSHOT method was used to extract genomic DNA from the ear notches or tail samples (Truett et al., 2000). A tissue sample was heated in HotSHOT lysis buffer (25 mM NaOH and 0.2 mM EDTA) at 95°C for 60 min. The solution was then neutralised using HotSHOT neutralisation buffer (40 mM Tris-HCl). The supernatant was isolated by centrifugation at 1600 g for 3 min. For the reaction, 1 µL of supernatant was combined with the primers IMR 6735 (1600 nM), IMR 6734 (800 nM) and IMR 2060 (800 nM) (Eurogentec, Belgium) (sequences listed in Table 2.2). GoTaq DNA polymerase in Green Reaction Buffer and 200 µM of dNTPs were used to amplify the polymerase chain reaction (PCR) product.

The cycling conditions for the PCR were 95°C for 2 min, and 35 cycles of 95°C for 30 s, 56°C for 30 s and 72°C for 30 s, then 72°C for 5 min. To separate PCR products, the samples were run on a 1.2 % (w/v) agarose gel stained with RedSafe (1:20000) at 130 V for 30 min, in TBE buffer (44 mM Tris, 44 mM boric acid, 1.6 mM EDTA). Samples were run against Hyperladder 1 kb DNA markers. DNA bands were then visualised under ultraviolet (UV) illumination. The WT product ran at 131 bp and the KO product ran at 400 bp.

2.3.2. Fmr1 KO SD rat

The genomic DNA from *Fmr1* rats was also extracted using the HotSHOT method as previously described (section 2.3.1). For the PCR reaction, 1 µL of extracted DNA was combined with the primers SDrat Fmr1 F (20 uM) and SDrat Fmr1 R (20 uM) (Eurogentec, Belgium) (sequences listed in Table 2.2). GoTaq Green Master Mix was used to amplify the PCR product.

The cycling conditions for the PCR were 95°C for 5 min, and 35 cycles of 95°C for 30 s, 60°C for 30 s and 68°C for 30 s, then 68°C for 5 min. To separate PCR products, the samples were run on a 2 % (w/v) agarose gel stained with RedSafe (1:20000) at 45 V for 35 min, in TBE buffer (44 mM Tris, 44 mM boric acid, 1.6 mM EDTA). Samples were run against Hyperladder 1 kb DNA markers. The WT product ran at 400 bp and the KO product ran at 278 bp.

2.3.3. SynGAP1 mouse

Genomic DNA was extracted using the Wizard SV Genomic DNA Purification System (Promega, Wisconsin USA; A2360) according to manufacturer's instructions for purification using a microcentrifuge. Briefly, tissue was incubated in Nuclei Lysis Solution, 0.5 M EDTA (pH 8.0), Proteinase K 20 mg/mL and RNase A Solution overnight at 55°C. After incubation, Wizard SV lysis buffer was added. The sample was then transferred to the Wizard SV Minicolumn Assembly and spun at 13000 g for 3 min. DNA was eluted using nuclease-free water.

Both WT and KO PCR reactions were set up for each sample. For the WT reaction, 4 uL of extracted DNA was combined with the primers Syn12R (800 nM) and Syn11> (800 nM) (Eurogentec, Belgium) (sequences listed in Table 2.2). For the KO reaction, 2 uL of extracted DNA was combined with primers Syn12R (800nM) and FCASS1a (800 nM) (Eurogentec, Belgium) (sequences listed in Table 2.2). GoTaq

DNA polymerase in Green Reaction Buffer and 200 μM of dNTPs were used to amplify the PCR product. The cycling conditions for the PCR were 95°C for 3 min, and 30 cycles of 94°C for 20 s, 56°C for 30 s and 68°C for 120 s, then 68°C for 3 min followed by holding at 4°C. To separate PCR products, the samples were run on a 0.8 % (w/v) agarose gel stained with RedSafe (1:20000) at 140 V for 20 min, in TBE buffer (44 mM Tris, 44 mM boric acid, 1.6 mM EDTA). Samples were run against Hyperladder 1 kb DNA markers. The WT product ran at 2.5 kb and the KO product ran at 1 kb.

2.3.4. Fmr1 KO LEH, SynGAP1 GAP deletion LEH, SynGAP1 KO LEH

Tissue samples from *Fmr1* KO LEH, *SynGAP GAP* LEH and *SynGAP* KO LEH were sent directly to Transnetyx (Cordova, Tennessee, USA) for genotyping. Genomic DNA was extracted, genotyped and sequenced using proprietary methods. Primers used for genotyping are found in Table 2.2.

Animal model	Primer	Sequence 5'-3'
Fmr1 KO mouse	IMR 6735	CTTCTGGCACCTCCAGCTT
Fmr1 KO mouse	IMR 6734	TGTGATAGAATATGCAGCATGTGA
Fmr1 KO mouse	IMR 2060	CACGAGACTAGTGAGACGTG
Fmr1 KO SD	SDrat Fmr1 F	TGGCATAGACCTTCAGTAGCC
Fmr1 KO SD	SDrat Fmr1 R	TATTTGCTTCTCTGAGGGGG
Fmr1 KO LEH	GFPF1	ACGTAAACGGCCACAAGTTC
Fmr1 KO LEH	GFPR1	ATGCCGTTCTTCTGCTTGTC
Fmr1 KO LEH	CelF1	CGAGGAAGGACGAGAAGATG
Fmr1 KO LEH	CelR1	CCGCTTCCCTGACTGAAC
SynGAP KO mouse	FCASS1a	TTCATGGAGCGGGAACACCTCATAT
SynGAP KO mouse	Syn12R	CATACAAGAATTGCTGCATAGAAC
SynGAP KO mouse	Syn11>	TTCATGGAGCGGGAACACCTCATAT
SynGAP GAP LEH	SynGAP For	GACTCCATTATCAAGCCAGTACA
SynGAP GAP LEH	SynGAP Rev	CGAGCCATGAAGGACTGAA
SynGAP KO LEH	Cel-1 F	GGGAGTGGTGGACGCTATT
SynGAP KO LEH	Cel-1 R	GGGGTACCACTGCTCTGTG

Table 2.2 Genotyping primer sequences

All primers were synthesised by Eurogentec (Belgium)

2.4. Cell culture

2.4.1. Primary neuronal cultures

The UK Home Office Schedule 1 methods were followed for sacrifice of the pregnant females and embryos. At day 16.5 to 18.5 of gestation for mice and day 18.5-19.5 of gestation for rats, pregnant females were sacrificed using cervical dislocation. Death of pregnant females was confirmed by onset of *rigor mortis*. Embryos were taken by caesarean section. All embryos were decapitated, and death

was confirmed by the destruction of brain. Tail samples were taken for genotyping purposes.

Due to the X-linked nature of FXS, in the case of the *Fmr1* KO mouse and rat, embryos were sexed and only males were chosen and dissected. Males could either have the KO or WT allele and thus could be used both for the experimental *Fmr1* KO group and WT littermate controls. To determine the sex of the embryos, the abdomen was dissected and the distinction between the sexes was made using the visible reproductive anatomy (Figure 2.1). For all other genotypes, embryos of either sex were dissected.

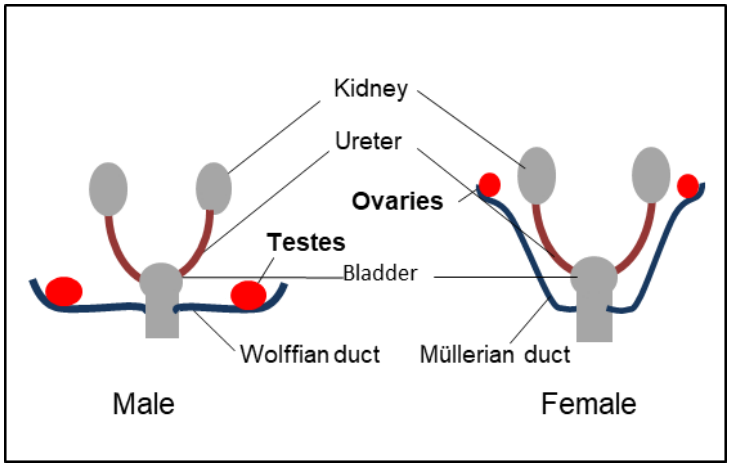

Figure 2.1 Embryonic reproductive organs

Figure adapted from Heikkila, 2002)
The sexes of embryos can be determined by the location of their reproductive organs (highlighted in red). In males, the testes can be found adjacent to the bladder. In females, the ovaries are located behind the kidneys.

Embryos were dissected in ice-cold phosphate buffered saline (PBS, 10 mM phosphate buffer, 2.7 mM KCl and 137 mM NaCl, pH 7.4). Hippocampi from each embryo were processed separately as to avoid contamination across genotypes. Tissue was digested in a 10 units/ml papain solution for 20 min at 37°C.

After the digestion, excess papain was removed and DMEM F12 supplemented with 10 % (v/v) foetal bovine serum (FBS) and 1 % (v/v) penicillin/streptomycin was added to neutralise the remaining papain. Cells were triturated to form a single cell suspension and centrifuged at 260 g for 5 min in a Universal 32 R Hettich centrifuge at room temperature. Neurons were resuspended in 100 uL/head of pre-warmed Neurobasal (NB) medium supplemented with 2 % (v/v) B-27 supplement, 0.5 mM L-glutamine and 1 % (v/v) penicillin/streptomycin.

Cells were counted using a haemocytometer and plated at 5x 10^4 cells per coverslip in a 50 µL spot of laminin (10 µg/ mL in supplemented NB medium) for live-cell imaging experiments and 3.5x 10^4 cells per coverslip for immunofluorescence staining experiments. Coverslips had been coated overnight with poly-D-lysine (PDL) (50 µg/mL) dissolved in boric acid (100 mM, pH 8.5).

After plating, cells were left to settle for 1 h, after which 2 mL of supplemented NB was added into each well. After 2-3 days of incubation (humidified Sanyo incubator, 37°C, 95 % air/5 % CO_2) 1 µM of cytosine arabinofuranoside (AraC) was added to each well to inhibit the proliferation of glia.

2.4.2. Transfection of primary neuronal cultures

High purity plasmid DNA was prepared using a HiSpeed Plasmid Maxi Kit (Qiagen, Hilden, Germany; 12643), according to manufacturer's instructions, using overnight cultures of TOP10 *Escherichia coli (E. coli)*. A Thermo Scientific Nanodrop 2000 spectrophotometer was used to quantify DNA yield and purity. All plasmids used can be found in Table 2.3.

Plasmid name	Species	Vector	Amount transfected	Obtained from
synaptophysin-pHluorin (sypHy)	Rat	pEGFP-C1	1 µg	Prof. L. Lagnado (LMB, University of Cambridge)
mCerN1	N/A	Clontech EGFP-N1	Variable 0.3 -1 µg	Cousin lab by replacing EGFP by mCer (Cheung et al., 2010)
vGLUT-pHluorin	Rat	pCAGGS	1 µg	Prof. R. Edwards (University of California, San Francisco, USA)
mCer-Dynamin1aa (Dyn1)	Rat	pEGFP-N1	0.3 µg	Cousin lab (Anggono et al., 2006)
VAMP4-pHluorin	Human	pEGFP-N1	1 µg	Cloned from viral VAMP4-pH from Prof. E. Kavalali (University of Texas South-Western Medical Centre, Texas, USA) (Nicholson-Fish et al., 2015)
shFMRP	Rat	pcDNA3.0	1 µg	Prof. A. Dolphin (University College London, London, UK)
shScr (FMRP)	Rat	pcDNA3.0	1 µg	Prof. A. Dolphin (University College London, London, UK)
mCer-Dynamin1aa G139R	Rat	pEGFP-N1	0.3 µg	Site directed mutagenesis
mCer-Dynamin1aa R237W	Rat	pEGFP-N1	0.3 µg	Site directed mutagenesis
mCer-Dynamin1aa I289F	Rat	pEGFP-N1	0.3 µg	Site directed mutagenesis
mCer-Dynamin1aa H396D	Rat	pEGFP-N1	0.3 µg	Site directed mutagenesis
mCer-Dynamin1aa A408T	Rat	pEGFP-N1	0.3 µg	Site directed mutagenesis
shSyndapin	Rat	pSuper	1 µg	Cousin lab (Clayton et al., 2009)
shScr (syndapin)	Rat	pSuper	1 µg	Cousin lab (Clayton et al., 2009)

Table 2.3 Plasmids used for transfections

For transfection of a 6-well plate, per well, 1 µL of Lipofectamine 2000 per 1 µg of the plasmid DNA was incubated in Minimal Essential Medium (MEM) for a total volume of 100 µL. Plasmid DNA was also incubated in 100 µL of MEM. After 5 min, both solutions were combined for a total volume of 200 µL/ well and left to incubate at room temperature for 20-30 min. During this incubation, growth medium

was removed from cells and replaced with pre-warmed and equilibrated MEM. The conditioned NB that was removed from the cultured neurons was conserved in the incubator. After incubation, the Lipofectamine 2000 and plasmid complexes were added dropwise to each well. The cells were left to incubate with the complexes for 2 h at 37°C before removing the MEM and replacing with the conditioned growth medium.

2.4.3. Cell line culture

HEK293T cells (obtained from Prof. Luke Chamberlain, University of Strathclyde, Glasgow, UK) were thawed out at passage 2. The cells were grown in Dulbecco's Modified Eagle Medium (DMEM) supplemented with 1 % (v/v) penicillin/streptomycin and 10 % (v/v) FBS and grown in T75 flasks. Cells were split twice a week upon confluence. Briefly, growth medium was removed from the cells and cells were washed with PBS. Cells were then incubated in pre-warmed (37°C) trypsin to detach them from growth surface. Once cells were detached, trypsin was quenched with pre-warmed supplemented DMEM. 1:15 of cell suspension was added to new flask.

2.4.4. Cell line transfection

The day prior to transfection cells were plated in 10 cm culture dishes at 80 % confluence. Cells were transfected using Lipofectamine 2000 according to manufacturer's instructions. Briefly, per plate, 14 ug of plasmid DNA complexes were made up to a volume of 500 uL in Opti-MEM reduced-serum medium. Per dish, 28 uL of Lipofectamine 2000 was left to incubate in 472 uL of Opti-MEM at room temperature for 5 min. After incubation, the Lipofectamine 2000 solution was added to the plasmid DNA for a total volume of 1 mL/10 cm dish. This solution was added drop-wise to the cells. Cells were harvested 48 h later. Plasmid DNA constructs used for transfection can be found in Table 2.3.

2.5. Site-directed mutagenesis

Single-base pair mutations in *DNM1* were obtained from a screen of patients with developmental delay and/or epilepsy by the Deciphering Developmental Disorders Consortium and provided to us by Dr Wayne Lam (Muir Maxwell Epilepsy Centre, University of Edinburgh). Site-directed mutagenesis was used to introduce patient mutations into the mCer-Dynamin1aa plasmid (mCer-Dyn1). The spontaneous $Dyn1_{A408T}$ mutation observed in fitful mice (Boumil et al., 2010) was also generated. The Stratagene approach was used to make single base pair changes in the plasmid. For each reaction, diluted template DNA was added to Pfu DNA polymerase 10 x buffer, 200 µM dNTPs, 0.5 µM sense primer (see Table 2.4 for primer details), 0.5 µM anti-sense complement primer, and 1 µL Pfu DNA polymerase. The cycling conditions for the PCR were were 96°C for 2 min, and 18 cycles of 96°C for 30 s, 52°C for 10 s and 72°C for 1 min/ kb of plasmid (7 min), then 72°C for 10 min. The base change was confirmed by Source Bioscience Sanger Sequencing (Glasgow, UK).

Mutation	Primers 5'- 3'	
$Dyn1_{G139R}$	Sense	CTAGTGGACCTGCCAAGAATGACCAAGGTCCCA
	Anti-sense	TGGGACCTTGGTCATTCTTGGCAGGTCCACTAG
$Dyn1_{R237W}$	Sense	ATTGGCGTGGTGAACTGGAGCCAGAAGGACATA
	Anti-sense	TATGTCCTTCTGGCTCCAGTTCACCACGCCAAT
$Dyn1_{I289F}$	Sense	CAACTGACCAACCACTTCCGGGACACGCTGCCG
	Anti-sense	CGGCAGCGTGTCCCGGAAGTGGTTGGTCAGTTG
$Dyn1_{H396D}$	Sense	GCTATCAAGAACATTGATGGCATCAGGACAGGC
	Anti-sense	GCCTGTCCTGATGCCATCAATGTTCTTGATAGC
$Dyn1_{A408T}$	Sense	TTCACTCCTGACCTCACTTTTGAAGCCACAGTG
	Anti-sense	CACTGTGGCTTCAAAAGTGAGGTCAGGAGTGAA

Table 2.4 Primers used for site-directed mutagenesis of mCer-Dyn1aa

2.6. Fluorescence live-cell imaging

Transfected hippocampal neurons were imaged on day *in vitro* (*DIV*) 13-15. Coverslips were mounted onto an imaging chamber embedded with parallel platinum wires and fluid perfusion ports (Warner Instruments, CT, USA; RC-21BRFS) using vacuum grease. Cells were viewed using a Zeiss Axio Observer D1 inverted epifluorescence microscope (Zeiss, Cambridge, UK). Cells were visualised with a Zeiss EC Plan Neofluar 40 ×/1.30 oil immersion objective. Excitation at 500 nm was used to visualise pHluorins (sypHy, VAMP4-pH, vGLUT-pH) and calcium reporters (GCaMP6f, Fluo-5F). Excitation at 430 nm was used to visualise vectors tagged with mCerulean (mCer-Dyn1 constructs, mCerN1). For both these excitation wavelengths, 515 nm dichroic filter and long-pass emission filter, >520 were used for emission collection. Unless otherwise specified, fluorescent images were acquired at 4 s intervals using an AxioCam 506 mono digital camera (Zeiss) at room temperature. Images were acquired using Zen Pro software (Zeiss).

Neurons were field stimulated using a Digitimer LTD MultiStim system-D33 stimulator (current output 100 mA, current width 1 ms, Hertfordshire, UK) with a low frequency train of 300 action potentials (APs) delivered at 10 Hz or high frequency train of 300 APs delivered at 50 Hz or 60 Hz, or 400 APs delivered at 40 Hz. Imaging time courses were acquired while undergoing constant perfusion with imaging buffer (119 mM NaCl, 2.5 mM KCl, 2 mM $CaCl_2$, 2 mM $MgCl_2$, 25 mM HEPES, 30 mM glucose at pH 7.4, supplemented with 10 μM 6-cyano-7-nitroquinoxaline-2,3-dione (CNQX) and 50 μM DL-2-Amino-5-phosphonopentanoic acid (AP-5) (Armbruster and Ryan, 2011). After stimulation, pHluorin-transfected neurons were left to recover before undergoing perfusion with imaging buffer containing 50 mM NH_4Cl substituted for 50 mM NaCl. NH_4Cl imaging buffer was used to unquench the synaptic pHluorin giving a measure of total fluorescence to quantify the total SV pool. The weak base NH_4^+ can reversibly dissociate into NH_3 and H^+. NH_3 is permeable and can enter the acidic SVs where it can associate with

the protons in the SV which alkalinises the pH of the SV lumen unquenching the pHluorins.

2.6.1. SypHy and vGLUT-pH imaging

For standard sypHy and vGLUT-pH experiments, cells were perfused with imaging buffer before being stimulated with a train of 300 APs delivered at either 10 Hz (low frequency), 50 Hz or 60 Hz (both high frequency). After recovery, neurons were perfused with NH_4Cl buffer to reveal the total SV pool (Figure 2.2). Precise time courses for individual experiments can be found in results figures.

For MaxiPost experiments, cells were incubated in imaging buffer with 0 µM, 3 µM, 10 µM or 30 µM of MaxiPost made up in dimethyl sulfoxide (DMSO) for 2 min prior to the start of imaging. MaxiPost was present in the imaging buffer for the duration of the experiment. Total concentration of DMSO in the imaging buffer was kept constant across conditions.

Images were analysed using the FIJI distribution of Image J (NIH). Images were aligned using the Rigid body model of the StackReg plugin (Thevenaz et al., 1998). Nerve terminal fluorescence was measured using the Time Series Analyser plugin (Balaji, 2007). Regions of interest (ROIs) 5 px in diameter were placed over nerve terminals that responded to the electrical stimulus. Per transfected axon, 10-148 ROIs were selected. Fluorescence intensity in these ROIs was measured across all the frames to produce a fluorescence time trace. The ROI Trace Selection v0.6 software (Stewart, 2013) was used to screen ROIs to ensure that all selected ROIs responded both to the electrical stimulation and NH_4Cl buffer. Any traces that did not meet these criteria were excluded. The baseline of traces displaying fluorescence decay were fitted with a mono-exponential curve. This curve was then subtracted from the whole trace.

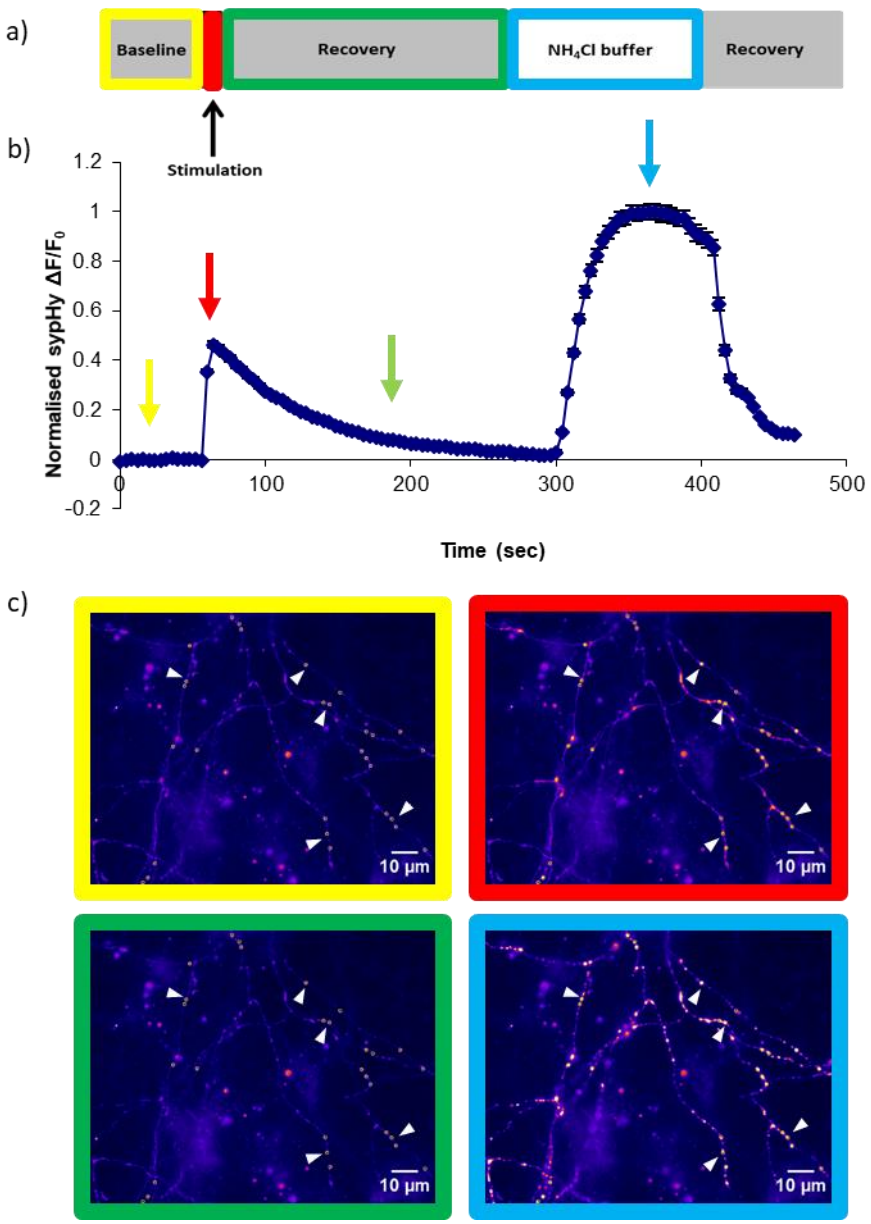

Figure 2.2 Example sypHy or vGLUT-pH trace

Hippocampal neurons transfected with sypHy or vGLUT-pH were imaged DIV 13-15 following the time course in a). Baseline (yellow), stimulation (red), recovery (green), NH_4Cl buffer (blue) b) Sample fluorescence trace. Coloured arrows correspond to the different stages of the protocol time course. c) Example images with selected ROIs which responded both to electrical stimulation and NH_4Cl pulse. Border colour corresponds to the different stages of the protocol time course. Arrow heads show responding nerve terminals

Data were firstly normalised to the fluorescence at baseline (F/F0), and then further normalised to either maximum response to stimulus to look at SV endocytosis or maximum fluorescence response (NH_4^+) to look at peak exocytosis. Fluorescence decay time constants (tau, τ, s) were calculated by fitting an exponential decay curve to data from the time point directly after the end of electrical stimulation to the point where the fluorescence plateaued (200 s from start of acquisition).

2.6.1.1.Surface fraction

The surface fraction assay provides a measure for how much reporter is stranded on the cell surface. For these imaging experiments, cells were perfused with imaging buffer, acid buffer (69 mM NaCl, 2.5 mM KCl, 2 mM $CaCl_2$, 2 mM $MgCl_2$, 25 mM MES, 30 mM glucose at pH 5.5) and NH_4Cl buffer. The acid buffer was used to quench all the sypHy at the surface (Figure 2.3). The NH_4Cl buffer was used to provide a measure for the total amount of SVs.

For the surface fraction traces, sypHy fluorescence was normalised to 100 in the NH_4Cl solution and to 0 in the acid buffer. Surface fraction was calculated for individual cells as a percentage of total fluorescence:

$$surface\ fraction = \left(\frac{\text{baseline fluorescence} - \text{minimum fluorescence}}{\text{maximum fluorescence} - \text{minimum fluorescence}}\right) \times 100$$

Where the baseline fluorescence is the average fluorescence when perfused with the imaging buffer taken for 20 s immediately before acid pulse and 20 s immediately before stimulation, the minimum fluorescence is the average fluorescence obtained from 20 s of plateaued acid buffer and maximum fluorescence is the average fluorescence obtained from the peak 20 s of NH_4Cl buffer.

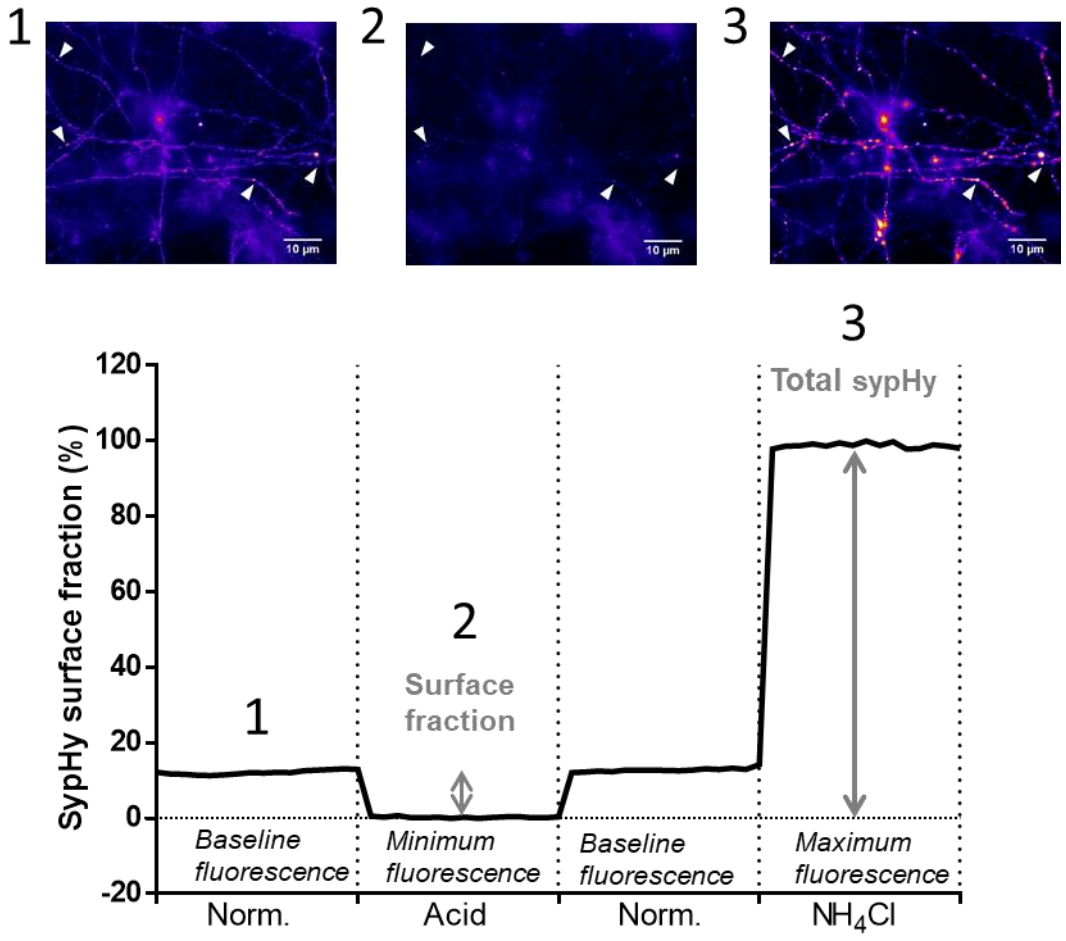

Figure 2.3 Surface fraction assay

Example surface fraction trace with fluorescence images from baseline fluorescence (1), minimum fluorescence with acid buffer (2) and maximum fluorescence with NH_4Cl buffer (3). Arrow heads show responding nerve terminals.

2.6.1.2.Reacidification

For reacidification experiments, surface sypHy fluorescence was quenched with a pulse of acid buffer during baseline. After recovery of surface fluorescence by perfusing over imaging buffer, cells were electrically stimulated with 300 APs at 10 Hz. After the end of the stimulation, another pulse of acid buffer was applied to the culture to quench any surface stranded sypHy. The sypHy that was already located in SVs was not quenched as the acid buffer is impermeable. This allowed for the monitoring of the reacidification kinetics of the SVs separately from the endocytosis rates as any further decrease in fluorescence would be due to the acidification of the SV (Kwon and Chapman, 2011).

Images were acquired every 1 s to ensure accurate monitoring of SV acidification which occurs on the order of ~ 5 s (Atluri and Ryan, 2006). Rate of acidification was calculated by fitting a mono exponential curve to the fluorescence drop after the second acid pulse.

2.6.1.3.37°C experiments

For experiments conducted at 37°C, an automatic temperature controller (Warner Instruments, CT, USA; TC-324C) was used to heat the imaging buffers. The temperature controller was set at 42°C so that the temperature of the buffers when they were being perfused over the cells was 37°C. This was confirmed by measuring the temperature of the imaging solution with an electronic thermometer at the level of the cells.

Images were acquired every 2 s during baseline, stimulation and recovery as to ensure accurate monitoring of SV kinetics, as the kinetics of SV recycling is faster at physiological temperatures (Micheva and Smith, 2005).

2.6.1.4.Bafilomycin

To determine exocytosis rate and total exocytosis amount we used the vacuolar-type H^+-ATPase blocker Bafilomycin A1 to inhibit reacidification of SVs.
Bafilomycin A1 diluted in DMSO was added to the imaging buffer for the duration of acquisition for a final concentration of 1 μM.

The average fluorescence of the final 20 s of electrical stimulation was used to obtain maximum fluorescence during electrical stimulation providing a measure for total exocytosis.

2.6.2. VAMP4-pH imaging

VAMP4-pH imaging was conducted as previously described (Nicholson-Fish et al., 2015; Nicholson-Fish et al., 2016). Briefly, after 19 frames of baseline, neurons were stimulated at 40 Hz 10 s then allowed to recover for 180 s before being perfused with NH_4Cl buffer to reveal the total SV pool. The fluorescence decay caused by bleaching due to 500 nm excitation was corrected by fitting a linear function to 19 frames of baseline and subtracting this function from each individual synaptic bouton's fluorescence trace using MATLAB (MathWorks, USA).

As VAMP4 is not an abundant protein, VAMP4-pH was always cotransfected with mCerN1 to allow for visualisation of the transfected cells. An image of the mCerN1 transfection was also captured to allow for identification of nerve terminals. Images were acquired using 3 x 3 px binning performed by Zen Pro software (Zeiss) to increase signal intensity. ROIs 3 px in diameter were selected using this image and fluorescence traces were obtained by translocating these ROIs onto the VAMP4-pH time trace images. Images were then processed in Microsoft Excel as previously

described (Nicholson-Fish et al., 2016). Briefly, VAMP4-pH fluorescence traces for each nerve terminal were normalised to the total SV pool as revealed by NH_4Cl. Fluorescence responses were then sorted into "up" or "down" traces depending on fluorescence 120 s after stimulation. If a nerve terminal's fluorescence trace was above baseline by this timepoint it was categorised as "up", whereas if the fluorescence trace was below baseline it was categorised as "down". Formula for segregation of traces obtained from Nicholson-Fish et al. (2016).

2.6.3. Calcium imaging

Due to the rapid kinetics of the calcium reporters used, images were acquired every 2 s. Cells were imaged in imaging buffer, however constant perfusion was not required for these experiments. After acquiring a 30 s baseline, neurons were stimulated with 300 APs delivered at either 10 Hz or 50 Hz as previous described in Section 2.6.1. Image processing was done as previously described in Section 2.6.1. Nerve terminal fluorescence was measured using the Time Series Analyser plugin (Balaji, 2007) to determine the fluorescence time trace of ROIs placed on synaptic boutons (as determined by morphology). Per transfected axon, 20-148 ROIs were selected. Fluorescence intensity in these ROIs was measured across all the frames to produce a fluorescence time trace. Only the fluorescence time traces of ROIs that responded to electrical stimulation were included.

For Fluo-5F experiments, cultures were incubated with 10 µM of Fluo-5F in imaging buffer for 30 min at room temperature prior to image acquisition. Image acquisition occurred in imaging buffer without Fluo-5F.

2.6.4. Dextran imaging

Neurons were loaded with 50 µM of tetramethylrhodamine (TMR) dextran, 40,000 MW in imaging buffer using 400 AP stimulation delivered at 40 Hz to elicit

ADBE. The dextran was then washed off with imaging buffer to remove all dextran that had not been taken up into ADBE endosomes. This ensured a low level of background fluorescence for image acquisition. Images were acquired undergoing constant perfusion to lower levels of background fluorescence.

Dextran images were acquired using a 556/25 excitation and 630/98 emission filter (Zeiss). Per coverslip, 5-7 different fields of view with roughly the same number of axons, and few cell bodies were imaged. The n for this experiment is number of coverslips. The dextran puncta on each image were counted using the Analyze Particles plugin of Image J (NIH) to select and count particles of 4-14 px. For each imaging day, for each condition, at least one unstimulated coverslip was imaged. As there was no loading of dextran, this condition was used as a control for the background level of dextran. The values for number of dextran puncta obtained from these conditions was subtracted from all experimental (stimulated) coverslips.

2.7. Immunofluorescence staining and fixed-cell imaging

Immunofluorescence staining and analysis was performed as previously described (Gordon et al., 2011). Briefly, hippocampal neurons plated on PDL-coated coverslips were fixed with 4% paraformaldehyde (PFA) in PBS. Cells were left to incubate in PFA for 15 min at room temperature. PFA was then removed and cells were quenched 2 x 5 min with 50 mM NH_4Cl in PBS. Cells were then washed 4 x 5 min with PBS. Fixed neurons were stored at 4°C until antibody labelling, (no longer than 1 week).

Before staining, cells were permeabilised in 1% bovine serum albumin (BSA) in PBS-Triton 1% for 5 min. Cells were then washed gently in PBS before being blocked in 1% BSA in PBS at room temperature for 1 h. After blocking, cells were left to incubate in primary antibody diluted in blocking solution for 30-45 min (see

Table 2.4 for antibodies). Following 4 x 5 min washes, cells were left to incubate in secondary antibody (see table 2.2 for antibodies) diluted in blocking buffer for 30-45 min at room temperature in the dark. After washing, coverslips were mounted to slides using FluorSave Reagent.

Alexa Fluor 488 and 568 images were acquired using a dual camera imaging system (Zeiss). The signal was filtered by a double band pass excitation filter (470/27 + 556/25) with beam splitter (490 + 575) and emission filters 512/30 and 630/98 (Zeiss) respectively. Alexa Fluor 647 was visualised with a 640 nm excitation and a 690/50 band pass emission filter.

For each image analysed, ROIs were placed over the transfected neuron, a non-transfected neuron and the background. This allowed measurement of levels of overexpression of mCer-Dyn1 within neurons on the same coverslip by comparing the overexpression to normal expression levels. Background fluorescence was subtracted from all signals. For each coverslip, 4-6 fields with transfected neurons were acquired. The n is the number of transfected cells imaged.

	Antibody	Dilution	Host	Supplier and product code
Primary antibodies	Anti-GFP	1:5000	Chicken	Abcam ab13970
	Anti-Synaptic vesicle glycoprotein 2A (SV2A)	1:200	Rabbit	Abcam ab32942
	Anti-Dynamin-1	1:200	Goat	Santa Cruz sc-6402
Secondary antibodies	Anti-chicken Alexa Fluor 488	1:1000	Goat	Invitrogen A11039
	Anti-rabbit Alexa Fluor 568	1:1000	Goat	Invitrogen A21069
	Anti-goat Alexa Fluor 647	1:1000	Donkey	Invitrogen A21447

Table 2.5 Antibodies used for immunofluorescence staining

2.8. Statistical analysis

Microsoft Excel and Prism 6 software (GraphPad software Inc., San Diego USA) were used for data processing and analysis. A response trace was calculated for each cell by averaging the individual traces from each selected ROI.

For all figures, results are presented with error bars as ± SEM, and the n in brackets for each condition represents the number of coverslips imaged unless otherwise specified. For each imaging assay, cells were obtained from at least two independent cultures. Mean pHluorin fluorescence differences across the time course were examined with two-way analysis of variance (ANOVA) with Dunnett's post hoc test comparing all traces to the control condition when three or more conditions were present. For all other data, statistical significance between two groups was evaluated using two-tailed Student t-tests. Statistical significance between three or more groups was evaluated using a one-way ANOVA with Dunnett's post hoc test to compare all results to control results unless otherwise stated.

2.9. GTPase assay

2.9.1. HEK293T lysis

HEK293T cells that were previously transfected with mCer-Dyn1 plasmids were harvested 48 h after transfection. Culture media was removed, and cells were rinsed with PBS. Two plates transfected with the same plasmid were pooled together to obtain sufficient protein for the GTPase assay experiments. Cells were then washed off the culture dish in 1 mL of PBS and centrifuged at 250 g for 2 min at 4°C. The supernatant was discarded. Pelleted cells were resuspended in 1 mL of sucrose lysis buffer (250 mM sucrose, 3 mM imidazole pH 7.4 supplemented with 2 µL/mL protease inhibitors and 1 mM phenylmethane sulfonyl fluoride). Cells were then placed into a primed ball-bearing cell cracker (EMBL, Heidelberg, Germany) and forced through the chamber 30 times. The solution with the mechanically broken

cells was collected and centrifuged at 1500 g for 15 min at 4°C to pellet all unbroken cells. The supernatant was collected and used for the following assays.

2.9.2. Immunoprecipitation using GFP-trap beads

Anti-GFP V_HH coupled to agarose beads for immunoprecipitation (IP) of GFP-fusion proteins (GFP-Trap) was used for IP of mCerN1, mCer-Dyn1$_{WT}$ or mutant mCer-Dyn1. GFP-Trap buffer was made substituting KCl for NaCl for consistency with the GTPase assay buffer. Beads were diluted 2:1 in GFP-Trap buffer. Following manufacturer's instructions, the beads were washed in GFP-Trap buffer and centrifuged at 2500 g for 2 min at 4°C. The mechanically lysed cells were added to the equilibrated GFP-trap beads and mixed top over bottom at 4°C for 1 h. Following the incubation, the beads and attached proteins were centrifuged at 2500 g for 2 min at 4°C. The supernatant was discarded. The beads were then washed 3 times as previously described.

2.9.3. Bradford

A Bradford assay was performed according to manufacturer's instructions to determine protein concentration of GFP-Trap-bound mCerN1 or mCer-Dyn1. For the standard curve, BSA was dissolved in GTPase assay buffer (20 mM HEPES pH 7.5, 50 mM KCl, 2 mM $MgCl_2$ (Leonard et al., 2005)) to create a standard curve (0, 1, 2, 4, 6, 8, 10 µg of BSA/ 100 µL buffer). 1 mL of Bradford solution was added to each concentration of the standard curve and to diluted GFP-Trap-bound protein samples. The absorbance of these dilutions was measured at 595 nm on a spectrophotometer and plotted to make a standard curve. The IP samples were diluted 1:10 in GTPase assay buffer and the concentration was determined based on the standard curve.

2.9.4. Malachite green colorimetric GTPase assay

A colorimetric assay was used to quantify GTPase activity of the different mCer-Dyn1 mutants (Leonard et al., 2005). The dye malachite green changes colour from yellow to blue-green when free inorganic phosphate is detected. This change in colour was then quantified using a plate reader to measure the absorbance at 650 nm.

GTP was made up to a 100 mM stock in 20 mM HEPES pH 7.4, snap frozen and stored at -80C. For each experiment, a fresh aliquot of GTP was thawed on ice and diluted in GTPase assay buffer (20 mM HEPES pH 7.5, 50 mM KCl - this low salt concentration allows for the oligomerisation of dynamin, 2 mM $MgCl_2$). GFP-Trap-bound mCer-Dyn1 mutants were diluted to a concentration of 1 µM in GTPase assay buffer.

All reactions were carried out on ice to limit GTP hydrolysis. For each reaction, 20 µL of 2 mM GTP diluted in GTPase assay buffer and 20 µL of 1 µM stock of mCer-Dyn1 was left to incubate in a 37°C water bath for 30 min. To terminate the reaction 10 µL of 0.5 M EDTA pH 8.0 was added. During the incubation, the standards were prepared at room temperature. KH_2PO_4 was diluted in GTPase assay buffer for the standards: 0 µM, 5 µM, 10 µM, 20 µM, 50 µM, 80 µM, 100 µM, 150 µM. After termination of the reaction, it was transferred to room temperature and 300 uL of filtered Malachite green solution (34 mg Malachite green carbinol base dissolved in 40 mL of 1 N HCl added to 1 g of ammonium molybdate tetrahydrate diluted in 14 mL of 4 N HCl up to 100 mL with ddH_2O) was added to each of the reactions as well as the standards. This step was done in the dark as Malachite green is light-sensitive. The reactions were mixed by pipetting up and down and then transferred to a 96-well plate. The absorbance of the standards and samples were read in a plate reader at 650 nm. The amount of inorganic phosphate released was calculated using the standard curve.

The controls included for each repeat of this experiment were: 1-GTP only reaction: as to measure the amount of GTP degradation occurring during the time course of the experiment, 2- GTPase addition after the termination of the reaction with EDTA: as to control for the GTPase having any effect on absorbance due to nucleotide contaminants, 3-No GTP for baseline inorganic phosphate levels in the reaction. These controls were not included in the results. Instead we used the mCerN1 reaction as a measure of basal release activity because it was a more accurate representation of basal inorganic phosphate release.

3. Characterisation of SV recycling defects in rodent models of SynGAP1 haploinsufficiency

3.1. Introduction

Mutations in the synaptic GTPase-activating protein 1 (*SYNGAP1*) gene lead to non-syndromic intellectual disability, autism spectrum disorder and epilepsy (Hamdan et al., 2009; Hamdan et al., 2011). The affected protein, SynGAP, is a brain-specific protein enriched at excitatory neuron synapses (Chen et al., 1998; J. H. Kim et al., 1998). SynGAP is expressed in the hippocampus and cortex prenatally and throughout development with expression reaching its peak on post-natal day (PND) 14 and levels decreasing into adulthood (J. H. Kim et al., 1998; Porter et al., 2005; Clement et al., 2012).

SynGAP plays an important role in synapse formation. Firstly, it competitively binds the PDZ domains of PSD-95 where it can regulate the composition of the postsynaptic density by preventing other proteins such as neuroligin, LRRTM and TARP from binding (Walkup et al., 2016). Secondly, although dendritic spine density was unchanged between *SynGAP1* heterozygous (Het) and WT dentate gyrus neurons, spine morphology was markedly different in Het neurons with more mushroom-type spines and fewer stubby-type spines (Clement et al., 2012). Moreover, dendritic spines in *SynGAP1* Het cortical neurons mature rapidly and, by PND 21, they are already undergoing pruning which is characteristic of mature neurons (Aceti et al., 2015).

SynGAP can also control synapse formation and strength through the regulation of protein translation in cortical neurons. It does this by suppressing the MAPK/ERK pathway and inhibiting protein translation (Rumbaugh et al., 2006; Wang et al., 2013). In fact, siRNA-mediated knock-down of SynGAP in cortical networks leads

to increased protein synthesis rates (Wang et al., 2013). SynGAP mediates AMPAR trafficking and its insertion in the plasma membrane through negative regulation of ERK (Rumbaugh et al., 2006). SynGAP can also limit AMPAR content through suppression of its synthesis by inhibiting the MAPK/ERK pathway (Wang et al., 2013). Altering the number of AMPAR at the plasma membrane directly impacts synaptic strength (reviewed in Anggono and Huganir, 2012).

SynGAP plays an important role in synapse formation during the critical period, in agreement with its pattern of expression. Het deletion of *SynGAP1* results in rapid maturation of synapses at PND 7 (Aceti et al., 2015) and increased neurotransmission in the hippocampus starting at PND 14 (Clement et al., 2012). The increase in mEPSC frequency and amplitude seen in Het mice at PND 14 is fully recovered to WT levels by PND 21 (Clement et al., 2012).

Although there is no direct evidence that SynGAP is localised at the presynapse (Moon et al., 2008) the increased mEPSC frequency in the hippocampus of Het mice during development (Clement et al., 2012) and in the cortex when SynGAP is knocked-down (Wang et al., 2013) could be due to presynaptic dysfunction. Furthermore, various SynGAP isoforms have been found to affect mEPSC frequency and amplitude differentially (McMahon et al., 2012). Additionally, overexpression of GFP-SynGAP in cultured neurons revealed decreased mEPSC frequency (Rumbaugh et al., 2006).

SynGAP1 Het mice behave differently to WT littermates in various experimental paradigms due to deficits in synapse and circuit formation. *SynGAP1* het mice display an anxiolytic phenotype compared to WT controls as shown by significantly more entries into the open arms of an elevated plus maze (Muhia et al., 2010). These mice also display deficits in hippocampal-dependent behaviour including no preference to enter the unvisited arm in a T-maze experiment, whereas on

hippocampal independent tasks such as novel object recognition, the Het mice showed no impairment (Muhia et al., 2010).

Thus, the highly abundant SynGAP protein plays multiple roles in synapse formation, protein translation, synaptic transmission and hippocampal learning. These roles could, in part, mediate the ASD, ID and epilepsy phenotypes observed in individuals with *SYNGAP1* haploinsufficiency

The aims of this work were to characterise SV recycling defects in preclinical models of *SynGAP1* haploinsufficiency. Furthermore, we also wanted to determine whether the defects observed were due to the enzymatic GAP activity of the SynGAP protein.

3.2. Results

3.2.1. SynGAP1 KO mouse hippocampal neurons show increased sypHy retrieval only at low frequency stimulation

The altered mEPSC described in various SynGAP haploinsufficiency models (Clement et al., 2012; McMahon et al., 2012; Wang et al., 2013) could suggest altered presynaptic function, particularly altered neurotransmitter release. To determine whether the mEPSC frequency phenotype was indeed due to presynaptic function, we used the genetically-encoded synaptic pHluorins to monitor synaptic vesicle recycling in a *SynGAP1* haploinsufficiency mouse model (Komiyama et al., 2002). PHluorins are pH-sensitive GFPs, which are fused to SV-associated proteins such as synaptophysin-pHluorin (sypHy) and located in the lumenal portion of the SV. When the synaptic pHluorin is exposed to an acidic pH as is the case in a SV (pH 5.5), the pHluorin is quenched. Upon exposure to a neutral pH, as is found in the

extracellular milieu (pH 7.4), the pHluorin fluoresces (Ryan, 2001; Sankaranarayanan and Ryan, 2000). PHluorins report the reacidification of SVs after endocytosis which happens on the order of ~5 s (Atluri and Ryan, 2006). Thus, the coupling between rate-limiting slow endocytosis, τ ~ 15-60 s, (Granseth et al., 2006; Sankaranarayanan and Ryan, 2000) and fast acidification allow for pHluorins to report SV endocytosis kinetics.

We first compared sypHy retrieval kinetics in dissociated hippocampal cultures from *SynGAP1* Het, KO and WT littermate controls to determine whether either the absence or a reduction of SynGAP had any effect on SV recycling.

As increased mEPSC frequency seen in previous studies could be due to increased SV fusion and neurotransmitter release, we first determined whether loss of SynGAP impacted SV exocytosis. SypHy time traces were normalised to the total synaptic vesicle pool by perfusion with NH_4Cl buffer which can diffuse through the membrane and neutralise acidic vesicles thus allowing for complete unquenching of the sypHy signal (Figure 3.1b). The amount of exocytosis can then be quantified as a proportion of fluorescence during stimulation compared to total fluorescence as revealed by NH_4Cl (Figure 3.1d). There were no significant differences (1-way ANOVA n.s. $p > 0.05$) in the normalised sypHy peak heights of *SynGAP1* Het (0.388 ± 0.026 units, n=16) or KO (0.332 ± 0.024 units, n=11) compared to control, WT (0.392 ± 0.032 units, n=19). Thus, partial or complete absence of SynGAP does not have an effect on SV exocytosis at low frequency stimulation.

Since there was no effect on SV exocytosis, we then investigated whether endocytosis was different across genotypes. Although all modes of SV endocytosis serve to replenish the SV pools, they are all distinct from each other with different proteins mediating the various steps of each (reviewed in Saheki and De Camilli, 2012). This means that loss of a specific protein may impair or accelerate a specific

endocytic pathway without affecting another. Similarly, different SV endocytosis modes are triggered by discrete stimulus intensities. Thus, different stimulation frequencies were used to mobilise different endocytosis pathways. We first started with low frequency stimulation, 10 Hz 30 s (Figure 3.1) which has been shown to predominantly recruit the CME pathway at room temperature (Granseth et al., 2006). Traces were normalised to the stimulation peak to examine sypHy retrieval (Figure 3.1c). Normalising to the peak of stimulation allows for a measurement of endocytosis without the confounds of exocytosis. Furthermore, it allows for quantification of the amount SVs endocytosed as a proportion of total amount exocytosed as determined by the fluorescence trace. When comparing time traces, sypHy retrieval was significantly different in KO hippocampal neurons compared to WT (2-way ANOVA using Dunnett's multiple comparisons $p < 0.01$). Single-phase decays can also be fitted to these curves to provide the sypHy retrieval time constant (τ). There were no differences (1-way ANOVA n.s. $p > 0.05$) between the τ values of Het (33.42 ± 2.73 s, n=16), KO (25.19 ± 1.99 s, n=11) and WT (33.66 ± 3.10 s, n=19). Thus, there was enhanced sypHy retrieved during the time course in *SynGAP1* KO hippocampal neurons compared to WT, however the rate of endocytosis remained constant across all genotypes.

To see if we could observe a similar phenotype at high frequency, we maintained the same number of action potentials (300 action potentials) and increased the frequency of stimulation, 50 Hz for 6 s (Figure 3.2). High frequency stimulation provides a higher intensity stimulus load which can lead to exaggeration of defects seen at lower frequency stimulation. Furthermore, during high frequency stimulation ADBE is thought to become the more dominant endocytic mode (Clayton et al., 2008). Although sypHy cannot be used to monitor ADBE (Nicholson-Fish et al., 2015), sypHy responses can still be examined to determine whether the reported endocytosis modes are perturbed when faced with a bigger stimulus load.

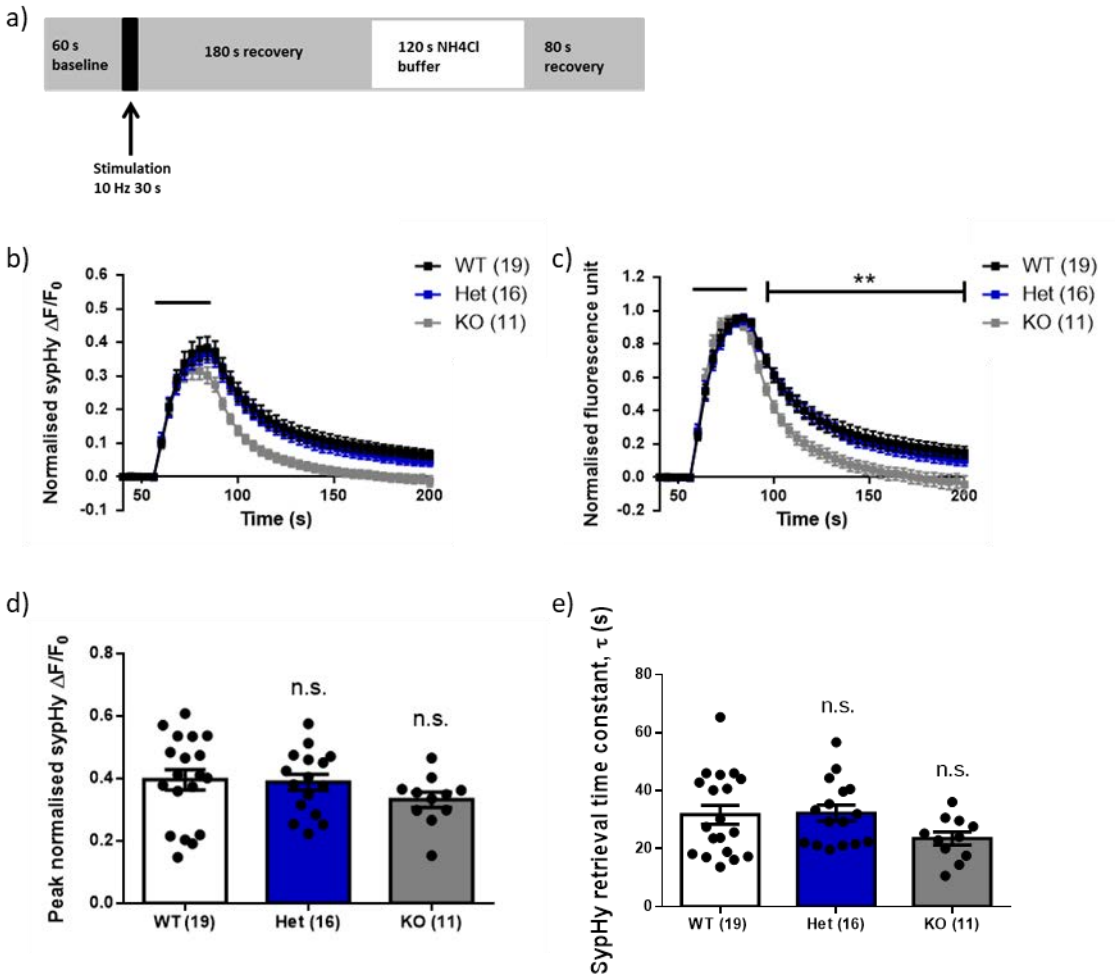

Figure 3.1 Increased sypHy retrieval in SynGAP1 KO hippocampal neurons compared to WT at low frequency stimulation (10 Hz 30 s)

*Hippocampal neurons derived from SynGAP1 Het and KO mice and WT littermate controls were transfected with sypHy on DIV 7 and imaged DIV 13-15. a) Time course of experiment. b-c) Mean sypHy fluorescence traces of WT (white), Het (blue) and KO (grey) hippocampal neurons. Bars indicate the period of stimulation, 10 Hz 30 s. b) normalised to the total vesicle number as revealed by NH_4Cl. c) normalised to the peak of stimulation. 2-way ANOVA ** $p < 0.01$. d) Mean and individual stimulation peak heights obtained from individual sypHy traces of data in b). e) Mean and individual sypHy retrieval time constants (τ) of data plotted in c). d-e) n.s. non-significant $p > 0.05$ by 1-way ANOVA.*
Experimental n shown in brackets, error bars in all panels ± SEM

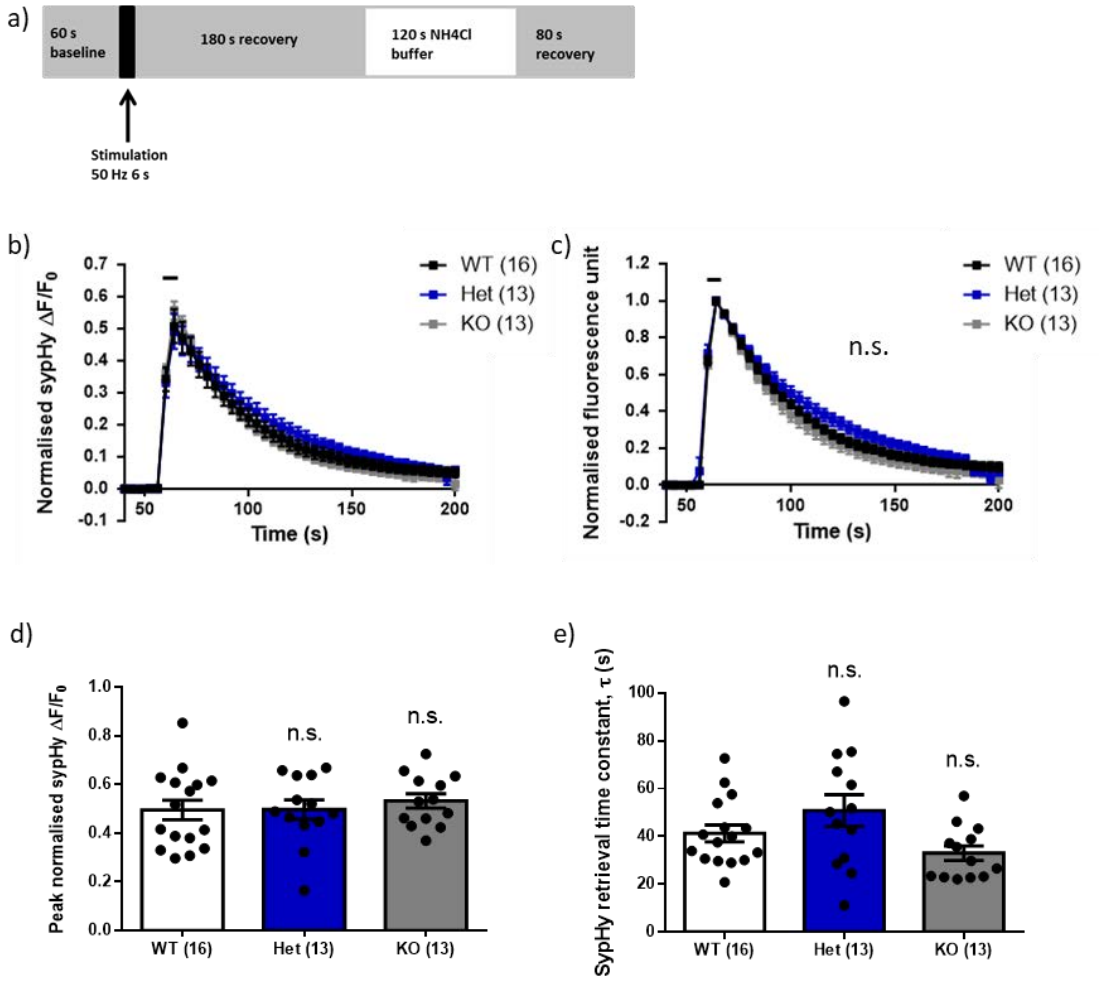

Figure 3.2 No difference in exocytosis or sypHy retrieval at high frequency stimulation (50 Hz 6 s) of SynGAP1 Het or KO compared to WT

Hippocampal neurons derived from SynGAP1 Het and KO mice and WT littermate controls were transfected with sypHy on DIV 7 and imaged DIV13-DIV15. a) Time course of experiment. b-c) Mean sypHy fluorescence traces of WT(white), Het (blue) and KO (grey) hippocampal neurons. Bars indicate the period of stimulation, 50 Hz 6 s. b) normalised to the total vesicle number as revealed by NH_4Cl. c) normalised to the peak of stimulation. 2-way ANOVA n.s non-significant $p > 0.05$. d) Mean and individual stimulation peak heights obtained from individual sypHy traces of data in b). e) Mean and individual sypHy retrieval time constants (τ) of data plotted in c). d-e) n.s. non-significant $p > 0.05$ by 1-way ANOVA. Experimental n shown in brackets, error bars in all panels ± SEM

We first examined exocytosis by looking at normalised sypHy peak heights (Figure 3.2b,d). There were no significant differences (1-way ANOVA n.s. $p > 0.05$) in the sypHy peak heights of *SynGAP1* Het (0.497 ± 0.040 units, n=13) or KO (0.532 ± 0.029 units, n=13) compared to control, WT (0.496 ± 0.040 units, n=16) at high frequency stimulation. Taken together with the results from Figure 3.1, these results suggest that there is no effect of *SynGAP1* deletion on exocytosis at either low or high frequency stimulation.

We next examined SV endocytosis during high frequency stimulation. As done previously, traces were normalised to the stimulation peak (Figure 3.2c) to examine sypHy retrieval. There was no difference between the traces (2-way ANOVA n.s. $p> 0.05$), suggesting that the amount of endocytosis occurring during the acquisition period was the same across all genotypes. Furthermore, there were no differences (1-way ANOVA n.s. $p > 0.05$) between the τ values of Het (50.82 ± 6.65 s, n=13), KO (33.01 ± 3.07 s, n=13) and WT (41.26 ± 3.51 s, n=16). Thus, sypHy retrieval is only affected at low frequency stimulation in *SynGAP1* KO neurons whereas there is no difference in either amount or rate of endocytosis at high frequency.

3.2.2. There is less sypHy stranded at the cell surface in KO neurons compared WT littermates

As there appeared to be more sypHy retrieval in *SynGAP1* KO compared to WT mouse hippocampal neurons (Figure 3.1c) we then determined whether this was indeed due to accelerated sypHy endocytosis or rather due to faster acidification of the vesicle. To do this we performed a reacidification experiment to be able to observe the acidification of recently retrieved SVs. In order to obtain an accurate timescale of reacidification, images were acquired at 1 s intervals. The cell was first perfused with acid buffer (pH 5.5) to quench all surface sypHy, and once again immediately after the end of stimulation (Figure 3.3a-b). With the second acid pulse, all surface sypHy was quenched, so it was possible to visualise the reacidification of the recently retrieved SVs in isolation. This was shown by a decrease in fluorescence

across all genotypes (Figure 3.3c). The rate of reacidification of the SVs could then be quantified by fitting an exponential decay to the curve for each individual pHluorin trace. Mean and average acidification rates are shown in Figure 3.3d). There was no significant difference in reacidification rates (1-way ANOVA n.s. $p > 0.05$) between Het (7.62 ± 0.71 s, n=7), KO (7.93 ± 1.30 s, n=9) and WT (8.28 ± 1.84 s, n=10). Taken together with the results in Figure 3.1, this would suggest that the accelerated sypHy retrieval is indeed due to accelerated endocytosis and not due to altered SV reacidification.

Defects in SV endocytosis can be reflected by a change in cargo at the plasma membrane as the SV cargo cannot be cleared efficiently (reviewed in Cousin, 2017). Since we saw increased endocytosis in *SynGAP1* KO hippocampal neurons compared to WT, we also looked at the surface fraction of sypHy to determine whether this defective endocytosis had an effect on the amount of sypHy at the surface of the plasma membrane.

Using both an impermeable acid and an NH_4Cl solution, it is possible to estimate the ratio of sypHy stranded at the surface. Perfusing on acid quenches all surface fluorescence whereas pulsing over NH_4Cl reveals the total SV pool. To determine the surface fraction, the minimum fluorescence obtained by perfusing over acid buffer was subtracted from both the baseline fluorescence (in normal buffer) and maximum fluorescence (NH_4Cl buffer). The ratio of corrected baseline fluorescence over maximum fluorescence gives the ratio of surface-to-vesicle pool fluorescence. Interestingly, there was a significant decrease in surface fraction between KO (8.57 ± 0.85%, n=7) and WT (13.23 ± 1.31, n=7) (1-way ANOVA with Dunnett's comparing all conditions to WT $p= 0.0487$), however the Het surface fraction (13.53 ± 1.73%, n=7) was not different from WT (1-way ANOVA with Dunnett's n.s. $p> 0.05$). Therefore, there is less sypHy at the plasma membrane in *SynGAP1* KO hippocampal neurons which could be a result of the enhanced endocytosis seen in Figure 3.1.

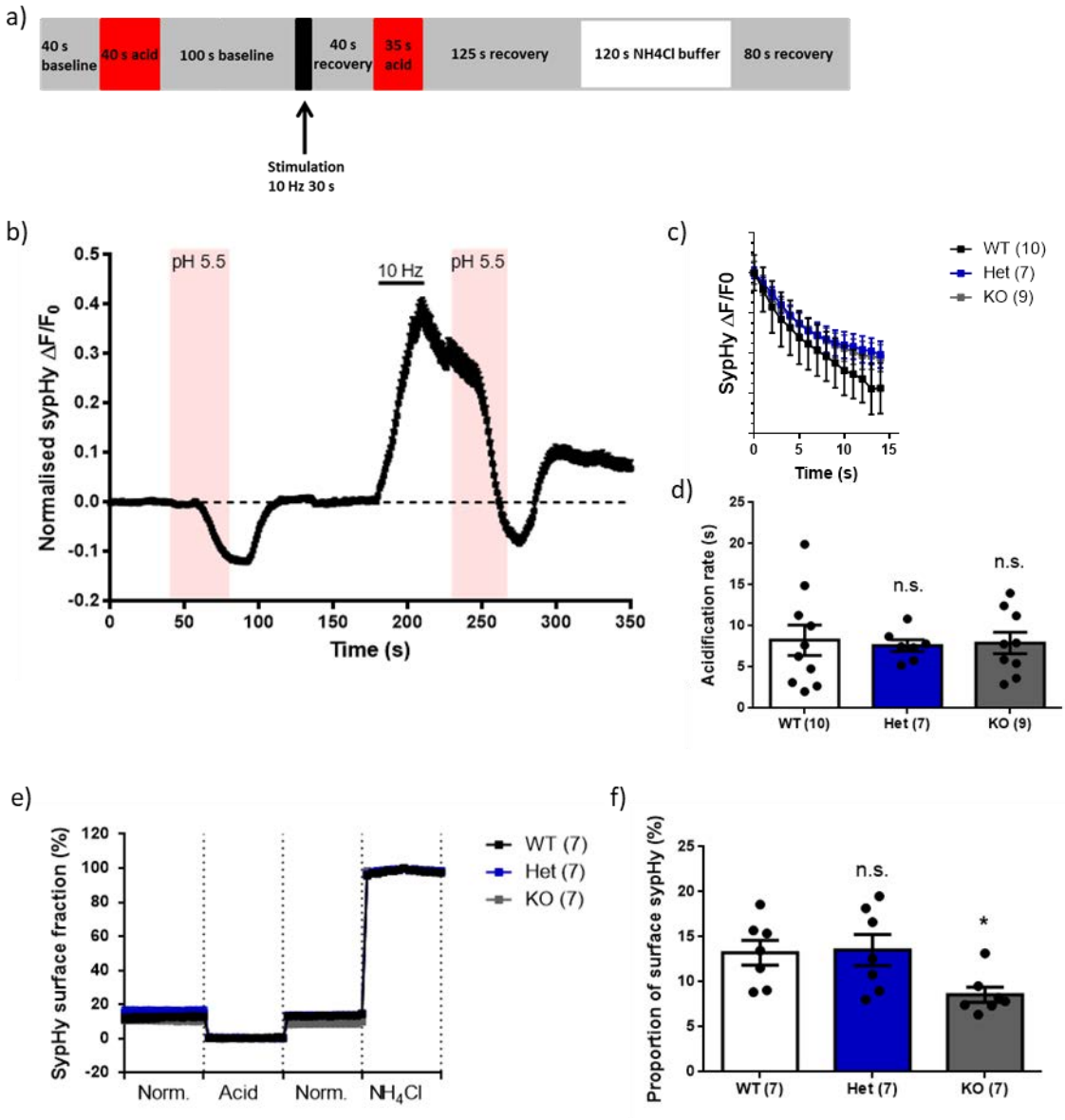

Figure 3.3 Less sypHy stranded at membrane surface in SynGAP1 KO hippocampal neurons compared to WT

Hippocampal neurons derived from SynGAP1 Het and KO mice and WT littermate controls were transfected with sypHy on DIV 7. a) Time course of experiment. Images were acquired at 1 Hz. b) Representative sypHy reacidification trace. c) Mean sypHy reacidification trace of WT(white), Het (blue) and KO (grey) neurons. d) Mean and individual reacidification rates obtained from fitting single exponential curves to fluorescence drop upon second acid pulse (pulse after stimulation) as shown in c). e) Mean normalised traces of sypHy fluorescence upon exposure to normal buffer (Norm.) 20 frames before acid pulse, acidic buffer (pH 5.5; 0% fluorescence) 20 frames of acid plateau, and NH_4Cl buffer (100% fluorescence) 20 frames of highest fluorescence. f) Mean and individual sypHy surface fraction (formula in methods). d,f) 1-way ANOVA with Dunnett's test comparing all means to WT (control condition). $p < 0.05$; n.s. non-significant $p > 0.05$.*
Experimental n shown in brackets, error bars in all panels ± SEM.

3.2.3. Increased endocytosis in SynGAP1 KO neurons is not due to absence of GAP domain

The GAP domain in SynGAP plays an important role in its function and is thought to be the functional domain responsible for most of SynGAP activity (J. H. Kim et al., 1998). Due to the importance of this domain, we used a rat model with a deletion of the SynGAP GAP domain. Rats that were Het or homozygous (Hom) for this deletion where used to determine whether the loss of this domain would replicate the SV recycling phenotype seen in the *SynGAP1* KO mouse model.

We first compared sypHy retrieval kinetics in dissociated hippocampal cultures from *SynGAP1 GAP* Het, Hom and WT littermate controls at low frequency stimulation, 10 Hz 30 s (Figure 3.4) since these were the stimulation conditions which revealed an endocytosis defect in *SynGAP1* KO mice.

To first check whether there was any effect on SV exocytosis, traces were normalised to total vesicle pool (Figure 3.4b) and sypHy peak heights were calculated (Figure 3.4d). There was no difference in sypHy peak heights between Het (0.350 ± 0.031 units, n=14), Hom (0.383 ± 0.031 units, n=14) and WT (0.382 ± 0.033 units, n=17) (1-way ANOVA n.s. non-significant $p > 0.05$). Thus, there was no effect of partial or complete GAP domain deletion on SV exocytosis at low frequency stimulation.

As we saw defective endocytosis in *SynGAP1* KO mouse neurons, we then went on to examine endocytosis in the GAP deletion rat model. There was no difference in amount of endocytosis as revealed by normalising the traces to the stimulation peak (2-way ANOVA n.s. $p> 0.05$, Figure 3.4c). The sypHy τ (Figure 3.4e) was also not significantly different (1-way ANOVA n.s. $p > 0.05$) between Het (35.49 ± 4.47 s, n=14), Hom (40.72 ± 5.29 s, n=14) and WT (40.19 ± 3.87 s, n=17). Therefore,

deletion of the *SynGAP1* GAP domain does not impair amount or rate of endocytosis at low frequency stimulation.

To determine whether the SynGAP GAP domain may interfere with other endocytic pathways, we next looked to see if there was any effect of GAP deletion on exocytosis or endocytosis at high frequency stimulation 50 Hz 6 s (Figure 3.5). We first examined exocytosis by normalising sypHy traces to total vesicle pool (Figure 3.2b) to calculate the normalised peak sypHy response (Figure 3.5d). There were no significant differences (1-way ANOVA n.s. $p > 0.05$) in the sypHy peak heights of *SynGAP1 GAP* Het (0.452 ± 0.029 units, n=16) or Hom (0.397 ± 0.026 units, n=15) compared to control, WT (0.427 ± 0.031 units, n=18) at high frequency stimulation. Thus, deletion of the *SynGAP1 GAP* domain does not affect exocytosis at high frequency stimulation.

Mouse KO cultures display no defect in endocytosis at high frequency stimulation, therefore we next determined whether this was also the case for GAP domain deletion mutants. Traces were normalised to the stimulation peak (Figure 3.2c) to examine sypHy retrieval as before. There was no significant difference in amount of sypHy retrieved (1-way ANOVA n.s. $p> 0.05$) when comparing sypHy fluorescence traces across genotypes. There were also no differences (1-way ANOVA n.s. $p > 0.05$) in the τ values between Het (40.07 ± 4.16 s, n=16), Hom (42.26 ± 4.74 s, n=15) and WT (41.67 ± 4.72 s, n=18). Therefore, GAP domain deletion does not alter SV endocytosis at high frequency stimulation. These results taken together suggest that it is not the loss of function of the GAP domain that is mediating the enhanced SV endocytosis seen in the *SynGAP1* KO mouse model at low stimulation frequencies.

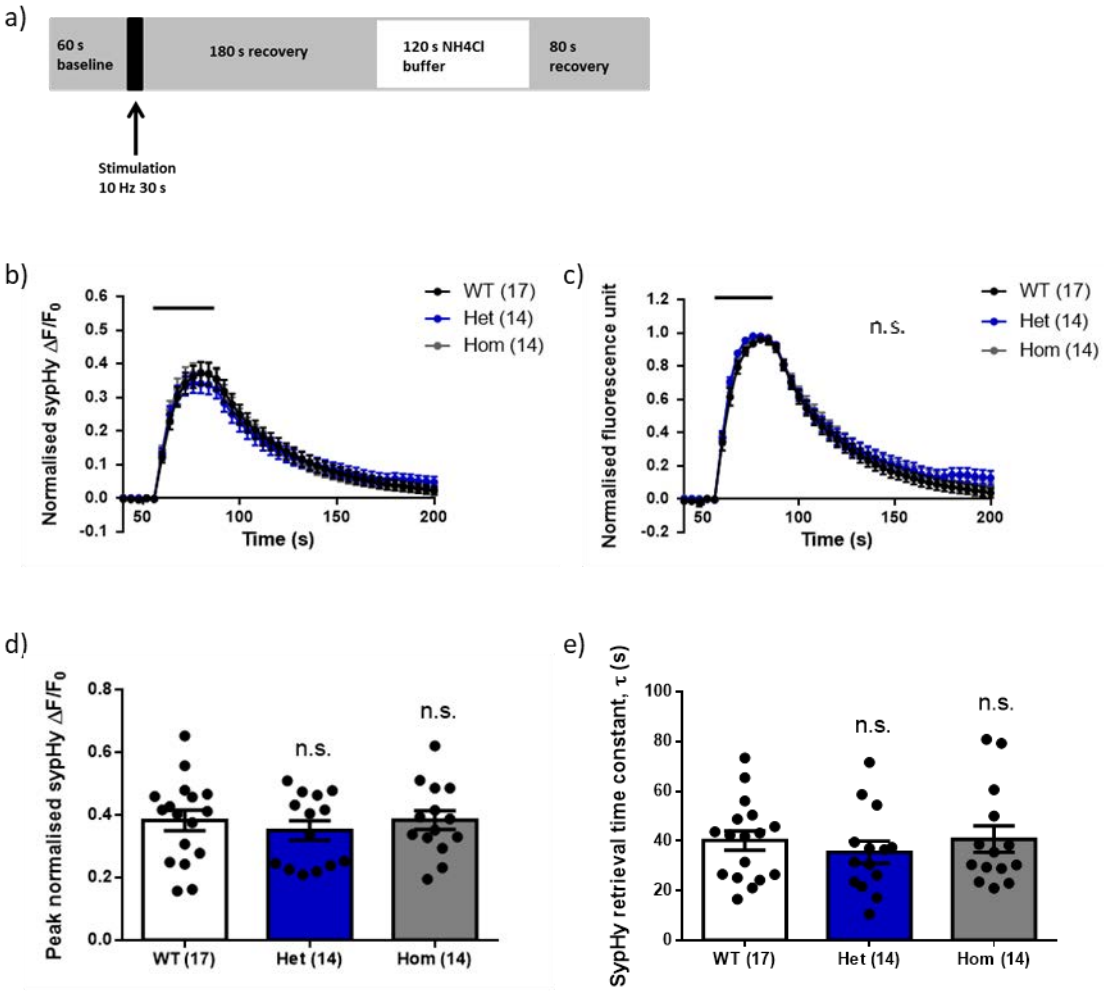

Figure 3.4 No difference in exocytosis or sypHy retrieval at low frequency stimulation (10 Hz 30 s) in SynGAP1 GAP deletion rat model

Hippocampal neurons derived from SynGAP1 rat GAP domain heterozygous (Het) or homozygous (Hom) deletion and WT littermate controls were transfected with sypHy on DIV 7 and imaged DIV 13-15. a) Time course of experiment. b-c) Mean sypHy fluorescence traces of WT (white), Het (blue) and Hom (grey) hippocampal neurons. Bars indicate the period of stimulation, 10 Hz 30 s. b) normalised to the total vesicle number as revealed by NH_4Cl. c) normalised to the peak of stimulation. 2-way ANOVA n.s. non-significant $p > 0.05$. d) Mean and individual stimulation peak heights obtained from individual sypHy traces of data in b). e) Mean and individual sypHy retrieval time constants (τ) of data plotted in c). d-e) 1-way ANOVA n.s. non-significant $p > 0.05$.
Experimental n shown in brackets, error bars in all panels ± SEM.

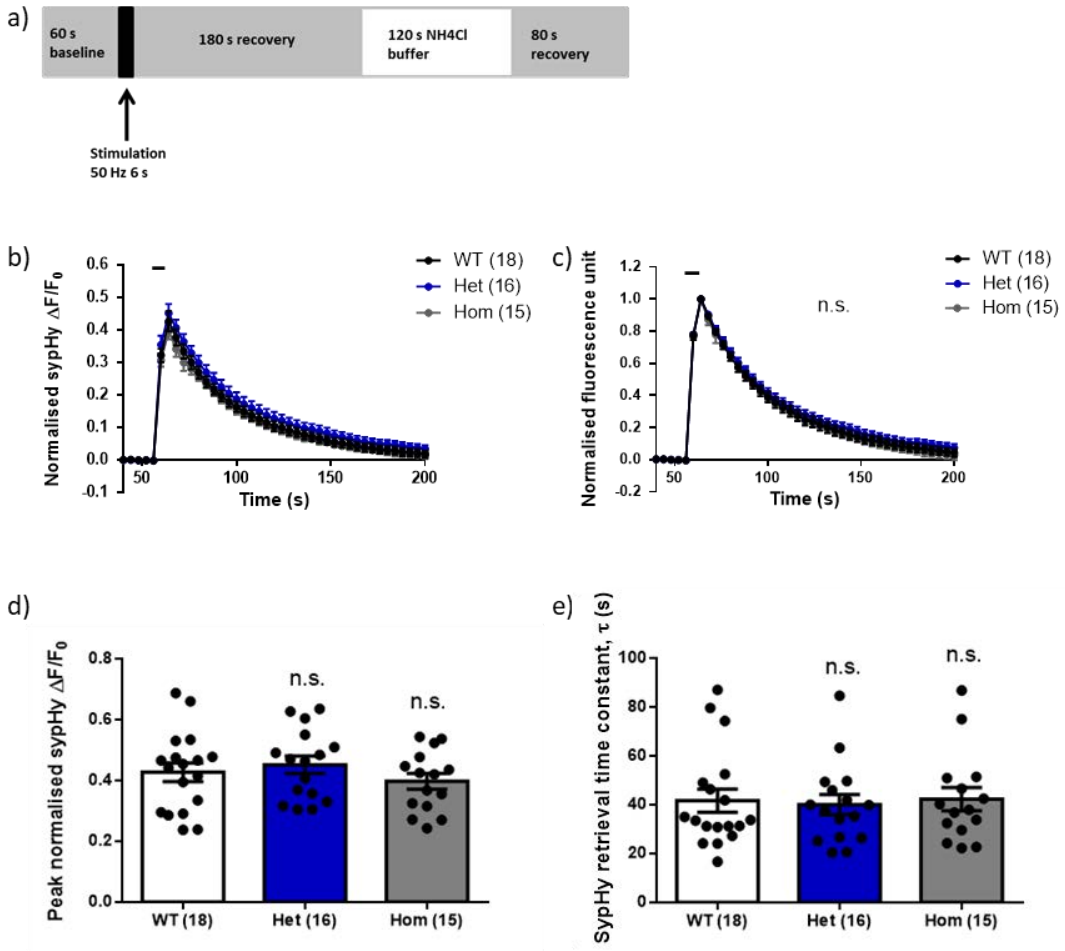

Figure 3.5 No difference in exocytosis or sypHy retrieval at high frequency stimulation (50 Hz 6 s) in SynGAP1 GAP deletion rat model

Hippocampal neurons derived from SynGAP1 rat GAP domain heterozygous (Het) or homozygous (Hom) deletion and WT littermate controls were transfected with sypHy on DIV 7 and imaged on DIV 13-15. a) Time course of experiment. b-c) Mean sypHy fluorescence traces of WT (white), Het (blue) and Hom (grey) hippocampal neurons. Bars indicate the period of stimulation, 50 Hz 6 s. b) normalised to the total vesicle number as revealed by NH_4Cl. c) normalised to the peak of stimulation. 2-way ANOVA n.s. non-significant $p > 0.05$. d) Mean and individual stimulation peak heights obtained from individual sypHy traces of data in b). e) Mean and individual sypHy retrieval time constants (τ) of data plotted in c) d-e) 1-way ANOVA n.s. non-significant $p > 0.05$.
Experimental n shown in brackets, error bars in all panels ± SEM.

3.2.4. SynGAP1 KO rat hippocampal neurons showed no effect on SV recycling

We did not observe the enhanced endocytosis at low frequency stimulation seen in the mouse KO hippocampal neurons using the GAP deletion rat model. This could be due to the loss of the GAP domain not being involved in the defective endocytic phenotype observed, alternatively, it could be due to species differences between mice and rats. Thus, we went on to study SV recycling in a novel *SynGAP1* KO rat model (Figures 3.6-3.8). If the enhanced SV endocytosis phenotype was seen in the rat KO neurons, then taken together with the results in Figure 3.4, it would suggest that the GAP domain is not required for SV endocytosis.

A new imaging protocol was used in this model (Figure 3.6a) to extract the maximum amount of information from a single experiment. We perfused acid buffer over the cells prior to stimulation to be able to calculate sypHy surface fraction. The cells were then stimulated at 10 Hz 30 s to examine the effect of low frequency stimulation. Following a five-minute recovery, cells were stimulated again, this time at 40 Hz for 10 s to determine the effect of high frequency stimulation on SV recycling. After further recovery NH_4Cl buffer was pulsed over the cells to reveal the total SV pool (Figure 3.6b).

We first examined SV exocytosis and found that there were no differences in sypHy peak height at low frequency stimulation (1-way ANOVA n.s. $p > 0.05$) between Het (0.524 ± 0.029 units, n= 11), KO (0.488 ± 0.025 units, n= 12) and WT (0.461 ± 0.030 units, n=12) (Figure 3.6c). Furthermore, there were no differences in sypHy peak height at high frequency stimulation (1-way ANOVA n.s. $p> 0.05$) between Het (0.401 ± 0.028 units, n=11), KO (0.427 ± 0.330 units, n=12) and WT (0.375 ± 0.024 units, n=12) (Figure 3.6d). The lack of difference in exocytosis across genotypes suggests that SynGAP is not required for SV exocytosis similar to what was observed in the mouse model.

We then normalised the sypHy traces to the peak of stimulation for each stimulus including a 15-frame baseline for the second stimulus to examine sypHy endocytosis (Figure 3.7a). When comparing the time traces across genotypes, there was no difference in the amount of endocytosis observed during imaging (2-way ANOVA n.s. $p > 0.05$). There was also no significant difference (1-way ANOVA n.s. $p > 0.05$) in sypHy retrieval rates either at low frequency (Figure 3.7b; Het: 42.98 ± 4.76 s, n=11; KO: 43.08 ± 5.47 s, n=12; WT: 46.61 ± 4.89 s, n=12) or at high frequency stimulation (Het: 48.27 ± 7.00 s, n=11; KO: 48.39 ± 6.73 s, n=12; WT 51.01 ± 5.11 s, n=12; 1-way ANOVA n.s. $p > 0.05$). Thus, in this rat model of *SynGAP1* haploinsufficiency, the loss of SynGAP does not precipitate any SV recycling defects.

As we saw decreased stranding of sypHy in the plasma membrane in *SynGAP1* KO mouse neurons compared to WT, we looked at whether the surface fraction of sypHy was altered in this rat model (Figure 3.8). The surface fraction traces (Figure 3.8a) were obtained by using the 5 frames from the start of acquisition (20 seconds) and 5 frames before stimulation (20 seconds) to determine baseline fluoresce levels as well as 5 frames of acid plateau and 5 frames of NH_4Cl plateau. There was no difference in surface fraction between *SynGAP1* Het (9.27 ± 1.52 %, n=9), KO (10.42 ± 0.84 %, n=8) and WT (9.90 ± 2.45 %, n=8) (1-way ANOVA n.s. $p > 0.05$). Taken together these results suggest that there is no effect of deletion of *SynGAP1* on SV recycling in rat hippocampal neurons. This is in contrast to the results seen in mouse hippocampal neurons (Figure 3.1) where there was enhanced sypHy retrieval at low frequency stimulation and less sypHy stranded on the plasma membrane.

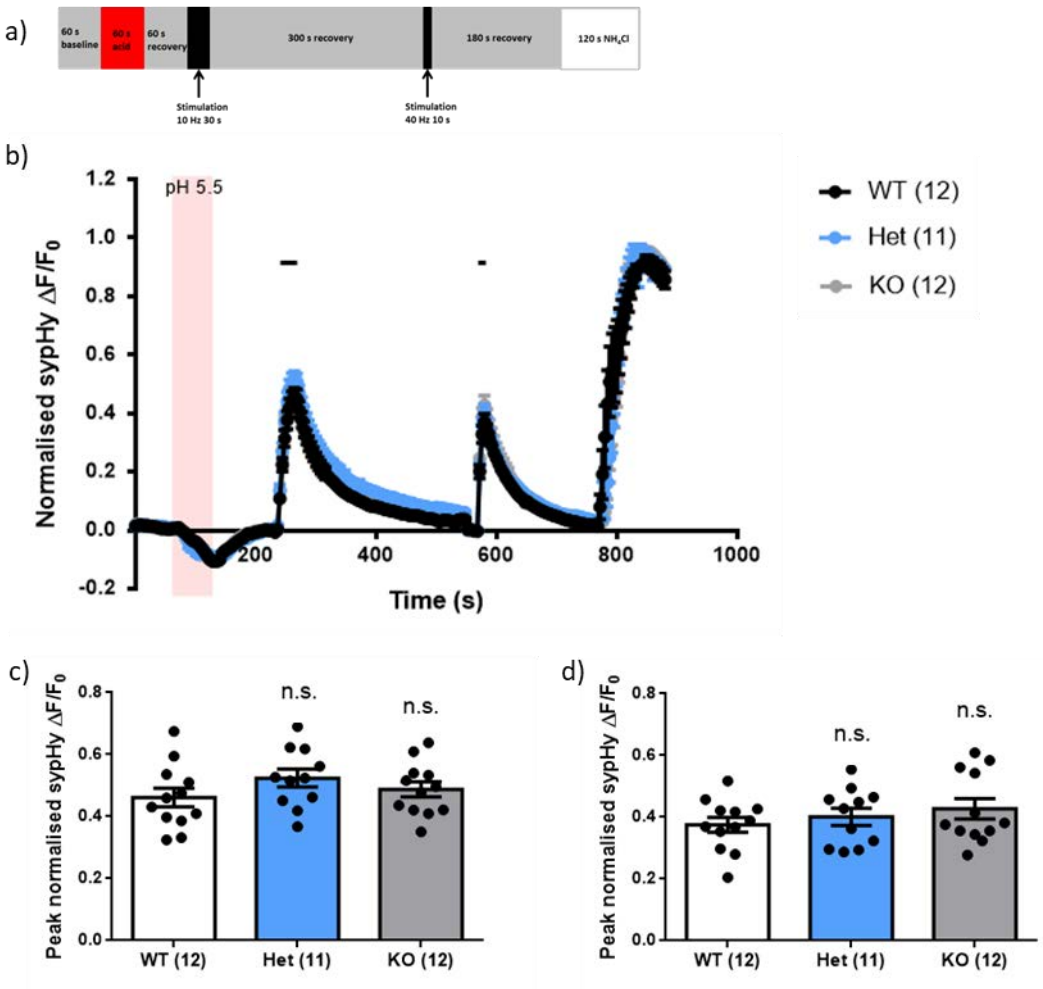

Figure 3.6 No difference in exocytosis at either low (10 Hz 30 s) or high frequency stimulation (40 Hz 10 s) in SynGAP1 KO rat model.

Hippocampal neurons derived from SynGAP1 heterozygous (Het) and knockout (KO) mice and WT littermate controls were transfected with sypHy on DIV 7 and imaged on DIV 13-15. a) Time course of experiment. b) Mean sypHy fluorescence traces of WT (white), Het (blue) and KO (grey) hippocampal neurons normalised to the total vesicle number as revealed by NH_4Cl. Bars indicate the period of stimulation, first bar: 10 Hz 30 s, second bar: 40 Hz 10 s. c) Mean and individual 10 Hz stimulation peak heights obtained from individual sypHy traces of data in a). d) Mean and individual 40 Hz stimulation peak heights obtained from individual sypHy traces of data in a). 1-way ANOVA n.s. non-significant $p > 0.05$.
Experimental n shown in brackets, error bars in all panels ± SEM.

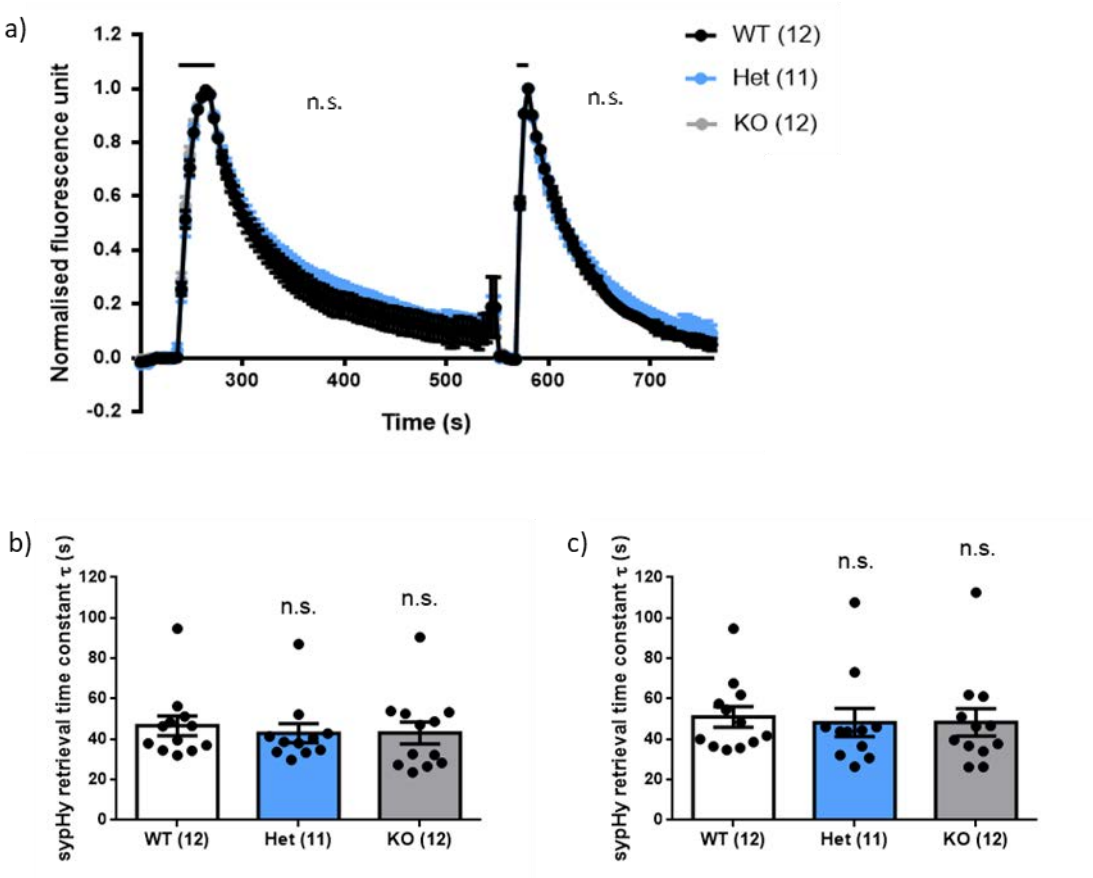

Figure 3.7 No difference in sypHy retrieval rate at either low (10 Hz 30 s) or high frequency stimulation (40 Hz 10 s) in SynGAP1 KO rat model.

Same data as in Figure 3.6 a) Mean sypHy fluorescence traces of SynGAP1 WT (white), Het (blue) and KO (grey) hippocampal neurons normalised to the peak of each stimulation. Bars indicate the period of stimulation, first bar: 10 Hz 30 s, second bar: 40 Hz 10 s. 2-way ANOVA n.s. non-significant $p > 0.05$. b-c) Mean and individual taus b) following 10 Hz stimulation; c) following 40 Hz stimulation. 1-way ANOVA n.s. non-significant $p > 0.05$. Experimental n shown in brackets, error bars in all panels ± SEM.

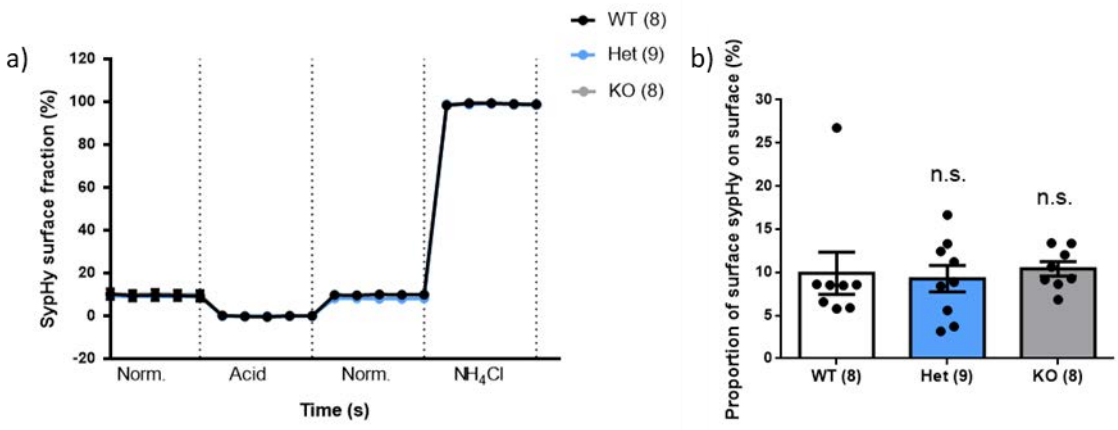

Figure 3.8 No difference in surface levels of sypHy

Data obtained from individual traces of data from figure 3.6. a) Mean normalised traces of sypHy fluorescence upon exposure to normal buffer (Norm.), acidic buffer (pH 5.5; 0% fluorescence) and NH_4Cl buffer (100% fluorescence) of WT (white), Het (blue) and KO (grey) hippocampal neurons. f) Mean and individual sypHy surface fraction (formula in methods). 1-way ANOVA n.s. non-significant $p > 0.05$.
Experimental n shown in brackets, error bars in all panels ± SEM.

3.3. Discussion

Using the genetically encoded reporter sypHy to monitor SV recycling in different rodent models of *SynGAP1* haploinsufficiency, we observed enhanced SV endocytosis at low frequency stimulation in *SynGAP1* KO mouse hippocampal neurons compared to WT littermate controls, however the rate at which the endocytosis occurred was not changed. Paired with this, we also found a decreased proportion of sypHy stranded on the plasma membrane. Interestingly, when the neurons were challenged with a higher stimulus load (50 Hz 6 s or 40 Hz 10 s) to mobilise the whole recycling pool (Denker and Rizzoli, 2010), there were no differences in endocytosis amount or rate between genotypes.

Previous electrophysiological evidence hinted toward a defect in presynaptic neurotransmitter release which could underlie the impaired mEPSC frequency in *SynGAP1* het neurons (Clement et al., 2012; McMahon et al., 2012; Wang et al., 2013). We used our pHluorin imaging assay to determine whether loss of SynGAP impaired SV exocytosis. The amount of exocytosis as a proportion of the total SV pool, as revealed by NH_4Cl buffer, was not different between genotypes at either low or high frequency stimulation. This suggests that release probability is unimpaired with loss of SynGAP. Thus, defects in mEPSC frequency could be due to impaired postsynaptic function as proposed by Clement et al. (2012).

SynGAP was first described as a RasGAP and most of its functions were thought to be mediated by its GAP activity, particularly the negative regulation of AMPAR trafficking to the postsynaptic membrane which mediates the altered synaptic plasticity observed in this model (J. H. Kim et al., 1998). However, in our GAP deletion rat model, we observed no SV recycling defects. This could suggest that the enhancement in SV endocytosis observed in *SynGAP1* full KO mouse hippocampal neurons is not mediated by the GAP domain as homozygous deletion of the SynGAP GAP domain does not alter SV endocytosis. Alternatively, this could also suggest a

species difference between mice and rats as the *SynGA1P* KO rat hippocampal neurons show no defects in SV recycling at either low or high frequency stimulation.

3.3.1. Species differences

As previously mentioned, the lack of effect of loss of SynGAP in rat KO neurons could suggest differing function of SynGAP across species. SynGAP may play different roles across species and may interact differently with other postsynaptic molecules which in turn could mediate the lack of SV endocytosis enhancement in hippocampal neurons. However, it would be highly unusual for a gene product to perform a completely different role within different mammalian systems.

It is important to note the KO of *SynGAP1* in each model was not generated the same way. The mouse model was created by deleting exons coding for the C2 and GAP domains and inserting stop codons and a neo-resistance cassette (Komiyama et al., 2002) whereas the rat was created using CRISPR/Cas9 technology to introduce a 2 bp deletion and 1 bp insertion at exon 8 introducing an early stop codon (Horizon Discovery, Saint Louis MO, USA). Although these models were generated in different ways, the loss of SynGAP has been verified by Western blotting in the mouse (Komiyama et al., 2002) and the rat (S. Basu, personal correspondence). SynGAP protein expression is down to 50% in Hets and absent in the KO. Although SynGAP expression levels have been studied extensively to characterise these models, it is possible that certain truncated portions of the proteins remain which may exert different effects on the synapse and neurotransmission and could underlie the differences observed across these models. To determine whether this is the case, an N-terminus-specific antibody to SynGAP could be used to detect the presence of a truncated protein.

Another possible explanation for why the enhanced SV endocytosis phenotype was absent in the rat could be the difference in critical periods between the two species (reviewed in Pressler and Auvin, 2013). SynGAP plays an important role in synapse formation during critical periods, particularly through accelerating maturation of dendritic spines (Aceti et al., 2015; Clement et al., 2012). Early during development (PND 7-9) there are no deficits in dendritic spine morphology or synaptic transmission in *SynGAP1* Het mice (Clement et al., 2012). Deficits only begin to appear at PND 14 where spines already have mature-like appearance (Clement et al., 2012). At PND 14 in *SynGAP1* Het mice there are fewer silent synapses (Rumbaugh et al., 2006) and there is altered neurotransmission (Clement et al., 2012). Interestingly these deficits did not persist through development. The more "mature synapse" phenotype was recovered by PND 60 when WT neurons reached maturity thus becoming comparable to the "prematurely aged" *SynGAP1* Het neurons (Aceti et al., 2015; Clement et al., 2012). Surprisingly, the altered mEPSC frequency and amplitude of *SynGAP1* het pyramidal neurons compared to WT observed at PND 14 is recovered by PND 21 as now WT spines and connectivity are more mature. Therefore, it appears that SynGAP is essential during this critical period. More support for this comes from work showing that conditional expression of *SynGAP1* in het animals during adulthood is not enough to rescue behavioural deficits (Clement et al., 2012).

The studies cited above have all examined these deficits in mice. It is possible that SynGAP has the same functions in rats, however the critical periods may be slightly shifted. A shift in critical periods could explain why there were no SV recycling deficits observed in both rat models (full KO and GAP deletion). It appears that loss of SynGAP is particularly important at PND 14. In our experiments, neurons were imaged at *DIV* 14 when synapse development has reached its peak (Kaech and Banker, 2006; Rao et al., 1998). This time point is roughly equivalent to this PND 14 developmental critical period, as it marks the peak of dendritic spine formation with dendritic spines just starting to form around the second week *in vitro* (Kaech and Banker, 2006).

The mEPSC amplitude and frequency deficits seen at PND 14 are absent at PND 7 and have been fully recovered by PND 21. This leaves a small window for this critical period. There is evidence to suggest that rat hippocampal neurons do not mature in the same way as mouse hippocampal neurons, at least in the case neurons arising from adult synaptogenesis (Snyder et al., 2009). It is therefore possible that the critical periods are subtly shifted between species in neuronal culture. If the critical period is indeed shifted, even by just a few days, it may explain why no enhanced SV endocytosis was seen in the rat model at *DIV* 13-15. It would be interesting to repeat these experiments in both mice and rats at both an earlier time-point such as *DIV* 10 and a later time-point such as *DIV* 21. As well as providing information on the role SynGAP plays in SV recycling, the results from these experiments could provide insight on synapse formation critical periods in rats.

3.3.2. Altered surface fraction

Cargo stranding at the plasma membrane surface can be due to multiple rounds of SV recycling occurring during stimulated or network activity in culture. It may also reflect a physiological cohort of cargo immediately available for retrieval distinct from the cargo released upon exocytosis of a specific SV (Fernandez-Alfonso et al., 2006; Hua et al., 2011). In *SynGAP1* KO hippocampal neurons we observed a decreased surface fraction of sypHy compared to WT levels. This could be due to the enhanced sypHy retrieval observed. If there is enhanced endocytosis, it may be expected that there is less sypHy on the plasma membrane or that the cargo is not present on the plasma membrane for as long before being retrieved to form new SVs. However, there was no defect in the extent of sypHy retrieval during low frequency stimulation, arguing against this explanation. Recent evidence suggests that the surface fraction of cargo proteins does not always correlate with deficits in SV recycling (Harper et al., 2017; Kaempf et al., 2015; Kononenko et al., 2013; Zhang et al., 2015). In fact, there can be more cargo stranded on the surface with faster endocytosis (Kaempf et al., 2015; Kononenko et al., 2013; Zhang et al., 2015).

Surface levels of cargo can also be unaltered when there is defective recycling (Harper et al., 2017; Kononenko et al., 2013). Thus, there is evidence that the surface stranding of SV cargo is independent of defective SV recycling.

Additionally, it is necessary to determine whether the amount of all SV cargo is decreased on the plasma membrane or whether this is sypHy-specific. Solely less sypHy on the membrane could suggest that there is more sypHy in newly-formed SVs. More synaptophysin on SVs would also lead to more recruitment of synaptobrevin-2 on SVs (Gordon et al., 2011; Gordon and Cousin, 2013; Gordon et al., 2016). This potential alteration in the composition of SVs could impair SV recycling through altered stoichiometry of SV proteins leading to altered interactions and recruitment of SV docking machinery. Conversely, a decrease in all SV cargo at the plasma membrane could be due to increased number of SVs within the nerve terminal depleting a limited stock of SV proteins (Wilhelm et al., 2014). Interestingly, increased SV number and pool size has been suggested to be a pathological feature in FXS (Deng et al., 2011), another condition which causes ASD, ID and epilepsy. The sypHy reporter does not provide an accurate estimate of SV numbers, since the signal is normalised to the total SV pool. SV pool size can be estimated with sypHy by depleting the recycling pool in the presence of bafilomycin and then estimating the remaining resting pool via addition of NH_4Cl (S. H. Kim and Ryan, 2013), thus stimulating neurons to depletion. Other optical approaches such as tracking SV numbers with FM dyes or morphological approaches will be required to conclusively determine alterations in absolute number of SVs inside nerve terminals (Deng et al 2011).

3.3.3. Lack of role of GAP domain

As previously suggested, the absence of effect of the deletion of the GAP domain on SV endocytosis could be due to species differences across mice and rats, as full KO of *SynGAP1* in the rat does not show any impaired SV recycling. However, it may

also be the case that the GAP domain does not mediate the role that SynGAP plays in SV recycling.

The N-terminal portion of SynGAP contains its GAP domain containing both a PH and C2 domain (J. H. Kim et al., 1998). SynGAP functions as a GAP that can negatively regulate Ras and Rap GTPases (Chen et al., 1998; Krapivinsky et al., 2004; Pena et al., 2008). The RasGAP activity of SynGAP can also regulate F-actin which is a major component of stable dendritic spines (Bar et al., 2016). In the absence of SynGAP there is no longer any negative modulatory effect on F-actin. Increased levels of F-actin can, in part, be responsible for the earlier time course of dendritic spine maturity observed in *SynGAP1* Het neurons. F-actin is also required for clustering SV proteins to the presynaptic membrane (Dason et al., 2014). Increasing the amount of F-actin could therefore increase clustering of SV proteins on the plasma membrane allowing them to be more readily retrieved during endocytosis and thus mediating accelerated SV retrieval.

Furthermore, together with the C2 domain, the GAP domain of SynGAP can take on a RapGAP role (Krapivinsky et al., 2004; Pena et al., 2008). Dephosphorylation activates SynGAP RapGAP activity which in turn inactivates Rap. With Rap inactivated, there is no activation of p38 MAPK which mediates AMPAR trafficking from the postsynaptic membrane (Krapivinsky et al., 2004; Rumbaugh et al., 2006; Zhu et al., 2002). SynGAP can mediate synaptic plasticity by preventing the removal of AMPAR from synapses. With the loss of SynGAP, there is no longer inactivation of Rap. This leads to increased p38 MAPK activity and removal of AMPAR from the postsynaptic membrane. Activation of the MAPK/ERK pathway can lead to increased phosphorylation of synapsin (Giachello et al., 2010) which may in part mediate any presynaptic defects observed in this model.

However, SynGAP is not just a GAP, it has other functions in the synapse. The C-terminus of SynGAP contains a PDZ-domain ligand that mediates its binding to the PDZ domains of PSD-95 (J. H. Kim et al., 1998). SynGAP can competitively bind all three slots of PSD-95, thus preventing other molecules, including TARP complexes, from binding (Opazo et al., 2012; Walkup et al., 2016). SynGAP can thus alter synaptic strength by limiting the binding of AMPAR complexes to the plasma membrane. SynGAP can also prevent the cell-adhesion molecules LRRTMs and neuroligins from binding the PDZ domains of PSD-95. This is particularly important as it is through these molecules and their interactions with the presynaptic protein neurexin that synapses are formed (Graf et al., 2004; Levinson et al., 2005; Scheiffele et al., 2000). The deletion of *SynGAP1* could therefore alter synapse composition and impair SV recycling.

Based on the results from our experiments, we cannot conclude whether the GAP domain mediates the presynaptic SV recycling defect observed. However, as outlined above, the GAP domain may indirectly play a role in SV recycling through the activation of other important presynaptic molecules involved in SV recycling including F-actin and synapsin.

There seems to be some redundancy across both major functions of SynGAP as it appears that both the GAP function and structural function of can mediate AMPAR localisation at the postsynapse which in turn mediates synaptic plasticity. Thus, it will be important to use both the *SynGAP1 GAP* deletion and the full deletion models to determine how SynGAP can mediate synaptic strength and transmission.

3.3.4. Potential mechanisms for acceleration of SV endocytosis

The observed acceleration of SV endocytosis in *SynGAP1* KO neurons, specifically during low frequency stimulation, could be due to different underlying mechanisms.

Because SynGAP is highly abundant in the PSD (Cheng et al., 2006), it can bind to approximately 10-15% of the PDZ domains of PSD-95 where it then determines synaptic composition (Walkup et al., 2016). Because of the 50 % decrease in protein levels duet to haploinsufficiency (Vazquez et al., 2004), SynGAP can no longer bind to as many PSD-95 PDZ domains and thus the composition of the synapses is altered (Walkup et al., 2016). In agreement, there is significantly increased binding of TARP, LRRTM-2, and neuroligin-2 to PSD-95, in PSD fractions from *SynGAP1* Het neurons (Walkup et al., 2016). Of particular interest to this work is the increased binding of the postsynaptic cell adhesion molecules LRRTM2 and neuroligin-2. Altering the binding of both these proteins to PSD-95 may have varying effects on synaptic development and strength.

LRRTMs are postsynaptic proteins that can bind PSD-95 through their cytoplasmic C-tail (Hung and Sheng, 2002), and presynaptic neurexins through their leucine-rich extracellular domains (Paatero et al., 2016). LRRTM-2 is predominantly expressed in the hippocampus (Lauren et al., 2003). Knocking-down LRRTM-2 in cultured neurons was found to decrease the number of excitatory synapses (de Wit and Ghosh, 2014). Although LRRTMs are postsynaptic proteins they have powerful synaptogenic effects. Expressing LRRTMs in non-neuronal cells elicited artificial synapse formation in the axons of co-cultured neurons including clustering of presynaptic proteins such as synaptophysin and bassoon on contacting axons (Linhoff et al., 2009; Siddiqui et al., 2013). It is through its binding to neurexin that LRRTM-2 mediates excitatory synapse development (Siddiqui et al., 2010).

Like LRRTM, neuroligin-2 has strong neurogenic effects. In co-culture assays, neuroligin-2 was found to induce the formation of presynaptic structures in contacting axons. These presynaptic structures included both gamma-aminobutyric acid (GABA)ergic and glutamatergic SVs which could undergo turnover (Graf et al., 2004; Scheiffele et al., 2000). Although neuroligin-2 is localised at inhibitory synapses, increasing PSD-95 levels can alter the distribution of neuroligin-2,

possibly through mediating its binding to the PDZ domain of PSD-95, allowing for more molecules to be associated with excitatory synapses (Levinson et al., 2005).

LRRTM-2 and neuroligin-1 bind to an overlapping region of neurexin and thus both cannot bind the same neurexin molecule (Siddiqui et al., 2010). However, these postsynaptic proteins can cooperate in an additive manner to recruit neurexin to form new glutamatergic synapses (Siddiqui et al., 2010). Neurexins play important roles in the presynapse (reviewed in Reissner et al., 2013). Most importantly, knocking-out the neurexin-1α isoform has been shown to impair spontaneous neurotransmitter release (Etherton et al., 2009), whereas knocking-out more isoforms also impairs evoked release (Kattenstroth et al., 2004; Missler et al., 2003).

It is therefore possible that postsynaptic SynGAP can exert an effect on presynaptic activity through modulating PSD composition. The SV recycling deficits observed with the loss of SynGAP, could be mediated by increased recruitment of neurexins to synapses by LRRTM-2 and neuroligin-2. This could be tested by knocking-down neurexin in *SynGAP1* KO cultures and seeing whether this can rescue the accelerated endocytosis observed in these neurons.

3.3.5. Limitations in experimental design

Our results suggest a novel role for SynGAP in mediating presynaptic activity at low frequency stimulation in mice however, there are still certain limitations of this work that need to be addressed.

We saw enhanced sypHy retrieval at low frequency stimulation in *SynGAP1* KO hippocampal neurons compared to WT littermate controls. Synaptophysin is an important abundant component of SVs, however to ensure that it is endocytosis in

general that is affected by loss of SynGAP, it would be important to repeat this experiment with a different synaptic pHluorin to ensure that it is not just synaptophysin retrieval that is defective in this model.

Additionally, it would be important to determine whether this enhanced SV endocytosis observed is due solely to enhanced endocytosis or whether it is compensation for increased exocytosis. It can be difficult to determine whether SV deficits are due to exocytic or endocytic defects as these two processes are tightly coupled. Endocytosis can start to occur during exocytosis particularly during the long stimulus train we used to elicit this effect (10 Hz 30 s) (Sankaranarayanan and Ryan, 2000). Using the vacuolar-type H^+-ATPase proton pump blocker, Bafilomycin A1 it is possible to dissociate these two processes during pHluorin imaging to isolate exocytosis. Bafilomycin A1 prevents reacidification of the vesicles after endocytosis, therefore once the pHluorin is within the vesicle, its fluorescence can no longer be quenched. This allows each SV fusing to only be monitored once (Sankaranarayanan and Ryan, 2000). It would be important to use Bafilomycin A1 to examine exocytosis in this model to determine whether the enhanced endocytosis is a homeostatic compensatory effect.

SynGAP is localised in the PSD of excitatory neurons (Chen et al., 1998; J. H. Kim et al., 1998). Although it may alter inhibitory neurotransmission through compensatory mechanisms (Clement et al., 2012) there is no evidence that SynGAP is localised in inhibitory neurons. In dissociated hippocampal cultures, there are various hippocampal cell-types including excitatory glutamatergic pyramidal neurons and inhibitory GABAergic interneurons. It is possible that some neurons sampled were inhibitory and thus *SynGAP1* KO may not have a direct effect on a cell-type where it is not expressed. Although these different cell-types can be distinguished based on morphology, it would be interesting to repeat these experiments looking solely at excitatory hippocampal neurons. This could be done by labelling neurons with vesicular GABA transporter (vGAT)- and vGLUT-oyster (as inhibitory and

excitatory markers respectively) during live-cell imaging to determine whether the effect of loss of SynGAP is excitatory synapse-specific (Petrini et al., 2014; Smith et al., 2012).

SypHy is a good reporter of CME (Granseth et al., 2006) which is the dominant endocytic pathway in hippocampal neurons at low frequency stimulation at room temperature (Granseth et al., 2006). However, there are other endocytic modes that cannot be reported by sypHy, particularly ADBE (Nicholson-Fish et al., 2015). ADBE is elicited after strong stimulus trains such as 50 Hz 6 s and 40 Hz 10 s (Clayton et al., 2008). ADBE can be monitored using labeled-dextrans or VAMP4-pH. Both reporters can report the number of nerve terminals undergoing ADBE in neuronal cultures. Additionally, horseradish peroxidase (HRP) uptake assays can determine how much ADBE is occurring in each nerve terminal. As different modes of endocytosis are all independent and require different molecules, it would be interesting to see if ADBE is affected by loss of SynGAP in future.

Overall, these experiments suggest a novel activity-dependent role of SynGAP in SV recycling. Furthermore, this novel role in SV endocytosis provides a new target for developing treatments for *SYNGAP1* haploinsufficiency, the leading genetic cause of ID and ASD (Jeyabalan and Clement, 2016).

4. Characterisation of SV recycling defects in rodent models of FXS

4.1. Introduction

Loss of FMRP results in FXS, which is a leading monogenic cause of ID and ASD (Mefford et al., 2012). FMRP is expressed throughout the brain (Gholizadeh et al., 2015) with peak expression within the first postnatal week in rodents. FMRP levels then decrease and reach a plateau in adulthood (Till et al., 2012; Till et al., 2015; Gholizadeh et al., 2015) Loss of FMRP disrupts synaptic plasticity (Harlow et al., 2010) and synapse formation during critical periods (Doll et al., 2017).

FMRP's main role is repressing protein translation of a subset of mRNAs, downstream of Group1 mGluRs, through polyribosome stalling (Darnell et al., 2011). In the absence of FMRP, there is no negative regulation of protein translation and the translation of Group1 mGluR-associated transcripts is upregulated (Dolen and Bear, 2009). The levels of several presynaptic and postsynaptic proteins are altered with the loss of FMRP (Zalfa et al., 2003; Osterweil et al., 2010; Darnell and Klann, 2013) which may in part mediate the synaptic defects observed in various models of FXS.

FXS is a synaptopathy, a disorder of the synapse. The loss of FMRP has been widely studied in the postsynapse, including its impact on spine morphology and dynamics (Cruz-Martin et al., 2010; Comery et al., 1997; Irwin et al., 2000; Galvez and Greenough, 2005; Levenga et al., 2011; Wijetunge et al., 2014), mGluR-LTD (Huber et al., 2002), and postsynaptic protein translation (Darnell and Klann, 2013). However, there is also evidence for a presynaptic role of FMRP, as there is faster synaptic vesicle recycling in *Fmr1* KO mouse hippocampal neurons as determined by faster FM1-43 unloading kinetics (Deng et al., 2011). These neurons also have a

larger RRP and a larger reserve pool compared to WT littermate controls (Deng et al., 2011). Furthermore knocking-down FMRP in dorsal root ganglion (DRG) neurons and hippocampal neurons enhances SV exocytosis during high frequency stimulation (Ferron et al., 2014).

Presynaptic defects observed in models of FXS are thought to be due to non-canonical roles of FMRP, despite 30.4% of presynaptic proteome mRNA transcripts being bound by FMRP. FMRP can also directly bind presynaptic ion channels (reviewed in Ferron, 2016) including Slack channels (Brown et al., 2010), N-type calcium channels (Ferron et al., 2014) and BK channels (Deng et al., 2013; Deng and Klyachko, 2016). FMRP can modulate synaptic strength through binding the regulatory subunit of BK channels to modulate their gating. Indeed, the BK channel's calcium-sensitivity is reduced in *Fmr1* KO neurons (Deng et al., 2013).

Thus, FMRP plays multiple pre-and post-synaptic roles in synapse and circuit formation and neurotransmission which may underlie the cognitive and behavioural deficits seen in FXS.

The aims of this work were to characterise SV recycling defects in both CME and ADBE in preclinical models of FXS. We first wanted to replicate previous findings that suggested altered SV recycling through the CME pathway (Deng et al., 2011; Ferron et al., 2014). We also wanted to establish whether FMRP could perform a direct role in SV recycling.

4.2. Results

4.2.1. No SV exocytosis or endocytosis deficits in Fmr1 KO mouse hippocampal neurons

FMRP is found in the presynapse (Christie et al., 2009; Akins et al., 2012) and regulates the translation of a third of the presynaptic proteome (Darnell et al., 2011) including SV recycling-related proteins such as dyn1. There is also evidence that FMRP plays a role in SV recycling, as FMRP KD in DRG neurons leads to increased exocytosis at higher frequency stimulation without any change in SV endocytosis rate (Ferron et al., 2014). Furthermore, SV turnover has been found to be faster in *Fmr1* KO hippocampal neurons (Deng et al., 2011).

Because of this evidence suggesting loss of FMRP may alter SV recycling, we decided to investigate this role further in order to establish a molecular mechanism. We started by using sypHy as a reporter of SV recycling. We first examined exocytosis, as there is evidence for increased exocytosis with FMRP KD (Ferron et al., 2014). Dissociated hippocampal neurons from *Fmr1* KO mice and WT littermate controls were stimulated with a train of low frequency APs (10 Hz 30 s, Figure 4.1). SypHy fluorescence traces were normalised to the total SV pool to measure the amount of exocytosis as a proportion of the total SV pool (Figure 4.1b, d). There was no significant difference (Student t-test n.s. $p > 0.05$) between KO (0.300 ± 0.030 units, n=16) and WT (0.342 ± 0.024 units, n=15). Thus, the loss of FMRP does not affect exocytosis during low frequency stimulation.

We used this low-frequency stimulation paradigm to determine whether CME, the dominant endocytic mode in these conditions (Granseth et al., 2006), was impaired in this model. SypHy fluorescence traces were normalised to the peak of stimulation so that CME kinetics could be compared across genotypes (Figure 4.1c). There was no significant difference between KO and WT fluorescence traces (2-way ANOVA, n.s. $p> 0.05$). Furthermore, the sypHy retrieval time constants, τ, were not different (Student t-test n.s. $p> 0.05$) between KO (25.44 ± 2.51 s, n=16) and WT ($32.62 \pm$

4.15 s, n=15) (Figure 4.1e). Therefore, the loss of FMRP does not impair endocytosis at low frequency stimulation.

There is evidence suggesting increased SV exocytosis at high frequency stimulation in hippocampal neurons with FMRP KD (Ferron et al., 2014). Additionally, the loss of FMRP has been found to enhance synaptic responses to high-frequency stimulation (Deng et al., 2011). Therefore, we next examined the effect of high-frequency stimulation (50 Hz 6 s) on SV recycling kinetics in *Fmr1* KO hippocampal cultures and WT controls (Figure 4.2). SypHy fluorescence traces were normalised to the total SV pool as revealed by NH_4Cl buffer to examine the amount of exocytosis that occurred during stimulation as a proportion of the total SV pool (Figure 4.1b, d). There was no difference (Student t-test n.s. $p > 0.05$) between KO (0.463 ± 0.035 units, n=17) and WT (0.431 ± 0.035 units, n=17). Taken together with the results from Figure 4.1, this suggests that the complete loss of FMRP does not affect SV exocytosis during either low- or high-frequency stimulation.

We then went on to examine SV endocytosis after high-frequency stimulation (Figure 4.2c, e) as faster SV recycling has been observed in *Fmr1* KO hippocampal neurons (Deng et al., 2011). There was no significant difference in sypHy fluorescence traces across genotypes (2-way ANOVA n.s. $p> 0.05$). There was also no difference in sypHy τ (Figure 4.2e, Student t-test n.s. $p > 0.05$) between KO (37.44 ± 5.11.s, n=17) and WT (44.71 ± 7.11 s, n=17). Taken together with the endocytosis findings in Figure 4.1, this suggests that loss of FMRP does not alter sypHy retrieval, and by extension SV endocytosis, at either low or high frequency stimulation. Taken all together, it appears that deletion of *Fmr1* does not play a role in SV recycling under these conditions.

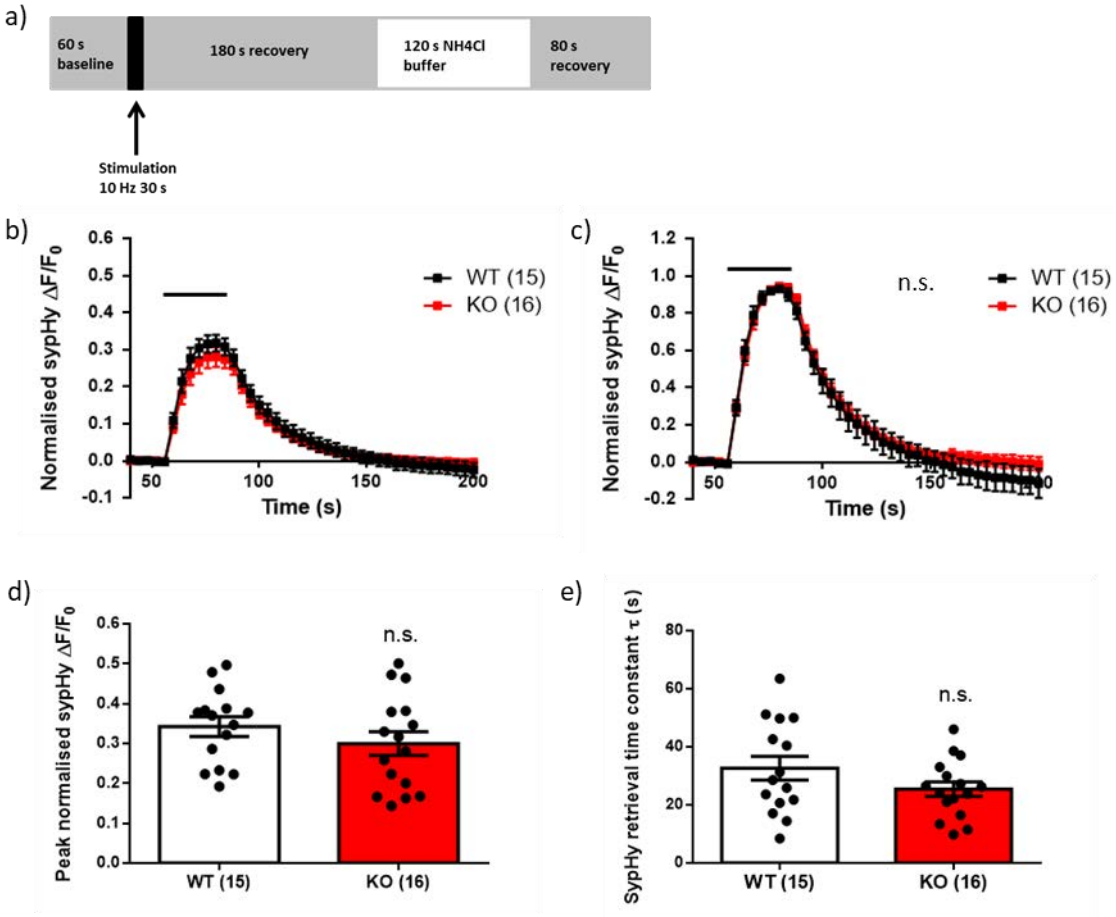

Figure 4.1 No difference in exocytosis or sypHy retrieval at low frequency stimulation (10 Hz 30 s)

Hippocampal neurons derived from Fmr1 KO mice and WT littermate controls were transfected with sypHy on DIV 7 and imaged DIV 13-15. a) Time course of experiment. b-c) Mean sypHy fluorescence traces of WT (white) and KO (red) hippocampal neurons. Bars indicate the period of stimulation, 10 Hz 30 s. b) normalised to the total vesicle number as revealed by NH_4Cl. c) normalised to the peak of stimulation. 2-way ANOVA n.s. $p > 0.05$. d) Mean and individual stimulation peak heights obtained from individual sypHy traces of data in b). e) Mean and individual sypHy retrieval time constants (τ) of data plotted in c). d-e) n.s. non-significant $p > 0.05$ by Student t-test.
Experimental n shown in brackets, error bars in all panels ± SEM.

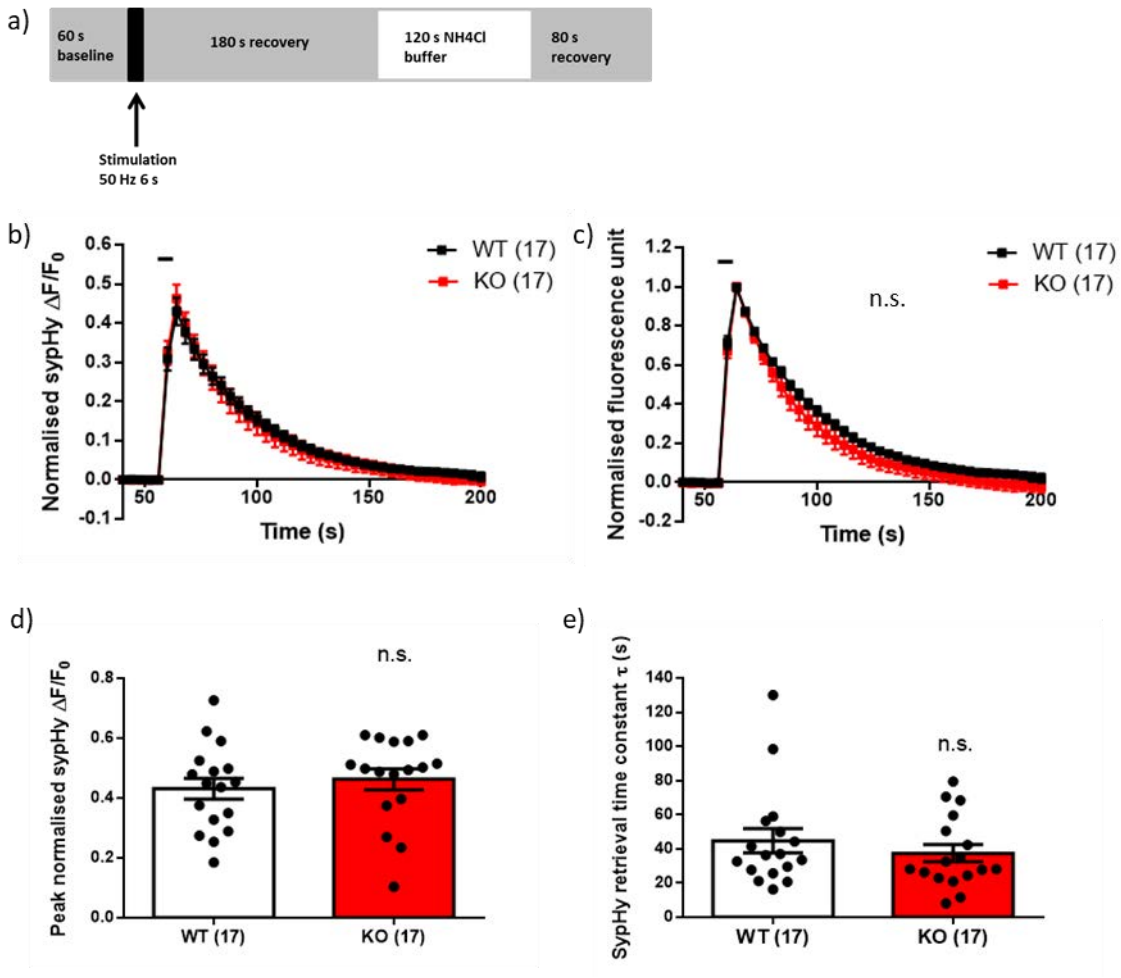

Figure 4.2 No difference in exocytosis or sypHy retrieval at high frequency stimulation (50 Hz 6 s)

Hippocampal neurons derived from Fmr1 KO mice and WT littermate controls were transfected with sypHy on DIV 7 and imaged DIV 13-15. a) Time course of experiment. b-c) Mean sypHy fluorescence traces of WT (white) and KO (red) hippocampal neurons. Bars indicate the period of stimulation, 10 Hz 30 s. b) normalised to the total SV number as revealed by NH_4Cl. c) normalised to the peak of stimulation; 2-way ANOVA non-significant n.s. p> 0.05. d) Mean and individual stimulation peak heights obtained from individual sypHy traces of data in b). e) Mean and individual sypHy retrieval time constants (τ) of data plotted in c). d-e) n.s. non-significant p > 0.05 by Student t-test.
Experimental n shown in brackets, error bars in all panels ± SEM.

4.2.2. No SV exocytosis deficits in immature Fmr1 KO mouse hippocampal neurons

Like SynGAP, FMRP plays an important role in synapse maturation and refinement during critical periods of circuit development (Doll et al., 2017; Harlow et al., 2010). FMRP expression in the brain peaks during the first postnatal week in mice and rats and expression levels decrease then plateau in adulthood (Till et al., 2012; Till et al., 2015). We decided to examine SV exocytosis at *DIV* 7, at peak FMRP expression (Figure 4.3), with either low or high frequency stimulation (Figure 4.3a). This was to ensure that the absence of SV exocytosis phenotypes in Figures 4.1 and 4.2 was not due to low expression levels of FMRP in *DIV* 13-15 WT hippocampal neurons masking any differences between KO and WT. SypHy fluorescence traces were normalised to NH_4Cl peak height (Figure 4.3b, d) to quantify exocytosis as a proportion of total SV pool. At low-frequency stimulation (10 Hz 30 s, Figure 4.3c), there was no difference (Student t-test n.s. $p > 0.05$) between KO (0.301 ± 0.018 units, n=3) and WT (0.377 ± 0.050 units, n= 4). Therefore, loss of FMRP during peak expression does not impair SV exocytosis at low frequency stimulation.

We also challenged the cells with a higher intensity stimulus load (50 Hz 6 s, Figure 4.3d-e) and again saw no difference (Student t-test n.s. $p> 0.05$) between KO (0.439 ± 0.088 units, n=3) and WT hippocampal neurons (0.432 ± 0.059 units n=3). Thus, there are no defects in SV exocytosis during high frequency stimulation in immature hippocampal neurons lacking FMRP. Taken together, this suggests that loss of FMRP does not impact SV recycling at either low or high frequency stimulation in developing hippocampal neurons in culture under our experimental conditions.

4.2.3. No defects in evoked synaptic calcium concentrations in Fmr1 KO mouse hippocampal neurons

FMRP can directly bind to $Ca_v2.2$ (N-type) calcium channels and modulate their density on the plasma membrane. Ferron et al. (2014) proposed that the increased SV exocytosis seen with shRNA-mediated FMRP is KD in DRG neurons is mediated by

the interaction of FMRP with these presynaptic channels. When FMRP is knocked-down, more channels can be inserted into the membrane which in turn increases calcium current density (Ferron et al., 2014). Increased calcium influx through N-type and P/Q-type voltage-gated calcium channels can also be observed in mouse *Fmr1* KO hippocampal neurons especially with high-frequency stimulation (Deng et al., 2011).

We decided to look at presynaptic calcium concentration during our two different stimulation paradigms because of the altered calcium influx previously reported with loss of FMRP (Deng et al., 2011; Deng et al., 2013; Ferron et al., 2014). We first used the genetically encoded reporter GCaMP6f (Chen et al., 2013) due to its fast kinetics, low calcium affinity (K_d: 375 ± 14 nM) and broad dynamic range compared to other transfected reporters (Akerboom et al., 2012; Chen et al., 2013). We first examined the change in intracellular free calcium concentration ($[Ca^{2+}]_i$) during low frequency stimulation (Figure 4.4b-c). There was no difference in peak GCaMP6f fluorescence during stimulation (Student t-test n.s. $p > 0.05$) between KO (2.919 ± 0.440 units, n=8) and WT (2.343 ± 0.400 units, n =8). Thus, there is no difference in evoked presynaptic $[Ca^{2+}]_i$ across genotypes at low frequency stimulation.

As exaggerated calcium influx was primarily observed during high-frequency stimulation (Deng et al., 2011; Deng et al., 2013; Ferron et al., 2014), we went on to compare evoked presynaptic $[Ca^{2+}]_i$ responses between *Fmr1* KO and WT littermate control neurons during high-frequency stimulation (Figure 4.4d-e). There was no difference in the evoked presynaptic $[Ca^{2+}]_i$ response between genotypes (Student t-test n.s. $p>0.05$, KO: 5.724 ± 0.350 units, n= 8; WT: 7.776 ± 1.186 units, n=7, Figure 4.4e), Therefore, loss of FMRP does not alter $[Ca^{2+}]_i$ during high-frequency stimulation.

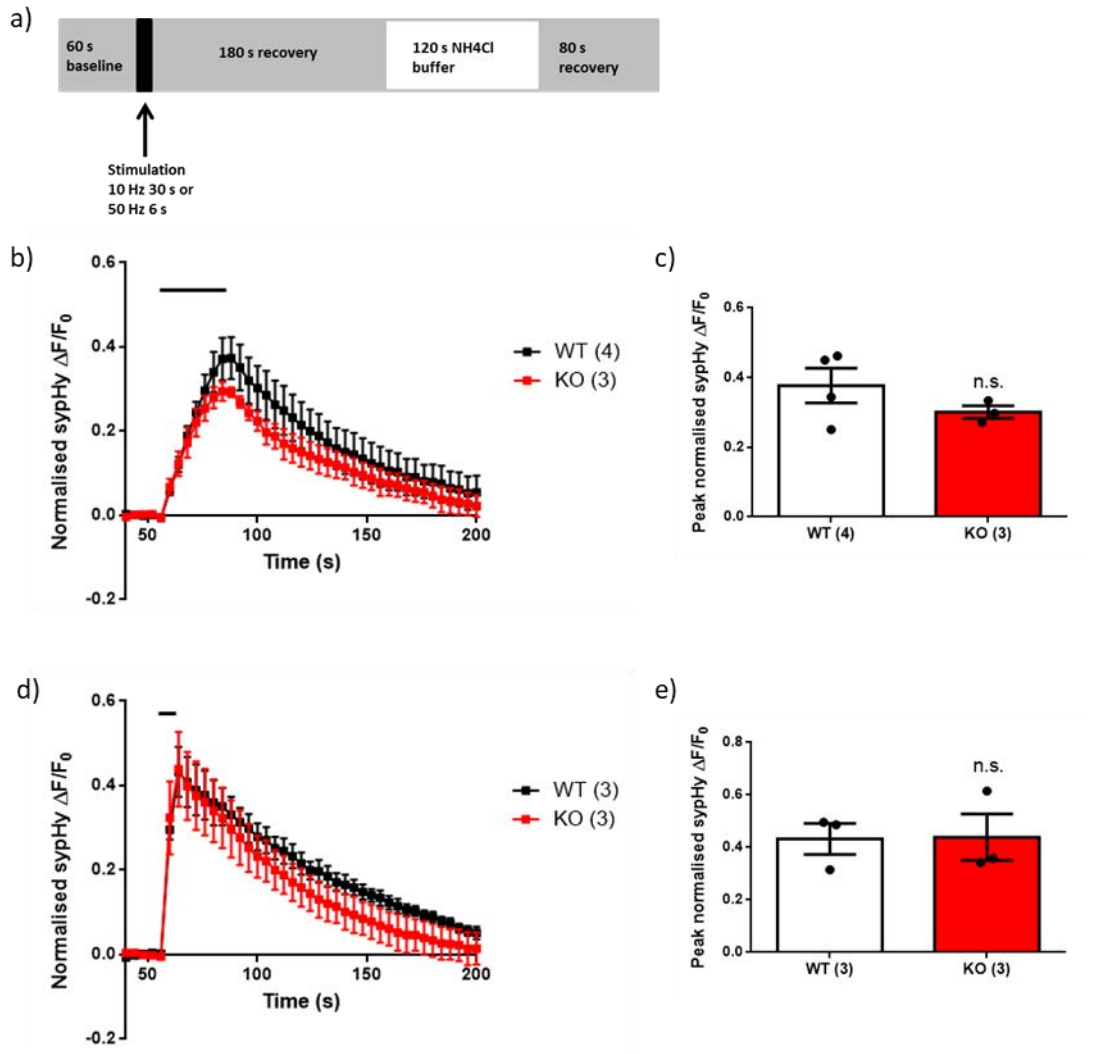

Figure 4.3 No difference in exocytosis at low or high frequency stimulation at DIV 7

Hippocampal neurons derived from Fmr1 KO mice and WT littermate controls were transfected with sypHy on DIV 3 and imaged at DIV 7. a) Time course of experiment. b) Mean sypHy fluorescence traces of WT (white) and KO (red) hippocampal neurons normalised to the total SV number as revealed by NH4Cl. Bar indicates period of stimulation (10 Hz 30 s) c) Mean and individual stimulation peak heights obtained from individual sypHy traces of data in b). d) Mean sypHy fluorescence traces of WT and KO hippocampal neurons normalised to the total vesicle number as revealed by NH_4Cl. Bar indicates period of stimulation (50 Hz 6 s). e) Mean and individual sypHy retrieval time constants (τ) of data plotted in d). Student t-test n.s. non-significant $p > 0.05$.
Experimental n shown in brackets, error bars in all panels ± SEM.

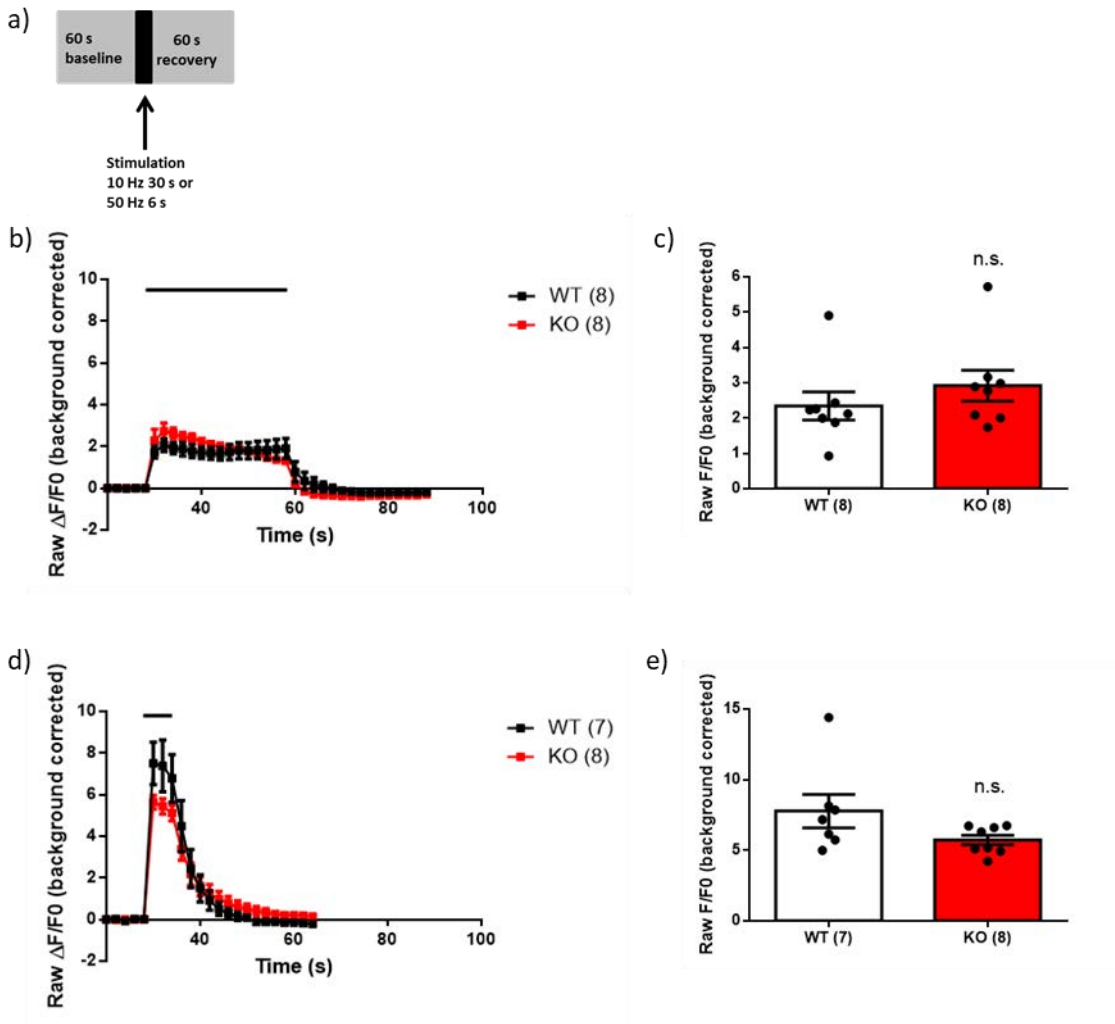

Figure 4.4 No difference in evoked presynaptic [Ca^{2+}]i using GCaMP6f

Hippocampal neurons derived from Fmr1 KO mice and WT littermate controls were transfected with GCaMP6f on DIV 7 and imaged DIV 13-15. a) Time course of experiment. b) Mean GCaMP6f fluorescence traces of WT (white) and KO (red) hippocampal neurons in response to 10 Hz 30 s stimulation. Bar indicates duration of stimulation. c) Mean and individual stimulation peak heights obtained from individual GCaMP6f traces of data in b). d) Mean GCaMP6f fluorescence traces of WT and KO hippocampal neurons in response to 50 Hz 6 s stimulation. Bar indicates duration of stimulation. e) Mean and individual stimulation peak heights obtained from individual GCaMP6f traces of data in d). n.s. p > 0.05 by Student t-test
Experimental n shown in brackets, error bars in all panels ± SEM

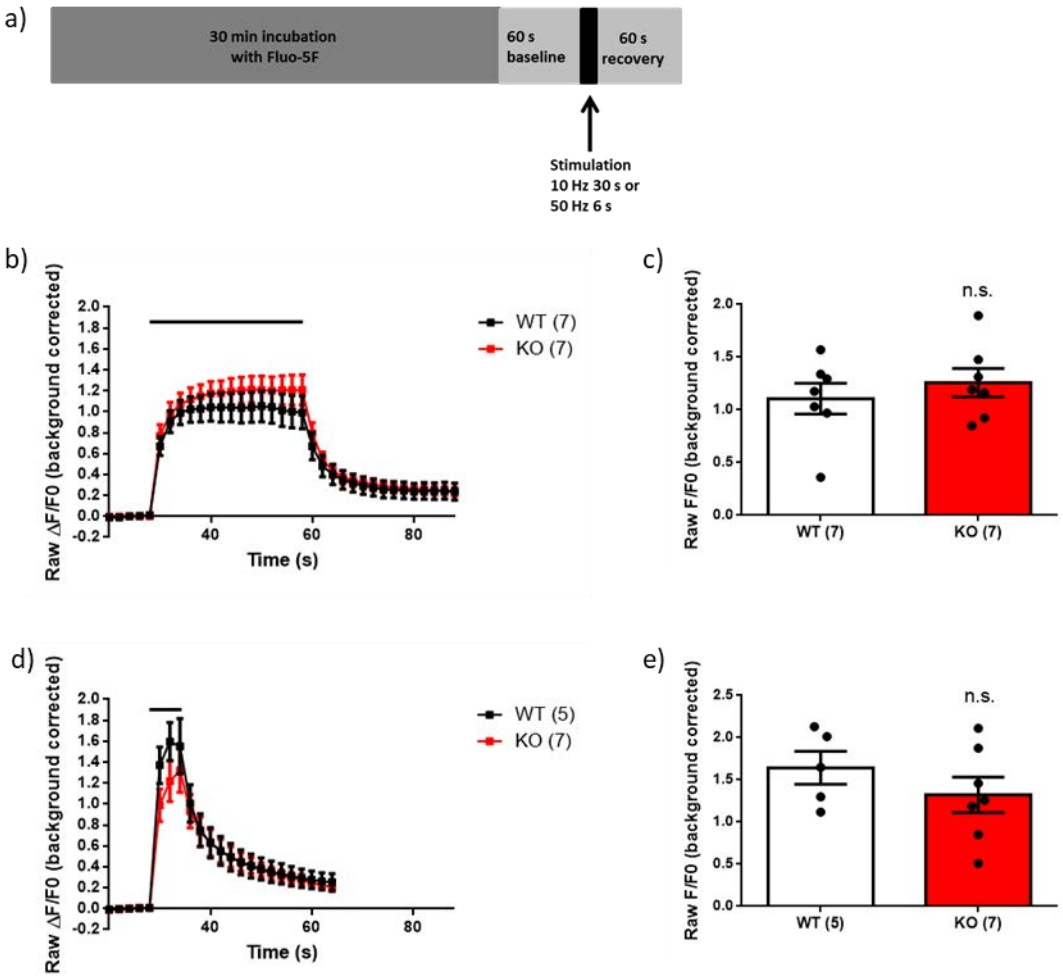

Figure 4.5 No difference in evoked presynaptic $[Ca^{2+}]i$ using Fluo-5F

Hippocampal neurons derived from Fmr1 KO mice and WT littermate controls were incubated in 10 μM Fluo-5F at room temperature for 30 min prior to imaging at DIV 13-15. a) Time course of experiment. b) Mean Fluo-5F fluorescence traces of WT (white) and KO (red) hippocampal neurons in response to 10 Hz 30 s stimulation. Bar indicates duration of stimulation. c) Mean and individual stimulation peak heights obtained from individual Fluo-5F traces of data in b). d) Mean Fluo-5F fluorescence traces of WT and KO hippocampal neurons in response to 50 Hz 6 s stimulation. Bar indicates duration of stimulation. e) Mean and individual stimulation peak heights obtained from individual Fluo-5F traces of data in d). n.s. non-significant $p > 0.05$ by Student t-test.
Experimental n shown in brackets, error bars in all panels ± SEM.

We also used Fluo-5F, a fluorescent calcium-reporter dye (Scott and Rusakov, 2006), to examine changes in $[Ca^{2+}]_i$, as it has lower calcium affinity (K_d: ~2.3 μM) and would not saturate as readily as GCaMP6f during high frequency stimulation to allow $[Ca^{2+}]_i$ to be monitored across a broader dynamic range. Once again, we examined the $[Ca^{2+}]_i$ response across genotypes using either a low frequency (Figure 4.5b-c) or high frequency (Figure 4.5d-e) stimulation paradigm. We found no difference in peak Ca^{2+} fluorescence at low frequency stimulation using Fluo-5F (Student t-test n.s. $p > 0.05$, Figure 4.5c) KO (1.259 ± 0.134 units, n=7) and WT (1.106 ± 0.146 units, n=7). There was also no difference at high frequency stimulation (Student t-test n.s. $p>0.05$, Figure 4.5e) between KO (1.321 ± 0.210 units, n=7) and WT (1.642 ± 0.196 units, n=5). Thus, loss of FMRP does not affect the presynaptic $[Ca^{2+}]_i$ response to action potential stimulation.

4.2.4. No effect of FMRP KD on SV exocytosis

The increased exocytosis previously described in neurons with FMRP KD was reported with vGLUT-pH (Ferron et al., 2014). We therefore investigated whether we could replicate the increased SV exocytosis phenotype observed in FMRP KD hippocampal results from Ferron et al. (2014). *Fmr1* KO mouse hippocampal neurons and WT littermate controls were transfected with vGLUT-pH and either shRNA against FMRP (shFMRP) or the scrambled shRNA vector (shScr). *Fmr1* KO neurons do not contain any FMRP, however they were also transfected to determine if there were any off-target effects of the shRNA. Hippocampal neurons were stimulated at high frequency (60 Hz 5 s) to mimic the previously published experimental conditions and SV exocytosis was measured (Figure 4.6). There was no difference in SV exocytosis peak heights across all conditions (1-way ANOVA n.s. $p > 0.05$) WT shFMRP (0.435 ± 0.090 units, n=6), WT scr (0.434 ± 0.035 units, n=6), KO shFMRP (0.418 ± 0.048 units, n=10) and KO scr (0.389 ± 0.053 units, n=8). Thus, knocking-down FMRP has no effect on SV exocytosis during high frequency stimulation.

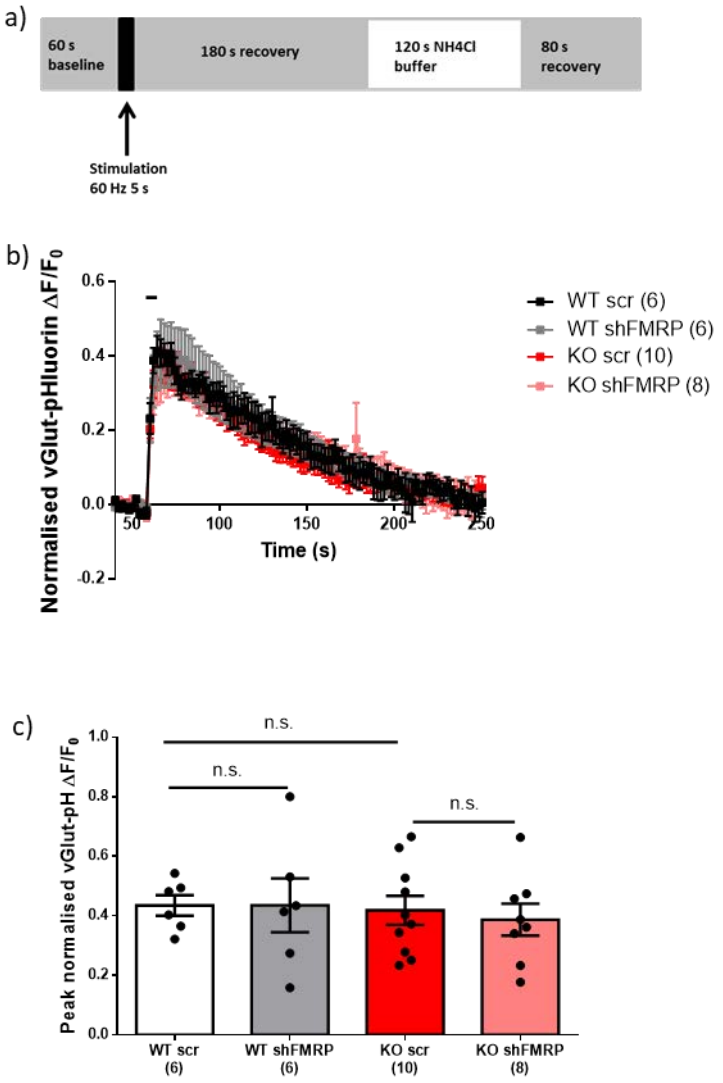

Figure 4.6 No difference in amount of SV exocytosis at high frequency stimulation (60 Hz 5 s) with FMRP KD

Hippocampal neurons derived from Fmr1 KO mice and WT littermate controls were transfected with vGlut-pH and either shFMRP or scrambled vector 4 days prior to imaging and imaged DIV 13-15. a) Time course of experiment, imaging frames were acquired at 2 s intervals. b) Mean vGlut-pH fluorescence traces of WT neurons transfected with scrambled vector (WT scr, white), WT neurons transfected with shFMRP (WT shFMRP, grey), KO neurons transfected with scrambled vector (KO scr, red) and KO neurons transfected with shFMRP (KO shFMRP, pink) normalised to the total SV number as revealed by NH_4Cl. Bar indicates period of stimulation (60 Hz 5 s). c) Mean and individual stimulation peak heights obtained from individual vGlut-pHluorin traces of WT and KO transfected hippocampal neuron data in b). n.s. non-significant $p > 0.05$ 1-way ANOVA with Bonferroni multiple comparisons test.
Experimental n shown in brackets, error bars in all panels ± SEM.

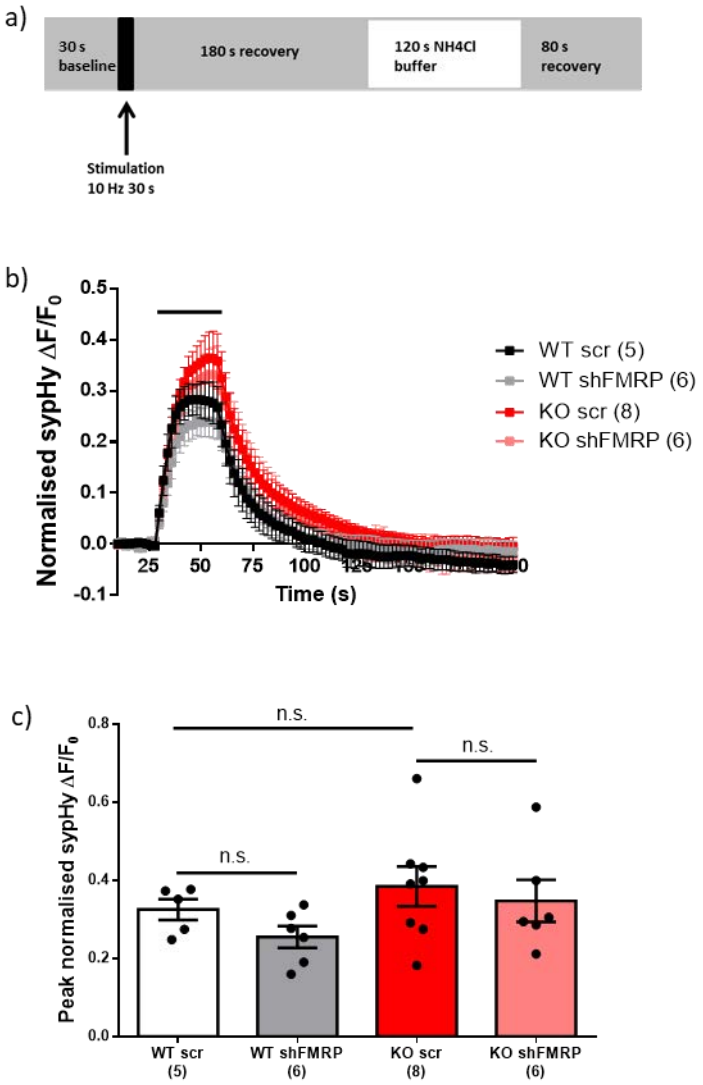

Figure 4.7 No difference in amount of SV exocytosis at low frequency stimulation (10 Hz 30 s) with KD of FMRP at physiological temperature

Hippocampal neurons derived from Fmr1 KO mice and WT littermate controls were transfected with sypHy and either shFMRP or scrambled vector 4 days prior to imaging and imaged DIV 13-15. a) Time course of experiment, imaging frames were acquired at 2 s intervals. b) Mean sypHy fluorescence traces of WT neurons transfected with scrambled vector (WT scr, white), WT neurons transfected with shFMRP (WT shFMRP, grey), KO neurons transfected with scrambled vector (KO scr, red) and KO neurons transfected with shFMRP (KO shFMRP, pink) normalised to the total SV number as revealed by NH_4Cl. Bar indicates period of stimulation (10 Hz 30 s). c) Mean and individual stimulation peak heights obtained from individual sypHy traces of WT and KO hippocampal neuron data in b). n.s. non-significant $p > 0.05$ 1-way ANOVA Bonferroni multiple comparisons test. Experimental n shown in brackets, error bars in all panels ± SEM.

One potential reason for the discrepancy with the work of Ferron et al. (2014) was that their imaging studies were performed at near-physiological temperature (30°C). We therefore also examined SV exocytosis with FMRP KD at physiological temperature (37°C, Figure 4.7). In this case we used sypHy as the reporter, so the pHluorin kinetics would be comparable to previous data (Figure 4.1). Dissociated hippocampal neurons from *Fmr1* KO or WT littermate controls were transfected with sypHy and either shFMRP or shScr. Neurons were stimulated at 10 Hz 30 s and peak amount of exocytosis during stimulation was quantified. There was no difference across conditions (1-way ANOVA n.s. $p > 0.05$; WT shFMRP 0.255 ± 0.028 units, n=6; WT scr 0.325 ± 0.027 units, n=5; KO shFMRP 0.348 ± 0.054 units, n=6; Figure 4.7c) and KO scr (0.385 ± 0.051 units, n=8). Therefore knocking-down FMRP in cultured hippocampal neurons does not alter SV exocytosis at low frequency stimulation at physiological temperatures.

4.2.5. No SV exocytosis or endocytosis deficits in mature Fmr1 KO rat hippocampal neurons

We then went on to examine SV recycling at both low and high frequency stimulation in a rat model of FXS (Till et al., 2015) to determine whether the role (or absence of role) of FMRP is conserved across species. We used sypHy to examine both exocytosis and endocytosis. We started by examining SV recycling during low frequency stimulation (10 Hz 30 s, Figure 4.8) in both *Fmr1* KO rat neurons and WT littermate controls. Fluorescence traces were normalised to the total SV pool to determine the amount of exocytosis as a proportion of the total SV pool (Figure 4.8b,d). There was no difference (Student t-test n.s. $p > 0.05$) between KO (0.386 ± 0.038 units, n=11) and WT (0.411 ± 0.044 units, n=9). Thus, the loss of FMRP does not affect SV exocytosis at low frequency stimulation in rats.

We then studied SV endocytosis by examining sypHy retrieval by normalising the fluorescence traces to the peak of stimulation so that kinetics could be compared across genotypes (Figure 4.8c). Fluorescence traces were not different between KO

and WT (2-way ANOVA, n.s. $p > 0.05$). Furthermore, the sypHy τ were not different (Student t-test n.s. $p > 0.05$) between KO (33.87 ± 2.63 s, n=11) and WT (44.43 ± 7.71 s, n=9) (Figure 4.8e). Therefore, the loss of FMRP does not impair SV endocytosis at low frequency stimulation in rat hippocampal neurons.

As the effects of loss of FMRP are exaggerated at high frequency stimulation (Deng et al., 2011; Deng et al., 2013; Ferron et al., 2014; Wang et al., 2014) we challenged *Fmr1* KO and WT littermate control neurons with high-frequency stimulation (50 Hz 6 s) and examined the effects on SV recycling kinetics (Figure 4.9). When fluorescence traces were normalised to maximum NH_4Cl fluorescence, there was no difference in peak exocytosis during stimulation (Student t-test n.s. $p > 0.05$, Figure 4.9b,d) between KO (0.432 ± 0.034 units, n=11) and WT (0.443 ± 0.041 units, n=10). Thus, loss of FMRP in rat hippocampal neurons does not affect SV exocytosis during high-frequency stimulation.

We then proceeded to examine SV endocytosis after high-frequency stimulation (Figure 4.9c, e). There was no difference in sypHy fluorescence traces across genotypes (2-way ANOVA n.s. $p > 0.05$). There was also no difference in sypHy τ (Figure 4.9e, Student t-test n.s. $p > 0.05$) between KO (39.58 ± 3.64 s, n=11) and WT hippocampal neurons (43.46 ± 4.87 s, n=17). This suggests that the loss of FMRP does not affect sypHy retrieval during high-frequency stimulation in this rat model. Taken together with Figure 4.8, these results suggest that SV recycling, as reported by sypHy, is not affected by the loss of FMRP in rat hippocampal neurons.

4.2.6. Fewer nerve terminals undergo ADBE in Fmr1 KO rat hippocampal neurons

SypHy is a good reporter of CME, however it cannot report ADBE (Nicholson-Fish et al., 2015) which is the main endocytic mode that occurs during high frequency train (Clayton et al., 2008). To determine whether the absence of FMRP impacts on

ADBE, we used the fluid-phase marker TMR dextran (40 kDa) in *Fmr1* KO rat neurons (using the novel *Fmr1* LEH model). TMR dextran is a fluorescent-labeled hydrophilic saccharide that can be taken up into bulk endosomes in the fluid phase upon endocytosis. 40 kDa TMR dextran is specifically accumulated via ADBE since its size limits uptake via CME (Clayton and Cousin, 2009). TMR dextran was loaded with a train of 40 Hz 10 s action potentials, a high frequency stimulation shown to trigger ADBE (Cheung et al., 2010; Clayton et al., 2008; Clayton and Cousin, 2009; Nicholson-Fish et al., 2016). The TMR dextran was then immediately washed off. The remaining fluorescent puncta represent TMR dextran that has been endocytosed during stimulation. Fluorescent puncta were then counted to get an overview of the amount of ADBE occurring in culture (Clayton and Cousin, 2009). The number of puncta in KO cultures were normalised to the WT puncta number to compare the data across genotypes (Figure 4.10). There were significantly fewer TMR dextran puncta (Student t-test ** p=0.0054) in the *Fmr1* KO hippocampal neurons (76.02 ± 5.17% of WT levels, n=14) relative to WT littermate controls (100 ± 5.97 % of WT levels, n=14). Thus, there is less ADBE occurring in *Fmr1* KO hippocampal neurons compared to WT controls. This suggests that FMRP may plays a role in ADBE as its deletion decreases the amount of nerve terminals where ADBE occurs.

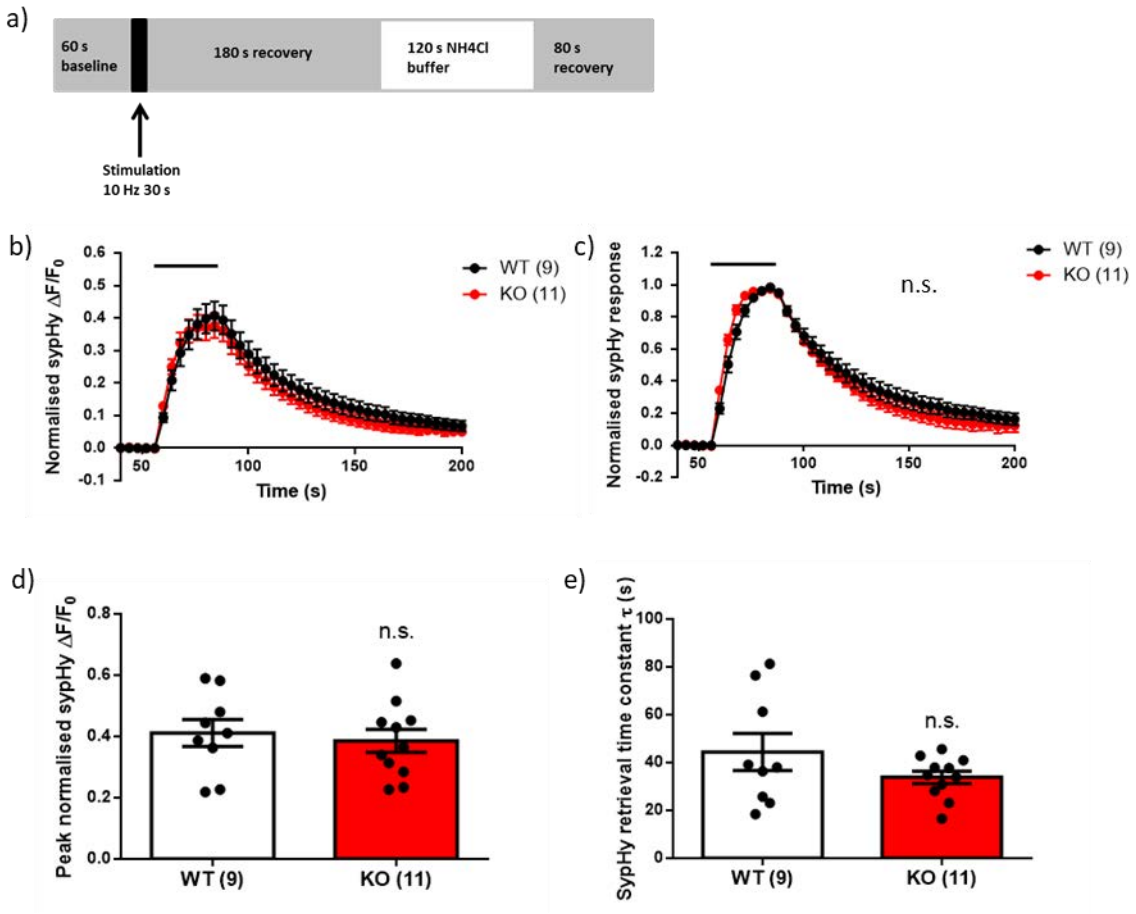

Figure 4.8 No difference in exocytosis or sypHy retrieval at low frequency stimulation (10 Hz 30 s) in Fmr1 SD rat model

Hippocampal neurons derived from Fmr1 KO rat (SD) and WT littermate controls were transfected with on DIV 7and imaged DIV 13-15. a) Time course of experiment. b-c) Mean sypHy fluorescence traces of WT (white) and KO (red) hippocampal neurons. Bars indicate the period of stimulation, 10 Hz 30 s. b) normalised to the total SV number as revealed by NH_4Cl. c) normalised to the peak of stimulation; 2-way ANOVA n.s. non-significant p> 0.05. d) Mean and individual stimulation peak heights obtained from individual sypHy traces of data in b). e) Mean and individual sypHy retrieval time constants (τ) of data plotted in c). n.s. non-significant p > 0.05 by Student t-test.
Experimental n shown in brackets, error bars in all panels ± SEM.

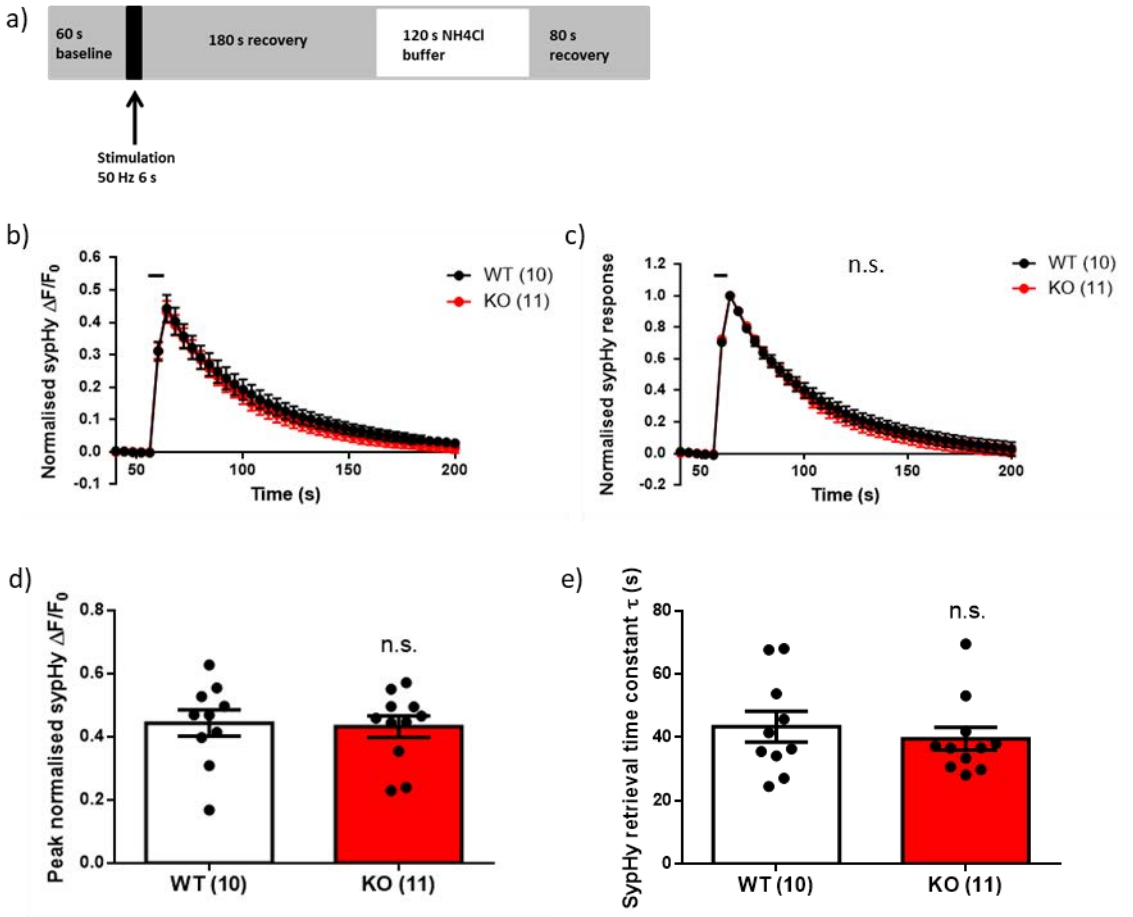

Figure 4.9 No difference in exocytosis or sypHy retrieval at high frequency stimulation (50 Hz 6 s) in Fmr1 SD rat model

Hippocampal neurons derived from Fmr1 KO rat (SD) and WT littermate controls were transfected with either sypHy at DIV 7 and imaged DIV 13-15. a) Time course of experiment. b-c) Mean sypHy fluorescence traces of WT (white) and KO (red) hippocampal neurons. Bars indicate the period of stimulation, 10 Hz 30 s. b) normalised to the total SV number as revealed by NH4Cl. c) normalised to the peak of stimulation; 2-way ANOVA n.s. non-significant p> 0.05. d) Mean and individual stimulation peak heights obtained from individual sypHy traces of data in b). e) Mean and individual sypHy retrieval time constants (τ) of data plotted in c) .n.s. non-significant p > 0.05 by Student t-test.
Experimental n shown in brackets, error bars in all panels ± SEM.

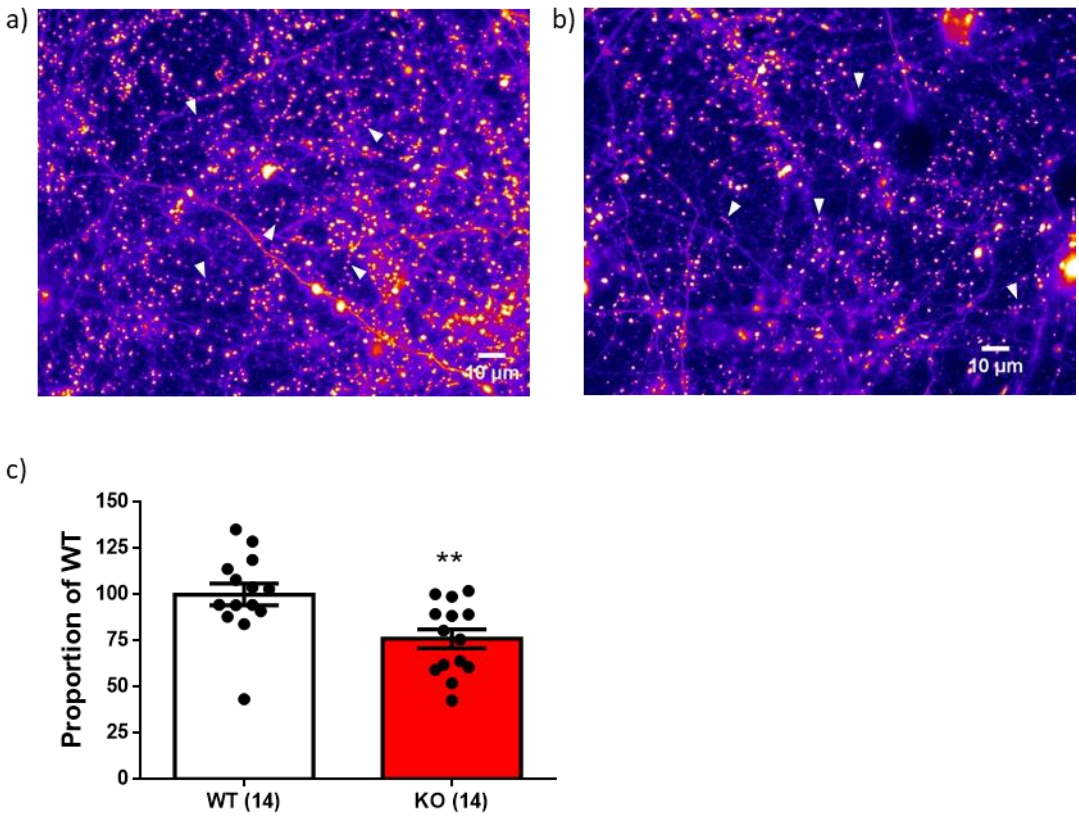

Figure 4.10 TMR Dextran uptake is impaired in Fmr1 KO neurons in Fmr1 LEH model

*Hippocampal neurons derived from Fmr1 KO LEH rat (KO, red) and WT littermate controls (white) were loaded with TMR dextran during a 40 Hz 10 s action potential train and imaged at DIV 13-15. a-b) Representative images of TMR dextran loaded nerve terminals of a) WT and b) Fmr1 KO hippocampal neurons. Arrow heads indicate selected nerve terminals that have taken up TMR dextran. c) Mean and individual dextran puncta uptake data as a proportion of total WT uptake. Student t-test ** $p < 0.05$.*
Experimental n shown in brackets, error bars in all panels ± SEM.

4.3. Discussion

We used a series of fluorescent reporters to examine SV recycling deficits in *Fmr1* KO neurons. In our hippocampal cultures at *DIV* 14 neither SV exocytosis nor SV endocytosis were affected by loss of FMRP. This was the case with both low and high frequency stimulation. We also looked at SV recycling at *DIV* 7, as FMRP expression peaks at PND 7, to ensure that we did not miss any shift in presynaptic activity during this synapse formation critical period. However, we did not see any SV exocytosis defects in immature *Fmr1* KO hippocampal neurons at either frequency.

We also measured presynaptic $[Ca^{2+}]_i$ to determine whether there was an effect of loss of FMRP as FMRP has been found to directly bind to N-type calcium channels (Ferron et al., 2014). We did not see any difference in evoked calcium concentration at the presynapse using the calcium reporters GCaMP6f or Fluo5f.

Impaired pHluorin recycling kinetics have been observed with FMRP KD at near physiological temperatures (Ferron et al., 2014). We attempted to replicate this phenotype in our own hippocampal cultures. However, there was no effect on SV exocytosis of FMRP KD during high frequency stimulation. We then examined the effect of physiological temperatures on SV exocytosis. We found no difference in exocytosis between *Fmr1* KO and WT neurons at low frequency stimulation.

We then monitored SV recycling kinetics in a rat model of *Fmr1* KO to determine whether there was a converging role of FMRP across species as there is some evidence that suggests a different role of FMRP across mouse and rat models. Specifically, loss of FMRP in both mouse and rat models leads to altered synaptic plasticity, particularly exaggerated protein synthesis-independent mGluR-LTD (Huber et al., 2002; Nosyreva and Huber, 2006; Till et al., 2015). Interestingly, *Fmr1*

KO SD rats show impaired hippocampal-dependent spatial learning, whereas *Fmr1* KO mice do not (Till et al., 2015). However, there were no differences in SV exocytosis or endocytosis across genotypes at either high or low frequency stimulation.

Finally, using a different rat model, *Fmr1* KO LEH, we discovered ADBE deficits in *Fmr1* KO hippocampal neurons compared to WT. There were fewer KO nerve terminals that underwent ADBE as determined by fewer fluorescent dextran puncta compared to WT littermate controls.

4.3.1. No SV exocytic defects at high frequency stimulation

4.3.1.1.Total vs partial loss of FMRP

Previous work has suggested that loss of FMRP can impair SV recycling, demonstrated by altered SV release kinetics using FM dyes (Deng et al., 2011) and increased vGLUT-pH exocytosis upon high frequency stimulation (Ferron et al., 2014). Ferron et al. found that partial loss of FMRP led to increased exocytosis in DRG neurons at high frequency stimulation. This also appeared to be the case in preliminary studies in FMRP KD hippocampal neurons (Ferron et al., 2014). Unfortunately, we could not replicate these findings in our cultures. In our shFMRP experiments, FMRP was knocked down at *DIV* 9-11 and imaged 4 days later consistent with experiments reported in Ferron *et al.* (2014). Synapse formation has already started to occur in hippocampal cultures at this stage (Kaech and Banker, 2006). It is therefore possible that synaptic plasticity may no longer be as reliant on FMRP as it is during synapse formation and neurite outgrowth (reviewed in Pfeiffer and Huber, 2009) which occurs earlier at *DIV* 4-7 in hippocampal cultures (Kaech and Banker, 2006). As well, it is important to note that this protocol was optimised for DRG neurons, it is possible that a 4-day KD of FMRP is insufficient to achieve optimal FMRP depletion in hippocampal neurons. The efficiency of FMRP KD under our experimental conditions would also need to be examined. A lack of FMRP

KD could explain the discrepancy between our work and what has previously been published by Ferron et al. (2014).

Furthermore, we do not see an SV exocytosis defect in *Fmr1* KO hippocampal neurons. This could be due to the role that FMRP plays in development. FMRP plays an important role in synapse formation during critical periods (Cruz-Martin et al., 2010; Doll et al., 2017). FMRP expression peaks early in development at PND 7 (Till et al., 2012; Till et al., 2015) when it is required for synapse pruning and maintenance (Pfeiffer et al., 2010). This is why we also looked at SV exocytosis in developing neurons at *DIV* 7, in the case where a SV recycling phenotype would be exaggerated. This was not the case, there were no SV exocytosis defects in Fmr1 KO hippocampal neurons compared to WT.

A possible explanation for the lack of effect of the complete loss of FMRP could be due to homeostatic compensation for the absence of the protein. In its absence, different pathways may be upregulated or downregulated to compensate for loss of FMRP activity. FMRP is involved in multiple cellular processes. Because of this, it is perhaps not unsurprising that the defects observed in FXS can be rescued by targeting multiple different molecules and pathways (reviewed in Wijetunge et al., 2013). In fact, all or a subset of the following pathophysiological phenotypes: dendritic spine morphology, increased protein translation, audiogenic seizures, and impaired synaptic plasticity can be rescued by altering BK channel opening pharmacologically (Hebert et al., 2014) or genetically (Deng and Klyachko, 2016), inhibiting mGluR activity pharmacologically (Chuang et al., 2005; Suvrathan et al., 2010; Yan et al., 2005) or genetically (Dolen et al., 2007), targeting the mammalian target of rapamycin (mTOR) pathway pharmacologically (Osterweil et al., 2013) or repressing protein synthesis of FMRP-target mRNAs pharmacologically (Gkogkas et al., 2014). Thus, there is considerable overlap between these pathways. This suggests that there may already be endogenous mechanisms in place that can compensate for absence of the protein. This could be tested using mass spectrometry to screen for

proteins that may be up-regulated or down-regulated in the absence of FMRP (Klemmer et al., 2011; Tang et al., 2015). We prepared synaptosomes from hippocampi and cortices isolated from adult *Fmr1* KO mice and WT littermate controls. These synaptosomes were then analysed by quantitative mass spectrometry (Prof Matthias Trost, Newcastle University, UK) to determine whether there was alteration in expression of any key presynaptic proteins (data not shown). We found a significant decrease in endophilin levels in both the hippocampal and cortical synaptosomes of the *Fmr1* KO brains compared to WT. This decrease in endophilin levels could potentially be responsible for the deficit in ADBE observed.

With a 4-day FMRP KD, FMRP levels are reduced by half in non-neuronal tsA-201 cells (Ferron et al., 2014). There may still be sufficient levels FMRP present in this model, therefore there would be no need for any compensatory mechanisms to be put in place. This could explain why there is deficient SV recycling with FMRP KD but not with complete loss of the protein. Indeed, it is interesting that a 50 % depletion of FMRP resulted in significantly increased exocytosis whereas we did not observe any defects in *Fmr1* KO neurons, This is especially surprising, since both mouse and human *Fmr1* Het females show milder FXS phenotypes compared with KO males (Clifford et al., 2007; Gauducheau et al., 2017).

Taken all together, our results suggest that FMRP may not play any role in SV recycling by the CME pathway.

4.3.1.2.Presynaptic calcium concentration

Another widely observed phenotype with loss of FMRP is increased calcium currents in the presynapse. FMRP binds to N-type calcium channels and, through this interaction, can modulate their density at the plasma membrane. This could partially mediate the increased presynaptic calcium response reported in *Fmr1* KO

hippocampal neurons (Deng et al., 2011; Deng et al., 2013; Ferron et al., 2014). However we did not observe any increased in $[Ca^{2+}]_i$ at the presynapse using the genetically encoded reporter, GCaMP6f. This reporter was chosen for its rapid kinetics, however it appeared our fluorescence signal was being saturated, as addition of ionomycin to the cells was not able to further increase fluorescence signal. Ionomycin is used to raise $[Ca^{2+}]_i$ and thus should cause an increase in reporter fluorescence due to the increased $[Ca^{2+}]_i$ present. We then went on to use Fluo-5F. Fluo-5F is a calcium indicator dye that increases fluorescence upon binding calcium. It was chosen since it had a lower affinity for calcium and it did not saturate during high frequency stimulation as application of ionomycin was able to increase fluorescence signal.

It should be noted that these reporters are not exclusively presynaptic and therefore do not exclusively report changes in presynaptic calcium levels. When we used the presynaptic calcium reporter SyGCaMP5f (GCaMP5f fused to synaptophysin, data not shown) we observed a significant trafficking of the reporter molecule from the presynapse which confounded our results (data not shown). Therefore we monitored presynaptic $[Ca^{2+}]_i$ using Fluo-5F selecting ROIs based on nerve terminal morphology.

The changes in presynaptic $[Ca^{2+}]_i$ previously reported were changes in Ca^{2+} currents measured through electrophysiological patch clamping onto the neuron or through two-photon imaging (Deng et al., 2011; Deng et al., 2013; Ferron et al., 2014). These recording techniques have better spatial resolution than epi-fluorescence microscopy and thus may be more sensitive to slight variations in calcium concentration at the AZ. It is possible that this increased $[Ca^{2+}]_i$ is very localised, and a cytosolic reporter may not report these minor fluctuations in calcium currents at least under our imaging conditions.

4.3.2. Role for FMRP in ADBE

Although we saw no effect of loss of FMRP on SV exocytosis or CME, we did observe fewer nerve terminals undergoing ADBE in *Fmr1* KO rat (*Fmr1* KO LEH) neurons as compared to WT controls. VAMP4-pH could also be used to confirm this phenotype as VAMP4 preferentially found as cargo on bulk endosomes (Nicholson-Fish et al., 2015). It is important to note that the dextran assay used to report ADBE only reports the number of nerve terminals undergoing ADBE, not the extent to which it happens in each nerve terminal (Clayton and Cousin, 2009). Therefore, it would also be important to perform an HRP uptake assay to label endosomes and SVs at the presynapse and image them using electron microscopy to determine how much ADBE is occurring at each nerve terminal (Cheung et al., 2010).

4.3.2.1. Translational effects

Our group has previously found that FMRP is enriched on bulk endosomes (Kokotos et al, unpublished data), therefore it may play an important role in this endocytic mode. FMRP may regulate ADBE through translational regulation of molecules involved in the pathway. FMRP's main function is to block protein translation downstream of mGluRs through repression of transcription initiation (Napoli et al., 2008) and elongation (Darnell et al., 2011). In its absence, there is increased translation of its target mRNAs (Darnell and Klann, 2013). A third of the presynaptic proteome is an FMRP target (Darnell et al., 2011). Increased translation and expression of these proteins may impair SV recycling by ADBE, especially since, in normal conditions, the number of proteins within a synaptic bouton are tightly regulated and present in limited amounts (Wilhelm et al., 2014). Mass spectrometry analyses performed by us and others confirm that there are indeed increased levels of presynaptic proteins important for SV recycling in *Fmr1* KO mouse brains including, amphiphysin-1 which has been found to be overexpressed in *Fmr1* KO mice during development (Tang et al., 2015). Amphiphysin-1 is only present in low levels on ADBE endosomes compared to SVs (Kokotos et al, unpublished data). Therefore, it

is possible that altered levels of this protein can impair endocytosis, particularly by biasing the nerve terminal to undergo CME rather than ADBE.

4.3.2.2.-Actin dynamics

FMRP can regulate protein synthesis by forming an inhibitory complex with CYFIP1 and eIF4E to suppress protein synthesis initiation (Napoli et al., 2008). Along with being an eIF4E-binding protein, CYFIP1 can also regulate actin remodelling. In the absence of FMRP, CYFIP1 preferentially takes on its role as a promoter of actin remodelling (Santini et al., 2017). FMRP and CYFIP1 act antagonistically on the mTOR pathway to maintain effective neurotransmission through regulation of dendritic spines (Abekhoukh et al., 2017). In the absence of FMRP, there is an increase in number of dendritic spines and altered morphology (Abekhoukh et al., 2017) similar to what is seen with overexpression of CYFIP1 (Pathania et al., 2014). Thus, FMRP plays an important role in synapse formation at the structural level. Furthermore, disruption of actin dynamics through loss of FMRP may mediate the decreased levels of ADBE occurring in this model as ADBE is actin-dependent (Kononenko et al., 2014) (see section 1.3.2.2).

4.3.2.3.Modulation of APs through presynaptic ion channels

Alternatively, FMRP could also be regulating ADBE through modulation of ion channel activity (Ferron, 2016). There is evidence that dysregulation of the Slack and N-type calcium channels may in part mediate the presynaptic deficits observed in FXS, however there is considerable evidence that defects in SV recycling are due to the loss of FMRP regulation of BK channels (Deng et al., 2013; Deng and Klyachko, 2016). In *Fmr1* KO neurons, there is no repression of the BK channel β4 subunit by FMRP binding (Deng et al., 2013). This leads to broader action potentials which in turn increases neurotransmission, enhances SV recycling as reported by FM1-43 recycling and increases seizure susceptibility in KO neurons (Deng et al., 2011; Deng et al., 2013; Deng and Klyachko, 2016). Interestingly, KO of β4 in *Fmr1* KO

neurons was able to rescue all the pathogenic phenotypes previously described (Deng and Klyachko, 2016). Administration of a BK channel opener to *Fmr1* KO mice rescued dendritic spine and behavioural phenotypes (Hebert et al., 2014). Therefore, it is highly probable that it is through this interaction that FMRP modulates presynaptic activity including SV recycling. Although currently there is no evidence tying BK channels to different modes of endocytosis, there is evidence that ion channels can differentially regulate both CME and ADBE (Yao et al., 2017).

4.3.2.4.Association with the endosomal sorting complex required for transport (ESCRT)

Another way in which FMRP could regulate ADBE is through its interaction with the endosomal sorting complex required for transport (ESCRT) complex. In *Drosophila melanogaster*, FMRP binds to the protein Shrub (CHMP4 in mammals) and can negatively regulate its expression during an early critical period (Vita and Broadie, 2017). Shrub is a core protein of the ESCRT-III complex. In endosomes, the ESCRT-III complex forms invaginated buds that trap important cargo protein. These invaginations can then form intraluminal vesicles through abscission of the endosomal membrane by the unfolding of the ESCRT-III by other ESCRT pathway proteins (reviewed in Williams and Urbe, 2007). Interestingly, in *Drosophila*, when Shrub was overexpressed, there was arrested membrane trafficking in synapses, including more endosomal structures and bigger intraluminal vesicle area. (Vita and Broadie, 2017). The same trafficking defects were seen in the *Drosophila* FXS model. Thus, the absence of FMRP could mediate defects in ADBE by loss of suppression of ESCRT-III complex activity.

4.3.3. Limitations

A key factor that should not be overlooked when comparing our results to the published work by Ferron et al. (2014) is the temperature at which we imaged our cells. All imaging experiments, other than those described in Figure 4.7, were conducted at room temperature. CME has been found to be the dominant endocytic

pathway at room temperature in hippocampal neurons (Granseth et al., 2006), however there is some debate as to whether these imaging parameters are physiologically relevant. At higher temperatures, the kinetics of SV recycling are accelerated and allow for faster replenishment of SV pools (Fernandez-Alfonso and Ryan, 2004; Renden and von Gersdorff, 2007). Physiological temperatures can also recruit different endocytic modes that do not occur at room temperature including ultrafast endocytosis (Watanabe et al., 2013) which occurs on faster timescales than CME. Thus, imaging at 37°C may be a more physiologically relevant imaging paradigm and may provide more insight into what actually occurs at functioning synapses in the brain. It is important to note that we did not observe any effect of FMRP KD with low frequency stimulation at physiological temperatures. No effect of FMRP KD has previously been reported in DRG neurons in these same conditions (Ferron et al., 2014). It would be important to repeat these experiments with high frequency stimulation as this should reveal any deficits due to the loss of FMRP (Deng et al., 2011; Deng et al., 2013; Ferron et al., 2014)

5. Characterisation of SV recycling defects associated with de novo mutations in DNM1 linked to epileptic encephalopathy

5.1. Introduction

Dynamin-1 (dyn1) is a large brain-specific GTPase. It is located in presynaptic nerve terminals, where it plays an essential role in SV recycling. Dyn1 is composed of a GTPase domain, a BSE, the stalk, a PH domain, and a PRD (Figure 5.1a). Dyn1 forms helical oligomers that wrap themselves around the neck of endocytic pits and upon GTP hydrolysis, dyn1 constricts the membrane and fission occurs (reviewed in Antonny et al., 2016). After fission, the dyn1 oligomer helices disassemble. Dyn1 GTPase activity plays essential roles in both CME and ADBE (reviewed in Rizzoli, 2014).

The PRD of dyn1 contains the S774 and S778 phosphorylation sites which are phosphorylated by GSK3β and Cdk5 respectively, and dephosphorylated by Ca^{2+}-dependent calcineurin (Clayton et al., 2009; Clayton et al., 2010). Mutating these residues has revealed additional roles of dyn1 in endocytosis including mediating the activity-dependent acceleration phase of endocytosis (Armbruster et al., 2013) and mediating ADBE (Clayton et al., 2009; Clayton et al., 2010). Activity-dependent dephosphorylation of dyn1 allows for it to interact with syndapin-1 which mediates endocytosis via ADBE (Clayton et al., 2009).

Recently, large-scale exome sequencing studies have revealed *de novo* mutations in *DNM1* to be important risk factors for neurodevelopmental disorders (EuroEPINOMICS-RES Consortium et al., 2014; von Spiczak et al., 2017). We have investigated *de novo* mutations in *DNM1* from patients with epileptic encephalopathy

(patient information acquired from the DDD consortium and provided by Dr Wayne Lam). These patients have one WT and one mutant allele of *DNM1,* suggesting that these mutants all express dominant-negative function. Epileptic encephalopathy presents itself with childhood-onset epilepsy associated with cognitive and behavioural deficits due to the seizures. It is often comorbid with moderate to severe intellectual disability and autism spectrum disorders (Epi4K Consortium et al., 2013; EuroEPINOMICS-RES Consortium et al., 2014; von Spiczak et al., 2017). Mutations human *DNM1* result in severe phenotypes including Lennox-Gastaut syndrome, severe intellectual disability, and dystonia (EuroEPINOMICS-RES Consortium et al., 2014; von Spiczak et al., 2017). Three of the mutations that are investigated in this chapter are novel, and one, R237W, has been characterised previously and appears to be a recurrent mutation appearing in multiple unrelated patients (EuroEPINOMICS-RES Consortium et al., 2014; von Spiczak et al., 2017). Three of the mutations are in the GTPase domain (G139R, R237W, I289F) and one in the stalk domain (H396D) (Figure 5.1a).

Dyn1 is necessary for sustained neurotransmission upon stimulation (Ferguson et al., 2007). Although *Dnm1* KO mice were viable and did not show any defects at birth, KO pups died within 2 weeks of birth (Ferguson et al., 2007). *Dnm1* KO cortical neurons could still undergo a few rounds of SV recycling, after which endocytic capacity became saturated (Ferguson et al., 2007). The KO nerve terminals exhibited accumulations of interconnected clathrin-coated buds and very few formed SVs (Ferguson et al., 2007), providing evidence that dyn1 is necessary for SV formation through endocytosis. It is important to note that *Dnm1,3* double KO (DKO) mice die within a few hours of birth and cultured neurons show significantly more SV endocytosis impairment than either *Dnm1* KO or *Dnm3* KO neurons (Ferguson et al., 2007; Raimondi et al., 2011). This suggests that the dynamins have some functional overlap which can explain why correctly formed SVs are still present in *Dnm1* KO nerve terminals.

In our studies, we also looked at the *Dnm1 ftfl* ($Dyn1_{A408T}$) mutation which spontaneously arose in mice that displayed non-lethal seizures (Boumil et al., 2010). Mice with heterozygous expression of this mutant allele displayed recurrent generalised tonic-clonic seizures. Mice homozygous for $Dyn1_{A408T}$ had lethal seizures by 3 weeks of age (Boumil et al., 2010). $Dyn1_{A408T}$ has also been found to have defective self-assembly (Boumil et al., 2010), a function which is critical for GTPase activity and membrane fission (Hinshaw and Schmid, 1995; Warnock et al., 1996). $Dyn1_{A408T}$ shows impaired endocytosis as measured by disrupted transferrin uptake in COS-7 fibroblast cells overexpressing this mutant. This can be rescued when $Dyn1_{A408T}$ is co-expressed with $Dyn1_{WT}$ (Asinof et al., 2016; Boumil et al., 2010).

The aim of this work was to determine whether these *de novo* mutations impaired SV recycling in cultured hippocampal neurons. This work could also provide mechanistic data which may explain the patient phenotypes. Studying the effect of these mutants on SV endocytosis could also provide insights on dyn1 function as the mutations are located within different protein functional domains. Additionally, we wanted to determine whether we could rescue any observed SV recycling defects.

5.2. Results

5.2.1. Overexpression of mutant mCer-Dyn1 impairs CME

De novo mutations in both the GTPase domain and stalk domain of dyn1 (Figure 5.1a) were found in patients suffering from neurodevelopmental disorders (Table 5.1). Due to the important role of dyn1 in both CME and ADBE, we decided to study the effects of these mutations on SV recycling through both of these pathways. We generated equivalent mutations in a mCerN1 vector which expresses rat dyn1. To

mimic the heterozygous condition found in patients, we transfected these mutants into WT mouse hippocampal neurons.

Human mutations		Linked disorders	Predicted effects based on in silico modelling
Protein change	**DNA change**		
G139R	c.415G>A	Seizures and developmental delay	Highly likely deleterious, destabilising
R237W	c.709C>T	Seizures and developmental delay	Highly likely deleterious, destabilising
I289F	c.865A>T	Seizures	Highly likely deleterious, destabilising
H396D	c.1186C>G	Developmental delay	Likely deleterious

Table 5.1 Dyn1 mutations identified by the DDD Consortium

Mutations were provided to us by Dr Wayne Lam (Muir Maxwell Epilepsy Centre, University of Edinburgh). In silico modelling was performed by Dr Dinesh Soares (American Chemical Society) See section 5.3.1

To mimic the patient condition as closely as possible, we attempted to titrate exogenous dyn1 levels to be equivalent to the endogenous isoform. All mutants except one (mCer-Dyn1$_{I289F}$) were significantly overexpressed when compared to endogenous dyn1 levels (1-way ANOVA with Dunnett's test comparing to mCerN1 empty vector 1.000 ± 0.089 fold overexpression, n=16); mCer-Dyn1$_{WT}$ (2.663 ± 0.402 fold overexpression, n=10, **p= 0.003), mCer-Dyn1$_{K44A}$ (2.397 ± 0.353 fold overexpression, n=10, *p= 0.014), mCer-Dyn1$_{G139R}$ (2.800 ± 0.369 fold overexpression, n=14, ***p= 0.0003), mCer-Dyn1$_{R237W}$ (2.759 ± 0.536 fold overexpression, n=9, **p= 0.002), mCer-Dyn1$_{I289F}$ (1.433 ± 0.189 fold overexpression, n=18, n.s. p> 0.05), mCer-Dyn1$_{H396D}$ (2.736 ± 0.447 fold overexpression, n=10, **p= 0.002), mCer-Dyn1$_{A408T}$ (2.147± 0.258 fold overexpression, n=21, *p= 0.019). Thus, transfection of the mCer-Dyn1 vectors under these conditions provided an overexpression of exogenous dyn1 in an approximate 2:1 ratio with the endogenous form in dissociated primary hippocampal cultures.

Since a number of human dyn1 mutants have alterations in their GTPase domains, we first examined the effects of overexpression of the well-characterised $Dyn1_{K44A}$ mutant on SV recycling using our sypHy imaging assay (Figure 5.2a). The $Dyn1_{K44A}$ mutation impairs both the GTPase activity of dyn1 and its ability to bind GTP (Damke et al., 1994; Damke et al., 2001). Previous studies using this mutant have revealed impaired transferrin uptake in HeLa cells, indicating an arrest of receptor-mediated endocytosis (Damke et al., 1994). However, to our knowledge, the effect of this mutation on CME has not been directly investigated in primary neuronal cultures. We first monitored the effect of mCer-$Dyn1_{K44A}$ on sypHy retrieval after low frequency stimulation (10 Hz 30 s), as this frequency evokes dyn1-dependent CME. We observed significant impairment in sypHy retrieval in neurons expressing the mCer-$Dyn1_{K44A}$ mutant (Figure 5.2b, 2-way ANOVA with Dunnett's test comparing to WT * $p< 0.05$, ** $p< 0.01$, **** $p< 0.0001$). In contrast, overexpression of mCer-$Dyn1_{WT}$ did not impair sypHy retrieval compared to mCerN1 empty vector (2-way ANOVA n.s. $p> 0.05$). Therefore, overexpression of mCer-$Dyn1_{K44A}$ impairs CME in primary neuronal cultures.

There is some evidence that dyn1 may play a role in hormone secretion in adrenal chromaffin cells, particularly through regulating the size of the fusion pore (Fulop et al., 2008). Dyn1 has also been proposed to regulate the kinetics of exocytic vesicle fusion pores in astrocytes (Lasic et al., 2017). Therefore, we also examined SV exocytosis by normalising the fluorescence trace to the fluorescence of the total vesicle pool (traces not shown). We observed no difference in SV exocytosis between the empty vector (mCerN1, 0.439 ± 0.036 units, n=9), mCer-$Dyn1_{K44A}$ (0.502 ± 0.028 units, n= 17) and mCer-$Dyn1_{WT}$ (0.553 ± 0.044 units, n=10). This suggests that mCer-$Dyn1_{K44A}$ mutant impairs SV endocytosis but not SV exocytosis.

We then determined whether overexpression of the other human dyn1 mutants or the $Dyn1_{A408T}$ mutant impacted SV endocytosis using the same imaging assay (Figure 5.3a). All fluorescent traces were compared to mCer-$Dyn1_{WT}$ traces to ensure that

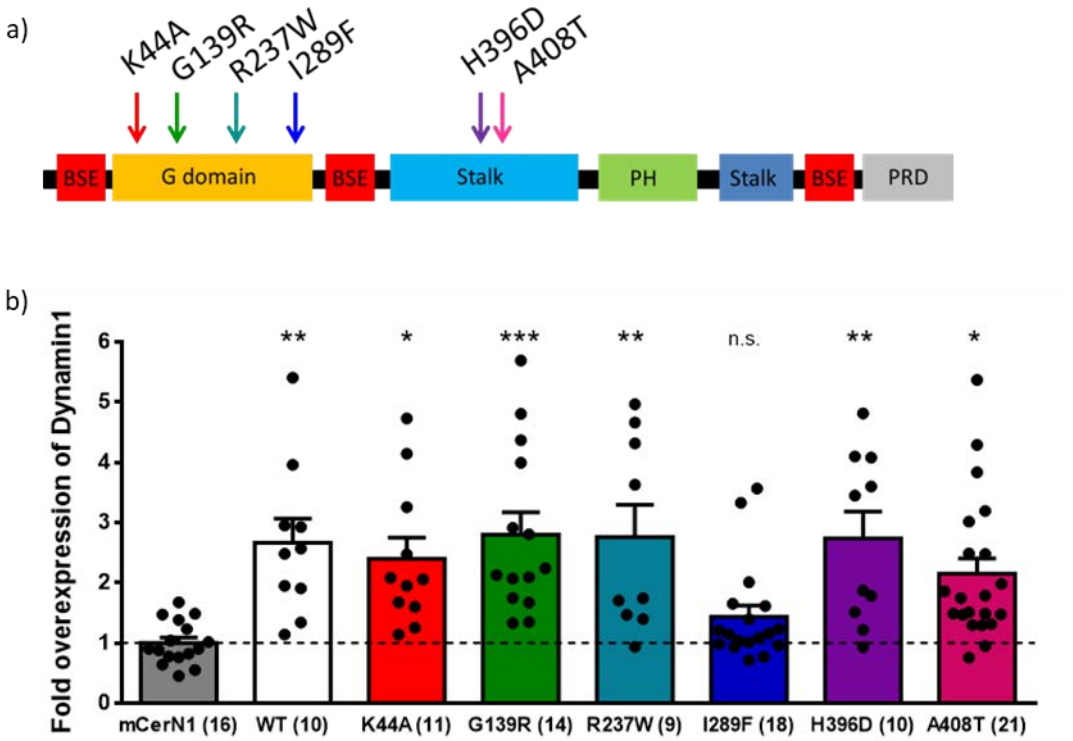

Figure 5.1 Overexpression of mCer-Dyn1 mutants in hippocampal cultures

*a) Schematic representation of the different functional domains of dyn1 and the location of the dyn1 mutations. b) Level of expression of dyn1 as a fold overexpression of mCerN1 (empty vector). Hippocampal neurons derived from wildtype mouse embryos were transfected with mCerN1(grey), or mCer-Dyn1$_{WT}$ (WT, white) or dyn1 mutants: mCer-Dyn1$_{K44A}$ (red), mCer-Dyn1$_{G139R}$ (green), mCer-Dyn1$_{R237W}$ (turquoise), mCer-Dyn1$_{I289F}$ (blue), mCer-Dyn1$_{H396D}$ (purple), mCer-Dyn1$_{A408T}$ (magenta) 2 days prior to fixing at DIV 13-14. Neurons were immunolabeled with anti-GFP to locate the transfected cells, anti-SV2A to locate synapses and anti-dyn1 for quantification. 1-way ANOVA with Dunnett's multiple comparison comparing values to mCerN1: * $p < 0.05$; ** $p < 0.01$; *** $p < 0.001$; n.s. $p > 0.05$. For each condition, experimental n in brackets and error bars ± SEM.*

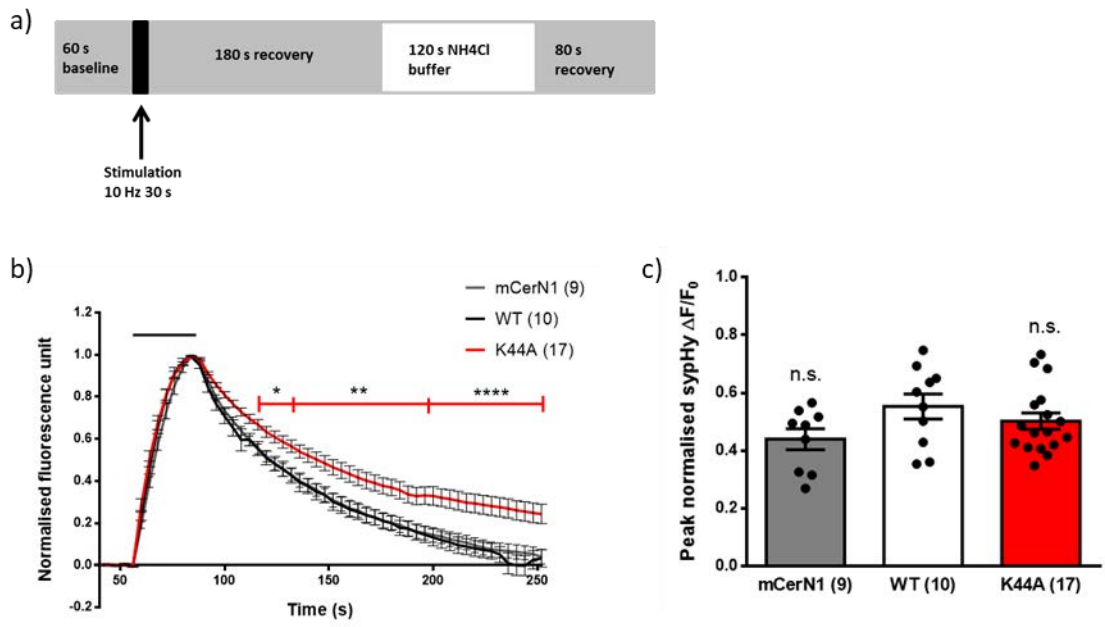

Figure 5.2 $Dyn1_{K44A}$ dominant negative mutant inhibits sypHy retrieval

*Hippocampal neurons derived from WT mouse cultures were transfected with sypHy and mCerN1 (grey), or mCer-$Dyn1_{WT}$ (WT; white) or mCer-$Dyn1_{K44A}$ (K44A; red) 2 days prior to imaging at DIV13-14. a) Time course of experiment b) Mean sypHy fluorescence traces normalised to the peak of stimulation. Bar indicates duration of stimulation, 10 Hz 30 s. 2-way ANOVA with Dunnett's multiple comparisons test comparing each trace to the mCer-$Dyn1_{WT}$ trace * $p < 0.05$; ** $p < 0.01$; **** $p<0.0001$. c) Mean and individual stimulation peak heights measuring exocytosis as a proportion of total SV pool revealed by NH_4Cl. 1-way ANOVA n.s. $p > 0.05$.*
For each condition, experimental n in brackets and error bars ± SEM.

any phenotype was due to the overexpression of the mutant copy of dyn1 and not due to excess dyn1 (Figure 5.3b). There was no significant difference in fluorescence traces after stimulation between mCer-Dyn1$_{G139R}$ or mCer-Dyn1$_{A408T}$ and mCer-Dyn1$_{WT}$ (Figure 5.3b,c,g, 2-way ANOVA with Dunnett's test comparing to mCer-Dyn1$_{WT}$: n.s. $p > 0.05$), however there was a significant difference in sypHy fluorescence traces post-stimulation between the mCer-Dyn1$_{R237W}$, mCer-Dyn1$_{I289F}$ and mCer-Dyn1$_{H396D}$ mutations compared to mCer-Dyn1$_{WT}$ (Figures 5.3b,d-f, 2-way ANOVA with Dunnett's test comparing to mCer-Dyn1$_{WT}$: * $p< 0.05$, ** $p< 0.01$, *** $p < 0.001$, **** $p < 0.0001$). Of note, sypHy τ was not calculated as the fluorescence decay could not be fit by an either a single or double exponential curve. Thus, overexpression of mCer-Dyn1$_{R237W}$, mCer-Dyn1$_{I289F}$ or mCer-Dyn1$_{H396D}$ impairs SV endocytosis at low frequency stimulation.

We also examined SV exocytosis in neurons expressing these mutants, because endocytosis and exocytosis are tightly coupled, and a defect in one may produce deficits in the other. We compared peak sypHy fluorescence during stimulation across mutants after normalisation to the total SV pool using NH_4Cl (Figure 5.4). There was a significant difference in peak sypHy fluorescence during stimulation (1-way ANOVA with Dunnett's test comparing to mCer-Dyn1$_{WT}$: * $p = 0.02$) between mCer-Dyn1$_{H396D}$ (0.3043 ± 0.028 units, n=10) and mCer-Dyn1$_{WT}$ (0.475 ± 0.042 units, n=16). However, there were no differences in sypHy peak height (1-way ANOVA: n.s. $p > 0.05$) between any of the other mutants (mCer-Dyn1$_{G139R}$: 0.589 ± 0.064 units, n=5; mCer-Dyn1$_{R237W}$: 0.427 ± 0.042 units, n=8; mCer-Dyn1$_{I289F}$: 0.414 ± 0.049 units, n=11; mCer-Dyn1$_{A408T}$: 0.479 ± 0.041 units, n=12) and mCer-Dyn1$_{WT}$. Therefore, the Dyn1$_{H396D}$ mutation in the stalk domain appears to impair SV exocytosis, whereas the other dyn1 mutations only appear to produce endocytic defects.

There is constant need for SV endocytosis to replenish SV pools to maintain neurotransmission, especially during long stimulus trains. Therefore, endocytosis

starts to occur during our electrical stimulation protocol. The decreased peak height observed with mCer-Dyn1$_{H396D}$ overexpression may reflect accelerated SV endocytosis, rather then decreased SV exocytosis. We investigated these neurons in the presence of Bafilomycin A1 (Sankaranarayanan et al., 2000) to determine whether the decreased sypHy peak height during stimulation is an endocytic or exocytic defect. Bafilomycin A1 uncouples the reporting of SV endocytosis and exocytosis by inhibiting the vacuolar-type H^+-ATPase that acidifies SVs after endocytosis. Therefore, once the sypHy on SVs has been exposed to the neutral pH upon exocytosis, it can no longer be quenched. SV exocytosis can be visualised without the confounds of SV endocytosis using this approach. Neurons expressing sypHy and either mCerN1, mCer-Dyn1$_{WT}$ or mCer-Dyn1$_{H396D}$ were stimulated at 10 Hz for 90 s to release the total recycling pool. There was no significant difference in amount of exocytosis (1-way ANOVA: n.s. $p > 0.05$; Figure 5.5c) between mCerN1 (0.516 ± 0.023 units, n= 11), mCer-Dyn1$_{WT}$ (0.500 ± 0.033 units, n=11) and mCer-Dyn1$_{H396D}$ (0.507 ± 0.028 units, n=7). Additionally, there was no difference in the rate of exocytosis (1-way ANOVA: n.s. $p > 0.05$; Figure 5.5d) between mCerN1 (0.017 ± 0.003 s, n=11) or mCer-Dyn1$_{H396D}$ (0.021 ± 0.004 s, n=7) and mCer-Dyn1$_{WT}$ (0.013 ± 0.002 s, =11). Taken together with the results from Figure 5.4, this suggests that the decreased exocytosis observed with overexpression of mCer-Dyn1$_{H396D}$ is not due to an exocytic defect, but rather an endocytic defect.

5.2.2. Overexpression of mCer-Dyn1$_{K44A}$ and mCer-Dyn1$_{H396D}$ impair ADBE

Thus far we have shown that dyn1 mutations identified in human patients result in a series of defects in SV recycling through CME. We next determined whether these dyn1 mutants also impacted on ADBE, as dyn1 may also play an important role in this endocytic mode (Clayton et al., 2009; Clayton et al., 2010; Nguyen et al., 2012; see also Y. Wu et al., 2014). To do this, we utilised the genetically-encoded reporter of ADBE: VAMP4-pH (Nicholson-Fish et al., 2015). Like TMR dextran, VAMP4-pH can provide a measure of the proportion of nerve terminals undergoing ADBE during high frequency stimulation (see section 1.4.1.2).

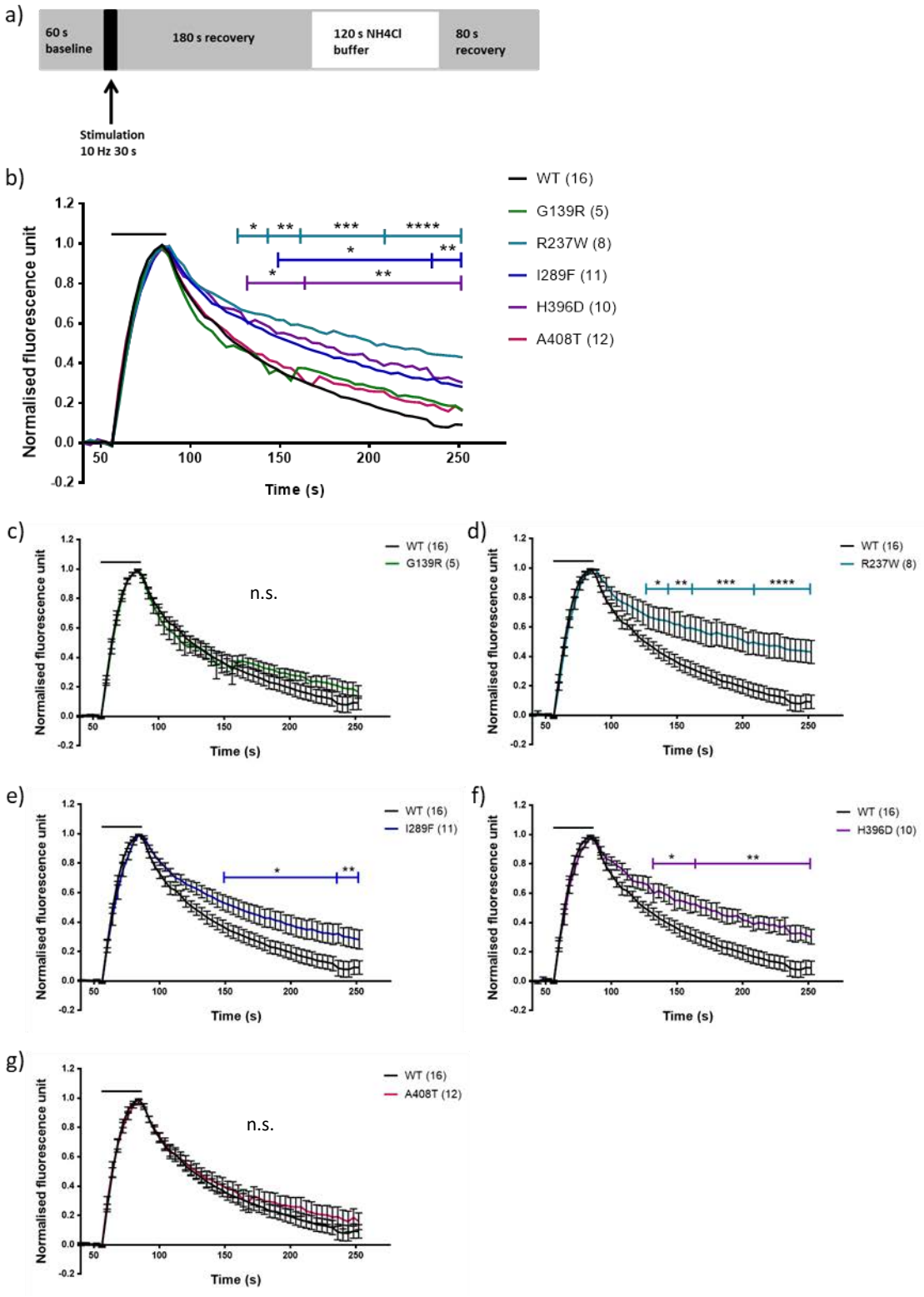

Figure 5.3 Overexpression of mCer-Dyn1$_{R237W}$, mCer-Dyn1$_{I289F}$, or mCer-Dyn1$_{H396D}$ significantly impairs SV endocytosis in hippocampal neurons

*Cultured hippocampal neurons derived from WT mice were transfected with sypHy and either mCer-Dyn1$_{WT}$ (WT, black) or dyn1 mutants: mCer-Dyn1$_{K44A}$ (red), mCer-Dyn1$_{G139R}$ (green), mCer-Dyn1$_{R237W}$ (turquoise), mCer-Dyn1$_{I289F}$ (blue), mCer-Dyn1$_{H396D}$ (purple), mCer-Dyn1$_{A408T}$ (magenta) 2 days prior to imaging on DIV 13-14. a) Time course of experiment b) Mean sypHy fluorescence traces normalised to the peak of 10 Hz 30 s stimulation for all mutations. Error bars were excluded for clarity but can be seen in c-g) Bar indicates duration of stimulation, 10 Hz 30 s. 2-way ANOVA with Dunnett's multiple comparisons test comparing each trace to the WT trace * p < 0.05; ** p < 0.01; *** p < 0.001; **** p < 0.0001. c-g) Mean sypHy traces from each mutant in b) plotted against WT sypHy trace c) G139R, d) R237W, e) I289F, f) H396D, g) A408T. Bars indicate duration of stimulation. Significance obtained from analysis in b).*
For each condition, experimental n in brackets and error bars ± SEM.

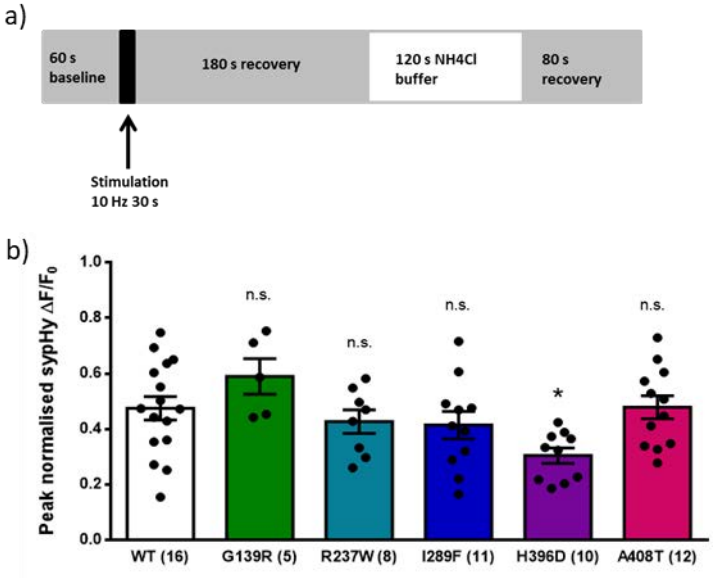

Figure 5.4 Altered sypHy fluorescence peak height with overexpression of mCer-Dyn1$_{H396D}$

*Data obtained from fluorescence traces in Figure 5.3. a) Time course of experiment. b) Mean and individual stimulation peak heights measuring exocytosis as a proportion of total SV pool revealed by NH_4Cl. 1-way ANOVA with Dunnett's test comparing values to mCer-Dyn1$_{WT}$ (white). * $p < 0.05$; n.s. $p > 0.05$.*
For each condition, experimental n in brackets and error bars ± SEM.

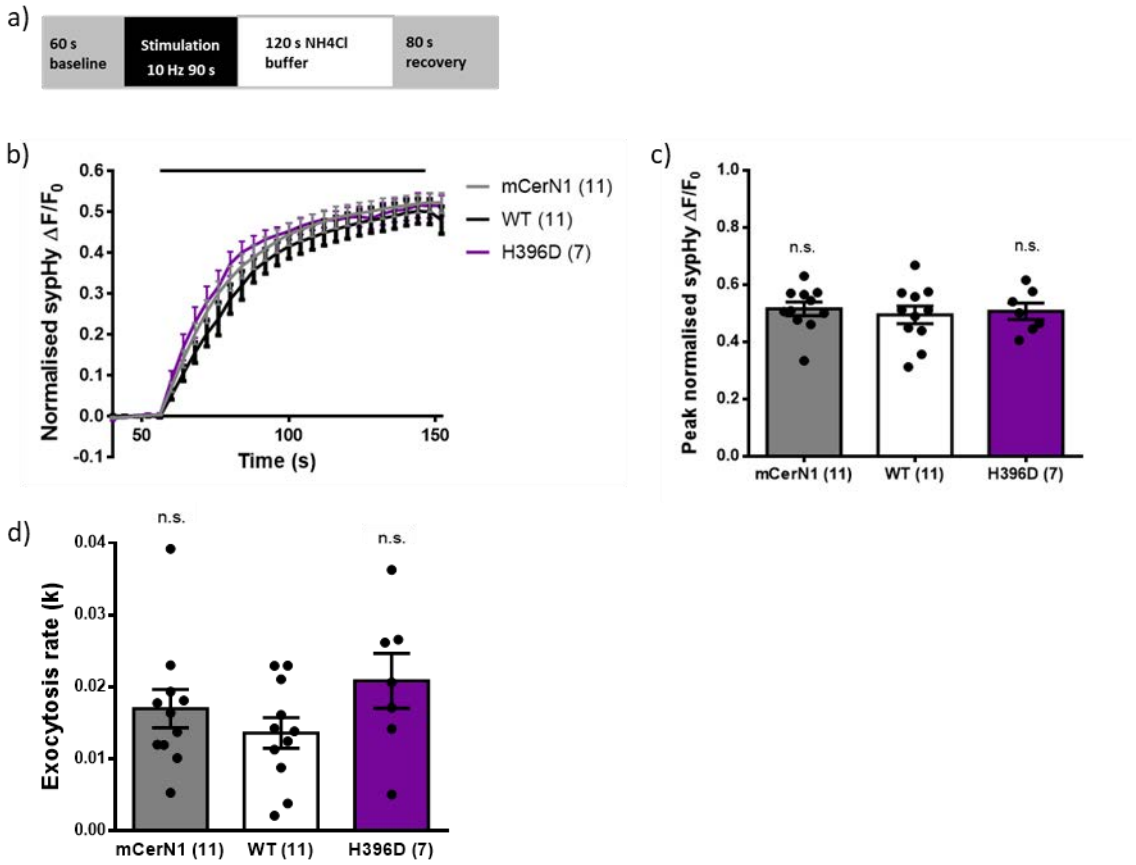

Figure 5.5 No impaired exocytosis with mCer-Dyn1$_{H396D}$ overexpression

Cultured hippocampal neurons derived from WT mice were transfected with sypHy and either mCerN1 (grey), mCer-Dyn1$_{WT}$ (WT, white) or mCer-Dyn1$_{H396D}$ mutant dyn1 (purple) 2 days prior to imaging on DIV 13-14. Imaging was performed in the presence of the vacuolar-type H$^+$-ATPase inhibitor Bafilomycin A1. a) Time course of experiment. b) Mean mCerN1, WT and H396D sypHy fluorescence traces normalised to the peak of 10 Hz 90 s stimulation. Bar indicates duration of stimulation, 10 Hz 90 s. c) Mean and individual stimulation peak heights measuring exocytosis as a proportion of total SV pool revealed by NH$_4$Cl buffer. d) Mean and individual exocytosis rates of data in b) obtained by calculating the slope of a linear regression fit to the first 3 timepoints after the start of stimulation. c-d) 1-way ANOVA n.s. p> 0.05.
For each condition, experimental n in brackets and error bars ± SEM.

Neurons expressing VAMP4-pH, mCerN1 and either mCer-Dyn1$_{WT}$ or mutant mCer-Dyn1 were challenged with high frequency stimulation to trigger ADBE. The fluorescence of each terminal was then sorted into "up" and "down" traces depending on the fluorescence 120 s after stimulation, as previously described (Nicholson-Fish et al., 2015; Nicholson-Fish et al., 2016). "Down" traces represent nerve terminals undergoing ADBE as the bulk endosomes slowly acidify over time quenching the VAMP4-pH. The proportion of "down" traces in mCer-Dyn1$_{K44A}$ expressing neurons (5.728 ± 1.456 %, n=12) was significantly different from mCer-Dyn1$_{WT}$ overexpression (1-way ANOVA with Dunnett's test comparing mCer-Dyn1$_{K44A}$ and mCerN1 17.660 ± 2.699 %, n=11 to mCer-Dyn1$_{WT}$ 18.800 ± 3.228 %, n=11; ** p= 0.002, n.s. p> 0.05; Figure 5.6a). The proportion of "down" traces with mCer-Dyn1$_{H396D}$ overexpression (8.714 ± 2.411 %, n=10) was also significantly different from mCer-Dyn1$_{WT}$ (Student t-test: * p= 0.021; Figure 5.6e). The proportion of "up" and "down" traces of all other mutants was not significantly different from WT (Student t-test: n.s. p> 0.05). This suggests that overexpression of mCer-Dyn1$_{K44A}$ and mCer-Dyn1$_{H396D}$ can decrease the number of nerve terminals undergoing ADBE.

We wanted to ensure that these differences were not due to differences in transfection conditions and overexpression of VAMP4-pH, since we observed lower levels of ADBE than previously reported by our group using this approach (~20% of nerve terminals performing ADBE in contrast to ~40% in Nicholson-Fish et al. (2015)). We transfected VAMP4-pH and mCerN1 for 7 days (17.210 ± 3.449 % down traces , n=7) or for 2 days prior to imaging (15.02 ± 3.415 % down traces, n=8) and saw no difference in the proportion of nerve terminals undergoing ADBE across transfection conditions (Student t-test: n.s. p > 0.05; Figure 5.7a). Thus, the number of days for which VAMP4-pH is expressed in hippocampal cultures does not alter the proportion of nerve terminals undergoing ADBE upon high frequency stimulation.

As a positive control, we also determined whether the proportion of ADBE occurring could be altered by knocking-down syndapin-1 (Figure 5.7b). Syndapin-1 is a neuronal protein in the BAR family that can interact with dyn1 through its C-terminal SH3 domain (reviewed in Quan and Robinson, 2013). In fact, the interaction between dyn1 and syndapin-1 is essential for ADBE (Clayton et al., 2009). Therefore, we predicted that knocking down syndapin-1 in our cultures should impair ADBE (Clayton et al., 2009). Indeed, there was a significantly lower proportion of WT hippocampal nerve terminals undergoing ADBE when transfected for 3 days with shRNA against Syndapin-1 (Syndapin KD: 9.773 ± 2.032 %, n=14) compared to the scrambled control (Scrambled: 22.110 ± 4.124 %, n=11; Student t-test: ** p= 0.009). These data show that an impairment in ADBE caused by knocking-down an essential component of this endocytic method can be observed using VAMP4-pH. This suggests that it is possible to impair ADBE by genetically interfering with proteins that are essential for its function.

5.2.3. BK channel opener may be able to rescue the endocytic defect observed in Dyn1$_{R237W}$ mutant

BK channels have long been proposed to be promising targets for treatment of epilepsy (reviewed in Leo et al., 2015; N'Gouemo, 2011), particularly because they can modulate action potential broadening and thus alter SV exocytosis and synaptic plasticity (Deng et al., 2013; Deng and Klyachko, 2016; Griguoli et al., 2016). There is evidence suggesting that a BK channel opener MaxiPost, can rescue both spine defects and behavioural deficits in a mouse model of FXS, a disorder in which epilepsy is often comorbid (Hebert et al., 2014). Furthermore, dyn1 has been found to associate with BK channels *in vivo* (Gorini et al., 2010). Thus, we decided to test whether modulation of BK channels could rescue the defective SV recycling observed with these dyn1 mutants.

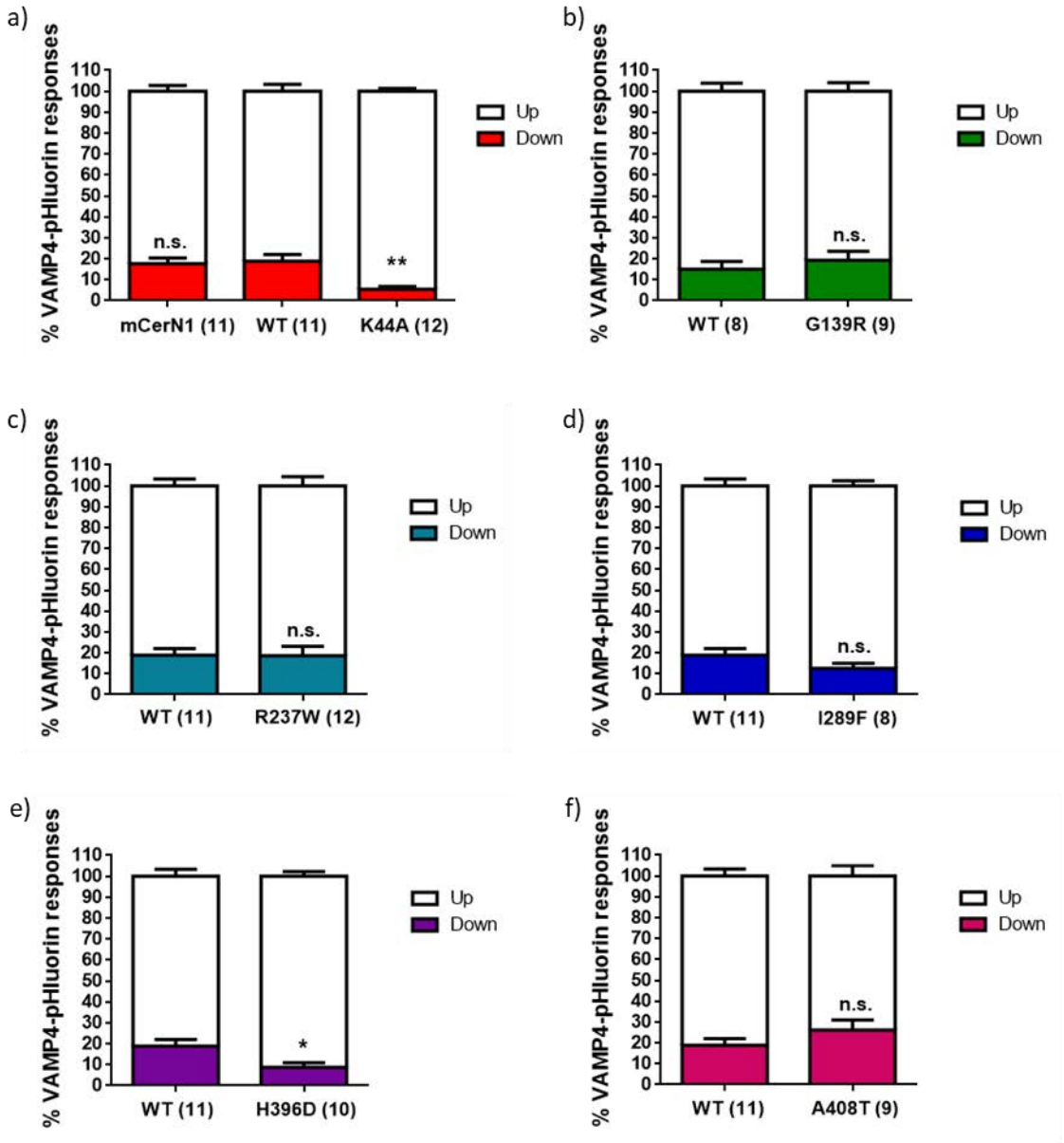

Figure 5.6 Overexpression of mCer-Dyn1$_{K44A}$ or mCer-Dyn1$_{H396D}$ decreases the proportion of nerve terminals undergoing ADBE

*Hippocampal neurons derived from WT mice were transfected with mCerN1, VAMP4-pH and either WT or mutant mCer-Dyn1, 2 days prior to imaging. a-f) The percentage of up and down VAMP4-pH responses in individual nerve terminals are displayed plotted against mCer-Dyn1$_{WT}$ a) mCer-Dyn1$_{K44A}$ (K44A, red) and mCerN1 empty vector 1-way ANOVA with Dunnett's test comparing values to WT: n.s. p> 0.05, ** p < 0.01. b) mCer-Dyn1$_{G139R}$ (G139R, green), c) mCer-Dyn1$_{R237W}$ (R237W, turquoise), d) mCer-Dyn1$_{I289F}$ (I289F, blue), e) mCer-Dyn1$_{H396D}$ (H396D, purple), f) mCer-Dyn1$_{A408T}$ (A408T, magenta). Down responses represent ABDE. Neurons were stimulated 40 Hz 10 s. Following stimulation, for each cell, fluorescence of each nerve terminals was measured and sorted if increased "up trace"; if decreased "down trace". "Down" traces are a measure of a nerve terminal undergoing ADBE. b-f) n.s. non-significant p > 0.05 by Student t-test, * p < 0.05.*
For each condition, experimental n in brackets and error bars ± SEM.

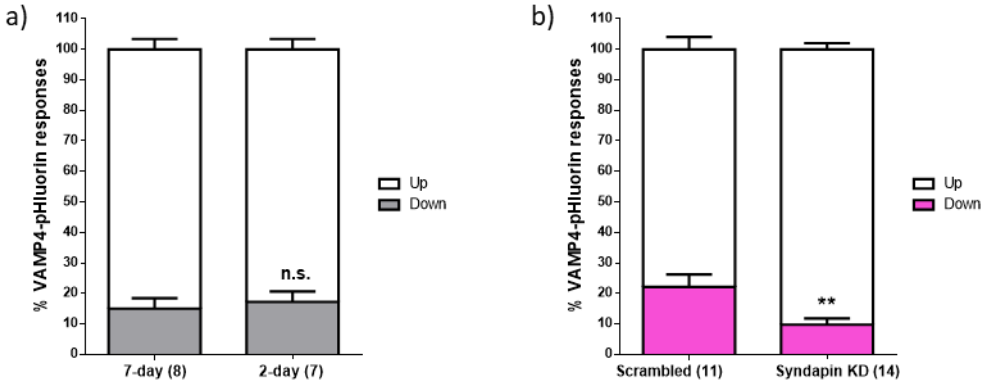

Figure 5.7 Proportion of nerve terminals undergoing ADBE can be genetically altered

*a) Hippocampal neurons derived from WT mice were transfected with mCerN1 and VAMP4-pH either 7 days or 2 days prior to imaging on DIV 13-14. Neurons were stimulated 40 Hz 10 s. Following stimulation, for each cell, fluorescence of each nerve terminals was measured and sorted into "up" or "down" traces. The percentage of up and down VAMP4-pH responses in individual nerve terminals. Down traces indicate the proportion of nerve terminals undergoing ADBE. b) Hippocampal neurons derived from wildtype cultures were transfected with mCerN1 and VAMP4-pH and either syndapin KD vector or scrambled vector 3 days prior to imaging. a-b) n.s. non-significant $p > 0.05$, * $p < 0.05$ by Student t-test. For each condition, experimental n in brackets and error bars ± SEM.*

We initially characterised the effect of different doses of the BK channel opener MaxiPost on SV recycling in WT hippocampal neurons using our sypHy imaging assay. WT neurons were transfected with sypHy and incubated in either DMSO, 3 μM, 10 μM or 30 μM MaxiPost for 120 s prior to imaging and throughout imaging. The neurons were stimulated at low frequency (300 action potentials, 10 Hz; Figure 5.8a). We first looked at SV exocytosis, since BK channels can modulate fusion of SVs through control of AP duration. SypHy fluorescence time traces were normalised to the total SV pool revealed by NH_4Cl buffer to examine exocytosis (Figure 5.8b). The amount of exocytosis was quantified as a proportion of total SV pool fluorescence (Figure 5.8d). There was a significant difference (1-way ANOVA with Dunnett's test comparing to DMSO: ** p=0.003) between MaxiPost 30 μM (0.239 ± 0.028 units, n=8) and DMSO (0.378 ± 0.021 units, n=10). There was no difference in peak exocytosis amount (1-way ANOVA with Dunnett's test comparing to DMSO: n.s. p> 0.05) between MaxiPost 3 μM (0.389 ± 0.036 units, n= 7), MaxiPost 10 μM (0.332 ± 0.028, n= 10) and DMSO. Thus, high doses of MaxiPost can decrease the amount of SV exocytosis occurring during low frequency stimulation, in agreement with its action at BK channels.

We then investigated whether endocytosis was altered with MaxiPost treatment. SypHy fluorescence traces were normalised to the stimulation peak to examine sypHy retrieval (Figure 5.8c). The fluorescence traces of 10 μM and 30 μM MaxiPost were significantly different (2-way ANOVA with Dunnett's to compare to DMSO: * $p < 0.05$, ** $p < 0.01$, *** $p < 0.001$, **** $p < 0.0001$). Single-phase decay curves were also fit to the traces to provide the sypHy τ (Figure 5.8e). There was a significant difference (1-way ANOVA with Dunnett's test comparing to DMSO control) between 10 μM MaxiPost (29.800 ± 2.345 s, n=10; * p= 0.012), 30 μM MaxiPost (21.560 ± 2.671 s, n=8; *** p = 0.0005) and DMSO (46.830 ± 6.091 s, n=10). However, there was no significant difference with 3 μM MaxiPost (35.650 ± 3.637 s, n=7; n.s. p > 0.05). Therefore, MaxiPost can accelerate SV endocytosis in WT neurons in a dose-dependent manner.

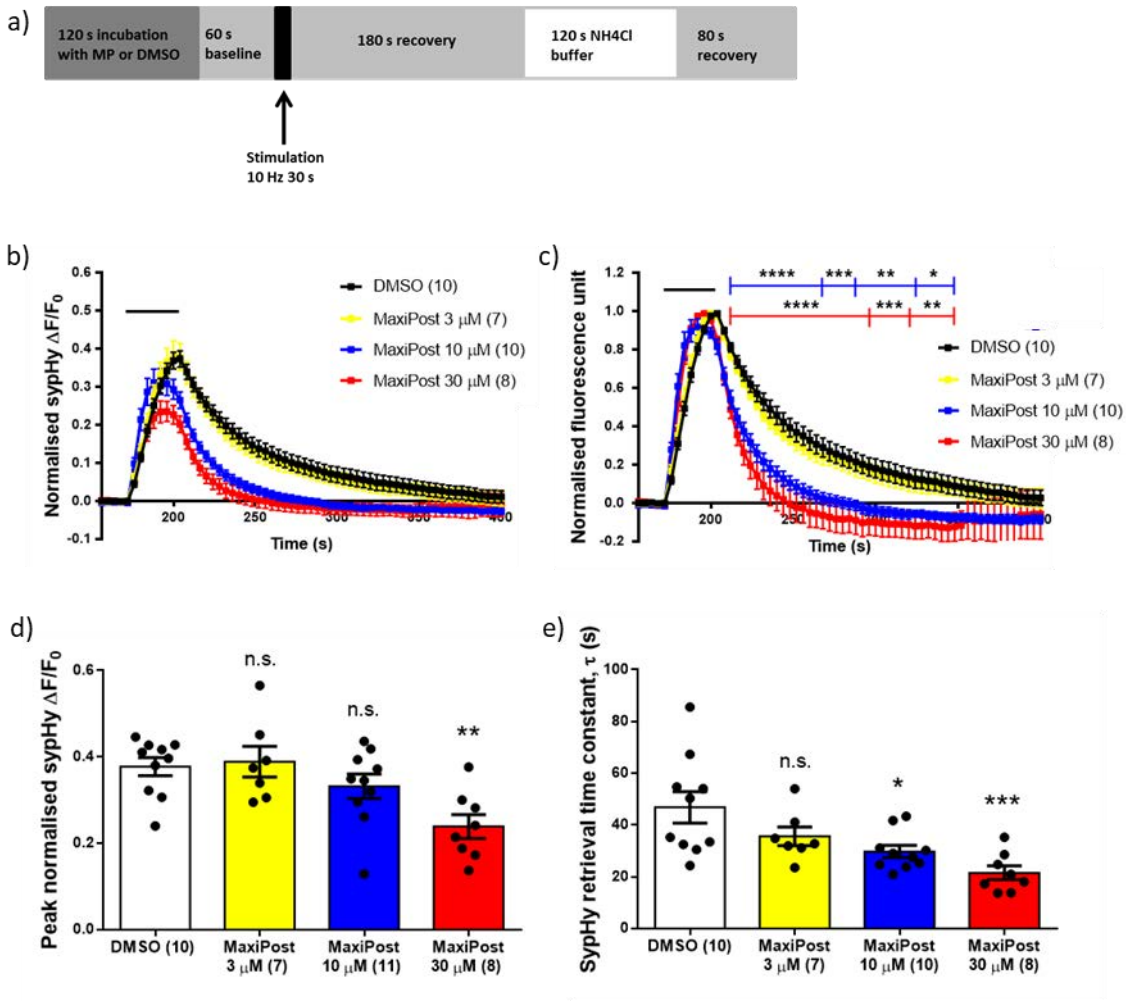

Figure 5.8 Effects of BK channel opener molecule MaxiPost on sypHy exocytosis and endocytosis at low frequency stimulation (10 Hz 30 s)

*Hippocampal neurons derived from WT mice were transfected with sypHy on DIV 7. Cells were perfused with DMSO (vehicle) or various MaxiPost concentrations for 120 s prior to imaging. Imaging was also performed in the presence of MaxiPost on DIV 13-15. a) Time course of experiment. b-c) Mean sypHy fluorescence traces of hippocampal neurons treated with DMSO (white), MaxiPost 3 μM (yellow),10 μM (blue), 30 μM (red). Bars indicate the period of stimulation, 10 Hz 30 s. b) normalised to the total SV number as revealed by NH_4Cl. c) normalised to the peak of stimulation. 2-way ANOVA with Dunnett's multiple comparisons test comparing each trace to the DMSO trace * $p < 0.05$; ** $p < 0.01$; *** $p < 0.001$; **** $p < 0.0001$ d) Mean and individual stimulation peak heights obtained from individual sypHy traces of data in b). e) Mean and individual sypHy retrieval time constants (τ) of data plotted in c). d-e) 1-way ANOVA with Dunnett's test comparing all means to DMSO (control condition): * $p < 0.05$; ** $p < 0.01$; *** $p < 0.001$; n.s. $p > 0.05$.*
For each condition, experimental n in brackets and error bars ± SEM.

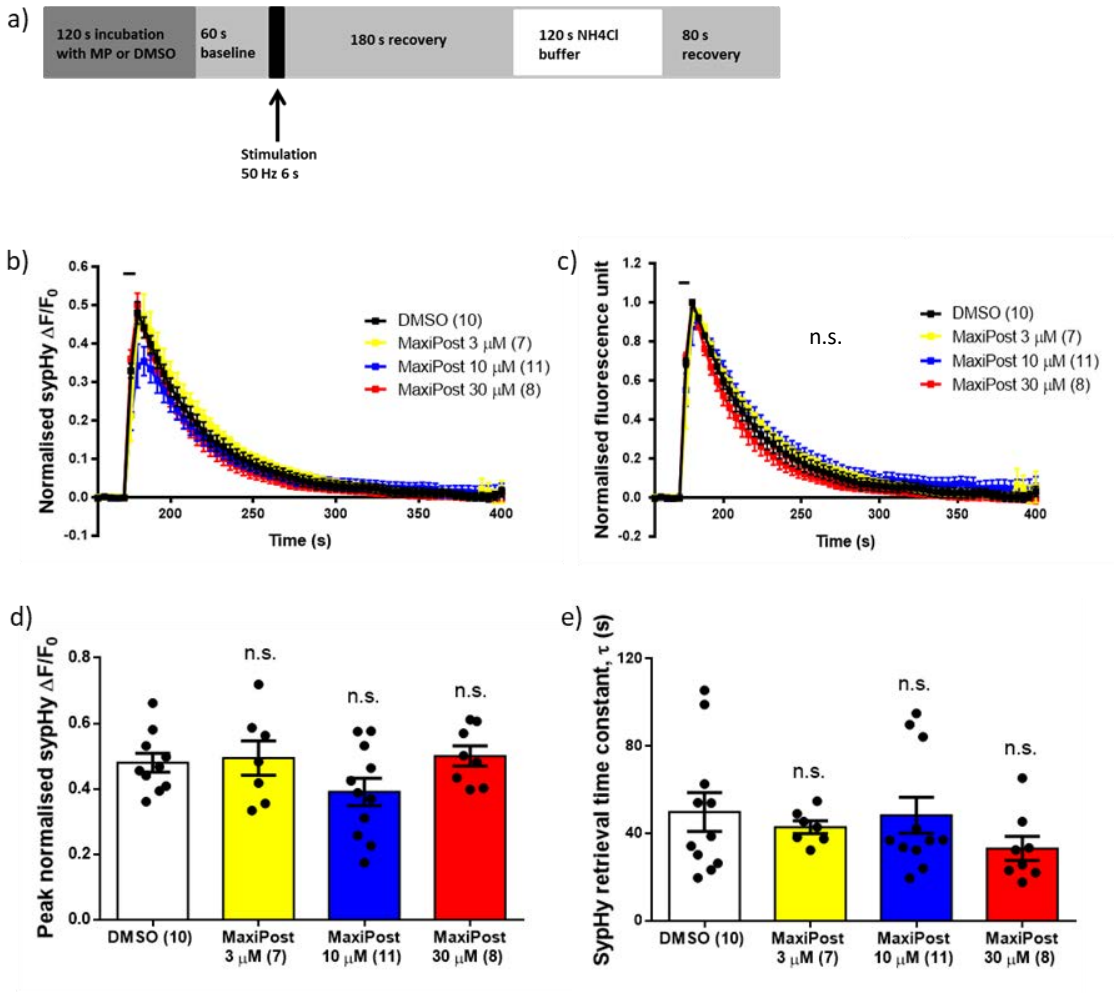

Figure 5.9 Effects of BK channel opener molecule MaxiPost on sypHy exocytosis and endocytosis at high frequency stimulation (50 Hz 6 s)

Hippocampal neurons derived from WT mice were transfected with sypHy on DIV 7. Cells were perfused with DMSO (vehicle) or various MaxiPost concentrations for 120 s prior to imaging. Imaging was also performed in the presence of MaxiPost at DIV 13-15. a) Time course of experiment. b-c) Mean sypHy fluorescence traces of hippocampal neurons treated with DMSO (white), MaxiPost 3 μM (yellow), 10 μM (blue), 30 μM (red). Bars indicate the period of stimulation, 50 Hz 6 s. b) normalised to the total SV number as revealed by NH_4Cl. c) normalised to the peak of stimulation. 2-way ANOVA n.s. $p > 0.05$. d) Mean and individual stimulation peak heights obtained from individual sypHy traces of data in b). e) Mean and individual sypHy retrieval time constants (τ) of data plotted in c). d-e) 1-way ANOVA n.s. $p > 0.05$.
For each condition, experimental n in brackets and error bars ± SEM.

We then repeated these experiments at high frequency stimulation to determine whether the effect of MaxiPost was frequency-dependent. Once again, WT neurons transfected with sypHy were incubated in either DMSO or 3 μM, 10 μM or 30 μM of MaxiPost for 120 s prior to imaging and imaged in the presence of MaxiPost. The neurons were stimulated at high frequency (50 Hz 6 s; Figure 5.9a). SypHy fluorescence time traces normalised to the total SV pool (Figure 5.8b) were used to determine the amount of exocytosis that occurred during stimulation (Figure 5.8d). There were no significant differences (1-way ANOVA n.s. $p > 0.05$) in the normalised sypHy peak heights of across MaxiPost doses (3 μM: 0.494 ± 0.052 units, n=7; 10 μM: 0.391 ± 0.042 units, n=11; 30 μM: 0.501 ± 0.031 units, n=8) and DMSO (0.480 ± 0.029 units, n=10). Thus, MaxiPost does not alter SV exocytosis at high frequency stimulation.

To determine whether endocytosis upon high frequency stimulation (50 Hz 6 s) was affected by MaxiPost, we normalised the traces to the peak of stimulation and saw no differences between MaxiPost traces and DMSO sypHy trace (2-way ANOVA n.s. $p> 0.05$; Figure 5.9c). We then calculated the sypHy τ and again found no differences between treatment conditions compared to DMSO (1-way ANOVA n.s. $p> 0.05$; 3 μM: 42.930 ± 2.874 s, n=7; 10 μM: 48.370 ± 8.262 s, n=11; 30 μM: 33.220 ± 5.511 s, n=8; DMSO: 49.860 ± 8.860 s, n=10; Figure 5.9e). Thus, treatment with MaxiPost does not alter SV endocytosis during high frequency stimulation. Taken all together, these data show that treatment with MaxiPost decreases SV exocytosis and accelerates SV endocytosis in a dose-dependent manner at low frequency stimulation.

We then investigated whether the decrease in SV exocytosis seen with high doses of MaxiPost treatment was due to the drug affecting SV exocytosis or due to the faster SV endocytosis seen with this concentration of MaxiPost. We used Bafilomycin A1 to uncouple exocytosis from endocytosis to determine the total amount of SV exocytosis occurring during low frequency stimulation (10 Hz 90 s).

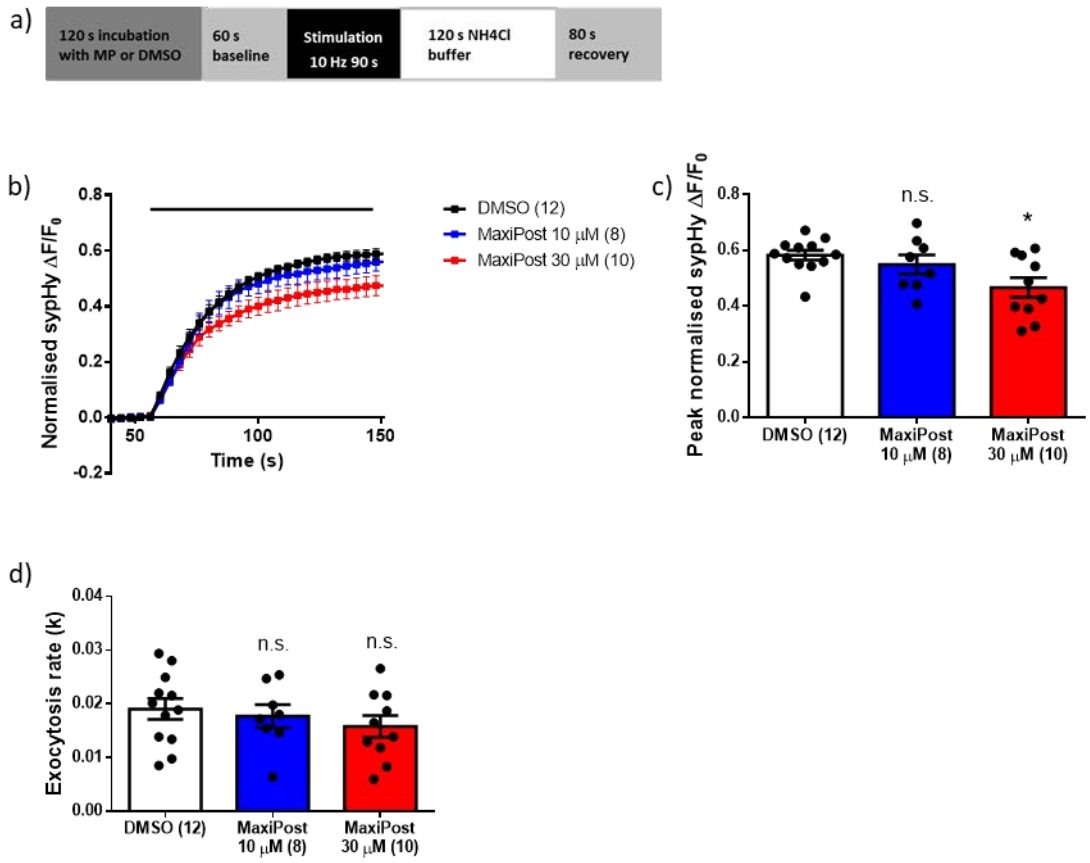

Figure 5.10 BK channel opener molecule MaxiPost impairs sypHy exocytosis at high doses

*Hippocampal neurons derived from WT mice were transfected with sypHy on DIV 7. Cells were perfused with Bafilomycin and either DMSO or various MaxiPost concentrations for 120 s prior to and for the duration of imaging. Neurons were imaged at DIV 13-15. a) Time course of experiment. b) Mean sypHy fluorescence traces of hippocampal neurons treated with DMSO (white), MaxiPost 10 µM (blue), 30 µM (red) normalised to the total SV number as revealed by NH_4Cl. Bar indicates the period of stimulation, 10 Hz 90 s. c) Mean and individual stimulation peak heights obtained from individual sypHy traces of data in b). d) Mean and individual exocytosis rates of data in b) obtained by calculating the slope of a linear regression fit to the first 3 timepoints after the start of stimulation. c-d) 1-way ANOVA with Dunnett's test comparing values to DMSO: * $p < 0.05$, n.s. $p > 0.05$.*
For each condition, experimental n in brackets and error bars ± SEM.

WT neurons transfected with sypHy were incubated in Bafilomycin A1 and either DMSO, 10 μM or 30 μM MaxiPost for 120 s and then imaged undergoing perfusion with imaging buffer containing these drugs (Figure 5.10a,b). Both concentrations of MaxiPost were used as they were both able to accelerate endocytosis upon low frequency stimulation. Although there was no difference in exocytic rate (1-way ANOVA: n.s. $p > 0.05$; 10 μM: 0.018 ± 0.002 s, n=8; 30 μM: 0.016 ± 0.002 s, n=10; DMSO: 0.019 ± 0.002 s, n=12; Figure 5.10d), there was a significant difference in amount of exocytosis (1-way ANOVA with Dunnett's test comparing to DMSO) with 30 μM (0.466 ± 0.035 units, n=10, * $p = 0.0101$) compared to DMSO (0.583 ± 0.017 units, n=12) but not with 10 μM (0.549 ± 0.034 units, n=8; n.s. $p > 0.05$). Therefore, a treatment with 30 μM MaxiPost impairs SV exocytosis and this is not due to the accelerated SV endocytosis observed in Figure 5.8c,e.

We determined that MaxiPost impairs CME, as sypHy retrieval was accelerated at low frequency stimulation which preferentially recruits this endocytosis mode in cultured hippocampal neurons (Granseth et al., 2006). We also wanted to investigate whether MaxiPost could alter ADBE. We transfected WT hippocampal neurons with VAMP4-pH to examine the impact of MaxiPost treatment on ADBE. Neurons were incubated in MaxiPost or DMSO for 120 s prior to imaging and imaged in their presence. Nerve terminals were divided into "up" or "down" traces depending on fluorescence signal following stimulation (40 Hz 10 s; Figure 5.11). There was no difference (1-way ANOVA n.s. $p > 0.05$) in the proportion of "down" traces representing ADBE between MaxiPost-treated (10 μM: 12.640 ± 2.009 %, n=4; 30 μM: 16.240 ± 4.610 %, n=4) and DMSO treated neurons (19.590 ± 5.113 %, n=6). Therefore, treatment with MaxiPost does not affect ADBE.

MaxiPost treatment with both 10 μM and 30 μM concentrations appears to enhance SV endocytosis, particularly CME, at low frequency stimulation. Therefore, we investigated whether treatment with MaxiPost could rescue the endocytic defect seen when overexpressing the *de novo* mCer-Dyn1 mutants.

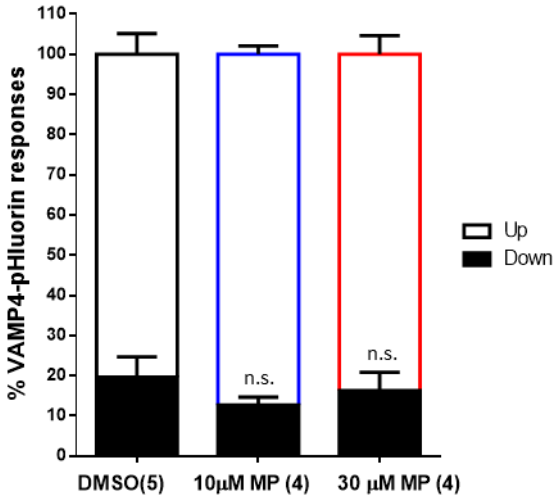

Figure 5.11 No effect of BK channel opener molecule MaxiPost on proportion of VAMP4-pH down traces

Hippocampal neurons derived from WT mice were transfected with mCerN1 and VAMP4-pH, 2 days prior to imaging. Cells were perfused with DMSO (black) or MaxiPost 10 µM (blue), 30 µM (red) for 120 s prior to imaging. Imaging was also performed in the presence of MaxiPost at DIV 13-14. a) The percentage of up and down VAMP4-pH responses in individual nerve terminals after 40 Hz 10 s stimulation are displayed.1-way ANOVA n.s. p> 0.05. Down responses represent ABDE. Neurons were stimulated 40 Hz 10 s. Following stimulation, for each cell, fluorescence of each nerve terminals was measured and sorted if increased "up"; if decreased "down". Down traces represent nerve terminals undergoing ADBE.
For each condition, experimental n in brackets and error bars ± SEM.

We first determined whether MaxiPost could accelerate endocytosis when mCer-Dyn1$_{WT}$ was overexpressed. We used the same protocol as previously described in Figure 5.8 (Figure 5.12a). WT hippocampal neurons overexpressing mCer-Dyn1$_{WT}$ and sypHy were treated with either DMSO or MaxiPost prior to and for the duration of imaging. SypHy fluorescence time traces were normalised to the peak of stimulation to look at endocytosis by comparing fluorescence traces (Figure 5.12b). There was a significant difference in the fluorescence trace (2-way ANOVA with Dunnett's comparing to DMSO: * $p< 0.05$) of 30 µM MaxiPost but not with 10 µM MaxiPost. Thus, high concentrations of MaxiPost can enhance SV endocytosis in neurons overexpressing mCer-Dyn1$_{WT}$.

We then looked at peak sypHy exocytosis during stimulation by normalising traces to the total SV pool fluorescence revealed by NH_4Cl (traces not shown). There was a significant difference (1-way ANOVA with Dunnett's test comparing to DMSO condition) in peak sypHy fluorescence during stimulation with 30 µM MaxiPost treatment (0.294 ± 0.046 units, n=6; * $p=0.022$) but not with 10 µM MaxiPost treatment (0.424 ± 0.074 units, n=8; n.s. $p> 0.05$) compared to DMSO (0.512 ± 0.367 units, n= 10). Therefore, high concentrations of MaxiPost (30 µM) decrease SV exocytosis in neurons overexpressing mCer-Dyn1$_{WT}$, as was the case in WT neurons (Figures 5.8, 5.10). Taken together, these data suggest that mCer-Dyn1$_{WT}$ overexpression does not impair MaxiPost treatment from altering both SV endocytosis and exocytosis at high concentration.

We next attempted to rescue the severe SV endocytosis impairment seen with overexpression of mCer-Dyn1$_{R237W}$ in our cultures (Figure 5.3b,d). We chose this mutant because it is a recurrent dyn1 mutation associated with a very severe seizure phenotype (EuroEPINOMICS-RES Consortium et al., 2014; von Spiczak et al., 2017). Furthermore, our assays show that this mutation only appeared to impair CME and not ADBE (Figure 5.4c). As we have found that MaxiPost only alters CME, this mutant should be a good rescue candidate.

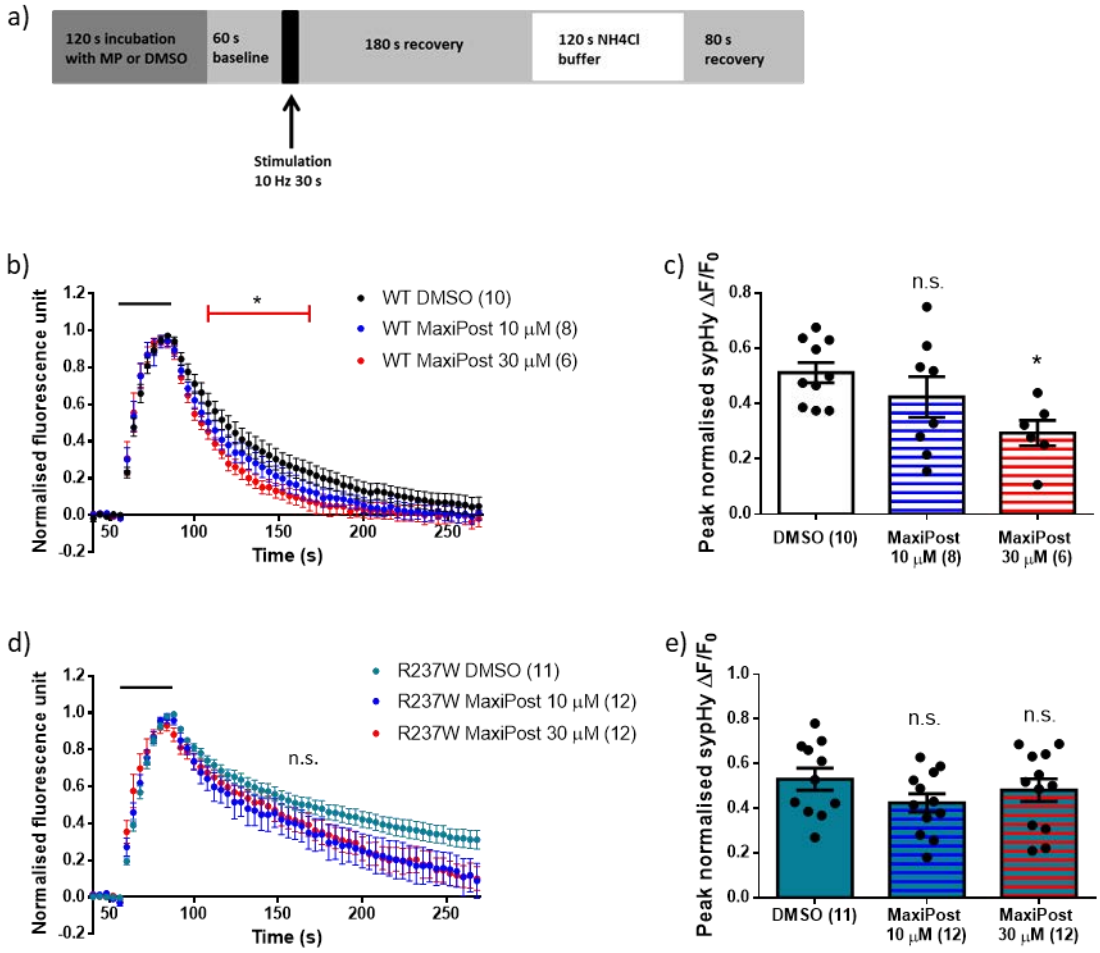

Figure 5.12 Effect of BK channel opener molecule, MaxiPost, on SypHy retrieval in hippocampal neurons overexpressing the mCer-Dyn1$_{R237W}$ mutant

*a) Time course of experiment. Cells were perfused with DMSO (vehicle) or MaxiPost for 120 s prior to imaging at DIV 13-14. Imaging was also performed in the presence of MaxiPost. b) Hippocampal neurons derived from WT mice were transfected with sypHy and mCer-Dyn1$_{WT}$ (WT) 2 days prior to imaging. Mean sypHy fluorescence traces of hippocampal neurons treated with DMSO (white), MaxiPost 10 μM (blue) or 30 μM (red). Bar indicates the period of stimulation, 10 Hz 30 s. 2-way ANOVA with Dunnett's multiple comparisons test comparing each trace to the DMSO trace * $p < 0.05$. c) Mean and individual stimulation peak heights obtained from individual sypHy traces of data in b). d) Hippocampal neurons derived from wildtype cultures were transfected with sypHy and mCer-Dyn1$_{R237W}$ 2 days prior to imaging. Mean sypHy fluorescence traces of hippocampal neurons treated with DMSO (turquoise), MaxiPost 10 μM (blue) or 30 μM (red). Bar indicates the period of stimulation, 10 Hz 30 s. e) Mean and individual stimulation peak heights obtained from individual sypHy traces of data in d). c,e) 1-way ANOVA with Dunnett's test comparing all means to DMSO (control condition): * $p < 0.05$; n.s. $p > 0.05$.*
For each condition, experimental n in brackets and error bars ± SEM.

We repeated our MaxiPost imaging assay in neurons overexpressing mCer-Dyn1$_{R237W}$ and sypHy. There was no significant difference in fluorescence traces across treatments (2-way ANOVA n.s. $p > 0.05$) however, there was a trend toward enhanced SV endocytosis with both MaxiPost concentrations tested. Therefore, although MaxiPost could not rescue the defect in SV endocytosis observed with overexpression of mCer-Dyn1$_{R237W}$ at the concentrations tested. The trend toward enhanced SV endocytosis observed suggest that these experiments should be repeated to reveal whether there is indeed a significant difference in fluorescence traces between treatment conditions.

We then looked at SV exocytosis during stimulation as a proportion of the total SV pool. Interestingly, there was no difference in sypHy exocytosis peak heights (1-way ANOVA: n.s. $p > 0.05$; 10 μM: 0.0425 ± 0.041 units, n=12; 30 μM: 0.481 ± 0.050 units, n=12; DMSO: 0.531 ± 0.050 units, n=11), suggesting that MaxiPost cannot affect SV exocytosis in the presence of this mutant.

5.2.4. Impaired GTPase activity of mCer-Dyn1$_{K44A}$, mCer-Dyn1$_{G139R}$ and mCer-Dyn1$_{R237W}$ mutants

Dyn1 mediates membrane fission during SV endocytosis through its GTPase activity (Antonny et al., 2016). The mutations studied were all predicted by *in silico* modelling to have deleterious effects on SV endocytosis (D. Soares personal correspondence). Specifically, Dyn1$_{G139R}$ and Dyn1$_{R237W}$ were predicted to impair GTPase activity of dyn1. We purified mCer-Dyn1$_{WT}$ and mutant mCer-Dyn1 to perform a GTPase assay to determine whether defective GTPase activity is responsible for the SV recycling deficits observed in our assays.

HEK293T cells were transfected with either mCerN1, mCer-Dyn1$_{WT}$ or mutant mCer-Dyn1. Cells were lysed and mCerN1, mCer-Dyn1$_{WT}$ and mutant

mCer-Dyn1$_{WT}$ was isolated by immunoprecipitation. Isolated proteins were then used for a colorimetric Malachite green GTPase assay which detects the release of inorganic phosphates (Pi). MCer-Dyn1$_{K44A}$ (93.630 ± 7.158 µM, n=4, 1-way ANOVA with Dunnett's test comparing to mCer-Dyn1$_{WT}$: * p= 0.014) had significantly less Pi release as compared to mCer-Dyn1$_{WT}$ (119.600 ± 5.840 µM, n=4; Figure 5.13a) in agreement with its inability to hydrolyse GTP. As predicted by *in silico* modelling, the mCer-Dyn1$_{G139R}$ (103.500 ± 7.796 µM, n=3, * p= 0.031) and mCer-Dyn1$_{R237W}$ (102.800 ± 3.943 µM, n=3, * p= 0.026) had significantly reduced Pi release compared to mCer-Dyn1$_{WT}$ (123.200 ± 2.706 µM, n=3). The mCer-Dyn1$_{I289F}$ mutant's Pi release was comparable to mCer-Dyn1$_{WT}$ levels (131.000 ± 0.887 µM, n=3, n.s. p > 0.05; Figure 5.13b). As expected, the mutations in the stalk did not impair Pi release compared to WT (1-way ANOVA n.s. p> 0.05, mCer-Dyn1$_{H396D}$: 122.700± 4.646 µM, n=3; mCer-Dyn1$_{A408T}$: 122.500 ± 1.185 µM, n=3; Figure 5.13c). For all experiments the mCerN1 vector produced significantly less Pi release than WT dyn1 control (1-way ANOVA with Dunnett's test **** p< 0.0001). Therefore, this condition represents basal Pi release in this assay. These data show that the mCer-Dyn1$_{K44A}$ mutant displays reduced GTPase activity, as previously reported (Damke et al., 1994). Furthermore, two GTPase domain mutants, mCer-Dyn1$_{G139R}$ and mCer-Dyn1$_{R237W}$ also impair GTPase activity, whereas the mCer-Dyn1$_{I289F}$, mCer-Dyn1$_{H396D}$ and mCer-Dyn1$_{A408T}$ do not affect dyn1 GTPase activity.

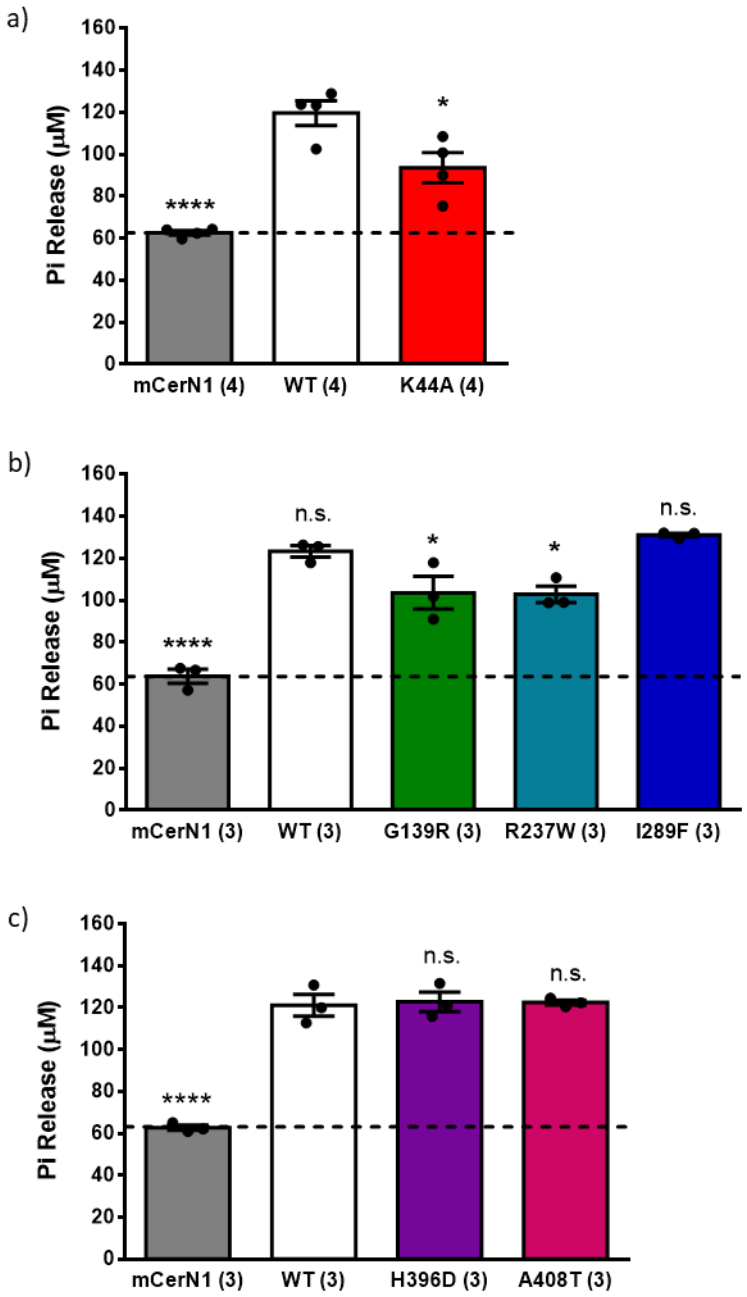

Figure 5.13 G139R and R237W mutations impair GTPase activity as predicted by in silico modelling

*HEK293T cells were transfected with mCerN1 empty vector (grey), mCer-Dyn1$_{WT}$ (WT, white) or mutant mCer-Dyn1$_{K44A}$ (K44A, red), mCer-Dyn1$_{G139R}$ (G139R, green), mCer-Dyn1$_{R237W}$ (R237W, turquoise), mCer-Dyn1I_{289F} (I289F, blue), mCer-Dyn1$_{H396D}$ (H396D, purple), mCer-Dyn1$_{A408T}$ (A408T, magenta) 48 h prior to lysis. Mutant proteins were isolated and GTPase activity was determined using a colorimetric GTPase assay based on the detection of free inorganic phosphate. a) GTPase deficient mCer-Dyn1$_{K44A}$ dominant negative mutant. b) mutations in dyn1 GTPase domain. c) mutations in dyn1 stalk domain. 1-way ANOVA with Dunnett's test comparing values to WT. * $p < 0.05$; **** $p < 0.0001$; n.s. $p > 0.05$.*
For each condition, experimental n in brackets and error bars ± SEM.

5.3. Discussion

In this work, we studied the effects of a series of dyn1 mutants on SV recycling, to determine whether any defects observed could be responsible for manifestation of the observed developmental disorders. We first characterised the $Dyn1_{K44A}$ mutation in dissociated primary neuronal cultures. This mutation was designed to impair both the binding of GTP and its hydrolysis (Damke et al., 1994) and impairs endocytosis in non-neuronal cell lines (Damke et al., 1994; Damke et al., 2001). The *de novo* $Dyn1_{G139R}$, $Dyn1_{R237W}$, $Dyn1_{I289F}$ and $Dyn1_{H396D}$ mutations were identified in patients suffering from seizures and/or developmental delay (DDD Consortium and W. Lam personal correspondence, Table 5.1). We also chose to investigate the effect of the $Dyn1_{A408T}$ *ftfl* mutation which spontaneously arose in mice and led to seizure phenotypes. We found that the *de novo* patient mutations had different effects on both CME and ADBE.

5.3.1. Modelling de novo dyn1 mutations

The crystal structure of dyn1 has been resolved (Faelber et al., 2011), therefore it is possible to use *in silico* modelling to predict whether *de novo* dyn1 mutations can impair its function. Previous studies have already predicted which functional defects may arise from *de novo* dyn1 mutations linked to epileptic encephalopathy. The predictions in these studies were based on their location in the protein and the amino acid substitution (von Spiczak et al., 2017). Our collaborator, Dr Dinesh Soares (American Chemical Society), used *in silico* pathogenicity detectors to determine whether the *de novo* mutations studied were likely to be deleterious to dyn1 function. $Dyn1_{G139R}$, $Dyn1_{R237W}$, $Dyn1_{I289F}$ were highly likely to be deleterious, whereas $Dyn1_{H396D}$ was predicted to be deleterious by PolyPhen-2 (Adzhubei et al., 2010) analysis but benign by SIFT analysis (Kumar et al., 2009) (D. Soares, personal correspondence). FoldFX forcefield was used to assess whether the mutations in the G domain destabilise the structure of dyn1. This analysis predicted that all mutations would be destabilising consistent with the non-conservative nature of the amino acid substitutions. Furthermore, both the $Dyn1_{G139R}$ and $Dyn1_{R237W}$ mutations were

predicted to impair GDP and GTP binding due to their proximity to the GDP binding site (D. Soares, personal correspondence). This work, therefore, was to determine whether these predicted deleterious mutations would impair SV recycling.

5.3.2. Effects of mutant dyn1 on SV recycling

5.3.2.1. Mutations in the GTPase domain

We found that $Dyn1_{K44A}$ impaired CME as determined by defective sypHy retrieval. Our results agree with what has previously been reported in non-neuronal cell lines, where $Dyn1_{K44A}$ impairs transferrin uptake (Damke et al., 1994; Damke et al., 2001). Furthermore, $Dyn1_{K44A}$ also impaired ADBE as determined by fewer VAMP4-pH "down" traces. These results were expected as this mutation impairs dyn1 GTPase activity which is essential for mediating membrane fission in both CME (Hinshaw and Schmid, 1995) and ADBE (Clayton et al., 2009). As for the mutations in the GTPase domain, $Dyn1_{R237W}$ and $Dyn1_{I289F}$ mutants severely impaired sypHy retrieval without having any effect on the proportion of nerve terminals undergoing ADBE. Interestingly, $Dyn1_{G139R}$ did not impair SV recycling through either mode of endocytosis. We also measured basal GTPase activity of these dyn1 mutants. We found that $Dyn1_{G139R}$ and $Dyn1_{R237W}$ mutants showed decreased GTPase activity as predicted by FoldX forcefield modelling (D. Soares, personal correspondence). This was expected as these residues are both in close proximity to where GDP binds, with R237 directly participating in GDP binding.

Our data suggest that defective basal GTPase activity is not sufficient to impair endocytosis as $Dyn1_{G139R}$ with defective GTP hydrolysis does not impair SV endocytosis. This lends support to previous work that shows that both effective GTP hydrolysis and a conformational change of dyn1 are required for endocytosis to occur (Damke et al., 2001; Marks et al., 2001). It was somewhat puzzling that $Dyn1_{G139R}$ mutation did not impair either form of endocytosis even though its GTPase activity was significantly impaired. Although basal GTPase activity of

Dyn1$_{G139R}$ way impaired, it is possible that evoked GTPase activity is not impaired. As previously described, self-assembly, phospholipid-binding and interactions with other the SH3 domain of other proteins can improve dyn1's GTPase activity. Therefore, it is possible that *in vivo* these factors can act together to promote GTPase activity for efficient membrane fission and SV endocytosis. Additionally, it is possible that Dyn1$_{G139R}$ dimerises with Dyn1$_{WT}$ *in vivo*. Dyn1$_{WT}$ present in cultures may be sufficient to rescue any SV recycling phenotype as what has been shown with Dyn1$_{A408T}$ (Asinof et al., 2016).

Dyn1$_{I289F}$ showed GTPase activity comparable to WT levels (Figure 5.13b), however SV endocytosis was impaired even though it was not significantly overexpressed (Figure 5.1b). Intact GTPase activity is not sufficient for dyn1-mediated endocytosis, dyn1 must also undergo a conformational for endocytosis to occur (Damke et al., 2001; Marks et al., 2001). Indeed, a previously characterised Dyn1$_{K142A}$ mutation showed mildly impaired GTPase activity but could still strongly inhibit transferrin endocytosis in COS-7 fibroblasts (Marks et al., 2001). Therefore, it is possible that the Dyn1$_{I289F}$ mutant is unable to change conformation upon GTP hydrolysis thus impairing SV endocytosis. This mutation was predicted to destabilise dyn1 structure but not affect GDP/GTP binding. Destabilising dyn1's structure may impair its interactions with phospholipids or with SH3 domains. This could prevent it from being recruited to endocytic pits by amphiphysin-1 and endophilin. Super resolution imaging of nanobodies to dyn1 could be used to determine whether this mutant can be targeted to invaginating endosome's necks. Mislocalisation of mCer-Dyn1$_{I289F}$ could explain why SV endocytosis is impaired in this model.

5.3.2.2. Mutations in the stalk domain

Dyn1$_{H396D}$ located in the stalk domain was the only *de novo* mutation that impaired both forms of SV endocytosis. This mutation corresponds to the Dyn1$_{G397D}$ mutation in rat dyn1 which has been shown to have impaired self-assembly (Ford et al., 2011).

The Dyn1$_{G397D}$ mutant was unable to form helical structures in the presence of lipid nanotubules which suggests that it may not be able to mediate efficient endocytosis (Ford et al., 2011). Dyn1$_{H396D}$'s inability to oligomerise may contribute to the defective SV recycling seen in this mutant. To determine whether this could be the case, we could generate the previously characterised Dyn1$_{G397D}$ mutant and determine whether we observe impaired CME and ADBE as observed with overexpression of mCer-Dyn1$_{H396D}$. This would provide confirmation as to whether defective dyn1 self-assembly can impair SV endocytosis.

Interestingly, we also observed increased endocytosis during exocytosis with this mutant. At physiological temperatures, there are two phases of endocytosis: an initial activity-dependent acceleration phase, followed by a slower endocytosis phase (Armbruster et al., 2013). These two phases may also be present at room temperature, but harder to dissociate. Dephosphorylation of dyn1 at S774 and S778 by calcineurin mediates this initial acceleration phase of endocytosis (Armbruster et al., 2013). The change from the positively charged histidine to the negatively charged aspartic acid in this mutation could impair dyn1 folding (Ford et al., 2011). We hypothesise that this change in folding could reveal the S774 and S778 residues and allow them to be readily dephosphorylated thus mediating the enhanced endocytosis seen during exocytosis without altering the later slow phase of endocytosis as seen in our model.

We also looked at the spontaneously occurring Dyn1$_{A408T}$ *ftfl* mutation. We did not observe any SV recycling defects in this model through either CME or ADBE. GTPase activity was comparable to Dyn1$_{WT}$ levels. Dyn1$_{A408T}$ has been previously described to show defective transferrin uptake when overexpressed in a COS-7 cell line (Boumil et al., 2010). Interestingly, there was also increased tubular networks connected to the plasma membrane in these cells (Boumil et al., 2010). These membrane tubules were similar to those that had been previously described when GTP hydrolysis was inhibited (Takei et al., 1995) or impaired (Marks et al., 2001).

This suggests that $Dyn1_{A408T}$ is unable to induce membrane fission despite being able to be recruited to the neck of invaginating pits (Takei et al., 1995). It is important to note, however, that this endocytic defect observed in COS-7 cells expressing $Dyn1_{A408T}$ could be rescued with $Dyn1_{WT}$ expression (Asinof et al., 2016) as this mutant can dimerise with $Dyn1_{WT}$ (Boumil et al., 2010). In our assay, we overexpressed $Dyn1_{A408T}$ in hippocampal neurons which already endogenously expressed $Dyn1_{WT}$. Therefore, in our hippocampal cultures, $Dyn1_{A408T}$ may be dimerising with the endogenous $Dyn1_{WT}$ to maintain efficient SV endocytosis. This may explain why we do not observe any endocytosis deficits with this mutant.

5.3.3. Rescue of endocytosis with MaxiPost

BK channels play an important role in SV recycling, particularly in SV exocytosis (reviewed in Griguoli et al., 2016). BK channels located in the presynapse colocalise with N-type and P/Q-type voltage-gated Ca^{2+} channels (Indriati et al., 2013; Loane et al., 2007). Upon depolarisation, the voltage-gated Ca^{2+} channels open and allow entry of Ca^{2+} into the cell. This is crucial for SV exocytosis as Ca^{2+} binding synaptotagmin-1 is essential for SV fusion. Ca^{2+} can then bind BK channels with high affinity which consequently lowers the $[Ca^{2+}]_i$ to subthreshold levels for neurotransmitter release (reviewed in Griguoli et al., 2016). Moreover, opening of the BK channel hyperpolarises the cell, further preventing neurotransmission by closing voltage-gated Ca^{2+} channels. Thus, BK channels can negatively regulate SV exocytosis.

We have shown that treatment of our hippocampal cultures with the BK channel fluoro oxindole opener molecule, MaxiPost, (Gribkoff et al., 2001), decreased exocytosis in a dose-dependent manner at low frequency stimulation (Figures 5.8, 5.10). This was expected as the opening of the BK channel would allow for an efflux of K^+ which would hyperpolarise the nerve terminal and close voltage-gated Ca^{2+} channels, thus preventing further SV fusion. These effects on SV recycling were not

present at high frequency stimulation. We propose that the absence of an effect on peak sypHy exocytosis was due to the short duration of stimulation in this condition rather than the frequency. This could be tested by stimulating at high frequency for a longer duration to see whether MaxiPost can still impair both SV exocytosis and endocytosis.

Our results suggest that BK channels may also play a role in SV endocytosis. It was surprising to us that MaxiPost had such a marked effect on CME in hippocampal neurons (Figure 5.8) as shown by significantly accelerated sypHy retrieval. There is a large body of evidence that BK channels play an important role in neurotransmission *in drosophila, c. elegans* and mice (Griguoli et al., 2016). However, as previously discussed, it mediates neurotransmitter release by modulation of AP length. It is possible that MaxiPost modulates SV endocytosis by regulating $[Ca^{2+}]_i$ through BK channel opening. There is no clear consensus as to whether increased $[Ca^{2+}]_i$ accelerates (Armbruster et al., 2013; Sankaranarayanan and Ryan, 2001) or slows endocytosis (Balaji et al., 2008; Cousin and Robinson, 2000; Leitz and Kavalali, 2011; Marland et al., 2016; Sankaranarayanan and Ryan, 2000). The localisation of presynaptic $[Ca^{2+}]_i$ can also determine how it affects SV endocytosis. There is evidence suggesting that prolonged, small increases in global Ca^{2+} can inhibit SV endocytosis, while transient, large increases in Ca^{2+} microdomains can trigger SV endocytosis (X. S. Wu and Wu, 2014). If it is indeed through modulating $[Ca^{2+}]_i$ that MaxiPost affects SV endocytosis, our data would suggest that decreased $[Ca^{2+}]_i$ accelerates endocytosis because the hyperpolarisation induced by the open BK channels would cause Ca^{2+} channels to close. To test this theory, we could increase $[Ca^{2+}]_i$ to determine whether it could slow SV endocytosis even further in this model.

Another possibility is that the interaction between dyn1 and the BK channel may underlie its role in SV endocytosis. The α-subunit which makes up the pore of BK

channels co-precipitates with dyn1 (Gorini et al., 2010). However, it remains unclear how this interaction mediates the activity of either component.

Alternatively, MaxiPost may have an off-target effect that modulates SV endocytosis. This could be tested by investigating whether another BK channel opener produces the same CME acceleration observed with MaxiPost treatment. It would also be interesting to determine whether a BK channel blocker such as paxilline or iberiotoxin would have the opposite effect and lead to a slowing of SV endocytosis.

MaxiPost can also activate non-inactivating potassium KCNQ channels (Jensen, 2002). These channels can regulate excitability of neurons and their response to synaptic input (reviewed in Jentsch, 2000). However as with the BK channels, there is no evidence that these channels can directly modulate SV endocytosis (Jentsch, 2000). It is important to note that MaxiPost cannot affect the number of nerve terminals undergoing ADBE (Figure 5.11). This may suggest that BK and KCNQ channels cannot modulate this endocytic mode. This work lends further support for different endocytic pathways having distinct regulatory mechanisms as pharmacological treatment can impair one mode but not another.

5.3.4. Different roles of dyn1 in CME and ADBE

Most studies looking at the effect of mutant dyn1 on endocytosis are performed in non-neuronal cell lines (Asinof et al., 2016; Boumil et al., 2010; Damke et al., 1994; Damke et al., 2001; Marks et al., 2001). Therefore, it was important to determine whether mutations known ($Dyn1_{K44A}$, $Dyn1_{A408T}$) or predicted ($Dyn1_{G139R}$, $Dyn1_{R237W}$, $Dyn1_{I289F}$, $Dyn1_{H396D}$) to impact GTP hydrolysis or dynamin self-assembly did indeed impair SV recycling in neurons. We found that these mutations

differentially impacted the CME or ADBE modes of endocytosis suggesting that different roles of dyn1 may regulate different modes of SV endocytosis.

Dyn1 can play multiple roles in SV endocytosis. Its different roles have been elucidated through the generation of a *Dnm1* KO mouse model (Ferguson et al., 2007) and by studying various mutations in different functional domains (Armbruster et al., 2013; Asinof et al., 2016; Baba et al., 1995; Boumil et al., 2010; Clayton et al., 2009; Damke et al., 1994; Damke et al., 2001; Marks et al., 2001).

Dyn1 can be recruited at the early stages of clathrin-coated pit formation where it can recruit more dyn1 to the forming pits to ensure efficient membrane fission through its GTPase activity (Taylor et al., 2012). Dyn1 is recruited to the neck of membrane invaginations in both CME (Hinshaw and Schmid, 1995) and ADBE (Clayton et al., 2009) where it can produce membrane fission through GTP hydrolysis and a subsequent conformational change (Damke et al., 2001; Marks et al., 2001). GTP-bound dyn1 is required for regulating clathrin-coated pit formation which is a rate limiting step in CME (Sever et al., 2000). In the absence of GTP, dyn1 forms a long scaffold around the necks of the invaginating clathrin-coated pits which stabilises their structure and prevents fission (Shnyrova et al., 2013). However, dyn1 bound to the non-hydrolisable GTPγS was also able to form stable scaffolds around the neck of invaginated membranes (Takei et al., 1995) which suggests that it may be the absence of GTP hydrolysis rather than the absence of GTP-binding that promotes dyn1 oligomerisation to form stable scaffolds. These findings suggest opposing roles of dyn1 depending on GTP-binding and hydrolysis.

In certain non-neuronal cell-lines that endogenously express dyn1, GSK3β phosphorylation of dyn1 can regulate the rate and formation of clathrin-coated pits (Reis et al., 2015). Indeed, GSK3β inactivation could drive SV endocytosis through a

compensatory rapid CME (Reis et al., 2015). This suggests that over-activation of dyn1 can dysregulate SV endocytosis at least in non-neuronal cells.

The other functional domains of dyn1 can also mediate efficient SV endocytosis. Dyn1 self-assembly via its stalk is required for SV endocytosis since $Dyn1_{A408T}$ located in the stalk domain impairs endocytosis in a transferrin uptake assay (Boumil et al., 2010). Additionally, $Dyn1_{G397D}$ impaired liposome-invoked GTPase activity which is required for SV endocytosis (Ford et al., 2011).

Dyn1's interactions with other proteins is also required for efficient SV endocytosis. The SH3 domains of different proteins can interact with the PRD domain of dyn1 to mediate its stability and GTPase activity to varying extents (Krishnan et al., 2015). To trigger ADBE, a dephosphorylation-rephosphorylation cycle of dyn1 is required in addition to GTPase activity for induction of membrane fission (Clayton et al., 2009). Dyn1 must be dephosphorylated in order to interact with the SH3 domain of syndapin which is required for this mode of endocytosis (Clayton et al., 2009).

These distinct functions of dyn1 may explain why the *de novo* mutations studied had varying effects on SV endocytosis. $Dyn1_{K44A}$ and $Dyn1_{H396D}$ impair both CME and ADBE perhaps by preventing efficient GTP hydrolysis *in vivo* which is required for both modes of endocytosis. $Dyn1_{R237W}$ and $Dyn1_{I289F}$ mutants only impair CME and not ADBE. These mutants are both predicted to destabilise dyn1 structure. It is possible that this unstable mutant dyn1 can no longer interact with the SH3 domains of amphiphysin-1 and endophilin and thus cannot be efficiently recruited to clathrin-coated pits. However, $Dyn1_{R237W}$ and $Dyn1_{I289F}$ may still retain the ability to interact with the SH3 domain of syndapin-1 which is required for ADBE. Interaction with syndapin-1's SH3 domain has been found to increase dyn1's assembly and GTPase activity (Krishnan et al., 2015) which may explain why ADBE is not affected despite the impaired basal GTPase activity of $Dyn1_{R237W}$. It could also be the case that the

unstable dyn1 preferentially forms long scaffold structures around the neck of clathrin-coated pits to prevent membrane fission, thus impairing CME.

5.3.5. Limitations

There are a few limitations of this work. Firstly, VAMP4-pH, like TMR dextran, does not provide a measure of the amount of ADBE occurring at nerve terminals (Nicholson-Fish et al., 2015). Therefore, although we have shown that ADBE still occurs at the same proportion of nerve terminals when overexpressing mutant mCer-Dyn1$_{G139R}$, mCer-Dyn$_{R237W}$, mCer-Dyn1$_{H396D}$, there may be less ADBE occurring at individual nerve terminals compared to WT. The VAMP4-pH assay cannot be used to investigate this. The amount of ADBE occurring in nerve terminals can be measured by using an HRP uptake assay to observe the number of bulk endosomes in nerve terminals (described in Section 4.3.3).

Endocytic membrane tubule structures have been observed when dyn1 GTP hydrolysis is impaired (Damke et al., 1994; Damke et al., 2001; Marks et al., 2001; Takei et al., 1995). It would be interesting to use electron microscopy to evaluate endosomal structures and determine whether we observe the same phenotype when overexpressing our mCer-Dyn1 mutants. It would be especially interesting to fix the cells after high frequency stimulation to observe the intermediary bulk endosome structures. This could determine whether it is indeed defective GTP hydrolysis *in vivo* that is mediating the SV recycling defects.

It is interesting to note that the patient with Dyn1$_{H396D}$ was the only patient to exhibit only developmental delay and not seizures. Moreover, this was the only *de novo* mutant to impair both modes of SV endocytosis studied. Therefore, it would be interesting to determine whether there is a correlation between patient phenotype severity, and the severity of the endocytic deficit. This may provide some evidence

for compensation by other molecular components of SV endocytosis, particularly in the case of the $Dyn1_{G139R}$ mutant where we do not observe any defects in SV endocytosis using our assays.

6. Discussion

In this work, we have studied SV recycling in three monogenic conditions that lead to ID, ASD and epilepsy. Using live-cell fluorescence imaging, we have shown that impaired SV endocytosis is a common feature across models of *SYNGAP1* haploinsufficiency, FXS and *DNM1* epileptic encephalopathy. Furthermore, the altered SV endocytosis observed in these models may contribute to the impaired synaptic function observed in these disorders.

We observed enhanced SV endocytosis in a mouse model of *SynGAP1* haploinsufficiency. *SynGAP1* KO hippocampal neurons showed enhanced sypHy retrieval only at low frequency stimulation, suggesting that CME is enhanced. SynGAP is enriched at excitatory PSDs where it can control synapse structure. PSD protein composition is altered in *SynGAP1* Het mice (Walkup et al., 2016). We propose that it is through altering protein composition at the postsynapse, including the localisation of the cell adhesion molecules neuroligin-2 and LRRTM, that SynGAP can enhance SV recycling. Interestingly, rat *SynGAP1* KO neurons did not display enhanced SV endocytosis, perhaps due to the altered time course of development between these rodent species.

SypHy retrieval was not altered with either low or high frequency stimulation in either a mouse or rat model of FXS compared to WT controls, suggesting that CME is not impaired. We did observe that fewer nerve terminals took up fluorescent TMR dextran in rat *Fmr1* KO hippocampal neurons compared to WT. These results suggest an impairment in ADBE, with fewer nerve terminals able to take part in this form of SV endocytosis. FMRP plays multiple roles in both the presynapse and the postsynapse, therefore it is still unclear which of FMRP's roles mediates efficient ADBE.

De novo mutations in *DNM1* associated with epileptic encephalopathy (DDD Consortium and DR. W. Lam, University of Edinburgh) had differential effects on both modes of SV endocytosis studied. Interestingly, deficits in GTPase activity were not always correlated with SV endocytosis deficits. $Dyn1_{G139R}$ showed impaired GTPase activity without impairing CME or ADBE. $Dyn1_{R237W}$, $Dyn1_{I289F}$ and $Dyn1_{H396D}$ all showed impaired sypHy retrieval compared to $Dyn1_{WT}$ with significantly less SV endocytosis occurring in these models. $Dyn1_{H396D}$ also impaired ADBE with fewer nerve terminals expressing this mutant undergoing ADBE as determined by fewer VAMP4-pH "down" traces. We also found that a BK channel opener can accelerate CME and thus may be able to rescue the impaired SV endocytosis caused by a subset of these mutants.

6.1. Axis of pathophysiology

Auerbach et al. (2011) proposed an axis of pathophysiology that could explain models of neurodevelopmental disorders. They proposed that decreased activity and increased activity of mGluRs fell on either side of an inverted U-shaped curve with optimal activity located at the peak (Auerbach et al., 2011). Evidence for this model was provided by the offspring of a genetic cross between *Fmr1* KO mice, that display increased mGluR activity, and *Tsc2* Het mice, that show decreased mGluR activity. The offspring carrying both mutations ($Fmr1^{-/y}$ $Tsc2^{+/-}$) displayed optimal mGluR activity with mGluR-LTD resembling WT mGluR-LTD (Auerbach et al., 2011). This suggests that there is an optimal level of mGluR activity required for efficient neural performance and deviation from this optimal level may lead to the phenotypes observed in both the *Fmr1* KO and *Tsc2* Het models (Auerbach et al., 2011).

Although the pathway was first suggested for mGluR activity, we propose that SV endocytosis can also be measured on a spectrum with either too little or too much SV

endocytosis leading to impaired neurotransmission and synaptic dysfunction (Figure 6.1). Dyn1$_{R237W}$, Dyn1$_{I289F}$ and Dyn1$_{H396D}$ mutations and FXS fall to one side of an inverted U-shaped curve with impaired SV endocytosis observed in these models. On the other side of the curve, there is *SYNGAP1* haploinsufficiency and *CDKL5* disorder which both show enhanced SV endocytosis. *CDKL5* disorder is another monogenic cause of ID and epilepsy (Kalscheuer et al., 2003). Our group has observed that more hippocampal nerve terminals undergo ADBE upon high frequency stimulation in this model compared to WT (E. Davenport, unpublished).

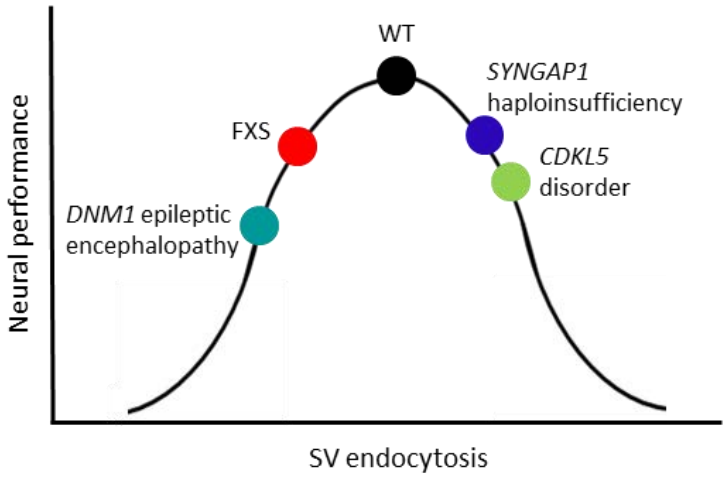

Figure 6.1 SV endocytosis axis of pathophysiology

Adapted from Auerbach et al. (2011)
Different monogenic causes of neurodevelopmental disorders have been placed on an inverted U-shaped curve with optimal SV endocytosis designated by WT (black). There are decreased levels of SV endocytosis in DNM1 epileptic encephalopathy (turquoise) and FXS (red). There is enhanced SV endocytosis in SYNGAP1 haploinsufficiency (blue) and CDKL5 disorder (green; E. Davenport unpublished).

6.2. Dysfunctional SV endocytosis and dysfunctional synapses

We propose that deviation from the optimal amount of SV endocytosis can impair neural performance through impairing synapse function. As previously mentioned, SV recycling is necessary for efficient neurotransmission, especially during increased or sustained neuronal activity. A decrease in levels of SV endocytosis

could lead to enhanced synaptic depression as new SVs cannot be formed to maintain neuronal activity (Chen et al., 2003; Shupliakov et al., 1997). This could lead to deficits in synaptic plasticity such as the exaggerated mGluR-LTD observed in FXS (Huber et al., 2002). In addition, neurotransmission failure could ultimately lead to death as is the case with the *Dnm1/3* DKO mouse that cannot undergo efficient CME following neuronal stimulation (Raimondi et al., 2011).

Altering SV endocytosis may also change synapse composition, however this is not always the case (Harper et al., 2017; Kaempf et al., 2015; Kononenko et al., 2013; Zhang et al., 2015). SVs fuse at the protein-dense presynaptic AZ. The protein composition of the AZ is tightly controlled to maintain efficient neurotransmission and ensure neurotransmitter release is performed at the right speed (reviewed in Sudhof, 2012). Addition of SV cargo to the active zone without SV endocytosis removing it may result in an unbalance in membrane homeostasis which could dysregulate synaptic function.

Alternatively, enhanced endocytosis may also alter presynaptic membrane composition, destabilising the finely-tuned balance of exocytosis and endocytosis. In the case of the *SynGAP1* KO mice, there is less cargo stranded at the plasma membrane which may also destabilise synaptic membrane homeostasis. This could be further exaggerated if exocytosis did not occur on a matching timescale. It would be important to use Bafilomycin A1 to determine both the rate and amount of exocytosis occurring during stimulation to better determine the extent of SV exocytosis and endocytosis uncoupling in this model.

Enhanced SV recycling, as observed in the *SynGAP1* KO mouse may suggest that neuronal activity cannot become as easily saturated during stimulation, since new SVs are being formed at a faster rate. This could perhaps alter the threshold for

synaptic depression which, in turn, could impair circuit remodelling resulting in altered network connectivity (Cohen et al., 2017).

6.3. Future directions

We have found that impaired SV endocytosis is a common feature across three different models of neurodevelopmental disorders. Mutations in other genes involved in synapse regulation including *DYRK1A* and *STXBP1* have also been linked to neurodevelopmental disorders (Deciphering Developmental Disorders Study, 2015). Using the live-cell imaging assays described, it would be possible to screen other models of neurodevelopmental disorders to determine whether impaired SV endocytosis is indeed a common feature across all these models. This would thus provide a pathway that could be used as a target when developing new treatments for ID, ASD and epilepsy.

Furthermore, we have also found that a BK channel opener, MaxiPost, may be able to rescue the decreased CME observed with overexpression of $Dyn1_{R237W}$. This drug was developed as a treatment for acute ischemic stroke, however it did not increase patient outcomes compared to control treatment in a phase 3 clinical trial (Gribkoff et al., 2001; Jensen, 2002). However, these studies did show that this drug was safely tolerated in subjects. Its safety may provide an additional incentive for MaxiPost to be studied further in the context of neurodevelopmental disorders especially as it may be able to rescue some of the synaptic dysfunction. There is also evidence that MaxiPost administration can rescue neurodevelopmental disorder-associated behavioural phenotypes in mice. Treatment of *Fmr1* KO mice with MaxiPost rescued cognitive and social behavioural deficits (Hebert et al., 2014). However, it is important to note that FMRP directly binds BK channels, therefore these results may be due to the rescue of other BK-channel mediated deficits in this syndrome.

In conclusion, *SYNGAP1* haploinsufficiency and FXS are both synaptopathies. Based on our results, *DNM1* epileptic encephalopathy can probably also be characterised as a disorder of the synapse based on the requirement of dyn1 for SV endocytosis. We propose that altered SV recycling may lead to the synaptic dysfunction observed in these models. This work provides a convergent mechanism underlying the various deficits observed in these models.

References

Abekhoukh, S., Sahin, H.B., Grossi, M., Zongaro, S., Maurin, T., Madrigal, I., Kazue-Sugioka, D., Raas-Rothschild, A., Doulazmi, M., Carrera, P., *et al.* (2017). New insights into the regulatory function of CYFIP1 in the context of WAVE- and FMRP-containing complexes. Dis. Model. Mech. 10, 463-474.

Aceti, M., Creson, T.K., Vaissiere, T., Rojas, C., Huang, W.C., Wang, Y.X., Petralia, R.S., Page, D.T., Miller, C.A., and Rumbaugh, G. (2015). Syngap1 haploinsufficiency damages a postnatal critical period of pyramidal cell structural maturation linked to cortical circuit assembly. Biol. Psychiatry 77, 805-815.

Adzhubei, I.A., Schmidt, S., Peshkin, L., Ramensky, V.E., Gerasimova, A., Bork, P., Kondrashov, A.S., and Sunyaev, S.R. (2010). A method and server for predicting damaging missense mutations. Nat. Methods 7, 248-249.

Akerboom, J., Chen, T.W., Wardill, T.J., Tian, L., Marvin, J.S., Mutlu, S., Calderon, N.C., Esposti, F., Borghuis, B.G., Sun, X.R., *et al.* (2012). Optimization of a GCaMP calcium indicator for neural activity imaging. J. Neurosci. 32, 13819-13840.

Akins, M.R., Leblanc, H.F., Stackpole, E.E., Chyung, E., and Fallon, J.R. (2012). Systematic mapping of fragile X granules in the mouse brain reveals a potential role for presynaptic FMRP in sensorimotor functions. J. Comp. Neurol. 520, 3687-3706.

Alabi, A.A., and Tsien, R.W. (2013). Perspectives on kiss-and-run: role in exocytosis, endocytosis, and neurotransmission. Annu. Rev. Physiol. 75, 393-422.

Alabi, A.A., and Tsien, R.W. (2012). Synaptic vesicle pools and dynamics. Cold Spring Harb Perspect. Biol. 4, a013680.

Alessi, D.R., James, S.R., Downes, C.P., Holmes, A.B., Gaffney, P.R., Reese, C.B., and Cohen, P. (1997). Characterization of a 3-phosphoinositide-dependent protein kinase which phosphorylates and activates protein kinase Balpha. Curr. Biol. 7, 261-269.

Alvarez, V.A., and Sabatini, B.L. (2007). Anatomical and physiological plasticity of dendritic spines. Annu. Rev. Neurosci. 30, 79-97.

American Psychiatric Association, and American Psychiatric Association. DSM-5 Task Force. (2013). Diagnostic and statistical manual of mental disorders: DSM-5 (Washington, D.C.: American Psychiatric Association).

American Psychiatric Association, and American Psychiatric Association. Task Force on DSM-IV. (1994). Diagnostic and statistical manual of mental disorders: DSM-IV (Washington, DC: American Psychiatric Association).

Andreae, L.C., and Burrone, J. (2017). The role of spontaneous neurotransmission in synapse and circuit development. J. Neurosci. Res.

Anggono, V., and Huganir, R.L. (2012). Regulation of AMPA receptor trafficking and synaptic plasticity. Curr. Opin. Neurobiol. 22, 461-469.

Anggono, V., Smillie, K.J., Graham, M.E., Valova, V.A., Cousin, M.A., and Robinson, P.J. (2006). Syndapin I is the phosphorylation-regulated dynamin I partner in synaptic vesicle endocytosis. Nat. Neurosci. 9, 752-760.

Antonny, B., Burd, C., De Camilli, P., Chen, E., Daumke, O., Faelber, K., Ford, M., Frolov, V.A., Frost, A., Hinshaw, J.E., *et al.* (2016). Membrane fission by dynamin: what we know and what we need to know. EMBO J. 35, 2270-2284.

Armbruster, M., Messa, M., Ferguson, S.M., De Camilli, P., and Ryan, T.A. (2013). Dynamin phosphorylation controls optimization of endocytosis for brief action potential bursts. Elife 2, e00845.

Asadi-Pooya, A.A. (2017). Lennox-Gastaut syndrome: a comprehensive review. Neurol. Sci.

Asinof, S.K., Mahaffey, C., Beyer, B., Frankel, W.N., and Boumil, R.M. (2016). Dynamin 1 isoform roles in a mouse model of severe childhood epileptic encephalopathy. Neurobiol. Dis. 95, 1-11.

Asinof, S.K., Sukoff Rizzo, S.J., Buckley, A.R., Beyer, B.J., Letts, V.A., Frankel, W.N., and Boumil, R.M. (2015). Independent Neuronal Origin of Seizures and Behavioral Comorbidities in an Animal Model of a Severe Childhood Genetic Epileptic Encephalopathy. PLoS Genet. 11, e1005347.

Atluri, P.P., and Ryan, T.A. (2006). The kinetics of synaptic vesicle reacidification at hippocampal nerve terminals. J. Neurosci. 26, 2313-2320.

Auerbach, B.D., Osterweil, E.K., and Bear, M.F. (2011). Mutations causing syndromic autism define an axis of synaptic pathophysiology. Nature 480, 63-68.

Avanzini, G., and Franceschetti, S. (2003). Cellular biology of epileptogenesis. Lancet Neurol. 2, 33-42.

Baba, T., Damke, H., Hinshaw, J.E., Ikeda, K., Schmid, S.L., and Warnock, D.E. (1995). Role of dynamin in clathrin-coated vesicle formation. Cold Spring Harb. Symp. Quant. Biol. 60, 235-242.

Bacaj, T., Wu, D., Yang, X., Morishita, W., Zhou, P., Xu, W., Malenka, R.C., and Sudhof, T.C. (2013). Synaptotagmin-1 and synaptotagmin-7 trigger synchronous and asynchronous phases of neurotransmitter release. Neuron 80, 947-959.

Balaji, J., Armbruster, M., and Ryan, T.A. (2008). Calcium control of endocytic capacity at a CNS synapse. J. Neurosci. 28, 6742-6749.

Banerjee, S., Riordan, M., and Bhat, M.A. (2014). Genetic aspects of autism spectrum disorders: insights from animal models. Front. Cell. Neurosci. 8, 58.

Bar, J., Kobler, O., van Bommel, B., and Mikhaylova, M. (2016). Periodic F-actin structures shape the neck of dendritic spines. Sci. Rep. 6, 37136.

Barnes, S.A., Wijetunge, L.S., Jackson, A.D., Katsanevaki, D., Osterweil, E.K., Komiyama, N.H., Grant, S.G., Bear, M.F., Nagerl, U.V., Kind, P.C., and Wyllie, D.J. (2015). Convergence of Hippocampal Pathophysiology in Syngap+/- and Fmr1-/y Mice. J. Neurosci. 35, 15073-15081.

Barylko, B., Binns, D., Lin, K.M., Atkinson, M.A., Jameson, D.M., Yin, H.L., and Albanesi, J.P. (1998). Synergistic activation of dynamin GTPase by Grb2 and phosphoinositides. J. Biol. Chem. 273, 3791-3797.

Barylko, B., Binns, D.D., and Albanesi, J.P. (2001). Activation of dynamin GTPase activity by phosphoinositides and SH3 domain-containing proteins. Methods Enzymol. 329, 486-496.

Bear, M.F., Huber, K.M., and Warren, S.T. (2004). The mGluR theory of fragile X mental retardation. Trends Neurosci. 27, 370-377.

Bell, M.V., Hirst, M.C., Nakahori, Y., MacKinnon, R.N., Roche, A., Flint, T.J., Jacobs, P.A., Tommerup, N., Tranebjaerg, L., and Froster-Iskenius, U. (1991). Physical mapping across the fragile X: hypermethylation and clinical expression of the fragile X syndrome. Cell 64, 861-866.

Berg, A.T., Berkovic, S.F., Brodie, M.J., Buchhalter, J., Cross, J.H., van Emde Boas, W., Engel, J., French, J., Glauser, T.A., Mathern, G.W., *et al.* (2010). Revised terminology and concepts for organization of seizures and epilepsies: report of the ILAE Commission on Classification and Terminology, 2005-2009. Epilepsia 51, 676-685.

Berry-Kravis, E. (2002). Epilepsy in fragile X syndrome. Dev. Med. Child Neurol. 44, 724-728.

Berthiaume, E.P., Medina, C., and Swanson, J.A. (1995). Molecular size-fractionation during endocytosis in macrophages. J. Cell Biol. 129, 989-998.

Bhattacharjee, A., and Kaczmarek, L.K. (2005). For K+ channels, Na+ is the new Ca2+. Trends Neurosci. 28, 422-428.

Boumil, R.M., Letts, V.A., Roberts, M.C., Lenz, C., Mahaffey, C.L., Zhang, Z.W., Moser, T., and Frankel, W.N. (2010). A missense mutation in a highly conserved

alternate exon of dynamin-1 causes epilepsy in fitful mice. PLoS Genet. 6, 10.1371/journal.pgen.1001046.

Bozzi, Y., Casarosa, S., and Caleo, M. (2012). Epilepsy as a neurodevelopmental disorder. Front. Psychiatry. 3, 19.

Brown, M.R., Kronengold, J., Gazula, V.R., Chen, Y., Strumbos, J.G., Sigworth, F.J., Navaratnam, D., and Kaczmarek, L.K. (2010). Fragile X mental retardation protein controls gating of the sodium-activated potassium channel Slack. Nat. Neurosci. 13, 819-821.

Cao, H., Garcia, F., and McNiven, M.A. (1998). Differential distribution of dynamin isoforms in mammalian cells. Mol. Biol. Cell 9, 2595-2609.

Charman, T. (2002). The prevalence of autism spectrum disorders. Recent evidence and future challenges. Eur. Child Adolesc. Psychiatry 11, 249-256.

Chen, H.J., Rojas-Soto, M., Oguni, A., and Kennedy, M.B. (1998). A synaptic Ras-GTPase activating protein (p135 SynGAP) inhibited by CaM kinase II. Neuron 20, 895-904.

Chen, M.S., Obar, R.A., Schroeder, C.C., Austin, T.W., Poodry, C.A., Wadsworth, S.C., and Vallee, R.B. (1991). Multiple forms of dynamin are encoded by shibire, a Drosophila gene involved in endocytosis. Nature 351, 583-586.

Chen, T.W., Wardill, T.J., Sun, Y., Pulver, S.R., Renninger, S.L., Baohan, A., Schreiter, E.R., Kerr, R.A., Orger, M.B., Jayaraman, V., *et al.* (2013). Ultrasensitive fluorescent proteins for imaging neuronal activity. Nature 499, 295-300.

Chen, Y., Deng, L., Maeno-Hikichi, Y., Lai, M., Chang, S., Chen, G., and Zhang, J.F. (2003). Formation of an endophilin-Ca2+ channel complex is critical for clathrin-mediated synaptic vesicle endocytosis. Cell 115, 37-48.

Cheng, D., Hoogenraad, C.C., Rush, J., Ramm, E., Schlager, M.A., Duong, D.M., Xu, P., Wijayawardana, S.R., Hanfelt, J., Nakagawa, T., Sheng, M., and Peng, J. (2006). Relative and absolute quantification of postsynaptic density proteome isolated from rat forebrain and cerebellum. Mol. Cell. Proteomics 5, 1158-1170.

Cheung, G., and Cousin, M.A. (2013). Synaptic vesicle generation from activity-dependent bulk endosomes requires calcium and calcineurin. J. Neurosci. 33, 3370-3379.

Cheung, G., and Cousin, M.A. (2012). Adaptor protein complexes 1 and 3 are essential for generation of synaptic vesicles from activity-dependent bulk endosomes. J. Neurosci. 32, 6014-6023.

Cheung, G., Jupp, O.J., and Cousin, M.A. (2010). Activity-dependent bulk endocytosis and clathrin-dependent endocytosis replenish specific synaptic vesicle pools in central nerve terminals. J. Neurosci. 30, 8151-8161.

Christie, S.B., Akins, M.R., Schwob, J.E., and Fallon, J.R. (2009). The FXG: a presynaptic fragile X granule expressed in a subset of developing brain circuits. J. Neurosci. 29, 1514-1524.

Chuang, S.C., Zhao, W., Bauchwitz, R., Yan, Q., Bianchi, R., and Wong, R.K. (2005). Prolonged epileptiform discharges induced by altered group I metabotropic glutamate receptor-mediated synaptic responses in hippocampal slices of a fragile X mouse model. J. Neurosci. 25, 8048-8055.

Chyung, E., LeBlanc, H.F., Fallon, J.R., and Akins, M.R. (2017). Fragile X granules are a family of axonal ribonucleoprotein particles with circuit-dependent protein composition and mRNA cargos. J. Comp. Neurol.

Clayton, E.L., Anggono, V., Smillie, K.J., Chau, N., Robinson, P.J., and Cousin, M.A. (2009). The phospho-dependent dynamin-syndapin interaction triggers activity-dependent bulk endocytosis of synaptic vesicles. J. Neurosci. 29, 7706-7717.

Clayton, E.L., and Cousin, M.A. (2009a). The molecular physiology of activity-dependent bulk endocytosis of synaptic vesicles. J. Neurochem. 111, 901-914.

Clayton, E.L., and Cousin, M.A. (2009b). Quantitative monitoring of activity-dependent bulk endocytosis of synaptic vesicle membrane by fluorescent dextran imaging. J. Neurosci. Methods 185, 76-81.

Clayton, E.L., Evans, G.J., and Cousin, M.A. (2008). Bulk synaptic vesicle endocytosis is rapidly triggered during strong stimulation. J. Neurosci. 28, 6627-6632.

Clayton, E.L., Evans, G.J., and Cousin, M.A. (2007). Activity-dependent control of bulk endocytosis by protein dephosphorylation in central nerve terminals. J. Physiol. 585, 687-691.

Clayton, E.L., Sue, N., Smillie, K.J., O'Leary, T., Bache, N., Cheung, G., Cole, A.R., Wyllie, D.J., Sutherland, C., Robinson, P.J., and Cousin, M.A. (2010). Dynamin I phosphorylation by GSK3 controls activity-dependent bulk endocytosis of synaptic vesicles. Nat. Neurosci. 13, 845-851.

Clement, J.P., Aceti, M., Creson, T.K., Ozkan, E.D., Shi, Y., Reish, N.J., Almonte, A.G., Miller, B.H., Wiltgen, B.J., Miller, C.A., Xu, X., and Rumbaugh, G. (2012). Pathogenic SYNGAP1 mutations impair cognitive development by disrupting maturation of dendritic spine synapses. Cell 151, 709-723.

Clifford, S., Dissanayake, C., Bui, Q.M., Huggins, R., Taylor, A.K., and Loesch, D.Z. (2007). Autism spectrum phenotype in males and females with fragile X full mutation and premutation. J. Autism Dev. Disord. 37, 738-747.

Coffee, B., Keith, K., Albizua, I., Malone, T., Mowrey, J., Sherman, S.L., and Warren, S.T. (2009). Incidence of fragile X syndrome by newborn screening for methylated FMR1 DNA. Am. J. Hum. Genet. 85, 503-514.

Cohen, E.J., Quarta, E., Bravi, R., Granato, A., and Minciacchi, D. (2017). Neural plasticity and network remodeling: From concepts to pathology. Neuroscience 344, 326-345.

Collins, S.C., Bray, S.M., Suhl, J.A., Cutler, D.J., Coffee, B., Zwick, M.E., and Warren, S.T. (2010). Identification of novel FMR1 variants by massively parallel sequencing in developmentally delayed males. Am. J. Med. Genet. A. 152A, 2512-2520.

Comery, T.A., Harris, J.B., Willems, P.J., Oostra, B.A., Irwin, S.A., Weiler, I.J., and Greenough, W.T. (1997). Abnormal dendritic spines in fragile X knockout mice: maturation and pruning deficits. Proc. Natl. Acad. Sci. U. S. A. 94, 5401-5404.

Cook, T., Mesa, K., and Urrutia, R. (1996). Three dynamin-encoding genes are differentially expressed in developing rat brain. J. Neurochem. 67, 927-931.

Cousin, M.A. (2017). Integration of Synaptic Vesicle Cargo Retrieval with Endocytosis at Central Nerve Terminals. Front. Cell. Neurosci. 11, 10.3389/fncel.2017.00234.

Cousin, M.A. (2015). Synaptic Vesicle Endocytosis and Endosomal Recycling in Central Nerve Terminals: Discrete Trafficking Routes? Neuroscientist 21, 413-423.

Cousin, M.A., and Robinson, P.J. (2000). Ca(2+) influx inhibits dynamin and arrests synaptic vesicle endocytosis at the active zone. J. Neurosci. 20, 949-957.

Cruz-Martin, A., Crespo, M., and Portera-Cailliau, C. (2010). Delayed stabilization of dendritic spines in fragile X mice. J. Neurosci. 30, 7793-7803.

Damke, H., Baba, T., Warnock, D.E., and Schmid, S.L. (1994). Induction of mutant dynamin specifically blocks endocytic coated vesicle formation. J. Cell Biol. 127, 915-934.

Damke, H., Binns, D.D., Ueda, H., Schmid, S.L., and Baba, T. (2001). Dynamin GTPase domain mutants block endocytic vesicle formation at morphologically distinct stages. Mol. Biol. Cell 12, 2578-2589.

Dar, S., Kamerkar, S.C., and Pucadyil, T.J. (2015). A high-throughput platform for real-time analysis of membrane fission reactions reveals dynamin function. Nat. Cell Biol. 17, 1588-1596.

Darnell, J.C., and Klann, E. (2013). The translation of translational control by FMRP: therapeutic targets for FXS. Nat. Neurosci.

Darnell, J.C., Van Driesche, S.J., Zhang, C., Hung, K.Y., Mele, A., Fraser, C.E., Stone, E.F., Chen, C., Fak, J.J., Chi, S.W., *et al.* (2011). FMRP stalls ribosomal translocation on mRNAs linked to synaptic function and autism. Cell 146, 247-261.

Dason, J.S., Smith, A.J., Marin, L., and Charlton, M.P. (2014). Cholesterol and F-actin are required for clustering of recycling synaptic vesicle proteins in the presynaptic plasma membrane. J. Physiol. 592, 621-633.

De Boulle, K., Verkerk, A.J., Reyniers, E., Vits, L., Hendrickx, J., Van Roy, B., Van den Bos, F., de Graaff, E., Oostra, B.A., and Willems, P.J. (1993). A point mutation in the FMR-1 gene associated with fragile X mental retardation. Nat. Genet. 3, 31-35.

de Vrij, F.M., Levenga, J., van der Linde, H.C., Koekkoek, S.K., De Zeeuw, C.I., Nelson, D.L., Oostra, B.A., and Willemsen, R. (2008). Rescue of behavioral phenotype and neuronal protrusion morphology in Fmr1 KO mice. Neurobiol. Dis. 31, 127-132.

de Wit, J., and Ghosh, A. (2014). Control of neural circuit formation by leucine-rich repeat proteins. Trends Neurosci. 37, 539-550.

Deciphering Developmental Disorders Study. (2015). Large-scale discovery of novel genetic causes of developmental disorders. Nature 519, 223-228.

Deng, P.Y., and Klyachko, V.A. (2016). Genetic upregulation of BK channel activity normalizes multiple synaptic and circuit defects in a mouse model of fragile X syndrome. J. Physiol. 594, 83-97.

Deng, P.Y., Rotman, Z., Blundon, J.A., Cho, Y., Cui, J., Cavalli, V., Zakharenko, S.S., and Klyachko, V.A. (2013). FMRP regulates neurotransmitter release and synaptic information transmission by modulating action potential duration via BK channels. Neuron 77, 696-711.

Deng, P.Y., Sojka, D., and Klyachko, V.A. (2011). Abnormal presynaptic short-term plasticity and information processing in a mouse model of fragile X syndrome. J. Neurosci. 31, 10971-10982.

Denker, A., and Rizzoli, S.O. (2010). Synaptic vesicle pools: an update. Front. Synaptic Neurosci. 2, 135.

Developmental Disabilities Monitoring Network Surveillance Year 2010 Principal Investigators, and Centers for Disease Control and Prevention (CDC). (2014). Prevalence of autism spectrum disorder among children aged 8 years - autism and developmental disabilities monitoring network, 11 sites, United States, 2010. MMWR Surveill. Summ. 63, 1-21.

Dhindsa, R.S., Bradrick, S.S., Yao, X., Heinzen, E.L., Petrovski, S., Krueger, B.J., Johnson, M.R., Frankel, W.N., Petrou, S., Boumil, R.M., and Goldstein, D.B. (2015). Epileptic encephalopathy-causing mutations in DNM1 impair synaptic vesicle endocytosis. Neurol. Genet. 1, e4.

Di Paolo, G., Sankaranarayanan, S., Wenk, M.R., Daniell, L., Perucco, E., Caldarone, B.J., Flavell, R., Picciotto, M.R., Ryan, T.A., Cremona, O., and De Camilli, P. (2002). Decreased synaptic vesicle recycling efficiency and cognitive deficits in amphiphysin 1 knockout mice. Neuron 33, 789-804.

Dolen, G., and Bear, M.F. (2009). Fragile x syndrome and autism: from disease model to therapeutic targets. J. Neurodev Disord. 1, 133-140.

Dolen, G., Osterweil, E., Rao, B.S., Smith, G.B., Auerbach, B.D., Chattarji, S., and Bear, M.F. (2007). Correction of fragile X syndrome in mice. Neuron 56, 955-962.

Doll, C.A., Vita, D.J., and Broadie, K. (2017). Fragile X Mental Retardation Protein Requirements in Activity-Dependent Critical Period Neural Circuit Refinement. Curr. Biol. 27, 2318-2330.e3.

Edwards, R.H. (2007). The neurotransmitter cycle and quantal size. Neuron 55, 835-858.

Egashira, Y., Takase, M., and Takamori, S. (2015). Monitoring of vacuolar-type H+ ATPase-mediated proton influx into synaptic vesicles. J. Neurosci. 35, 3701-3710.

Epi4K Consortium. (2016). De Novo Mutations in SLC1A2 and CACNA1A Are Important Causes of Epileptic Encephalopathies. Am. J. Hum. Genet. 99, 287-298.

Epi4K Consortium, Epilepsy Phenome/Genome Project, Allen, A.S., Berkovic, S.F., Cossette, P., Delanty, N., Dlugos, D., Eichler, E.E., Epstein, M.P., Glauser, T.*, et al.* (2013). De novo mutations in epileptic encephalopathies. Nature 501, 217-221.

Etherton, M.R., Blaiss, C.A., Powell, C.M., and Sudhof, T.C. (2009). Mouse neurexin-1alpha deletion causes correlated electrophysiological and behavioral changes consistent with cognitive impairments. Proc. Natl. Acad. Sci. U. S. A. 106, 17998-18003.

EuroEPINOMICS-RES Consortium, Epilepsy Phenome/Genome Project, and Epi4K Consortium. (2014). De novo mutations in synaptic transmission genes including DNM1 cause epileptic encephalopathies. Am. J. Hum. Genet. 95, 360-370.

Evstratova, A., Chamberland, S., Faundez, V., and Toth, K. (2014). Vesicles derived via AP-3-dependent recycling contribute to asynchronous release and influence information transfer. Nat. Commun. 5, 5530.

Faelber, K., Posor, Y., Gao, S., Held, M., Roske, Y., Schulze, D., Haucke, V., Noe, F., and Daumke, O. (2011). Crystal structure of nucleotide-free dynamin. Nature 477, 556-560.

Fahrner, J.A., Liu, R., Perry, M.S., Klein, J., and Chan, D.C. (2016). A novel de novo dominant negative mutation in DNM1L impairs mitochondrial fission and presents as childhood epileptic encephalopathy. Am. J. Med. Genet. A. 170, 2002-2011.

Faire, K., Trent, F., Tepper, J.M., and Bonder, E.M. (1992). Analysis of dynamin isoforms in mammalian brain: dynamin-1 expression is spatially and temporally regulated during postnatal development. Proc. Natl. Acad. Sci. U. S. A. 89, 8376-8380.

Fan, F., Funk, L., and Lou, X. (2016). Dynamin 1- and 3-Mediated Endocytosis Is Essential for the Development of a Large Central Synapse In Vivo. J. Neurosci. 36, 6097-6115.

Farsad, K., Ringstad, N., Takei, K., Floyd, S.R., Rose, K., and De Camilli, P. (2001). Generation of high curvature membranes mediated by direct endophilin bilayer interactions. J. Cell Biol. 155, 193-200.

Feng, Y., Absher, D., Eberhart, D.E., Brown, V., Malter, H.E., and Warren, S.T. (1997). FMRP associates with polyribosomes as an mRNP, and the I304N mutation of severe fragile X syndrome abolishes this association. Mol. Cell 1, 109-118.

Ferguson, S.M., Brasnjo, G., Hayashi, M., Wolfel, M., Collesi, C., Giovedi, S., Raimondi, A., Gong, L.W., Ariel, P., Paradise, S., *et al.* (2007). A selective activity-dependent requirement for dynamin 1 in synaptic vesicle endocytosis. Science 316, 570-574.

Ferguson, S.M., and De Camilli, P. (2012). Dynamin, a membrane-remodelling GTPase. Nat. Rev. Mol. Cell Biol. 13, 75-88.

Fernandez-Alfonso, T., Kwan, R., and Ryan, T.A. (2006). Synaptic vesicles interchange their membrane proteins with a large surface reservoir during recycling. Neuron 51, 179-186.

Fernandez-Alfonso, T., and Ryan, T.A. (2004). The kinetics of synaptic vesicle pool depletion at CNS synaptic terminals. Neuron 41, 943-953.

Ferron, L. (2016). Fragile X mental retardation protein controls ion channel expression and activity. J. Physiol. 594, 5861-5867.

Ferron, L., Nieto-Rostro, M., Cassidy, J.S., and Dolphin, A.C. (2014). Fragile X mental retardation protein controls synaptic vesicle exocytosis by modulating N-type calcium channel density. Nat. Commun. 5, 3628.

Fesce, R., Grohovaz, F., Valtorta, F., and Meldolesi, J. (1994). Neurotransmitter release: fusion or 'kiss-and-run'? Trends Cell Biol. 4, 1-4.

Folstein, S., and Rutter, M. (1977). Infantile autism: a genetic study of 21 twin pairs. J. Child Psychol. Psychiatry 18, 297-321.

Ford, M.G., Jenni, S., and Nunnari, J. (2011). The crystal structure of dynamin. Nature 477, 561-566.

Ford, M.G., Mills, I.G., Peter, B.J., Vallis, Y., Praefcke, G.J., Evans, P.R., and McMahon, H.T. (2002). Curvature of clathrin-coated pits driven by epsin. Nature 419, 361-366.

Ford, M.G., Pearse, B.M., Higgins, M.K., Vallis, Y., Owen, D.J., Gibson, A., Hopkins, C.R., Evans, P.R., and McMahon, H.T. (2001). Simultaneous binding of PtdIns(4,5)P2 and clathrin by AP180 in the nucleation of clathrin lattices on membranes. Science 291, 1051-1055.

Fredj, N.B., and Burrone, J. (2009). A resting pool of vesicles is responsible for spontaneous vesicle fusion at the synapse. Nat. Neurosci. 12, 751-758.

Fu, Y.H., Kuhl, D.P., Pizzuti, A., Pieretti, M., Sutcliffe, J.S., Richards, S., Verkerk, A.J., Holden, J.J., Fenwick, R.G.,Jr, and Warren, S.T. (1991). Variation of the CGG repeat at the fragile X site results in genetic instability: resolution of the Sherman paradox. Cell 67, 1047-1058.

Fulop, T., Doreian, B., and Smith, C. (2008). Dynamin I plays dual roles in the activity-dependent shift in exocytic mode in mouse adrenal chromaffin cells. Arch. Biochem. Biophys. 477, 146-154.

Gad, H., Ringstad, N., Low, P., Kjaerulff, O., Gustafsson, J., Wenk, M., Di Paolo, G., Nemoto, Y., Crun, J., Ellisman, M.H., *et al.* (2000). Fission and uncoating of synaptic clathrin-coated vesicles are perturbed by disruption of interactions with the SH3 domain of endophilin. Neuron 27, 301-312.

Galvez, R., and Greenough, W.T. (2005). Sequence of abnormal dendritic spine development in primary somatosensory cortex of a mouse model of the fragile X mental retardation syndrome. Am. J. Med. Genet. A. 135, 155-160.

Gantois, I., Khoutorsky, A., Popic, J., Aguilar-Valles, A., Freemantle, E., Cao, R., Sharma, V., Pooters, T., Nagpal, A., Skalecka, A., *et al.* (2017). Metformin ameliorates core deficits in a mouse model of fragile X syndrome. Nat. Med. 23, 674-677.

Gauducheau, M., Lemaire-Mayo, V., D'Amato, F.R., Oddi, D., Crusio, W.E., and Pietropaolo, S. (2017). Age-specific autistic-like behaviors in heterozygous Fmr1-KO female mice. Autism Res. 10, 1067-1078.

Gholizadeh, S., Halder, S.K., and Hampson, D.R. (2015). Expression of fragile X mental retardation protein in neurons and glia of the developing and adult mouse brain. Brain Res. 1596, 22-30.

Giachello, C.N., Fiumara, F., Giacomini, C., Corradi, A., Milanese, C., Ghirardi, M., Benfenati, F., and Montarolo, P.G. (2010). MAPK/Erk-dependent phosphorylation of synapsin mediates formation of functional synapses and short-term homosynaptic plasticity. J. Cell. Sci. 123, 881-893.

Gkogkas, C.G., Khoutorsky, A., Cao, R., Jafarnejad, S.M., Prager-Khoutorsky, M., Giannakas, N., Kaminari, A., Fragkouli, A., Nader, K., Price, T.J., *et al.* (2014). Pharmacogenetic inhibition of eIF4E-dependent Mmp9 mRNA translation reverses fragile X syndrome-like phenotypes. Cell. Rep. 9, 1742-1755.

Gordon, S.L., and Cousin, M.A. (2013). X-linked intellectual disability-associated mutations in synaptophysin disrupt synaptobrevin II retrieval. J. Neurosci. 33, 13695-13700.

Gordon, S.L., Harper, C.B., Smillie, K.J., and Cousin, M.A. (2016). A Fine Balance of Synaptophysin Levels Underlies Efficient Retrieval of Synaptobrevin II to Synaptic Vesicles. PLoS One 11, e0149457.

Gordon, S.L., Leube, R.E., and Cousin, M.A. (2011). Synaptophysin is required for synaptobrevin retrieval during synaptic vesicle endocytosis. J. Neurosci. 31, 14032-14036.

Gorini, G., Ponomareva, O., Shores, K.S., Person, M.D., Harris, R.A., and Mayfield, R.D. (2010). Dynamin-1 co-associates with native mouse brain BKCa channels: proteomics analysis of synaptic protein complexes. FEBS Lett. 584, 845-851.

Gormal, R.S., Nguyen, T.H., Martin, S., Papadopulos, A., and Meunier, F.A. (2015). An acto-myosin II constricting ring initiates the fission of activity-dependent bulk endosomes in neurosecretory cells. J. Neurosci. 35, 1380-1389.

Gout, I., Dhand, R., Hiles, I.D., Fry, M.J., Panayotou, G., Das, P., Truong, O., Totty, N.F., Hsuan, J., Booker, G.W., Campbell, I.D., and Waterfield, M.D. (1993). The GTPase dynamin binds to and is activated by a subset of SH3 domains. Cell *75,* 25-36.

Graf, E.R., Zhang, X., Jin, S.X., Linhoff, M.W., and Craig, A.M. (2004). Neurexins induce differentiation of GABA and glutamate postsynaptic specializations via neuroligins. Cell 119, 1013-1026.

Granseth, B., Odermatt, B., Royle, S.J., and Lagnado, L. (2006). Clathrin-mediated endocytosis is the dominant mechanism of vesicle retrieval at hippocampal synapses. Neuron 51, 773-786.

Gribkoff, V.K., Starrett, J.E.,Jr, Dworetzky, S.I., Hewawasam, P., Boissard, C.G., Cook, D.A., Frantz, S.W., Heman, K., Hibbard, J.R., Huston, K., *et al.* (2001). Targeting acute ischemic stroke with a calcium-sensitive opener of maxi-K potassium channels. Nat. Med. 7, 471-477.

Grigliatti, T.A., Hall, L., Rosenbluth, R., and Suzuki, D.T. (1973). Temperature-sensitive mutations in Drosophila melanogaster. XIV. A selection of immobile adults. Mol. Gen. Genet. 120, 107-114.

Griguoli, M., Sgritta, M., and Cherubini, E. (2016). Presynaptic BK channels control transmitter release: physiological relevance and potential therapeutic implications. J. Physiol. 594, 3489-3500.

Gronskov, K., Brondum-Nielsen, K., Dedic, A., and Hjalgrim, H. (2011). A nonsense mutation in FMR1 causing fragile X syndrome. Eur. J. Hum. Genet. 19, 489-491.

Hagerman, P.J. (2008). The fragile X prevalence paradox. J. Med. Genet. 45, 498-499.

Hall, B.J., Ripley, B., and Ghosh, A. (2007). NR2B signaling regulates the development of synaptic AMPA receptor current. J. Neurosci. 27, 13446-13456.

Hamdan, F.F., Daoud, H., Piton, A., Gauthier, J., Dobrzeniecka, S., Krebs, M.O., Joober, R., Lacaille, J.C., Nadeau, A., Milunsky, J.M., *et al.* (2011). De novo SYNGAP1 mutations in nonsyndromic intellectual disability and autism. Biol. Psychiatry 69, 898-901.

Hamdan, F.F., Gauthier, J., Spiegelman, D., Noreau, A., Yang, Y., Pellerin, S., Dobrzeniecka, S., Cote, M., Perreau-Linck, E., Carmant, L., *et al.* (2009). Mutations in SYNGAP1 in autosomal nonsyndromic mental retardation. N. Engl. J. Med. 360, 599-605.

Hamilton, S.M., Green, J.R., Veeraragavan, S., Yuva, L., McCoy, A., Wu, Y., Warren, J., Little, L., Ji, D., Cui, X., Weinstein, E., and Paylor, R. (2014). Fmr1 and Nlgn3 knockout rats: novel tools for investigating autism spectrum disorders. Behav. Neurosci. 128, 103-109.

Harata, N., Pyle, J.L., Aravanis, A.M., Mozhayeva, M., Kavalali, E.T., and Tsien, R.W. (2001). Limited numbers of recycling vesicles in small CNS nerve terminals: implications for neural signaling and vesicular cycling. Trends Neurosci. 24, 637-643.

Harata, N.C., Aravanis, A.M., and Tsien, R.W. (2006). Kiss-and-run and full-collapse fusion as modes of exo-endocytosis in neurosecretion. J. Neurochem. 97, 1546-1570.

Harlow, E.G., Till, S.M., Russell, T.A., Wijetunge, L.S., Kind, P., and Contractor, A. (2010). Critical period plasticity is disrupted in the barrel cortex of FMR1 knockout mice. Neuron 65, 385-398.

Harper, C.B., Mancini, G.M.S., van Slegtenhorst, M., and Cousin, M.A. (2017). Altered synaptobrevin-II trafficking in neurons expressing a synaptophysin mutation associated with a severe neurodevelopmental disorder. Neurobiol. Dis. 108, 298-306.

Haucke, V., and De Camilli, P. (1999). AP-2 recruitment to synaptotagmin stimulated by tyrosine-based endocytic motifs. Science 285, 1268-1271.

Haucke, V., Neher, E., and Sigrist, S.J. (2011). Protein scaffolds in the coupling of synaptic exocytosis and endocytosis. Nat. Rev. Neurosci. 12, 127-138.

Hayashi, M., Raimondi, A., O'Toole, E., Paradise, S., Collesi, C., Cremona, O., Ferguson, S.M., and De Camilli, P. (2008). Cell- and stimulus-dependent heterogeneity of synaptic vesicle endocytic recycling mechanisms revealed by studies of dynamin 1-null neurons. Proc. Natl. Acad. Sci. U. S. A. 105, 2175-2180.

Hebert, B., Pietropaolo, S., Meme, S., Laudier, B., Laugeray, A., Doisne, N., Quartier, A., Lefeuvre, S., Got, L., Cahard, D., *et al.* (2014). Rescue of fragile X syndrome phenotypes in Fmr1 KO mice by a BKCa channel opener molecule. Orphanet J. Rare Dis. 9, 124-014-0124-6.

Hecht, F., and Bixenman, H.A. (1990). Location of FRAXD in Xq27.2. Fragile sites on the X chromosome. Cancer Genet. Cytogenet. 49, 137-138.

Heerssen, H., Fetter, R.D., and Davis, G.W. (2008). Clathrin dependence of synaptic-vesicle formation at the Drosophila neuromuscular junction. Curr. Biol. 18, 401-409.

Henne, W.M., Boucrot, E., Meinecke, M., Evergren, E., Vallis, Y., Mittal, R., and McMahon, H.T. (2010). FCHo proteins are nucleators of clathrin-mediated endocytosis. Science 328, 1281-1284.

Henne, W.M., Kent, H.M., Ford, M.G., Hegde, B.G., Daumke, O., Butler, P.J., Mittal, R., Langen, R., Evans, P.R., and McMahon, H.T. (2007). Structure and analysis of FCHo2 F-BAR domain: a dimerizing and membrane recruitment module that effects membrane curvature. Structure 15, 839-852.

Heuser, J.E., and Reese, T.S. (1973). Evidence for recycling of synaptic vesicle membrane during transmitter release at the frog neuromuscular junction. J. Cell Biol. 57, 315-344.

Hinshaw, J.E., and Schmid, S.L. (1995). Dynamin self-assembles into rings suggesting a mechanism for coated vesicle budding. Nature 374, 190-192.

Hirst, M., Grewal, P., Flannery, A., Slatter, R., Maher, E., Barton, D., Fryns, J.P., and Davies, K. (1995). Two new cases of FMR1 deletion associated with mental impairment. Am. J. Hum. Genet. 56, 67-74.

Hollopeter, G., Lange, J.J., Zhang, Y., Vu, T.N., Gu, M., Ailion, M., Lambie, E.J., Slaughter, B.D., Unruh, J.R., Florens, L., and Jorgensen, E.M. (2014). The membrane-associated proteins FCHo and SGIP are allosteric activators of the AP2 clathrin adaptor complex. Elife 3, 10.7554/eLife.03648.

Holt, M., Cooke, A., Wu, M.M., and Lagnado, L. (2003). Bulk membrane retrieval in the synaptic terminal of retinal bipolar cells. J. Neurosci. 23, 1329-1339.

Hou, L., Antion, M.D., Hu, D., Spencer, C.M., Paylor, R., and Klann, E. (2006). Dynamic translational and proteasomal regulation of fragile X mental retardation protein controls mGluR-dependent long-term depression. Neuron 51, 441-454.

Hua, Y., Sinha, R., Thiel, C.S., Schmidt, R., Huve, J., Martens, H., Hell, S.W., Egner, A., and Klingauf, J. (2011). A readily retrievable pool of synaptic vesicles. Nat. Neurosci. 14, 833-839.

Huber, K.M., Gallagher, S.M., Warren, S.T., and Bear, M.F. (2002). Altered synaptic plasticity in a mouse model of fragile X mental retardation. Proc. Natl. Acad. Sci. U. S. A. 99, 7746-7750.

Hulbert, S.W., and Jiang, Y.H. (2017). Cellular and Circuitry Bases of Autism: Lessons Learned from the Temporospatial Manipulation of Autism Genes in the Brain. Neurosci. Bull. 33, 205-218.

Hung, A.Y., and Sheng, M. (2002). PDZ domains: structural modules for protein complex assembly. J. Biol. Chem. 277, 5699-5702.

Indriati, D.W., Kamasawa, N., Matsui, K., Meredith, A.L., Watanabe, M., and Shigemoto, R. (2013). Quantitative localization of Cav2.1 (P/Q-type) voltage-dependent calcium channels in Purkinje cells: somatodendritic gradient and distinct somatic coclustering with calcium-activated potassium channels. J. Neurosci. 33, 3668-3678.

Irwin, S.A., Galvez, R., and Greenough, W.T. (2000). Dendritic spine structural anomalies in fragile-X mental retardation syndrome. Cereb. Cortex 10, 1038-1044.

Jensen, B.S. (2002). BMS-204352: a potassium channel opener developed for the treatment of stroke. CNS Drug Rev. 8, 353-360.

Jentsch, T.J. (2000). Neuronal KCNQ potassium channels: physiology and role in disease. Nat. Rev. Neurosci. 1, 21-30.

Jeyabalan, N., and Clement, J.P. (2016). SYNGAP1: Mind the Gap. Front. Cell. Neurosci. 10, 32.

Johnson, C.P., Myers, S.M., and American Academy of Pediatrics Council on Children With Disabilities. (2007). Identification and evaluation of children with autism spectrum disorders. Pediatrics 120, 1183-1215.

Kaech, S., and Banker, G. (2006). Culturing hippocampal neurons. Nat. Protoc. 1, 2406-2415.

Kaempf, N., Kochlamazashvili, G., Puchkov, D., Maritzen, T., Bajjalieh, S.M., Kononenko, N.L., and Haucke, V. (2015). Overlapping functions of stonin 2 and SV2 in sorting of the calcium sensor synaptotagmin 1 to synaptic vesicles. Proc. Natl. Acad. Sci. U. S. A. 112, 7297-7302.

Kaeser, P.S., Deng, L., Wang, Y., Dulubova, I., Liu, X., Rizo, J., and Sudhof, T.C. (2011). RIM proteins tether Ca2+ channels to presynaptic active zones via a direct PDZ-domain interaction. Cell 144, 282-295.

Kalscheuer, V.M., Tao, J., Donnelly, A., Hollway, G., Schwinger, E., Kubart, S., Menzel, C., Hoeltzenbein, M., Tommerup, N., Eyre, H., *et al.* (2003). Disruption of the serine/threonine kinase 9 gene causes severe X-linked infantile spasms and mental retardation. Am. J. Hum. Genet. 72, 1401-1411.

Kanner, L. (1943). Autistic Disturbances of Affective Contact. Nervous Child 2, 217-250.

Kasprowicz, J., Kuenen, S., Miskiewicz, K., Habets, R.L., Smitz, L., and Verstreken, P. (2008). Inactivation of clathrin heavy chain inhibits synaptic recycling but allows bulk membrane uptake. J. Cell Biol. 182, 1007-1016.

Kattenstroth, G., Tantalaki, E., Sudhof, T.C., Gottmann, K., and Missler, M. (2004). Postsynaptic N-methyl-D-aspartate receptor function requires alpha-neurexins. Proc. Natl. Acad. Sci. U. S. A. 101, 2607-2612.

Kavalali, E.T. (2015). The mechanisms and functions of spontaneous neurotransmitter release. Nat. Rev. Neurosci. 16, 5-16.

Kavalali, E.T., and Jorgensen, E.M. (2014). Visualizing presynaptic function. Nat. Neurosci. 17, 10-16.

Kim, S.H., and Ryan, T.A. (2013). Balance of calcineurin Aalpha and CDK5 activities sets release probability at nerve terminals. J. Neurosci. 33, 8937-8950.

Kim, J.H., Lee, H.K., Takamiya, K., and Huganir, R.L. (2003). The role of synaptic GTPase-activating protein in neuronal development and synaptic plasticity. J. Neurosci. 23, 1119-1124.

Kim, J.H., Liao, D., Lau, L.F., and Huganir, R.L. (1998). SynGAP: a synaptic RasGAP that associates with the PSD-95/SAP90 protein family. Neuron 20, 683-691.

Klemmer, P., Meredith, R.M., Holmgren, C.D., Klychnikov, O.I., Stahl-Zeng, J., Loos, M., van der Schors, R.C., Wortel, J., de Wit, H., Spijker, S., *et al.* (2011). Proteomics, ultrastructure, and physiology of hippocampal synapses in a fragile X syndrome mouse model reveal presynaptic phenotype. J. Biol. Chem. 286, 25495-25504.

Knuesel, I., Elliott, A., Chen, H.J., Mansuy, I.M., and Kennedy, M.B. (2005). A role for synGAP in regulating neuronal apoptosis. Eur. J. Neurosci. 21, 611-621.

Komiyama, N.H., Watabe, A.M., Carlisle, H.J., Porter, K., Charlesworth, P., Monti, J., Strathdee, D.J., O'Carroll, C.M., Martin, S.J., Morris, R.G., O'Dell, T.J., and Grant, S.G. (2002). SynGAP regulates ERK/MAPK signaling, synaptic plasticity, and learning in the complex with postsynaptic density 95 and NMDA receptor. J. Neurosci. 22, 9721-9732.

Kononenko, N.L., Diril, M.K., Puchkov, D., Kintscher, M., Koo, S.J., Pfuhl, G., Winter, Y., Wienisch, M., Klingauf, J., Breustedt, J., *et al.* (2013). Compromised fidelity of endocytic synaptic vesicle protein sorting in the absence of stonin 2. Proc. Natl. Acad. Sci. U. S. A. 110, E526-35.

Kononenko, N.L., and Haucke, V. (2015). Molecular mechanisms of presynaptic membrane retrieval and synaptic vesicle reformation. Neuron 85, 484-496.

Kononenko, N.L., Puchkov, D., Classen, G.A., Walter, A.M., Pechstein, A., Sawade, L., Kaempf, N., Trimbuch, T., Lorenz, D., Rosenmund, C., Maritzen, T., and Haucke, V. (2014). Clathrin/AP-2 mediate synaptic vesicle reformation from endosome-like vacuoles but are not essential for membrane retrieval at central synapses. Neuron 82, 981-988.

Krapivinsky, G., Medina, I., Krapivinsky, L., Gapon, S., and Clapham, D.E. (2004). SynGAP-MUPP1-CaMKII synaptic complexes regulate p38 MAP kinase activity and NMDA receptor-dependent synaptic AMPA receptor potentiation. Neuron 43, 563-574.

Krishnan, S., Collett, M., and Robinson, P.J. (2015). SH3 Domains Differentially Stimulate Distinct Dynamin I Assembly Modes and G Domain Activity. PLoS One 10, e0144609.

Krol, A., and Feng, G. (2017). Windows of opportunity: timing in neurodevelopmental disorders. Curr. Opin. Neurobiol. 48, 59-63.

Kumar, P., Henikoff, S., and Ng, P.C. (2009). Predicting the effects of coding non-synonymous variants on protein function using the SIFT algorithm. Nat. Protoc. 4, 1073-1081.

Kwon, S.E., and Chapman, E.R. (2011). Synaptophysin regulates the kinetics of synaptic vesicle endocytosis in central neurons. Neuron 70, 847-854.

Lachiewicz, A.M., Dawson, D.V., and Spiridigliozzi, G.A. (2000). Physical characteristics of young boys with fragile X syndrome: reasons for difficulties in making a diagnosis in young males. Am. J. Med. Genet. 92, 229-236.

Lai, Y., Choi, U.B., Leitz, J., Rhee, H.J., Lee, C., Altas, B., Zhao, M., Pfuetzner, R.A., Wang, A.L., Brose, N., Rhee, J., and Brunger, A.T. (2017). Molecular Mechanisms of Synaptic Vesicle Priming by Munc13 and Munc18. Neuron 95, 591-607.e10.

Lasic, E., Stenovec, M., Kreft, M., Robinson, P.J., and Zorec, R. (2017). Dynamin regulates the fusion pore of endo- and exocytotic vesicles as revealed by membrane capacitance measurements. Biochim. Biophys. Acta 1861, 2293-2303.

Lauren, J., Airaksinen, M.S., Saarma, M., and Timmusk, T. (2003). A novel gene family encoding leucine-rich repeat transmembrane proteins differentially expressed in the nervous system. Genomics 81, 411-421.

Lee, K.J., Lee, Y., Rozeboom, A., Lee, J.Y., Udagawa, N., Hoe, H.S., and Pak, D.T. (2011). Requirement for Plk2 in orchestrated ras and rap signaling, homeostatic structural plasticity, and memory. Neuron 69, 957-973.

Leitz, J., and Kavalali, E.T. (2011). Ca(2)(+) influx slows single synaptic vesicle endocytosis. J. Neurosci. 31, 16318-16326.

Lemmon, S.K. (2001). Clathrin uncoating: Auxilin comes to life. Curr. Biol. 11, R49-52.

Leo, A., Citraro, R., Constanti, A., De Sarro, G., and Russo, E. (2015). Are big potassium-type Ca(2+)-activated potassium channels a viable target for the treatment of epilepsy? Expert Opin. Ther. Targets 19, 911-926.

Leonard, H., and Wen, X. (2002). The epidemiology of mental retardation: challenges and opportunities in the new millennium. Ment. Retard. Dev. Disabil. Res. Rev. 8, 117-134.

Leonard, M., Song, B.D., Ramachandran, R., and Schmid, S.L. (2005). Robust colorimetric assays for dynamin's basal and stimulated GTPase activities. Methods Enzymol. 404, 490-503.

Levenga, J., de Vrij, F.M., Buijsen, R.A., Li, T., Nieuwenhuizen, I.M., Pop, A., Oostra, B.A., and Willemsen, R. (2011). Subregion-specific dendritic spine abnormalities in the hippocampus of Fmr1 KO mice. Neurobiol. Learn. Mem. 95, 467-472.

Levinson, J.N., Chery, N., Huang, K., Wong, T.P., Gerrow, K., Kang, R., Prange, O., Wang, Y.T., and El-Husseini, A. (2005). Neuroligins mediate excitatory and inhibitory synapse formation: involvement of PSD-95 and neurexin-1beta in neuroligin-induced synaptic specificity. J. Biol. Chem. 280, 17312-17319.

Li, W., Okano, A., Tian, Q.B., Nakayama, K., Furihata, T., Nawa, H., and Suzuki, T. (2001). Characterization of a novel synGAP isoform, synGAP-beta. J. Biol. Chem. 276, 21417-21424.

Li, Y.C., Chanaday, N.L., Xu, W., and Kavalali, E.T. (2017). Synaptotagmin-1- and Synaptotagmin-7-Dependent Fusion Mechanisms Target Synaptic Vesicles to Kinetically Distinct Endocytic Pathways. Neuron 93, 616-631.e3.

Lin, H.C., Barylko, B., Achiriloaie, M., and Albanesi, J.P. (1997). Phosphatidylinositol (4,5)-bisphosphate-dependent activation of dynamins I and II lacking the proline/arginine-rich domains. J. Biol. Chem. 272, 25999-26004.

Linhoff, M.W., Lauren, J., Cassidy, R.M., Dobie, F.A., Takahashi, H., Nygaard, H.B., Airaksinen, M.S., Strittmatter, S.M., and Craig, A.M. (2009). An unbiased expression screen for synaptogenic proteins identifies the LRRTM protein family as synaptic organizers. Neuron 61, 734-749.

Loane, D.J., Lima, P.A., and Marrion, N.V. (2007). Co-assembly of N-type Ca2+ and BK channels underlies functional coupling in rat brain. J. Cell. Sci. 120, 985-995.

Lopez-Murcia, F.J., Royle, S.J., and Llobet, A. (2014). Presynaptic clathrin levels are a limiting factor for synaptic transmission. J. Neurosci. 34, 8618-8629.

Lou, X., Fan, F., Messa, M., Raimondi, A., Wu, Y., Looger, L.L., Ferguson, S.M., and De Camilli, P. (2012). Reduced release probability prevents vesicle depletion and transmission failure at dynamin mutant synapses. Proc. Natl. Acad. Sci. U. S. A. 109, E515-23.

Lugenbeel, K.A., Peier, A.M., Carson, N.L., Chudley, A.E., and Nelson, D.L. (1995). Intragenic loss of function mutations demonstrate the primary role of FMR1 in fragile X syndrome. Nat. Genet. 10, 483-485.

Marks, B., Stowell, M.H., Vallis, Y., Mills, I.G., Gibson, A., Hopkins, C.R., and McMahon, H.T. (2001). GTPase activity of dynamin and resulting conformation change are essential for endocytosis. Nature 410, 231-235.

Marland, J.R., Hasel, P., Bonnycastle, K., and Cousin, M.A. (2016). Mitochondrial Calcium Uptake Modulates Synaptic Vesicle Endocytosis in Central Nerve Terminals. J. Biol. Chem. 291, 2080-2086.

Martens, S., Kozlov, M.M., and McMahon, H.T. (2007). How synaptotagmin promotes membrane fusion. Science 316, 1205-1208.

Mazarati, A.M., Lewis, M.L., and Pittman, Q.J. (2017). Neurobehavioral comorbidities of epilepsy: Role of inflammation. Epilepsia 58 Suppl 3, 48-56.

McMahon, A.C., Barnett, M.W., O'Leary, T.S., Stoney, P.N., Collins, M.O., Papadia, S., Choudhary, J.S., Komiyama, N.H., Grant, S.G., Hardingham, G.E., Wyllie, D.J., and Kind, P.C. (2012). SynGAP isoforms exert opposing effects on synaptic strength. Nat. Commun. 3, 900.

McMahon, H.T., and Boucrot, E. (2011). Molecular mechanism and physiological functions of clathrin-mediated endocytosis. Nat. Rev. Mol. Cell Biol. 12, 517-533.

Mefford, H.C., Batshaw, M.L., and Hoffman, E.P. (2012). Genomics, intellectual disability, and autism. N. Engl. J. Med. 366, 733-743.

Meijer, H., de Graaff, E., Merckx, D.M., Jongbloed, R.J., de Die-Smulders, C.E., Engelen, J.J., Fryns, J.P., Curfs, P.M., and Oostra, B.A. (1994). A deletion of 1.6 kb proximal to the CGG repeat of the FMR1 gene causes the clinical phenotype of the fragile X syndrome. Hum. Mol. Genet. 3, 615-620.

Micheva, K.D., and Smith, S.J. (2005). Strong effects of subphysiological temperature on the function and plasticity of mammalian presynaptic terminals. J. Neurosci. 25, 7481-7488.

Miesenbock, G., De Angelis, D.A., and Rothman, J.E. (1998). Visualizing secretion and synaptic transmission with pH-sensitive green fluorescent proteins. Nature 394, 192-195.

Miller, T.M., and Heuser, J.E. (1984). Endocytosis of synaptic vesicle membrane at the frog neuromuscular junction. J. Cell Biol. 98, 685-698.

Missler, M., Zhang, W., Rohlmann, A., Kattenstroth, G., Hammer, R.E., Gottmann, K., and Sudhof, T.C. (2003). Alpha-neurexins couple Ca2+ channels to synaptic vesicle exocytosis. Nature 423, 939-948.

Moon, I.S., Sakagami, H., Nakayama, J., and Suzuki, T. (2008). Differential distribution of synGAP alpha1 and synGAP beta isoforms in rat neurons. Brain Res. 1241, 62-75.

Moretto, E., Murru, L., Martano, G., Sassone, J., and Passafaro, M. (2017). Glutamatergic synapses in neurodevelopmental disorders. Prog. Neuropsychopharmacol. Biol. Psychiatry

Muhia, M., Yee, B.K., Feldon, J., Markopoulos, F., and Knuesel, I. (2010). Disruption of hippocampus-regulated behavioural and cognitive processes by heterozygous constitutive deletion of SynGAP. Eur. J. Neurosci. 31, 529-543.

Muhlberg, A.B., Warnock, D.E., and Schmid, S.L. (1997). Domain structure and intramolecular regulation of dynamin GTPase. EMBO J. 16, 6676-6683.

Myrick, L.K., Deng, P.Y., Hashimoto, H., Oh, Y.M., Cho, Y., Poidevin, M.J., Suhl, J.A., Visootsak, J., Cavalli, V., Jin, P.*, et al.* (2015). Independent role for presynaptic

FMRP revealed by an FMR1 missense mutation associated with intellectual disability and seizures. Proc. Natl. Acad. Sci. U. S. A. 112, 949-956.

Nakashima, M., Kouga, T., Lourenco, C.M., Shiina, M., Goto, T., Tsurusaki, Y., Miyatake, S., Miyake, N., Saitsu, H., Ogata, K., Osaka, H., and Matsumoto, N. (2016). De novo DNM1 mutations in two cases of epileptic encephalopathy. Epilepsia 57, e18-23.

Nakata, T., Iwamoto, A., Noda, Y., Takemura, R., Yoshikura, H., and Hirokawa, N. (1991). Predominant and developmentally regulated expression of dynamin in neurons. Neuron 7, 461-469.

Napoli, I., Mercaldo, V., Boyl, P.P., Eleuteri, B., Zalfa, F., De Rubeis, S., Di Marino, D., Mohr, E., Massimi, M., Falconi, M., *et al.* (2008). The fragile X syndrome protein represses activity-dependent translation through CYFIP1, a new 4E-BP. Cell 134, 1042-1054.

N'Gouemo, P. (2011). Targeting BK (big potassium) channels in epilepsy. Expert Opin. Ther. Targets 15, 1283-1295.

Nguyen, T.H., Maucort, G., Sullivan, R.K., Schenning, M., Lavidis, N.A., McCluskey, A., Robinson, P.J., and Meunier, F.A. (2012). Actin- and dynamin-dependent maturation of bulk endocytosis restores neurotransmission following synaptic depletion. PLoS One 7, e36913.

Nicholson-Fish, J.C., Cousin, M.A., and Smillie, K.J. (2016). Phosphatidylinositol 3-Kinase Couples Localised Calcium Influx to Activation of Akt in Central Nerve Terminals. Neurochem. Res. 41, 534-543.

Nicholson-Fish, J.C., Kokotos, A.C., Gillingwater, T.H., Smillie, K.J., and Cousin, M.A. (2015). VAMP4 Is an Essential Cargo Molecule for Activity-Dependent Bulk Endocytosis. Neuron 88, 973-984.

Nicholson-Fish, J.C., Smillie, K.J., and Cousin, M.A. (2016). Monitoring activity-dependent bulk endocytosis with the genetically-encoded reporter VAMP4-pHluorin. J. Neurosci. Methods 266, 1-10.

Nosyreva, E.D., and Huber, K.M. (2006). Metabotropic receptor-dependent long-term depression persists in the absence of protein synthesis in the mouse model of fragile X syndrome. J. Neurophysiol. 95, 3291-3295.

Obar, R.A., Collins, C.A., Hammarback, J.A., Shpetner, H.S., and Vallee, R.B. (1990). Molecular cloning of the microtubule-associated mechanochemical enzyme dynamin reveals homology with a new family of GTP-binding proteins. Nature 347, 256-261.

Opazo, P., Sainlos, M., and Choquet, D. (2012). Regulation of AMPA receptor surface diffusion by PSD-95 slots. Curr. Opin. Neurobiol. 22, 453-460.

Osterweil, E.K., Chuang, S.C., Chubykin, A.A., Sidorov, M., Bianchi, R., Wong, R.K., and Bear, M.F. (2013). Lovastatin corrects excess protein synthesis and prevents epileptogenesis in a mouse model of fragile X syndrome. Neuron 77, 243-250.

Osterweil, E.K., Krueger, D.D., Reinhold, K., and Bear, M.F. (2010). Hypersensitivity to mGluR5 and ERK1/2 leads to excessive protein synthesis in the hippocampus of a mouse model of fragile X syndrome. J. Neurosci. 30, 15616-15627.

Paatero, A., Rosti, K., Shkumatov, A.V., Sele, C., Brunello, C., Kysenius, K., Singha, P., Jokinen, V., Huttunen, H., and Kajander, T. (2016). Crystal Structure of an Engineered LRRTM2 Synaptic Adhesion Molecule and a Model for Neurexin Binding. Biochemistry 55, 914-926.

Park, R.J., Shen, H., Liu, L., Liu, X., Ferguson, S.M., and De Camilli, P. (2013). Dynamin triple knockout cells reveal off target effects of commonly used dynamin inhibitors. J. Cell. Sci. 126, 5305-5312.

Parker, M.J., Fryer, A.E., Shears, D.J., Lachlan, K.L., McKee, S.A., Magee, A.C., Mohammed, S., Vasudevan, P.C., Park, S.M., Benoit, V., *et al.* (2015). De novo, heterozygous, loss-of-function mutations in SYNGAP1 cause a syndromic form of intellectual disability. Am. J. Med. Genet. A. 167A, 2231-2237.

Paschal, B.M., Shpetner, H.S., and Vallee, R.B. (1987). MAP 1C is a microtubule-activated ATPase which translocates microtubules in vitro and has dynein-like properties. J. Cell Biol. 105, 1273-1282.

Patel, A.B., Loerwald, K.W., Huber, K.M., and Gibson, J.R. (2014). Postsynaptic FMRP promotes the pruning of cell-to-cell connections among pyramidal neurons in the L5A neocortical network. J. Neurosci. 34, 3413-3418.

Pathania, M., Davenport, E.C., Muir, J., Sheehan, D.F., Lopez-Domenech, G., and Kittler, J.T. (2014). The autism and schizophrenia associated gene CYFIP1 is critical for the maintenance of dendritic complexity and the stabilization of mature spines. Transl. Psychiatry. 4, e374.

Pena, V., Hothorn, M., Eberth, A., Kaschau, N., Parret, A., Gremer, L., Bonneau, F., Ahmadian, M.R., and Scheffzek, K. (2008). The C2 domain of SynGAP is essential for stimulation of the Rap GTPase reaction. EMBO Rep. 9, 350-355.

Petrini, E.M., Ravasenga, T., Hausrat, T.J., Iurilli, G., Olcese, U., Racine, V., Sibarita, J.B., Jacob, T.C., Moss, S.J., Benfenati, F., *et al.* (2014). Synaptic recruitment of gephyrin regulates surface GABAA receptor dynamics for the expression of inhibitory LTP. Nat. Commun. 5, 3921.

Pfeiffer, B.E., and Huber, K.M. (2009). The state of synapses in fragile X syndrome. Neuroscientist 15, 549-567.

Pfeiffer, B.E., Zang, T., Wilkerson, J.R., Taniguchi, M., Maksimova, M.A., Smith, L.N., Cowan, C.W., and Huber, K.M. (2010). Fragile X mental retardation protein is required for synapse elimination by the activity-dependent transcription factor MEF2. Neuron 66, 191-197.

Pieretti, M., Zhang, F.P., Fu, Y.H., Warren, S.T., Oostra, B.A., Caskey, C.T., and Nelson, D.L. (1991). Absence of expression of the FMR-1 gene in fragile X syndrome. Cell 66, 817-822.

Pitkanen, A., and Sutula, T.P. (2002). Is epilepsy a progressive disorder? Prospects for new therapeutic approaches in temporal-lobe epilepsy. Lancet Neurol. 1, 173-181.

Poodry, C.A., and Edgar, L. (1979). Reversible alteration in the neuromuscular junctions of Drosophila melanogaster bearing a temperature-sensitive mutation, shibire. J. Cell Biol. 81, 520-527.

Porter, K., Komiyama, N.H., Vitalis, T., Kind, P.C., and Grant, S.G. (2005). Differential expression of two NMDA receptor interacting proteins, PSD-95 and SynGAP during mouse development. Eur. J. Neurosci. 21, 351-362.

Pressler, R., and Auvin, S. (2013). Comparison of Brain Maturation among Species: An Example in Translational Research Suggesting the Possible Use of Bumetanide in Newborn. Front. Neurol. 4, 36.

Qian, Y., Corum, L., Meng, Q., Blenis, J., Zheng, J.Z., Shi, X., Flynn, D.C., and Jiang, B.H. (2004). PI3K induced actin filament remodeling through Akt and p70S6K1: implication of essential role in cell migration. Am. J. Physiol. Cell. Physiol. 286, C153-63.

Quan, A., and Robinson, P.J. (2013). Syndapin--a membrane remodelling and endocytic F-BAR protein. FEBS J. 280, 5198-5212.

Raimondi, A., Ferguson, S.M., Lou, X., Armbruster, M., Paradise, S., Giovedi, S., Messa, M., Kono, N., Takasaki, J., Cappello, V., *et al.* (2011). Overlapping role of dynamin isoforms in synaptic vesicle endocytosis. Neuron 70, 1100-1114.

Raingo, J., Khvotchev, M., Liu, P., Darios, F., Li, Y.C., Ramirez, D.M., Adachi, M., Lemieux, P., Toth, K., Davletov, B., and Kavalali, E.T. (2012). VAMP4 directs synaptic vesicles to a pool that selectively maintains asynchronous neurotransmission. Nat. Neurosci. 15, 738-745.

Ramachandran, R., Pucadyil, T.J., Liu, Y.W., Acharya, S., Leonard, M., Lukiyanchuk, V., and Schmid, S.L. (2009). Membrane insertion of the pleckstrin homology domain variable loop 1 is critical for dynamin-catalyzed vesicle scission. Mol. Biol. Cell 20, 4630-4639.

Ramachandran, R., Surka, M., Chappie, J.S., Fowler, D.M., Foss, T.R., Song, B.D., and Schmid, S.L. (2007). The dynamin middle domain is critical for tetramerization and higher-order self-assembly. EMBO J. 26, 559-566.

Rami, A. (2003). Ischemic neuronal death in the rat hippocampus: the calpain-calpastatin-caspase hypothesis. Neurobiol. Dis. 13, 75-88.

Rao, A., Kim, E., Sheng, M., and Craig, A.M. (1998). Heterogeneity in the molecular composition of excitatory postsynaptic sites during development of hippocampal neurons in culture. J. Neurosci. 18, 1217-1229.

Reis, C.R., Chen, P.H., Srinivasan, S., Aguet, F., Mettlen, M., and Schmid, S.L. (2015). Crosstalk between Akt/GSK3beta signaling and dynamin-1 regulates clathrin-mediated endocytosis. EMBO J. 34, 2132-2146.

Reissner, C., Runkel, F., and Missler, M. (2013). Neurexins. Genome Biol. 14, 213.

Renden, R., and von Gersdorff, H. (2007). Synaptic vesicle endocytosis at a CNS nerve terminal: faster kinetics at physiological temperatures and increased endocytotic capacity during maturation. J. Neurophysiol. 98, 3349-3359.

Richards, D.A., Guatimosim, C., and Betz, W.J. (2000). Two endocytic recycling routes selectively fill two vesicle pools in frog motor nerve terminals. Neuron 27, 551-559.

Ritvo, E.R., Freeman, B.J., Mason-Brothers, A., Mo, A., and Ritvo, A.M. (1985). Concordance for the syndrome of autism in 40 pairs of afflicted twins. Am. J. Psychiatry 142, 74-77.

Rizo, J., and Xu, J. (2015). The Synaptic Vesicle Release Machinery. Annu. Rev. Biophys. 44, 339-367.

Rizzoli, S.O. (2014). Synaptic vesicle recycling: steps and principles. EMBO J. 33, 788-822.

Rizzoli, S.O., and Betz, W.J. (2005). Synaptic vesicle pools. Nat. Rev. Neurosci. 6, 57-69.

Robertson, L. (2013). **mGlu5 as a potential therapeutic target for the treatment of fragile X syndrome**. Bioscience Horizons 6,

Ropers, H.H., and Hamel, B.C. (2005). X-linked mental retardation. Nat. Rev. Genet. 6, 46-57.

Rosenberg, R.E., Law, J.K., Yenokyan, G., McGready, J., Kaufmann, W.E., and Law, P.A. (2009). Characteristics and concordance of autism spectrum disorders among 277 twin pairs. Arch. Pediatr. Adolesc. Med. 163, 907-914.

Rousseau, F., Rouillard, P., Morel, M.L., Khandjian, E.W., and Morgan, K. (1995). Prevalence of carriers of premutation-size alleles of the FMRI gene--and implications for the population genetics of the fragile X syndrome. Am. J. Hum. Genet. 57, 1006-1018.

Rubenstein, J.L., and Merzenich, M.M. (2003). Model of autism: increased ratio of excitation/inhibition in key neural systems. Genes Brain Behav. 2, 255-267.

Rumbaugh, G., Adams, J.P., Kim, J.H., and Huganir, R.L. (2006). SynGAP regulates synaptic strength and mitogen-activated protein kinases in cultured neurons. Proc. Natl. Acad. Sci. U. S. A. 103, 4344-4351.

Ryan, T.A. (2001). Presynaptic imaging techniques. Curr. Opin. Neurobiol. 11, 544-549.

Saheki, Y., and De Camilli, P. (2012). Synaptic vesicle endocytosis. Cold Spring Harb Perspect. Biol. 4, a005645.

Sander, J.W., and Shorvon, S.D. (1996). Epidemiology of the epilepsies. J. Neurol. Neurosurg. Psychiatry. 61, 433-443.

Sankaranarayanan, S., Atluri, P.P., and Ryan, T.A. (2003). Actin has a molecular scaffolding, not propulsive, role in presynaptic function. Nat. Neurosci. 6, 127-135.

Sankaranarayanan, S., De Angelis, D., Rothman, J.E., and Ryan, T.A. (2000). The use of pHluorins for optical measurements of presynaptic activity. Biophys. J. 79, 2199-2208.

Sankaranarayanan, S., and Ryan, T.A. (2001). Calcium accelerates endocytosis of vSNAREs at hippocampal synapses. Nat. Neurosci. 4, 129-136.

Sankaranarayanan, S., and Ryan, T.A. (2000). Real-time measurements of vesicle-SNARE recycling in synapses of the central nervous system. Nat. Cell Biol. 2, 197-204.

Santini, E., Huynh, T.N., Longo, F., Koo, S.Y., Mojica, E., D'Andrea, L., Bagni, C., and Klann, E. (2017). Reducing eIF4E-eIF4G interactions restores the balance between protein synthesis and actin dynamics in fragile X syndrome model mice. Sci. Signal. 10, 10.1126/scisignal.aan0665.

Sarbassov, D.D., Guertin, D.A., Ali, S.M., and Sabatini, D.M. (2005). Phosphorylation and regulation of Akt/PKB by the rictor-mTOR complex. Science 307, 1098-1101.

Scheiffele, P., Fan, J., Choih, J., Fetter, R., and Serafini, T. (2000). Neuroligin expressed in nonneuronal cells triggers presynaptic development in contacting axons. Cell 101, 657-669.

Schettler, T. (2001). Toxic threats to neurologic development of children. Environ. Health Perspect. 109 Suppl 6, 813-816.

Schmid, S.L., and Frolov, V.A. (2011). Dynamin: functional design of a membrane fission catalyst. Annu. Rev. Cell Dev. Biol. 27, 79-105.

Scott, R., and Rusakov, D.A. (2006). Main determinants of presynaptic Ca2+ dynamics at individual mossy fiber-CA3 pyramidal cell synapses. J. Neurosci. 26, 7071-7081.

Sever, S., Damke, H., and Schmid, S.L. (2000). Dynamin:GTP controls the formation of constricted coated pits, the rate limiting step in clathrin-mediated endocytosis. J. Cell Biol. 150, 1137-1148.

Shimada, A., Niwa, H., Tsujita, K., Suetsugu, S., Nitta, K., Hanawa-Suetsugu, K., Akasaka, R., Nishino, Y., Toyama, M., Chen, L., *et al.* (2007). Curved EFC/F-BAR-domain dimers are joined end to end into a filament for membrane invagination in endocytosis. Cell 129, 761-772.

Shnyrova, A.V., Bashkirov, P.V., Akimov, S.A., Pucadyil, T.J., Zimmerberg, J., Schmid, S.L., and Frolov, V.A. (2013). Geometric catalysis of membrane fission driven by flexible dynamin rings. Science 339, 1433-1436.

Shpetner, H.S., and Vallee, R.B. (1989). Identification of dynamin, a novel mechanochemical enzyme that mediates interactions between microtubules. Cell 59, 421-432.

Shupliakov, O., Bloom, O., Gustafsson, J.S., Kjaerulff, O., Low, P., Tomilin, N., Pieribone, V.A., Greengard, P., and Brodin, L. (2002). Impaired recycling of synaptic vesicles after acute perturbation of the presynaptic actin cytoskeleton. Proc. Natl. Acad. Sci. U. S. A. 99, 14476-14481.

Shupliakov, O., Low, P., Grabs, D., Gad, H., Chen, H., David, C., Takei, K., De Camilli, P., and Brodin, L. (1997). Synaptic vesicle endocytosis impaired by disruption of dynamin-SH3 domain interactions. Science 276, 259-263.

Siddiqui, T.J., Pancaroglu, R., Kang, Y., Rooyakkers, A., and Craig, A.M. (2010). LRRTMs and neuroligins bind neurexins with a differential code to cooperate in glutamate synapse development. J. Neurosci. 30, 7495-7506.

Siddiqui, T.J., Tari, P.K., Connor, S.A., Zhang, P., Dobie, F.A., She, K., Kawabe, H., Wang, Y.T., Brose, N., and Craig, A.M. (2013). An LRRTM4-HSPG complex mediates excitatory synapse development on dentate gyrus granule cells. Neuron 79, 680-695.

Smillie, K.J., and Cousin, M.A. (2012). Akt/PKB controls the activity-dependent bulk endocytosis of synaptic vesicles. Traffic 13, 1004-1011.

Smillie, K.J., and Cousin, M.A. (2011). The Role of GSK3 in Presynaptic Function. Int. J. Alzheimers Dis. 2011, 263673.

Smillie, K.J., Pawson, J., Perkins, E.M., Jackson, M., and Cousin, M.A. (2013). Control of synaptic vesicle endocytosis by an extracellular signalling molecule. Nat. Commun. 4, 2394.

Smith, K.R., Muir, J., Rao, Y., Browarski, M., Gruenig, M.C., Sheehan, D.F., Haucke, V., and Kittler, J.T. (2012). Stabilization of GABA(A) receptors at endocytic zones is mediated by an AP2 binding motif within the GABA(A) receptor beta3 subunit. J. Neurosci. 32, 2485-2498.

Snyder, J.S., Choe, J.S., Clifford, M.A., Jeurling, S.I., Hurley, P., Brown, A., Kamhi, J.F., and Cameron, H.A. (2009). Adult-born hippocampal neurons are more numerous, faster maturing, and more involved in behavior in rats than in mice. J. Neurosci. 29, 14484-14495.

Sontheimer, H. (2015). Chapter 11 - Neurodevelopmental Disorders. In Diseases of the Nervous System, Sontheimer, Harald ed., (San Diego: Academic Press) pp. 319-347.

Sudhof, T.C. (2012). The presynaptic active zone. Neuron 75, 11-25.

Sudhof, T.C. (2004). The synaptic vesicle cycle. Annu. Rev. Neurosci. 27, 509-547.

Sudhof, T.C., and Rizo, J. (2011). Synaptic vesicle exocytosis. Cold Spring Harb Perspect. Biol. 3, 10.1101/cshperspect.a005637.

Sutcliffe, J.S., Nelson, D.L., Zhang, F., Pieretti, M., Caskey, C.T., Saxe, D., and Warren, S.T. (1992). DNA methylation represses FMR-1 transcription in fragile X syndrome. Hum. Mol. Genet. 1, 397-400.

Suvrathan, A., Hoeffer, C.A., Wong, H., Klann, E., and Chattarji, S. (2010). Characterization and reversal of synaptic defects in the amygdala in a mouse model of fragile X syndrome. Proc. Natl. Acad. Sci. U. S. A. 107, 11591-11596.

Sweitzer, S.M., and Hinshaw, J.E. (1998). Dynamin undergoes a GTP-dependent conformational change causing vesiculation. Cell 93, 1021-1029.

Szpir, M. (2006). New thinking on neurodevelopment. Environ. Health Perspect. 114, A100-7.

Takei, K., McPherson, P.S., Schmid, S.L., and De Camilli, P. (1995). Tubular membrane invaginations coated by dynamin rings are induced by GTP-gamma S in nerve terminals. Nature 374, 186-190.

Tamanini, F., Willemsen, R., van Unen, L., Bontekoe, C., Galjaard, H., Oostra, B.A., and Hoogeveen, A.T. (1997). Differential expression of FMR1, FXR1 and FXR2 proteins in human brain and testis. Hum. Mol. Genet. 6, 1315-1322.

Tan, T.C., Valova, V.A., Malladi, C.S., Graham, M.E., Berven, L.A., Jupp, O.J., Hansra, G., McClure, S.J., Sarcevic, B., Boadle, R.A., *et al.* (2003). Cdk5 is essential for synaptic vesicle endocytosis. Nat. Cell Biol. 5, 701-710.

Tang, B., Wang, T., Wan, H., Han, L., Qin, X., Zhang, Y., Wang, J., Yu, C., Berton, F., Francesconi, W., *et al.* (2015). Fmr1 deficiency promotes age-dependent alterations in the cortical synaptic proteome. Proc. Natl. Acad. Sci. U. S. A. 112, E4697-706.

Tanifuji, S., Funakoshi-Tago, M., Ueda, F., Kasahara, T., and Mochida, S. (2013). Dynamin isoforms decode action potential firing for synaptic vesicle recycling. J. Biol. Chem. 288, 19050-19059.

Taylor, B., Jick, H., and Maclaughlin, D. (2013). Prevalence and incidence rates of autism in the UK: time trend from 2004-2010 in children aged 8 years. BMJ Open 3, e003219-2013-003219.

Taylor, M.J., Lampe, M., and Merrifield, C.J. (2012). A feedback loop between dynamin and actin recruitment during clathrin-mediated endocytosis. PLoS Biol. 10, e1001302.

Taylor, M.J., Perrais, D., and Merrifield, C.J. (2011). A high precision survey of the molecular dynamics of mammalian clathrin-mediated endocytosis. PLoS Biol. 9, e1000604.

Teng, H., Lin, M.Y., and Wilkinson, R.S. (2007). Macroendocytosis and endosome processing in snake motor boutons. J. Physiol. 582, 243-262.

The Dutch-Belgian Fragile X Consortium. (1994). Fmr1 knockout mice: a model to study fragile X mental retardation. Cell 78, 23-33.

Thevenaz, P., Ruttimann, U.E., and Unser, M. (1998). A pyramid approach to subpixel registration based on intensity. IEEE Trans. Image Process. 7, 27-41.

Thomas, A.M., Bui, N., Perkins, J.R., Yuva-Paylor, L.A., and Paylor, R. (2012). Group I metabotropic glutamate receptor antagonists alter select behaviors in a mouse model for fragile X syndrome. Psychopharmacology (Berl) 219, 47-58.

Thomas, S., Hovinga, M.E., Rai, D., and Lee, B.K. (2017). Brief Report: Prevalence of Co-occurring Epilepsy and Autism Spectrum Disorder: The U.S. National Survey of Children's Health 2011-2012. J. Autism Dev. Disord. 47, 224-229.

Till, S.M., Asiminas, A., Jackson, A.D., Katsanevaki, D., Barnes, S.A., Osterweil, E.K., Bear, M.F., Chattarji, S., Wood, E.R., Wyllie, D.J., and Kind, P.C. (2015).

Conserved hippocampal cellular pathophysiology but distinct behavioural deficits in a new rat model of FXS. Hum. Mol. Genet. 24, 5977-5984.

Till, S.M., Wijetunge, L.S., Seidel, V.G., Harlow, E., Wright, A.K., Bagni, C., Contractor, A., Gillingwater, T.H., and Kind, P.C. (2012). Altered maturation of the primary somatosensory cortex in a mouse model of fragile X syndrome. Hum. Mol. Genet. 21, 2143-2156.

Trimbuch, T., and Rosenmund, C. (2016). Should I stop or should I go? The role of complexin in neurotransmitter release. Nat. Rev. Neurosci. 17, 118-125.

Truett, G.E., Heeger, P., Mynatt, R.L., Truett, A.A., Walker, J.A., and Warman, M.L. (2000). Preparation of PCR-quality mouse genomic DNA with hot sodium hydroxide and tris (HotSHOT). BioTechniques 29, 52, 54.

Tuma, P.L., Stachniak, M.C., and Collins, C.A. (1993). Activation of dynamin GTPase by acidic phospholipids and endogenous rat brain vesicles. J. Biol. Chem. 268, 17240-17246.

van der Bliek, A.M., and Meyerowitz, E.M. (1991). Dynamin-like protein encoded by the Drosophila shibire gene associated with vesicular traffic. Nature 351, 411-414.

van der Bliek, A.M., Redelmeier, T.E., Damke, H., Tisdale, E.J., Meyerowitz, E.M., and Schmid, S.L. (1993). Mutations in human dynamin block an intermediate stage in coated vesicle formation. J. Cell Biol. 122, 553-563.

van Loo, K.M., and Martens, G.J. (2007). Genetic and environmental factors in complex neurodevelopmental disorders. Curr. Genomics 8, 429-444.

Vazquez, L.E., Chen, H.J., Sokolova, I., Knuesel, I., and Kennedy, M.B. (2004). SynGAP regulates spine formation. J. Neurosci. 24, 8862-8872.

Verkerk, A.J., Pieretti, M., Sutcliffe, J.S., Fu, Y.H., Kuhl, D.P., Pizzuti, A., Reiner, O., Richards, S., Victoria, M.F., and Zhang, F.P. (1991). Identification of a gene (FMR-1) containing a CGG repeat coincident with a breakpoint cluster region exhibiting length variation in fragile X syndrome. Cell 65, 905-914.

Verstreken, P., Kjaerulff, O., Lloyd, T.E., Atkinson, R., Zhou, Y., Meinertzhagen, I.A., and Bellen, H.J. (2002). Endophilin mutations block clathrin-mediated endocytosis but not neurotransmitter release. Cell 109, 101-112.

Verstreken, P., Koh, T.W., Schulze, K.L., Zhai, R.G., Hiesinger, P.R., Zhou, Y., Mehta, S.Q., Cao, Y., Roos, J., and Bellen, H.J. (2003). Synaptojanin is recruited by endophilin to promote synaptic vesicle uncoating. Neuron 40, 733-748.

Vita, D.J., and Broadie, K. (2017). ESCRT-III Membrane Trafficking Misregulation Contributes To Fragile X Syndrome Synaptic Defects. Sci. Rep. 7, 8683-017-09103-6.

Voglmaier, S.M., Kam, K., Yang, H., Fortin, D.L., Hua, Z., Nicoll, R.A., and Edwards, R.H. (2006). Distinct endocytic pathways control the rate and extent of synaptic vesicle protein recycling. Neuron 51, 71-84.

von Spiczak, S., Helbig, K.L., Shinde, D.N., Huether, R., Pendziwiat, M., Lourenco, C., Nunes, M.E., Sarco, D.P., Kaplan, R.A., Dlugos, D.J., *et al.* (2017). DNM1 encephalopathy: A new disease of vesicle fission. Neurology

Walkup, W.G.,4th, Mastro, T.L., Schenker, L.T., Vielmetter, J., Hu, R., Iancu, A., Reghunathan, M., Bannon, B.D., and Kennedy, M.B. (2016). Correction: A model for regulation by SynGAP-alpha1 of binding of synaptic proteins to PDZ-domain 'Slots' in the postsynaptic density. Elife 5, 10.7554/eLife.22495.

Walkup, W.G.,4th, Washburn, L., Sweredoski, M.J., Carlisle, H.J., Graham, R.L., Hess, S., and Kennedy, M.B. (2015). Phosphorylation of synaptic GTPase-activating protein (synGAP) by Ca2+/calmodulin-dependent protein kinase II (CaMKII) and cyclin-dependent kinase 5 (CDK5) alters the ratio of its GAP activity toward Ras and Rap GTPases. J. Biol. Chem. 290, 4908-4927.

Wang, C.C., Held, R.G., and Hall, B.J. (2013). SynGAP regulates protein synthesis and homeostatic synaptic plasticity in developing cortical networks. PLoS One 8, e83941.

Wang, X.S., Peng, C.Z., Cai, W.J., Xia, J., Jin, D., Dai, Y., Luo, X.G., Klyachko, V.A., and Deng, P.Y. (2014). Activity-dependent regulation of release probability at excitatory hippocampal synapses: a crucial role of fragile X mental retardation protein in neurotransmission. Eur. J. Neurosci. 39, 1602-1612.

Warnock, D.E., Hinshaw, J.E., and Schmid, S.L. (1996). Dynamin self-assembly stimulates its GTPase activity. J. Biol. Chem. 271, 22310-22314.

Watanabe, S., and Boucrot, E. (2017). Fast and ultrafast endocytosis. Curr. Opin. Cell Biol. 47, 64-71.

Watanabe, S., Liu, Q., Davis, M.W., Hollopeter, G., Thomas, N., Jorgensen, N.B., and Jorgensen, E.M. (2013). Ultrafast endocytosis at Caenorhabditis elegans neuromuscular junctions. Elife 2, e00723.

Watanabe, S., Rost, B.R., Camacho-Perez, M., Davis, M.W., Sohl-Kielczynski, B., Rosenmund, C., and Jorgensen, E.M. (2013). Ultrafast endocytosis at mouse hippocampal synapses. Nature 504, 242-247.

Watanabe, S., Trimbuch, T., Camacho-Perez, M., Rost, B.R., Brokowski, B., Sohl-Kielczynski, B., Felies, A., Davis, M.W., Rosenmund, C., and Jorgensen, E.M. (2014). Clathrin regenerates synaptic vesicles from endosomes. Nature 515, 228-233.

Weiler, I.J., Irwin, S.A., Klintsova, A.Y., Spencer, C.M., Brazelton, A.D., Miyashiro, K., Comery, T.A., Patel, B., Eberwine, J., and Greenough, W.T. (1997). Fragile X mental retardation protein is translated near synapses in response to neurotransmitter activation. Proc. Natl. Acad. Sci. U. S. A. 94, 5395-5400.

Wijetunge, L.S., Angibaud, J., Frick, A., Kind, P.C., and Nagerl, U.V. (2014). Stimulated emission depletion (STED) microscopy reveals nanoscale defects in the developmental trajectory of dendritic spine morphogenesis in a mouse model of fragile X syndrome. J. Neurosci. 34, 6405-6412.

Wijetunge, L.S., Chattarji, S., Wyllie, D.J., and Kind, P.C. (2013). Fragile X syndrome: from targets to treatments. Neuropharmacology 68, 83-96.

Wilhelm, B.G., Mandad, S., Truckenbrodt, S., Krohnert, K., Schafer, C., Rammner, B., Koo, S.J., Classen, G.A., Krauss, M., Haucke, V., Urlaub, H., and Rizzoli, S.O. (2014). Composition of isolated synaptic boutons reveals the amounts of vesicle trafficking proteins. Science 344, 1023-1028.

Williams, R.L., and Urbe, S. (2007). The emerging shape of the ESCRT machinery. Nat. Rev. Mol. Cell Biol. 8, 355-368.

Wright, C.F., Fitzgerald, T.W., Jones, W.D., Clayton, S., McRae, J.F., van Kogelenberg, M., King, D.A., Ambridge, K., Barrett, D.M., Bayzetinova, T., *et al.* (2015). Genetic diagnosis of developmental disorders in the DDD study: a scalable analysis of genome-wide research data. Lancet 385, 1305-1314.

Wright, J., Pickard, N., Whitfield, A., and Hakin, N. (2000). A population-based study of the prevalence, clinical characteristics and effect of ethnicity in epilepsy. Seizure *9,* 309-313.

Wu, X.S., and Wu, L.G. (2014). The yin and yang of calcium effects on synaptic vesicle endocytosis. J. Neurosci. 34, 2652-2659.

Wu, Y., O'Toole, E.T., Girard, M., Ritter, B., Messa, M., Liu, X., McPherson, P.S., Ferguson, S.M., and De Camilli, P. (2014). A dynamin 1-, dynamin 3- and clathrin-independent pathway of synaptic vesicle recycling mediated by bulk endocytosis. Elife 3, e01621.

Yan, Q.J., Rammal, M., Tranfaglia, M., and Bauchwitz, R.P. (2005). Suppression of two major Fragile X Syndrome mouse model phenotypes by the mGluR5 antagonist MPEP. Neuropharmacology 49, 1053-1066.

Yao, C.K., Liu, Y.T., Lee, I.C., Wang, Y.T., and Wu, P.Y. (2017). A Ca2+ channel differentially regulates Clathrin-mediated and activity-dependent bulk endocytosis. PLoS Biol. 15, e2000931.

Yizhar, O., Fenno, L.E., Prigge, M., Schneider, F., Davidson, T.J., O'Shea, D.J., Sohal, V.S., Goshen, I., Finkelstein, J., Paz, J.T., *et al.* (2011). Neocortical excitation/inhibition balance in information processing and social dysfunction. Nature 477, 171-178.

Yoshida, Y., and Takei, K. (2005). Stimulation of Dynamin GTPase Activity by Amphiphysin. Methods in Enzymology *404,* 528-537.

Zalfa, F., Giorgi, M., Primerano, B., Moro, A., Di Penta, A., Reis, S., Oostra, B., and Bagni, C. (2003). The fragile X syndrome protein FMRP associates with BC1 RNA and regulates the translation of specific mRNAs at synapses. Cell 112, 317-327.

Zang, T., Maksimova, M.A., Cowan, C.W., Bassel-Duby, R., Olson, E.N., and Huber, K.M. (2013). Postsynaptic FMRP bidirectionally regulates excitatory synapses as a function of developmental age and MEF2 activity. Mol. Cell. Neurosci. 56, 39-49.

Zhang, J., Hou, L., Klann, E., and Nelson, D.L. (2009). Altered hippocampal synaptic plasticity in the FMR1 gene family knockout mouse models. J. Neurophysiol. 101, 2572-2580.

Zhang, N., Gordon, S.L., Fritsch, M.J., Esoof, N., Campbell, D.G., Gourlay, R., Velupillai, S., Macartney, T., Peggie, M., van Aalten, D.M., Cousin, M.A., and Alessi, D.R. (2015). Phosphorylation of synaptic vesicle protein 2A at Thr84 by casein kinase 1 family kinases controls the specific retrieval of synaptotagmin-1. J. Neurosci. 35, 2492-2507.

Zheng, J., Cahill, S.M., Lemmon, M.A., Fushman, D., Schlessinger, J., and Cowburn, D. (1996). Identification of the Binding Site for Acidic Phospholipids on the PH Domain of Dynamin: Implications for Stimulation of GTPase Activity. Journal of Molecular Biology *255,* 14-21.

Zhu, J.J., Qin, Y., Zhao, M., Van Aelst, L., and Malinow, R. (2002). Ras and Rap control AMPA receptor trafficking during synaptic plasticity. Cell 110, 443-455.